
THE UNIVERSITY *of* EDINBURGH

# Smart Wearable TENS Device For Overactive Bladder Management


**Wei Ju**

*A thesis submitted in partial fulfillment of the requirements for the degree of*

Doctor of Philosophy

School of Engineering
The University of Edinburgh

8 July 2025

“ 青，取之于蓝，而青于蓝；冰，水为之，而寒于水。木直中绳，輮以为轮，其曲中规。虽有槁暴，不复挺者，輮使之然也。故木受绳则直，金就砺则利，君子博学而日参省乎己，则知明而行无过矣。故不登高山，不知天之高也；不临深溪，不知地之厚也。”

—《荀子 • 劝学》

*“Indigo is derived from blue, but it is greener than blue; Ice is formed from water, but it is colder than water. Wood's straightness is measurable by carpenter's ink line, but heat-softening can turn it into a wheel with the roundness prescribed by a compass. Even if it is dried up by harsh weather elements, it will not be unbent again. It is the softening that has made it as such. So wood gauged by string is perpendicular, and metal upon whetted is sharp. Righteous man needs to be well-read and self-assessed daily, then he would conduct himself wisely and flawlessly. Therefore one cannot appreciate how high the sky is without climbing up a tall mountain. He cannot know how thick the ground is without going down an abyss.”*[1]

*— XUN ZI • AN EXHORTATION TO STUDY*

[1] It was translated by: alexcwlin; edited by: Adam Lam.

# Abstract

Overactive bladder (OAB) syndrome is a chronic condition of global prevalence that greatly affects patient quality of life. While percutaneous tibial nerve stimulation (PTNS) is now a well-established treatment, its invasiveness limits its usability. Recent advances in transcutaneous tibial nerve stimulation (TTNS) treatments have shown great promise, but most commercially available neuro-stimulator are relatively large, reliant on adhesive gel electrodes and require professional help. This makes them particularly difficult to use by older home-bound patients with sensitive/fragile skin, who are often the target demographic. These limitations reduce patient adherence and consistency in treatment. To address these issues, this thesis details the development of a compact, wearable device (TENS*mini*, weighing 31 g), specifically designed to be connected to a washable sock featuring conductive textile electrodes. This unobtrusive device allows users to control stimulation parameters wirelessly via mobile devices, enabling tailored TTNS treatments. Necessary features, including consistent electrode positioning, galvanic isolation and automated disconnection detection, were incorporated to ensure enhanced user protection. In two pilot studies involving 57 healthy participants, the TENS*mini* device effectively stimulated the tibial nerve (measured via electromyographic (EMG) recording) and demonstrated short-term inhibitory effects on bladder control, with performance comparable to a clinical-grade stimulator. While further clinical studies are needed to evaluate its long-term therapeutic effectiveness, the TENS*mini* offers patients enhanced safety, usability, and the potential for considerable improvements in adherence to home-based OAB management.

# Lay Summary

Overactive bladder (OAB) is a long-term health issue which causes people to experience sudden, frequent urges to urinate, even when the bladder is not full. This condition can disrupt daily to day activities and significantly lower quality of life, especially in older people.

A common treatment for OAB involves electrically stimulating the tibial nerve (found behind the ankle joint) to relieve symptoms. While some methods of stimulating this nerve such as invasive *percutaneous* tibial nerve stimulation (PTNS) (which uses a thin 34-gauge needle), or non-invasive *transcutaneous* tibial nerve stimulation (TTNS) (that utilises two gel-based electrode pads), can help, they nevertheless possess several limitations.

PTNS requires consistent visits to a medical clinic as well as invasive needle injections, while most TTNS devices are bulky and rely on adhesive pads that may irritate sensitive skin. Additionally, the range of buttons on the device's body can make it difficult for older users to operate them independently at home. These challenges make it difficult for OAB patients to adhere consistently to treatment sessions.

To address these issues, this project aimed to develop a smart, wearable, device called TENS*mini*. This small, lightweight machine can connect to a washable and reusable sock embedded with conductive fabric electrodes that eliminate the need for sticky gel pads or invasive needles. Its users can wirelessly adjust the intensity and timing of the nerve stimulation over Bluetooth® via their smartphones, allowing personalised treatment.

The device's safety features include an automatic shut-off if the sock shifts out of place, and protections against electrical risks. In early tests with 57 healthy volunteers, the TENS*mini* successfully activated the tibial nerve (measured by muscle responses in the foot) and showed short-term effects on bladder function comparable to a clinical-grade device benchmark.

More studies are needed to confirm its long-term benefits for OAB patients. However, the TENS*mini* offers a practical and comfortable solution for home-based use. Its simple, easy-to-wear, design, and Bluetooth control help users adhere to their treatment more consistently. By making TTNS safer and more user-friendly, this innovation aims to empower patients with OAB and other lower urinary tract conditions to manage their symptoms effectively, thereby improving their quality of life.

# Acknowledgements

I would like to express my sincere gratitude to the supervision team including Prof. Srinjoy Mitra and Prof. Susan D. Shenkin (Usher Institute), for their invaluable guidance and support throughout the entire postgraduate research project. Their insightful feedback has been instrumental in shaping this work. I am also deeply grateful to another senior academic, Prof. Kianoush Nazarpour (School of Informatics), for his expert advice on experimental methodology, statistical analysis, and academic writing, which has significantly refined key aspects of the study.

I extend my appreciation to my collaborative peers and colleagues, including Dr. Sadeque Reza Khan (Heriot-Watt University), Aidan McConnell-Trevillion (School of Informatics), and David Alejandro Vaca-Benavides, for their constructive discussions and internal reviews, which have contributed to the quality and impact of the entire work.

My gratitude also goes to Prof. Ian Underwood, Prof. Joanne Booth (Glasgow Caledonian University; Retired), Dr. Shiwei Wang (王师惟), Dr. Chang Liu (刘畅), Dr. Xinyu Jiang (姜新雨; School of Informatics), Dr. Andreas Tsiamis, Dr. Lichen Yao (姚力宸; Eindhoven University of Technology), Dr. Yinhuan Dong (董银幻), Pablo Gilberto Ledesma Lopez, Tiantao Jiang (姜天涛; Heriot-Watt University), and many other mentors, friends and colleagues for their encouragement and research guidance. I would also like to acknowledge the laboratory technicians, particularly Iain Gold and Alasdair Christie, for their kind assistance to resolve some technical issues.

Lastly, I would like to extend my thanks to my close friends in London, Wei Liu (刘炜) and Dr. Chen Xie (谢琛), for their consistent encouragement throughout my doctoral research journey. I am especially grateful to my partner, Fan Ye (叶蕃), and my parents, Junlong Ju (鞠军龙) and Dongmei Fu (辅冬梅), for their steadfast emotional and financial support. I would also like to sincerely thank my mother-in-law, Dongmei Han (韩冬美), for her invaluable help and dedication in taking care of my daily needs during the thesis writing period. Without their support, completing this doctorate would have been much far more difficult.

Additionally, the entire research work has been financially supported in part by the Legal & General Research Grant (to establish of the independent Advanced Care Research Centre at The University of Edinburgh), the Economic and Social Research Council (ESRC) Research Grant [ES/W006359/1], and the Engineering and Physical Sciences Research Council (EPSRC) Research Grant [EP/W031493/1]. Their financial contributions toward the dissemination of my research outcomes, through journal publications and conference presentations, are gratefully acknowledged.

# Contents

# List of Figures

# List of Tables

# Nomenclature

### Greek Symbols

| | |
|---|---|
| $\alpha_m$ | Small-signal gain factor, which is equal to $g_m^{-1}(R_4/R_3)$ |
| $\alpha$ | Temperature coefficient of a thermistor |
| $\varepsilon$ | Dielectric permittivity |
| $\varepsilon_0$ | Permittivity of free space ($8.854 \times 10^{-12}\,\mathrm{F\,m^{-1}}$) |
| $\varepsilon_r$ | Relative dielectric permittivity |
| $\mu_c$ | Core permeability of transformer |
| $\tau$ | Time constant |

### Other Symbols

| | |
|---|---|
| * | Estimated |
| A | Ampere (SI unit for electric current) |
| $A_c$ | Cross-sectional area of transformer's core (transformer) |
| $A_{ES}$ | Contact area between electrode and skin |
| Ag | Silver |
| AgCl | Silver chloride |

| | |
|---|---|
| $A_p$ | Overlapped area between capacitor plates |
| $\beta$-3 | Adrenergic agonist |
| $C_F$ | Feedback capacitor (boost converter) |
| $C_x$ | Capacitor ($x = 1 \cdots n$) |
| $d_s$ | Separation between capacitor plates |
| F | Farad (SI unit of capacitance) |
| $f_{SW}$ | Switching frequency (boost converter) |
| ft | Foot (imperial unit for length) |
| $g_m$ | Transconductance gain |
| $h_{FE}$ | Forward current transfer ratio (BJT) |
| H | Henry (SI unit of inductance) |
| h | Hour |
| $HV_{CC}$ | High-level supply voltage |
| $HV_{CC,\ ADJ}$ | Adjustable high-level supply voltage |
| Hz | Hertz (SI unit for frequency) |
| $I_{out}$ | Output current |
| $I_{RMS}$ | RMS value of pulsed current |
| $J$ | Current density |
| $K$ | Coupling coefficient (transformer) |
| $K_{ISET}$ | Fast-charging current factor |

| | |
|---|---|
| K | Kelvin (SI temperature unit) |
| $L$ | Inductance |
| $l_F$ | Flux path length in transformer's core (transformer) |
| L | Litre (SI unit of volume) |
| $L_P$, $L_S$ | Primary/Secondary winding inductance (transformer) |
| $L_n$ | Inductor ($x = 1 \cdots n$) |
| $M$ | Mutual inductance (transformer) |
| $M_2$, $M_3$ | Muscarinic acetylcholine receptors |
| m | Meter (SI unit for length) |
| $N$ | Number of turns (transformer) |
| N | Newton (SI unit of force) |
| °C | Degrees Celsius |
| Ω | Ohm (SI unit of electrical resistance) |
| $Q_x$ | Transistor ($x = 1 \cdots n$) |
| $R_F$ | Feedback resistor |
| $r$, $r_s$ | Sensing resistor |
| $R_{T1}$, $R_{T2}$ | Thermistor resistance at temperature $T_1$ and $T_2$ |
| $R_x$ | Resistor ($x = 1 \cdots n$) |
| s | Second (SI unit for time) |
| $S_x$ | Switch ($x = 1 \cdots n$) |

| | |
|---|---|
| $t_{DELAY}$ | Configured delay (boost converter) |
| $T_x$ | Temperature ($x$ = 1 or 2) |
| $V_C$ | Collector voltage (BJT) |
| $V_{CE}$ | Collector-emitter voltage (BJT) |
| $V_E$ | Emitter voltage (BJT) |
| $V_{in}$ | Input voltage (boost converter) |
| $V_{in}$ | Input voltage |
| $V_{out}$ | Output voltage (boost converter) |
| $V_{out}$ | Output voltage |
| $V_{REF}$ | Reference voltage (boost converter) |
| V | Volt (SI unit for electric voltage) |
| $\bar{x}$, $x_i$ | Mean and normalised grayscale values (RMS contrast) |
| $Z_{ab}$, $Z_{bc}$, $Z_{ac}$ | Impedance between points ((a)–(b); (a)–(c); (b)–(c)) |
| $Z_{Cb}$ | Contact impedance at midpoint (b) |
| $Z_{Load}$ | Load impedance |

**Acronyms / Abbreviations**

| | |
|---|---|
| AC | Alternating Current |
| ADC | Analogue-to-Digital Converter |
| Amp. | Amplitude |
| ANOVA | Analysis of Variance |

| | |
|---|---|
| Apvl. | Approval |
| AUA | American Urological Association |
| BAT | Battery |
| B.C. | Boost Converter |
| BJT | Bipolar Junction Transistor |
| BLE | Bluetooth® Low Energy |
| BTM. | Bottom |
| CAP. | Capacitor |
| C | Cycle (hand-washing) |
| CC | Constant Current |
| CcC | Composite-coated Copper |
| CE | Conformité Européene |
| CF | Conductive Fabric |
| Chan. | Channel |
| CHGR | Charger |
| CM | Customised |
| Coef. | Coefficient |
| Conn. | Connector |
| Cont. | Continuous |
| CV | Constant Voltage |

| | |
|---|---|
| DAC | Digital-to-Analogue Converter |
| DC | Direct Current |
| Dim. | Dimension |
| DMA | Direct Memory Access |
| DO | Detrusor Overactivity |
| DW | Deionised Water |
| EEG | Electroencephalography |
| Elctrd. | Electrode |
| Ele. | Electrolytic |
| EMG | Electromyography |
| ETI | Electrode-Tissue Impedance |
| EU | European Union |
| EUS | External Urethral Sphincter |
| FB | Feedback |
| FES | Functional Electrical Stimulation |
| Galv. | Galvanic |
| GE | Gel Electrode |
| GPIO | General-Purpose Input/Output |
| HCS | Howland Current Source |
| HG | Hydro Gel |

| | |
|---|---|
| HOR. | Horizontal |
| HSE | High-Speed External (system clock) |
| IC | Integrated Circuit |
| ICS | International Continence Society |
| IP | Interphase |
| Iso. | Isolation |
| IUS | Internal Urethral Sphincter |
| LDO | Low-Dropout (regulator) |
| LED | Light-Emitting Diode |
| LiPo | Lithium Polymer |
| Li-ion | Lithium-ion |
| LSE | Low-Speed External (system clock) |
| LUTS | Lower Urinary Tract Symptoms |
| Mag. | Magnetic |
| MAN | Management |
| Max. | Maximum |
| MCU | Microcontroller Unit |
| MEP | Motor Evoked Potential |
| MHRA | Medicines and Healthcare products Regulatory Agency |
| MOSFET | Metal-Oxide-Semiconductor Field-Effect Transistor |

| | |
|---|---|
| MR | Moisturiser |
| N/A | Not Applicable |
| NCC | Normalised Cross-Correlation |
| NMES | Neuromuscular Electrical Stimulation |
| NP | Negative Phase |
| NS | Not Specified |
| NTC | Negative Temperature Coefficient |
| NVIC | Nested Vectored Interrupt Controller |
| OAB | Overactive Bladder |
| OA | Operational Amplifier |
| O/W | Oil-in-Water |
| PAG | Periaqueductal Gray |
| PCB | Printed Circuit Board |
| PC. | Piece |
| PLA | Polylactic Acid |
| PMC | Pontine Micturition Centre |
| Pos. | Position |
| PP | Positive Phase |
| PTNS | Percutaneous Tibial Nerve Stimulation |
| PU | Polyurethane |

| | |
|---|---|
| PWR | Power |
| Qt. | Quantity |
| RCC | Reset and Clock Controller |
| REF | Reference (electrode) |
| Reg. | Regulatory |
| Rehab. | Rehabilitation |
| RES. | Resistor |
| RFID | Radio-Frequency Identification |
| RMS | Root-Mean-Square |
| SG | Silicone Graphite |
| SS | Stainless Steel |
| STIM | Stimulation |
| Sync. | Synchronisation |
| SWD | Serial Wire Debug |
| SYS | System |
| tDCS | Transcranial Direct Current Stimulation |
| TENS | Transcutaneous Electrical Nerve Stimulation |
| TE | Textile Electrode |
| TIM | Timer |
| TPU | Thermoplastic Polyurethane |

| | |
|---|---|
| TRSM. | Transformer |
| TTL | Transistor-Transistor Logic |
| TTNS | Transcutaneous Tibial Nerve Stimulation |
| UI | Urinary Incontinence |
| UKCA | UK Conformity Assessed |
| UK | United Kingdom |
| USART | Universal Synchronous/Asynchronous Receiver/Transmitter |
| US | United States |
| VCCS | Voltage-Controlled Current Source |
| VERT. | Vertical |
| WCM | Wilson Current Mirror |
| WOS | Web of Science |
| W/O | Water-in-Oil |

# Chapter 1

# Introduction

## 1.1 Overactive Bladder Syndrome

The normal function of the lower urinary tract depends on simultaneous ability for the bladder to store urine and enable its voiding at a time convenient to the individual [1]. In a typical adult's bladder, the total capacity is approximately 300 to 400 mL [2], [3]. According to epidemiological studies [4], on average a healthy individual urinates approximately eight times per day, with no more than one occurrence happening during the night.

Disruptions in bladder function are characterised by a number of lower urinary tract symptoms (LUTS), which have been categorised by the International Continence Society (ICS) into three subgroups [5]. These include: (1) storage symptoms, such as increased daytime urinary frequency, urgency, nocturia, and, in some cases, urge urinary incontinence (UI) [6]; (2) voiding symptoms, including slow or intermittent stream, hesitancy, straining, and terminal dribbling [7]; and (3) post-micturition such as incomplete emptying and post-void dribbling [8]. Of these, storage symptoms, including overactive bladder (OAB) syndrome (often accompanied by UI), are recognised as the most prevalent. As a result, they are widely reported to have a significant impact on patients' health-related quality of life.

OAB syndrome is defined by the ICS as "*urinary urgency, usually accompanied by frequency and nocturia, with or without urgency UI, in the absence of urinary tract infection or other obvious pathology*" [9]. It is a highly prevalent condition that affects millions of people worldwide [10]. In 2005, a large-scale epidemiological investigation (the EPIC study) conducted across five countries—Canada, Germany, Italy, Sweden, and the United Kingdom (UK)—reported a prevalence of OAB symptoms in 10.8% of men and 12.8% of women [11]. Notably, women were more likely than men to report urinary frequency exceeding eight times per day [11]. More recently, a UK-based study (FUTURE) reported that 12–14% of women were affected by OAB [12]. These findings are consistent with a range of other epidemiological studies conducted in the United States (US), which also support a substantial OAB prevalence [13] [14].

However, these estimates likely underestimate the true burden of OAB, as many patients experiencing urinary symptoms may be reluctant to seek medical attention due to social stigma and embarrassment [15]. While recent data of OAB prevalence on male populations are limited, existing evidence suggests that its prevalence increases with age in both genders [16]. Moreover, no significant difference in prevalence has been observed between urban and rural populations [16]. Although OAB symptoms are generally more frequently reported by women, this pattern tends to reverse with advancing age [13]. Specifically, in individuals over 60 years, urinary symptoms are more frequently observed in men, likely due to age-related prostate conditions and bladder outlet obstruction, both of which are prevalent in older male population [13].

The trend is further illustrated in Fig. 1.1, which presents the prevalence rate of OAB syndrome across different age groups in Finland. The figure reinforces findings from the literature by highlighting the increase in OAB prevalence with age, underscoring the growing demands for effective treatment options, particularly among older people [17]. Although some of the epidemiological data may be dated, studies conducted across diverse countries and regions consistently demonstrate an increasing prevalence of OAB with age [11], [14]. This persistent trend underscores the need for continued clinical and public health attention.

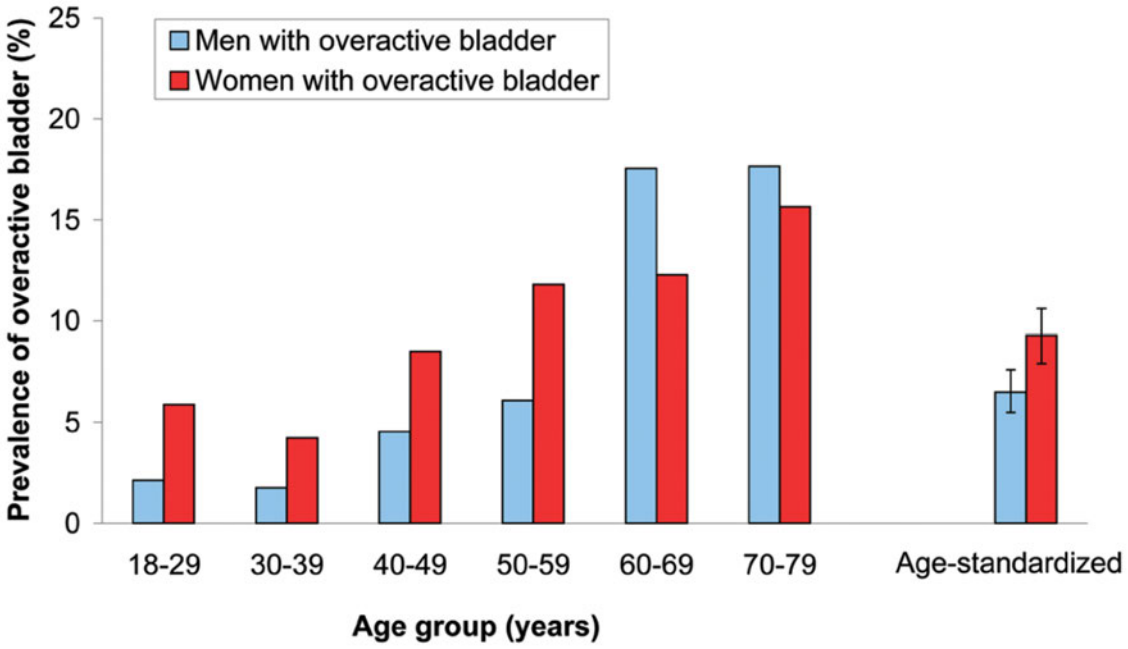


Fig. 1.1. Prevalence of OAB syndrome in both genders across different age groups in Finland [17].

## 1.2 Treatments

Given its high prevalence and the significant impact on patients' quality of life, OAB syndrome represents a substantial clinical and public health concern. As the condition can affect individuals across age groups and is associated with both physical and psychological burden, effective management remains a key therapeutic priority. A range of treatment strategies has been introduced through guidelines over time, including conservative stepwise approach from behavioural to neuromodulatory therapies and latest shared-decision approach. The following sections outline the progression of these treatment modalities, highlighting both established and emerging therapeutic strategies for OAB management.

### 1.2.1 Conventional Stepwise Strategy

#### First-line Treatment

Behavioural therapies, such as bladder training and pelvic floor muscle exercises are recommended as first-line interventions for OAB and have demonstrated effectiveness in symptom reduction; however, they are often limited by patience adherence [18]. Furthermore, current clinical evidence supporting these therapies is of low to moderate quality with inconsistencies in protocols and limited long-term outcomes [19]. As such, behavioural interventions alone may be insufficient for patients with chronic, treatment-resistant OAB, and are typically complemented by pharmacological or other modalities to achieve an optimal control of urinary symptoms [20].

#### Second-line Treatment

The second-line OAB treatments include prescription of muscarinic antagonists (e.g., Oxybutynin, Tolterodine) and $\beta$-3 adrenergic agonists (e.g., Mirabegron, Vibegron) medication [20]. If urinary symptoms persist, dose adjustments may be considered [21]. These two drug classes target different neurotransmitter receptors associated with bladder function and therefore offer distinct therapeutic benefits and limitations. Muscarinic receptor antagonists were designed to block $M_2$ and $M_3$ muscarinic receptors on the detrusor[1] muscle, thereby inhibiting acetylcholine-induced muscle contractions that occur during bladder filling [22]. This suppression of detrusor reduces urinary urgency and frequency [23], [24]. However, as muscarinic receptors are found throughout the human body, blocking them may cause unintended side effects, such as dry mouth, constipation, blurred vision, and an increased risk of complications in older patients [24]. These side effects often limit the long-term use of muscarinic medication, with many patients discontinuing pharmacological therapy due to their tolerability concerns.

[1] Refers to a specialised smooth muscle that forms the bladder wall.

Table 1.1. Physiological characteristics of medications commonly used in the OAB management.

| **Features** | **Muscarinic Antagonists** | **$\beta$-3 Adrenergic Agonists** |
|---|---|---|
| *Nervous system pathway* | Parasympathetic | Sympathetic |
| *Action on bladder* | Inhibit contraction (via $M_3$ block) | Promote relaxation (via $\beta$-3 activation) |
| *Have cognitive side effects?* | Yes | No |
| *Common side effects* | Confusion (Cognitive); Dry mouth; Constipation | Mild hypertension (Rare); Changed heart rhythms (Rare) |
| *Suitability for older patients* | Limited usage (due to side effects) | Better tolerated; Safer profile |

The development of $\beta$-3 adrenergic agonists represents an alternative pharmacological option for OAB management with an improved side-effect profile compared to muscarinic antagonists [25]. These agents act on $\beta$-3 adrenergic receptors in the bladder detrusor muscle to promote bladder muscle relaxation during the filling phase, increasing bladder capacity and reducing urinary urgency [26]. Due to their low risk of cognitive (e.g., confusion) and anticholinergic effects, this type of medicine is well-suited for elderly patients or those with pre-existing conditions. However, caution is still advised, as some patients may experience common side effects such as mild hypertension, nasopharyngitis, and headaches [27]. Therefore, healthcare professionals should prescribe and monitor these adrenergic medications carefully, especially for OAB patients with uncontrolled hypertension [28].

Key difference between muscarinic antagonists and and $\beta$-3 adrenergic agonists is presented in Table 1.1. More detailed insights into the receptor-mediated regulation of bladder function, especially through muscarinic and adrenergic mechanisms, are available in the literature [29]. In essence, the physiological advantage of $\beta$-3 agonists in older users comes from their selective action on bladder muscle without interfering with neurotransmitters involved in cognition, making them a comparably sustainable long-term option for older patients with OAB.

Table 1.2. Conventional stepwise approach for OAB management.

| Line of Treatment | Intervention |
|---|---|
| First-line (Conservative) | *Lifestyle & behavioural:*<br>– Bladder training (minimum 6 weeks);<br>– Fluid/caffeine restriction;<br>– Pelvic floor muscle training ($\geq$ 3 months);<br>– Weight loss (if body mass index $>$ 25). |
| Second-line (Pharmacological) | *Medications:*<br>– Muscarinic antagonists: Oxybutynin; Tolterodine; Darifenacin; Trospium.<br>– $\beta$-3 adrenergic agonists: Mirabegron. |
| Third-line (Advanced Non-surgical) | *Invasive/non-invasive therapies:*<br>– Botulinum toxin A injections;<br>– Neuromodulation (via different peripheral nerves). |

### Third-line Treatment

Due to the inadequate evidence of effectiveness for first-line treatments, and the presence of side effects and patient complications (particularly older people) associated with pharmacological approaches, clinical advancements have explored the third-line approach, including intra-detrusor Botulinum toxin A (i.e., onabotulinumtoxinA) injection and neuromodulation techniques [21]. While effective, Botulinum toxin A injections require regular clinic visits approximately every six months due to their time-constraint therapeutic effects, which increases treatment burden and may lead to patient non-compliance [30]. Fortunately, neuromodulation has emerged as a promising alternative therapy for the management of OAB symptoms. The entire stepwise OAB treatment procedure is summarised in Table 1.2.

Historically, neuromodulation for OAB began with sacral nerve stimulation, a procedure that involves surgically implanting electrodes near the sacral nerves, which are connected to a subcutaneous pulse generator, providing continuous urinary symptoms relief [31]. Although sacral nerve stimulation has demonstrated sustained clinical efficacy, its surgical invasiveness, potential complications such as lead migration, and requirement for device maintenance or replacement have prompted researchers to explore

Table 1.3. Key nerves involved in bladder control.

| Nerve | Spinal Segment Level | Primary Muscle(s) Innervated | Role in Bladder Function |
|---|---|---|---|
| Sacral Nerve | S2–S4 | Detrusor muscle; Pelvic floor muscles | Controls detrusor contraction and coordinates bladder emptying; Modulates storage/voiding reflexes. |
| Pudendal Nerve | S2–S4 | External urethral sphincter; Perineal muscles | Provides voluntary control over urination by contracting the external sphincter. |
| Tibial Nerve | L4–S3 | Calf/foot muscles | Indirectly modulates bladder reflexes via shared sacral roots; Inhibits the overactivity of detrusor. |

alternative neuromodulation strategies [32]. Subsequently, pudendal nerve stimulation was introduced, targeting nerves closer to pelvic structures. This neuromodulation technique offered lower stimulation thresholds and provided an additional option for patients unresponsive to sacral stimulation; however, its application is technically complex due to the clinical difficulty of accessing the pudendal nerve located deep within the pelvis, often requiring precise needle placement through the ischiorectal fossa [33]. This complexity, coupled with limited long-term clinical data as well as the absence of widespread regulatory approval, may restrict its routine clinical use [33].

To further reduce invasiveness and procedural complexity, percutaneous tibial nerve stimulation (PTNS; a minimally invasive neuromodulation technique) was developed in 1990s [34]. It targets the tibial nerve to modulate central neural circuits involved in lower urinary tract control, offering an effective treatment for OAB. However, PTNS requires the insertion of a needle electrode, which typically necessitates skilled medical professionals and contributes to higher treatment costs [34]. Recent studies have demonstrated that transcutaneous tibial nerve stimulation (TTNS; a non-invasive alternative using surface electrodes) provides comparable effectiveness to PTNS, while offering greater patient comfort and acceptability [35], [36], [37]. To better understand the rationale behind these neuromodulatory strategies, it is important to consider the anatomical origins of the stimulation-targeted nerves, as outlined in Table 1.3.

### 1.2.2 Recent Shared-decision Strategy

The latest guidelines from the American Urological Association (AUA) have revised the traditional stepwise approach (i.e., first-, second-, or third-line therapies) to OAB treatment [38]. In this updated framework, treatment choices are made through shared decision-making, an interactive discussion in which clinicians and patients together weigh benefits, risks, and personal goals before agreeing on the option that best fits the patients' preferences [38]. In practice, this means that when presented with options, many patients may gravitate toward TTNS due to its non-invasive nature, safety, and at-home practicality. Indeed, the recent clinical approval of TTNS devices and recognition of anticholinergic medication risks (e.g. cognitive side effects) have prompted calls to elevate tibial nerve stimulation from a "third-line" to an earlier therapy in OAB care [39].

By enabling therapy in the patient's own home, TTNS would eliminate the logistical and cost burdens of weekly clinic-based PTNS sessions. Urology clinics have begun offering TTNS alongside traditional options, giving OAB patients a choice between office-based PTNS and take-home TTNS devices as part of the treatment plan [40]. Early real-world audits also confirm that TTNS is an effective alternative to PTNS, with a considerable proportion of patients reporting symptomatic improvement within weeks of daily use [40]. Expert consensus now characterises TTNS as a "non-invasive, cost-effective, and convenient" therapy for OAB management, making it as a patient-preferred solution in the setting of shared decision-making [41], [42]. This recent patient-centric strategy has therefore accelerated the adoption of TTNS, as individuals increasingly prefer this safe, home-administered modality that delivers effective OAB relief without compromising their quality of life.

## 1.3 Basic Physiology of Urinary Bladder

The underlying cause of OAB remains incompletely understood, and no therapeutic approach has yet proved definitively curative [43], [44]. Detrusor overactivity (DO) nevertheless accounts for most cases, being demonstrated in more than 60% of patients by cystometry[2] [45]. During cystometric filling, simultaneous measurement of intravesical and abdominal pressures enables quantitative assessment of bladder sensation, volume capacity, and compliance, and it also exposes involuntary detrusor muscle contractions that characterise DO [46]. This abnormal activation of the detrusor, whose contraction is physiologically confined to the voiding phase, interrupts normal storage and produces the urgency and frequency typical of OAB [47]. Since muscle contractions are initiated by the nervous system, gaining insight into basic physiology of urinary bladder may help in identifying the optimal neuromodulatory treatments.

### 1.3.1 Neural Innervation

The bladder receives dual autonomic[3] innervation (i.e., parasympathetic[4] and sympathetic[5]) and somatic[6] innervation, as illustrated in Fig. 1.2. The parasympathetic nerves originate from spinal segments S2–S4 (pelvic nerves). Their afferent[7] fibres convey sensory information about bladder stretch and pain, and

[2]It is part of urodynamic testing and is used to measure the bladder pressure during a controlled filling of saline into the bladder via a catheter.

[3]Refers to one subdivision of peripheral nervous system (i.e., all nervous system excluding brain and spinal cord). This type of nerve regulates involuntary physiologic processes, such as heart rate, blood pressure, respiration, etc. It contains three anatomically distinct divisions: sympathetic, parasympathetic, and enteric.

[4]Refers to the part of the nervous system responsible for regulating the body's unconscious (e.g., "rest-and-digest" or "feed-and-breed") activities that occur when the body is at rest, especially after eating, including sexual arousal, salivation, lacrimation (tears), urination, digestion, and defecation.

[5]Refers to the part of the nervous system responsible for "fight-or-flight" responses, such as increased heart rate, blood pressure, breathing rate and pupil size.

[6]Refers to the other subdivision of peripheral nervous system. This type of nerve allows you to move and control muscles, and it also feeds information from four of senses (e.g., smell, sound, taste and touch) into the brain

[7]Afferent neurons carry information from sensory receptors of the skin and other organs to the central nervous system (i.e., brain and spinal cord)

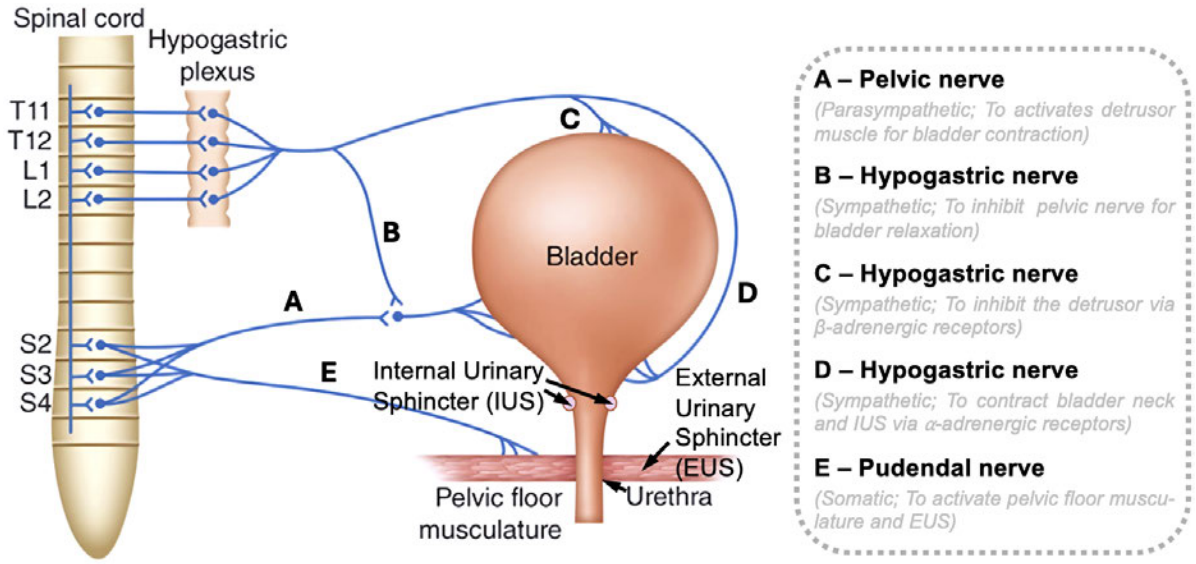


Fig. 1.2. Neural innervation of urinary bladder.

their efferent[8] fibres stimulate the contraction of the bladder's detrusor muscle and relaxation of the internal urethral sphincter[9] (IUS), thereby facilitating urination.

The sympathetic nerves originate from spinal segments T11–L2 (hypogastric nerves). They convey sensory information about bladder fullness through afferent fibres. Efferently, these nerves induce relaxation of the detrusor and contraction of the IUS, contributing to the bladder's storage function by preventing leakage and allowing bladder filling.

The somatic innervation delivered via the pudendal nerve (originating from spinal segments S2–S4), is responsible for voluntary control of the external urethral sphincter (EUS). Somatic afferents detect stretch and tension in this sphincter, while somatic efferents enable voluntary sphincter contraction to control the timing of voiding.

[8]Efferent neurons carry motor information away from the central nervous system to the muscles and glands of the body.

[9]Refers to a ring-shaped muscle that relaxes or tightens to open or close a passage or opening in the body.

### 1.3.2 Neural Control of Micturition

The process of micturition (or urination) involves a coordinated sequence of autonomic and somatic neural activities that govern both the storage and voiding phases. In Stage 1 (Bladder fills; Fig. 1.3), urine from the kidneys enters the bladder, causing gradual distension of the bladder wall. This triggers a "Storage Reflex", whereby sympathetic fibres from the thoracolumbar segment (i.e, T11–L2) of spinal cord, transmitted via the hypogastric nerve, activate $\beta$-adrenergic receptors in the detrusor muscle to promote relaxation. Concurrently, $\alpha$-adrenergic receptors at the IUS are stimulated to maintain closure. The pudendal nerve (originating from sacral segments; S2–S4) maintains tonic contraction of the EUS, allowing for voluntary continence through somatic motor control [48], [49].

As the bladder continues to fill, Stage 2 (First sensation to void; Fig. 1.3) occurs when stretch receptors in the bladder wall transmit afferent signals via pelvic nerves to the spinal cord and brainstem [49]. These signals ascend to the periaqueductal gray (PAG) and pontine storage centre (PMC), leading to activation of the "Guarding Reflex". This reflex enhances contraction of the EUS and pelvic floor muscles, preserving continence despite rising bladder pressure [48], [50]. Although the bladder is partially full at this point, the individual becomes consciously aware of the filling but can voluntarily suppress voiding.

Progressing to Stage 3 (Normal desire to void; Fig. 1.3), bladder volume reaches a threshold where afferent input intensifies and is processed by higher brain centres including the prefrontal cortex and PMC [52]. Although the desire to void is perceived, micturition is voluntarily delayed by sustained pudendal nerve activity, maintaining the contraction of EUS [52]. This decision-making phase allows the postponement of urination.

Finally, in Stage 4 (Micturition; Fig. 1.3), voluntary relaxation of the pelvic floor musculature initiates the "Voiding Reflex". The PMC sends descending excitatory signals to parasympathetic neurons in the sacral spinal cord, activating pelvic nerves that release acetylcholine onto $M_3$ muscarinic receptors of the detrusor, resulting in muscle contraction. Simultaneously, sympathetic outflow via the hypogastric nerve is inhibited, leading to the IUS relaxation. The pudendal nerve is also suppressed, allowing the EUS to relax. These coordinated events result in bladder emptying through the urethra [53].

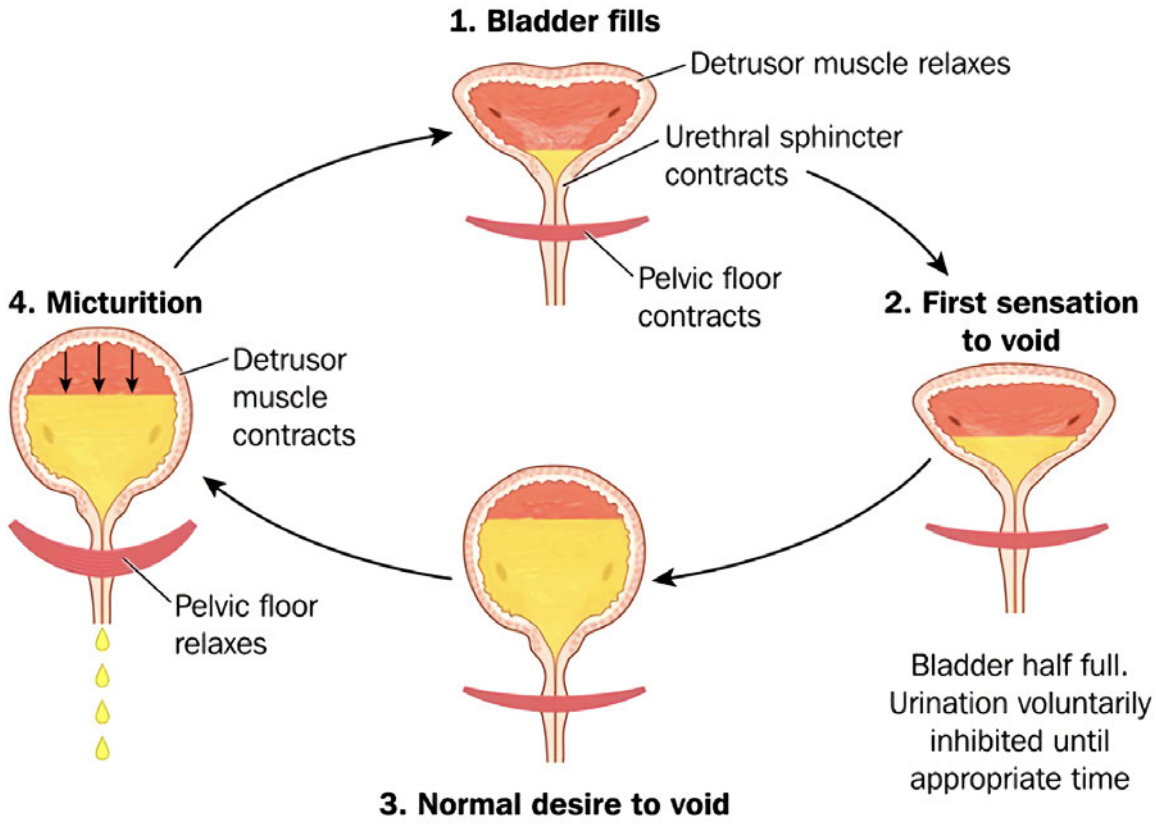


Fig. 1.3. A full bladder storage and voiding cycle [51].

### 1.3.3 Summary

Bladder regulation relies on the dynamic coordination between involuntary and voluntary neural pathways to ensure appropriate timing of urine storage and release. Signals from the lower urinary tract are integrated within spinal and brain centres, allowing the urinary system to adapt based on sensory input and conscious decisions. This integration enables the body to postpone or initiate urination according to internal bladder pressure and external circumstances. The overall mechanism of bladder control is summarised in Fig. 1.4 for a better illustration.

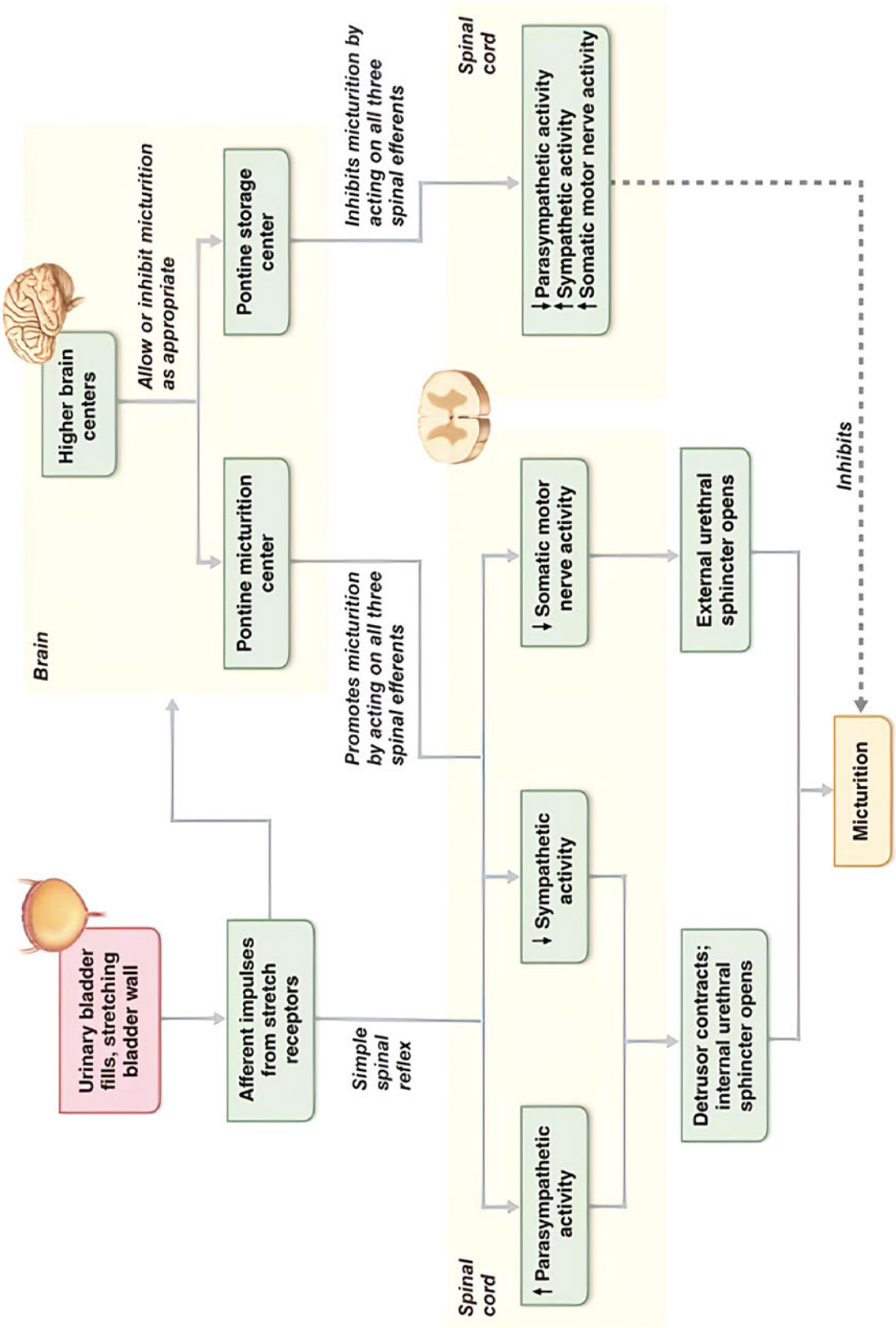


Fig. 1.4. Illustration of bladder control mechanism.

## 1.4 Tibial Neuromodulation Mechanism for Bladder Activity

### 1.4.1 Afferent Pathways and Spinal Reflex Modulation

The tibial nerve arises from the L4 to S3 spinal nerve roots, with partial overlap of the sacral segments (S2–S4), which also contribute to the pelvic and pudendal nerves responsible for innervating the detrusor and sphincters [54]. This shared spinal circuitry provides an anatomic basis for tibial neuromodulatory effects on bladder reflexes. Electrical stimulation of peripheral nerves in the sacral network (e.g., the pelvic nerve, pudendal nerve, or even distal branches like the tibial nerve) can reflexively inhibit the spinal micturition centre and bladder activity [55].

Unlike pharmacological agents that act directly on the detrusor, tibial nerve stimulation primarily influences afferent signalling pathways [55]. It is thought to prevent abnormal sensory inputs from the bladder to the sacral spinal cord, thereby avoiding activation of the voiding reflex. This neuromodulatory effect occurs through the activation of sensory fibres, which influence reflex pathways in the spinal cord and brain, without directly stimulating bladder motor fibres [55]. As a result, tibial neuromodulation increases bladder capacity and reduces the involuntary contraction of detrusor, as observed in many clinical studies [41], [42], [56], [57].

### 1.4.2 Supraspinal Effects and Hypothesised Pathways

Although the precise mechanisms of tibial neuromodulation are still being investigated, emerging evidence suggests involvement of ascending neural pathways that engage central inhibitory circuits [58]. Afferent signals from the tibial nerve travel to the sacral spinal cord and can ascend to brainstem centres via the sciatic nerve root pathways [59]. Some hypotheses suggest that tibial nerve stimulation modulates the activity of the pontine storage center and the PMC, resetting their rhythmic output to the bladder [60].

In essence, the tibial afferent input may enhance the regulatory control exerted by the pons and cortex over bladder function, thereby restoring a more normal balance between facilitation and inhibition of voiding reflexes [48]. In line with this hypothesis, a previous study demonstrated that tibial nerve stimulation extends the inter-void interval in animal models by modulating the bladder afferent feedback

pathway [61]. Tibial neuromodulation is proposed to recruit somatic afferents converging at the sacral spinal cord, thereby activating inhibitory interneurons and supraspinal centres to suppress the DO [62].

### 1.4.3 Summary

In summary, although tibial neuromodulation is not directly associated with bladder motor fibres, it engages the sacral neural circuitry to modulate the micturition reflex arc at both spinal and supraspinal levels. This modulation has been shown to reduce urinary urgency and frequency in patients, despite ongoing investigations into the specific neural mechanisms involved. However, this thesis does not provide an in-depth introduction of urinary system neurophysiology. Rather, it focuses on the development of an advanced device for TTNS with primary emphasis on technical enhancements.

## 1.5 Research Aim and Objectives

Transcutaneous electrical nerve stimulation (TENS) devices have been widely used for decades, particularly in the management of chronic and acute pain. These systems deliver electrical pulses through the skin to stimulate peripheral nerves, modulating pain perception. Due to their non-invasive nature and neuromodulatory capability, these TENS devices have been adapted for a range of clinical applications beyond analgesia, including neuromodulation for OAB and urinary incontinence via TTNS.

Currently, several TENS devices, such as the NeuroTrac® Continence (Verity Medical, Ireland) [63], TPN 200 Premier Plus (Performance Health, UK) [64], and geko™ T-1 (Firstkind, UK) [65], have been utilised in clinical settings for the management of OAB via TTNS. However, these devices often pose challenges for older and frail patients when used independently in home settings. Key issues include the precise placement of surface electrodes and the configuration of stimulation parameters, which could be difficult for this demographic to use devices effectively Furthermore, most conventional TENS devices for TTNS rely on adhesive gel electrodes (GEs), which may cause skin irritation or allergic reactions with long-term or repeated use [66], [67]. Additionally, the removal of these GEs also presents a concern, as it could potentially damage the fragile skin of older users [68], [69].

To address these, recent advancements in TENS technology for OAB management have focused on the development of miniaturised wearable solutions incorporating alternative electrode designs. Examples include the TENSI+ (Stimuli Technology, France) [70], Zida® Control Sock (Zida, Israel) [71], and more recent Vivally® (Avation Medical, US) [72]. These devices aim to improve user comfort and ease of operation. A detailed review of the technical specifications and differences among these devices is provided in Chapter 2.

However, challenges remain, such as ensuring accurate electrode positioning and enhancing overall usability. To address remaining issues, the development of a smart, compact, and wearable TENS device is demanded. This device is intended to address the technical shortcomings of existing solutions, thereby facilitating home-based OAB management. The proposed device (Chapter 4) would be particularly beneficial for older patients, offering a more user-friendly approach to treat their urinary symptoms.

## 1.6 Contributions to Knowledge

The thesis makes several contributions to the field of electrical stimulation devices, with a particular focus on TENS devices for OAB management via TTNS. The contributions are outlined as follows:

1. **Comprehensive Review of Wearable and Non-invasive Electrical Stimulators:** A literature review of existing wearable electrical stimulators was conducted, with an in-depth analysis of technical parameters and drive circuit topologies. This comprehensive review provides insights into the design requirements for developing a safe, smart, and wearable electrical stimulator intended for home-based OAB management.

2. **Feasibility of Conductive Textile Electrodes in TENS Applications:** A feasibility study was undertaken to evaluate the use of conductive (TEs) as an alternative to conventional GEs in TTNS. The study demonstrated that TEs exhibit comparable efficacy to GEs, validating their potential for integration into wearable TENS devices. This finding has led to further exploration of a TEs-integrated wearable system compatible with the proposed TENS device. This work has been presented at the *21st IEEE Interregional NEWCAS Conference* [73].

3. **Design of a Smart, Wearable TENS Device for Home-based Overactive Bladder Management:** A smart, compact wearable TENS device (named TENS*mini*) was developed for home-based OAB management. Integrated with a washable sock containing conductive TEs, the device could offer an unobtrusive solution for administering TTNS. Its wireless connectivity with mobile devices enables users to easily customise stimulation parameters, thus facilitating tailored treatment protocols. This development offers a potential approach to personalised, home-based neuromodulation therapy for OAB management. The hardware design details and selected validation experiments have been published in the *Proceedings of the 22nd IEEE Mediterranean Electrotechnical Conference* [74] and the *IEEE Transactions on Biomedical Circuits and Systems* [75].

4. **Pilot Studies on Short-term Physiological Efficacy using the Proposed Wearable Device:** Two pilot studies were conducted under ethically approved protocols (with a total of 57 healthy human participants recruited) to assess the short-term feasibility of the TENS*mini*. Both studies confirmed the device's capability to effectively recruit the tibial nerve and elicit physiological responses associated with bladder function. These findings offer valuable preliminary insights for future clinical research aimed at validating the device's therapeutic effectiveness for patients with lower urinary tract conditions including OAB, UI, and urinary retention. The first study has been disseminated via the *IEEE Transactions on Biomedical Circuits and Systems* [75], while the second one has been published on the *IEEE Transactions on Neural Systems and Rehabilitation Engineering* [76].

The findings of the thesis have been disseminated through multiple peer-reviewed conference and journal publications. Collaborative research efforts have resulted in additional publications that partially support findings of the thesis. A list of publications resulting from the entire research programme is provided below, summarising the research outcomes and their dissemination.

## 1.7 List of Publications

### Lead-author Publications

[1] **W. Ju**, A.M.-Trevillion, D.A.V.-Benavides, S.D. Shenkin, S. Mitra, K. Nazarpour, "Benchmarking TENS*mini* for neuromodulation via tibial nerve stimulation," *IEEE Trans. Neural Syst. Rehabil. Eng.*, vol. 33, pp. 2135–2141, Jun. 2025. DOI: 10.1109/TNSRE.2025.3575009.

[2] **W. Ju**, A.M.-Trevillion, D.A.V.-Benavides, S.R. Khan, S.D. Shenkin, K. Nazarpour, S. Mitra, "Smart wearable TENS device for home-based overactive bladder management," *IEEE Trans. Biomed. Circuits Syst.*, pp. 1–12, Jan. 2025. DOI: 10.1109/TBCAS.2025.3527343. (Accepted)

[3] **W. Ju**, D.A.V.-Benavides, A.M.-Trevillion, S.D. Shenkin, K. Nazarpour, S. Mitra, "TENS*mini*: a smart wearable device for home-based management of overactive bladder syndrome," in *21st European Geriatric Medicine Society Congress*, Reykjavik, Iceland, Sep. 2025. (Accepted)

[4] **W. Ju**, S.R. Khan, K. Nazarpour, S. Mitra, "TENS*mini*: a wearable electrical nerve stimulator for urinary incontinence management," in *22nd IEEE MELECON*, Porto, Portugal, Jun. 2024, pp. 1111–1115. DOI: 10.1109/MELECON56669.2024.10608726.

[5] **W. Ju**, A. M.-Trevillion, S.R. Khan, K. Nazarpour, S. Mitra, "A feasibility study on textile electrodes for transcutaneous electrical nerve stimulation," in *21st IEEE Interregional NEWCAS Conf.*, Edinburgh, UK, Jun. 2023, pp. 1–5. DOI: 10.1109/NEWCAS57931.2023.10198106.

### Other-author Publications

[6] D.A.V.-Benavides, W. Ju, C. Gonzalez, P. Aitken, A.K.A.N.S. Amma, S. Mitra, S.D. Shenkin, "The importance of electrical parameters on transcutaneous tibial nerve stimulation (TTNS) for overactive bladder syndrome: a systematic review and meta-analysis," *Age Ageing*, May 2025. (Accepted)

[7] D.A.V.-Benavides, **W. Ju**, S.D. Shenkin, S. Mitra, "The effect of electrical parameters on transcutaneous tibial nerve stimulation for overactive bladder syndrome: a systematic review and

meta-analysis," in *21st European Geriatric Medicine Society Congress*, Reykjavik, Iceland, Sep. 2025. (Accepted)

[8] A.M.-Trevillion, M. Jabbari, **W. Ju**, E. Lister, A. Erfanian, S. Mitra, K. Nazarpour, "The frequency-dependent effects of tibial nerve stimulation on bladder function," in *28th Annual Conf. of the IFESS*, Chicago, US, May 2025. (Accepted)

[9] A.M.-Trevillion, M. Jabbari, **W. Ju**, E. Lister, A. Erfanian, S. Mitra, K. Nazarpour, "Low-frequency tibial neuromodulation increases voiding activity—a human pilot study and computational model," *eLife*, Jun. 2025. DOI: 10.7554/eLife.106174.1. (Accepted)

[10] S.R. Khan, X. Wang; T. Jiang, **W. Ju**, N. Radacsi, M. A. Kadir, K. S.-e. Rabbani, S. Cunningham, S. Mitra, "Multi-modal portable respiratory rate monitoring device for childhood pneumonia detection," *Micromachines*, vol. 14, no. 70, 2023, Art. no. 708. DOI: 10.3390/mi14040708.

## 1.8 Structure of Thesis

Chapter 1 introduces the worldwide prevalence and chronic nature of OAB syndrome and emphasises the need for effective therapeutic approaches that ensure high patient adherence and satisfaction. In this chapter, some research gaps are identified, particularly the technical limitations of existing wearable TENS devices, and the main contributions of the work are outlined.

Chapter 2 provides a comprehensive review of wearable electrical stimulators and their applications across various medical domains, including pain relief, rehabilitation of motor dysfunction, and management of lower urinary tract disorders including OAB and UI. This review investigates the technical parameters and drive circuit topologies used in stimulators as documented in both the academic and commercial databases. In doing so, it establishes the foundational knowledge required for the design and development of a novel wearable stimulator specifically tailored for OAB management.

Chapter 3 presents a feasibility study that investigates the potential of TEs as a replacement for conventional GEs for OAB management via TTNS. The findings from this study demonstrate the viability of TEs, supporting their integration into wearable garments, such as socks, and informing the subsequent electronic design process.

Chapter 4 details the design, development, and implementation of a smart, wearable TENS device (i.e., TENS*mini*). This chapter covers the integration of conductive textiles into wearable forms (e.g., socks) and provides a clear explanation of the circuit design. It also discusses safety considerations and hardware miniaturisation, as well as the device's potential for home-based application.

Chapter 5 builds on the established design framework (Chapter 4) by presenting and discussing the simulation and measurement results of multiple experiments. These results validate the wearable TEs' usability and washability as well as the TENS*mini*'s safety and functionality.

Chapter 6 describes two human pilot studies conducted with a total of 57 healthy participants. These studies evaluate the short-term efficacy of the wearable TENS*mini* device by assessing basic physiological responses, including evoked electromyography, and demonstrating the inhibitory effects on bladder storage activity via TTNS. The results offer preliminary support for the TENS*mini*'s potential in managing OAB, indicating that further clinical studies are necessary.

Chapter 7 concludes the thesis by summarising the key findings and discussing their implications. It also outlines potential directions for future research, including qualitative usability studies, long-term clinical trials, and further technical optimisations to enhance the device's performance and applicability.

# Chapter 2

# Literature Review

Neuromodulation can be implemented via the targeted delivery of pharmacological agents or through electrical stimulation of the neuromuscular system. This approach is used to manage various neurological disorders and conditions by altering neural pathways to improve physiological functions. Electrical stimulation is primarily employed for pain relief. The modern application of electrical stimulation for analgesia is based on the Gate Control Theory of Pain introduced by Melzack and Wall in 1965 [77]. In 1967, Shealy implemented electrical stimulation of the dorsal columns using invasive electrodes, leading to the development of the first implantable spinal cord stimulator by Medtronic PLC in 1968 [78].

Subsequent studies have indicated that stimulation of peripheral afferents [79], [80], [81], [82], [83], [84], [85], dorsal columns [78], [86], and descending pain inhibitory pathways [87], [88] can reduce pain. Electrical stimulation has also been applied to address urinary symptoms such as overactive bladder (OAB) and urinary incontinence (UI). Early work by Brindley in the 1970s [89] and later studies, including a pilot study by Tanagho and Schmidt in the 1980s [90] and the development of Percutaneous Tibial Nerve Stimulation (PTNS) by Stoller in the late 1990s [91], demonstrated the potential of this technique to improve bladder control.

Historically, invasive methods such as benchtop stimulators with needle electrodes or implanted devices with integrated electrodes, have also been employed by Moe and Post to rehabilitate motion disorders in patients with neurological impairments [92]. Advances in electronics and electrode technology have

refined these neuromodulation practices. Currently, established invasive strategies are increasingly complemented by non-invasive techniques. Modern non-invasive methods use surface electrodes in conjunction with wearable electrical stimulators. These devices are generally classified into two categories: transcutaneous electrical nerve stimulation (TENS) and neuromuscular or functional electrical stimulation (NMES/FES).

In subsequent sections, the state-of-the-art developments in non-invasive wearable electrical stimulation devices is introduced. A systematic search methodology was co-designed by Aidan McConnell-Trevillion (AMT) and myself (WJ) to conduct a comprehensive review of existing qualified devices developed over the past decade. The review process involved querying multiple academic databases and relevant resources using keywords and inclusion criteria to ensure the identification of literature, thereby providing an up-to-date assessment of the current technological landscape in wearable neuromodulation systems.

## 2.1 Search Methodology

### 2.1.1 Overview

A systematic, three-pronged search strategy (Table 2.1) was employed to comprehensively cover the range of applications for electrical stimulation. Two reviewers (i.e., AMT and WJ) independently conducted searches in three academic databases, including MEDLINE, Web of Science (WOS), and IEEE Xplore, and exported full-text publications spanning the past ten years up to 18 July 2023.

### 2.1.2 Selection Criteria for Academic Databases

All resources retrieved from the three databases were imported into Covidence software (Veritas Health Innovation, Australia). Data extraction was performed using the following exclusion criteria:

- Non-English publications;

Table 2.1. The search strategy used for three academic databases.

| Databases | Search Factors | Search terms |
|---|---|---|
| MEDLINE & WOS (via Ovid®) | Intervention | "Functional Electric* Stimulation" OR "FES" OR "Neuromuscular Electric* Stimulation" OR "NMES" OR "Transcutaneous Electric* Nerve Stimulation" OR "Transcutaneous Electric* Stimulation" OR "Transcutaneous Nerve Stimulation" OR "Transcutaneous Neuromodulation Therapy" OR "TENS" |
| | Condition | "Lower Urinary Tract Dysfunction" OR "Urinary Tract Dysfunction" OR "LUTD" OR "Lower Urinary Tract Symptoms" OR "LUTS" OR "Analgesia" OR "Analgesic Effects" OR "Pain Relief" OR "Pain Reduction" OR "Pain Management" OR "Akinesia" OR "Dyskinesia" OR "Gait Dysfunction" OR "Movement Disorder" OR "Motor Disorder" OR "Motor Impairment" OR "Motor Dysfunction" |
| | Protocol | "Circuit*" OR "System*" OR "Design*" OR "Application*" NOT "Implant*" |
| IEEE Xplore | Document Title | "Functional Electric* Stimulation" OR "FES" OR "Neuromuscular Electric* Stimulation" OR "NMES" OR "Transcutaneous Electric* Nerve Stimulation" OR "TENS" |
| | Full Text & Metadata | "Circuit*" OR "System*" OR "Design*" OR "Application*" NOT "Implant*" |
| | Applied Filters | "Conference" OR "Journal" |

- Insufficient disclosure of the circuit schematic or block diagram pertaining to the complete or partial invention, or absence of information regarding the model/make of any commercially available device;
- Use of invasive probes or electrodes;
- Non-wearable devices;
- Devices that are not battery-powered.

The extracted data were subsequently cross-checked, and any disagreement between reviewers (i.e., AMT and WJ) were resolved by consensus.

### 2.1.3 Identification of Studies from Other Sources

#### Amazon Database Search

An initial exploratory search on Amazon UK was conducted to identify key product categories for non-invasive electrical stimulators. This search was led by AMT, with three categories were identified: (1) muscle and nerve stimulators, (2) pelvic floor toners, and (3) fitness electric stimulators. A web-scraping programme extracted key information, including product name, price, average review score, listing date, number of reviews, and instruction manuals, for the top 50 devices in each category. For devices with unavailable or non-English instruction manuals, the device reference number was used to locate the documentation from alternative sources. Duplicate listings by the same company were consolidated by retaining only the best-selling device in each set.

#### Other Searches

To comprehensively cover the range of commercially available devices, additional searches were performed using both Google Images and the United States (US) Food and Drug Administration (FDA) 510(k) database. Search keywords such as “Functional Electrical Stimulation”, “Transcutaneous Electrical Nerve Stimulation” and “Neuromuscular Electrical Stimulation” along with their abbreviations

and other identifiers (e.g., company name and registered trademark) were employed. The visual search using Google Images allowed for rapid cross-referencing with data previously extracted from academic research databases to facilitate duplicate removal and screening.

### 2.1.4 Exclusion Criteria

After initial screening, devices identified in the literature were excluded if they met any of the following criteria:

- Insufficient or lack of technical information;
- Bulky or heavy construction;
- Limited wearability (defined as devices attached via belt clip or lanyard rather than fully worn) or an invasive nature;
- Unsuitability or low quality of resources;
- Overly similar research or commercial design;
- Primarily focused on application-specific integrated circuit (ASIC) design rather than system or device design.

### 2.1.5 Search Outcome

Database searches yielded 1445 relevant results (1237 from three academic research databases and 208 from other sources). After removing 67 duplicates, 1377 unique records remained. Full texts were retrieved for 336 publications (139 from academic databases and 197 from other sources). Due to limitations in the disclosure of information by the original publications, two additional minor searches were conducted during eligibility screening, resulting in nine eligible records from manufacturers' official websites. The study selection process is summarised by a flowchart, as shown in Fig. 2.1.

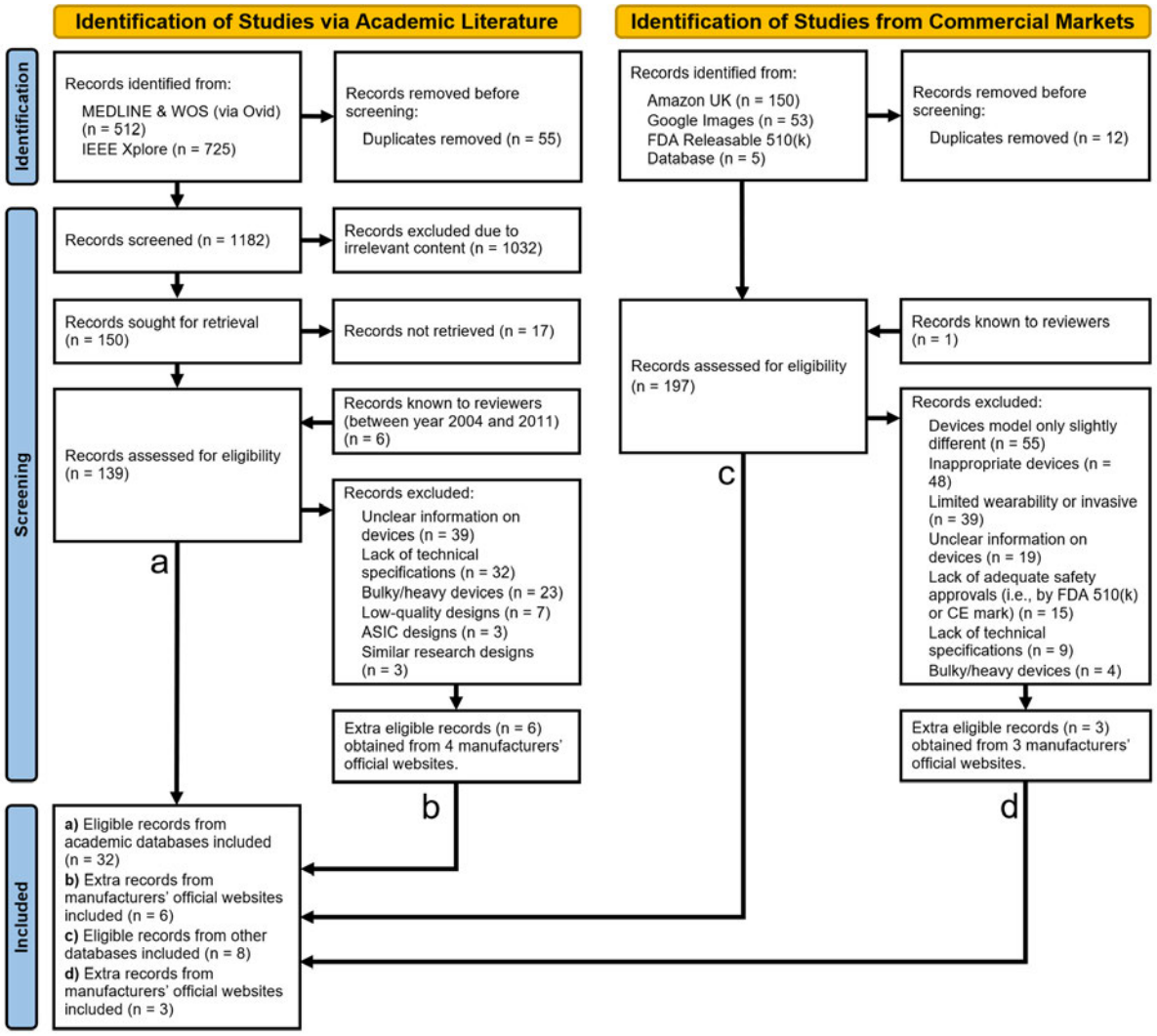


Fig. 2.1. Flowchart for literature collection, screening and inclusion.

## 2.2 Wearable Electrical Stimulators

### 2.2.1 TENS Applications

#### Overview

Although effective in alleviating pain, invasive electrical stimulation techniques are often associated with surgical risks and long-term maintenance challenges. In contrast, TENS offers a non-invasive alternative that delivers low-level electrical currents through surface electrodes applied to the skin. TENS

is widely employed in both clinical and home settings for managing acute and chronic pain conditions by stimulating peripheral nerves to disrupt nociceptive signal transmission and activate endogenous pain inhibitory mechanisms. Additionally, TENS technology has been adapted for transcutaneous tibial nerve stimulation (TTNS), a non-invasive approach for treating urinary symptoms, including OAB and UI.

### Recent Developments

Several wearable TENS devices have been developed to address a broad range of pain relief applications. For instance, the Quell® device [93], developed by NeuroMatrix Inc., is a wearable TENS system designed for temporary pain alleviation associated with sore, aching muscles in the lower extremities due to physical exertion, as well as for managing chronic intractable pain. It employs gel electrodes (GEs) that snap into a wearable leg cuff positioned approximately 1–2 inches below the knee.

Similarly, Chattanooga® Wireless Professional device [94] was specifically engineered for pain management and neuromuscular stimulation in both clinical and home settings. This device is particularly useful for post-surgical and chronic pain management, as well as for muscular re-education. It features wireless stimulation modules that connect to the skin via surface electrodes available in various sizes, allowing for flexible placement over targeted painful areas.

Compact and portable TENS devices, such as Compex Mini [95] and Paingone Easy [96] target pain relief from conditions including muscle strain, chronic pain, and arthritis. Both devices utilise snap-on adhesive GEs that attach to the skin around the pain sites to deliver stimulation impulses. Similarly, the Beurer EM 50 [97] also features GEs and is specifically designed for the relief of menstrual cramps and endometriosis pain by adhering directly to the lower abdomen of female users.

Beyond these general pain management applications, several TENS devices have been developed for the treatment and prevention of migraines—a form of acute pain. Notable examples include the Cefaly® [98], TensCare Mynd [99], and Paingone Qalm [100] devices. While Cefaly® and TensCare Mynd are recommended for patients aged 18 and above, Paingone Qalm is approved for use by children aged eight and above under adult supervision, although its efficacy in individuals under 18 remains unproven. Cefaly® distinguishes itself with advanced technical features such as Bluetooth® control and


Fig. 2.2. The geko™ T-1 device used for OAB treatment [65].

radio-frequency identification (RFID) for electrode detection, whereas Paingone Qalm and TensCare Mynd employ manual controls.

An additional innovative approach is presented by an intelligent analgesic bracelet proposed by Shi *et al.* [101]. This wearable TENS device, based on wrist-ankle acupuncture theory, consists of a flexible 25.5 cm bracelet equipped with two gold metal electrodes spaced 4.2 cm apart. Stimulation parameters can be manually adjusted using knobs on the device body, enabling personalised control of therapeutic settings.

Building on the versatility of TENS technology in alleviating pain, recent developments have extended its application to the treatment of lower urinary tract disorders. Specifically, several wearable TENS devices have been implemented to supply TTNS for managing urinary conditions.

The geko™ T-1 device, introduced by Firstkind Ltd. as a CE-marked TENS system and originally approved for the prevention of deep vein thrombosis, has also been evaluated for its effectiveness in treating OAB symptoms, as shown in Fig. 2.2. Seth and colleagues [65] assessed this self-adhesive, ambulatory device in a cohort of 48 patients with idiopathic and neurogenic OAB. The device delivers a constant current of 27 mA at 1 Hz with an adjustable pulse width ranging from 70 to 560 µs when applied


Fig. 2.3. TENS devices used for urinary symptoms (e.g., OAB and UI) management via TTNS: (a) A butterfly-shaped device [103]; (b) TENSI+ device [70]; (c) Zida® Control Sock [71]; (d) Vivally® system [72].

behind the medial malleolus. The treatment protocol, which involved 30-minute sessions conducted either daily or weekly over a 12-week period, resulted in 53% of participants experiencing moderate to significant improvement in OAB-related symptoms [65]. Recently, the latest geko™ T-3 device [102] has been developed, targeting the enhancement of blood circulation in the deep veins of the lower limbs.

A notable advancement in TENS devices for OAB treatment is a butterfly-shaped system evaluated in a single-centre, self-controlled pilot study [103]. The device (Fig. 2.3(a)) comprises a compact stimulation unit ($58.3 \times 55.6 \times 12.8$ mm$^3$, 70 g) powered by a rechargeable lithium battery. It employs removable conductive silicone electrodes and provides adjustable stimulation parameters, including an intensity of up to 30 mA, a frequency range of 1–200 Hz, and a pulse width range of 100–1000 µs. Control is facilitated via onboard buttons or a smartphone application through Bluetooth®, enabling

precise modulation of stimulation when targeting the tibial nerve [103]. In a four-week study with daily 60-minute sessions (20 Hz, 200 µs, and current intensity adjusted per patient comfort), a 20.5% reduction in daily micturition frequency and a 32.5% improvement in quality of life scores were achieved [103].

Further enhancements in wearable TENS technology for managing lower urinary tracts symptoms are exemplified by the TENSI+ device (Fig. 2.3(b)) designed by Stimuli Technology [70]. This CE-marked system is specifically developed for TTNS. Worn as an ankle wristband with two plugged-in silicone graphite electrodes, the TENSI+ demonstrated a 68% treatment persistence rate at three months in a multicentre retrospective study involving 103 patients who self-administered daily 20-minute sessions. Additionally, 70.9% of patients reported improvements based on the patient global impression of improvement score [70].

Another interesting design, the Zida® Control Sock [71] (Fig. 2.3(c)), incorporates conductive textile electrodes (TEs) directly into the fabric of a sock to facilitate TTNS for OAB management. The TEs positioned near the medial malleolus, deliver monophasic stimulation pulses at 20 Hz with an adjustable intensity of up to 156 mA. A clinical trial involving 40 OAB patients reported a 50% reduction in urgency voids and a 30% reduction in 24-hour urinary frequency following 12 weeks of weekly 30-minute sessions [104].

More recently, Vivally® system [72] (Fig. 2.3(d)) offers another wearable option for managing OAB and urge UI. This ankle-worn system employs surface electrodes to stimulate the tibial nerve and incorporates electromyography (EMG) feedback for personalised therapy adjustments. An integrated EMG sensor is placed at the dorsal foot to continuously monitor muscle activity for assessing nerve recruitment during TTNS. This closed-loop feedback mechanism enables verification of nerve activation and allows for adaptive control of stimulation parameters. The entire system allows for wireless control via a Bluetooth®-enabled mobile device, thereby potentially improving its usability.

### 2.2.2 NMES/FES Applications

#### Overview

NMES or FES is a widely used application of electrical stimulation for motion rehabilitation. Unlike physical exercise, NMES induces involuntary muscle contractions through external electrical impulses. However, it is not classified as a passive therapy, as active muscle engagement occurs during stimulation [105]. In clinical practice, NMES delivers electrical impulses to paralysed muscles that retain intact innervation, eliciting controlled muscle contractions to restore functional mobility [106]. This modality mitigates physical impairments and enhances patients' capacity to perform voluntary activities, such as muscle strengthening, shoulder subluxation correction, spasticity reduction, and movement facilitation [105]. NMES systems are typically classified into two broad categories [107]:

- Functional NMES: Applied to improve functional activity in patients with neurological impairments (e.g., spinal cord injury or stroke).
- Therapeutic NMES: Delivered to resting-state muscles to prevent atrophy and maintain muscle mass.

The functional form of NMES, commonly termed FES, is specifically designed to restore limb movement in patients with spinal cord injury or stroke [107]. Modern NMES/FES systems are implemented as wearable devices that deliver programmable electrical impulses to activate weakened or paralysed muscles in a controlled, sequence-dependent manner. These systems are increasingly integrated into rehabilitation protocols to promote neuroplasticity and functional recovery.

#### Recent Developments

The Bioness H200® wireless hand rehabilitation system [108] is designed to support the recovery of hand function in users with hemiplegia resulting from stroke or upper limb paralysis (due to spinal cord injury). The system comprises a wearable orthosis and a wireless controller that deliver electrical stimulation to the forearm and hand. The orthosis stabilises the wrist and supports both the flexor and

extensor muscles, while five embedded GEs or TEs deliver stimulation to assist movement and improve overall hand function.

The L300 Go® [109] is an FDA-cleared medical device recently developed by Bioness Inc. to assist users with foot drop in restoring mobility. The system includes a lower leg cuff, a stimulation unit, and a wireless controller, with optional components such as a foot sensor and a thigh cuff to address thigh muscle weakness. The compact stimulator can be worn with the leg cuff that incorporates two GEs or TEs for delivering stimulation to the targeted sites.

The WalkAide® system [110] addresses foot drop in patients with upper motor neuron damage or impairments in brain or spinal cord pathways. The device aims to improve gait by delivering electrical stimulation during the swing phase of walking. It consists of a battery-operated control unit, an electrode-embedded leg cuff, and an electrode lead cable. The system employs an optional foot sensor to detect the appropriate point in the gait cycle during stimulation, and visual as well as auditory indicators to display its operational status.

The XFT-2001E nerve and muscle stimulator [111] is intended to enhance ankle dorsiflexion in individuals with upper motor neuron damage or disruptions in spinal cord pathways. This system comprises a rechargeable, battery-powered stimulation unit and a lightweight cuff with integrated stainless-steel electrodes. A built-in Bluetooth® module enables wireless control via a smartphone application, providing users with a convenient and flexible option.

A hybrid FES system proposed by Ha *et al.* [112] combines a powered lower limb exoskeleton with a functional electrical stimulator for gait restoration in individuals with paraplegia. The exoskeleton is equipped with electric motors at the hip and knee joints and is controlled by a central control board. It is complemented by a four-channel stimulator that targets the quadriceps and hamstrings to enable coordinated muscle activation during walking.

Jung *et al.* [113] proposed a wearable EMG-controlled FES system for lower limb rehabilitation. This system integrates EMG sensors and inertial measurement units to facilitate volitional control. It consists of a main controller and four stimulation modules, with two modules designed for the thigh and two for the calf, each secured using wearable straps. Additionally, Nam *et al.* [114] developed an EMG-driven "exoneuromusculoskeleton" that integrates an NMES device, soft pneumatic muscles, and exoskeleton

technology for self-assisted upper limb rehabilitation following stroke. This system is designed to assist the elbow, wrist, and fingers in executing sequential reaching and withdrawal tasks, with voluntary control facilitated by EMG signals.

The eight-channel FES-assistive system (named STIMGRASP) developed by Barelli *et al.* [115] is intended to restore grasp function in patients with tetraplegia or hemiplegia. The proposed system comprises a limb orthosis embedded with multiple GEs, which is worn by users to receive electrical impulses. A build-in lithium-ion battery (3100 mAh) provides the entire system to operate consistently over ten hours.

Collectively, these systems demonstrate the breadth of MNES/FES applications, addressing both upper and lower limb rehabilitation as well as gait and grasp restoration. Their designs incorporate advanced features such as wireless control, integrated sensors, and multi-channel stimulation to cater to the specific needs of patients.

### 2.2.3 Summary

The technical specifications of the wearable electrical stimulation devices are summarised in Table 2.2. Since the main research objective in this thesis is to develop a TENS device for TTNS in OAB management, the relevant parameters, including device dimensions, electrical properties, and electrode types, are presented in Table 2.3. This overview is intended to provide readers with a clear understanding of the existing stimulators in the current literature.

Table 2.2. Technical summary of wearable electrical stimulators collated from academic and commercial databases.

| Ref. | General | | | | Electrode | | Electrical | | | | | Reg. Apvl. |
|---|---|---|---|---|---|---|---|---|---|---|---|---|
| | Make, Model | Intended Use | Dim. ($mm^3$) | Weight (g) | Type | Qt. Needed [Pos.] | Classification of Waveform (Patterns) | Other Stim. Parameters | Max. RMS Current (mA) | Max. Current Density ($mA/cm^2$) | Galv. Iso. | |
| [108] | Bioness, H200® | Upper Limb Rehab. | 270×110×90 | 300 | CF | 5 [Forearm & Hand:Palmer] | Symmetric Biphasic (PP&NP:100–300 µs, and IP:50 µs) | Burst/Cont., CC, 0–80 mA, 20–45 Hz, 0–5 kΩ | 13.21* | 1.67* | NS | FDA |
| [115] | STIMGRASP | Grasp Restoration | 100×39×25 | NS | SG | 8* [Elbow, Forearm, Hand: Palmar & Dorsal] | Symmetric Biphasic (PP&NP:300 µs and IP:0 µs) | Cont., CC, 0–40 mA, 20 Hz, 1 kΩ | 4.38* | NS | YES | N/A |
| [114] | N/A | Upper Limb Rehab. | NS | 358 | HG | 2 [Elbow] | Monophasic (PP:0–300 µs) | Cont., CV, 70 V, 40 Hz, NS | NS | NS | NS | N/A |
| [110] | Innovative Neurotronics, WalkAide® | Gait Restoration | 82×61×21 | 87.9 | HG/SS 316 | 2 [Lower Leg] | Unbalanced, Asymmetric Biphasic (PP:25–300 µs and NP:NS) | Burst, CV, 0–110 V, 16.7–33.3 Hz, 0.5–1 kΩ | NS | 25.3 (Peak) | NS | FDA, CE |
| [109] | Bioness, L300 Go® | Gait Restoration | 82×47×15 | 60 | HG/CF | 1/2 [Lower Leg] & 2 [Thigh] | Symmetric Biphasic (PP&NP:100–300 µs, and IP:50–200 µs)/Balanced, Asymmetric Biophasic (PP:100–300 µs, NP: 300–900 µs, and IP:50–200 µs) | Burst/Cont., CC, 0–100 mA, 10–45 Hz, 0.1–80 kΩ | 16.43 | 1.63 | YES | FDA, CE |
| [111] | Shenzhen XFT Medical, XFT-2001E | Gait Restoration | 419×103×13 | 155 | SS 316L | 7 [Lower Leg] | Balanced, Asymmetric Biphasic (PP:100–300 µs, NP:NS, and IP:NS) | Burst, CC, 0–90 mA, 16–50 Hz, 0.5–10 kΩ | 15.58 | 0.53 | NS | FDA, CE |
| [112] | N/A | Gait Restoration | NS | NS | NS | 2* [Thigh] + 2* [Knee] | Symmetric Biphasic (PP&NP:200 µs and IP:0 µs) | Cont., CC, 0–45 mA, 25/50 Hz*, NS | 6.36* | NS | NS | N/A |

(Continued)

| Ref. | General | | | | Electrode | | Electrical | | | | | Reg. Apvl. |
|---|---|---|---|---|---|---|---|---|---|---|---|---|
| | Make, Model | Intended Use | Dim. ($mm^3$) | Weight (g) | Type | Qt. Needed [Pos.] | Classification of Waveform (Patterns) | Other Stim. Parameters | Max. RMS Current (mA) | Max. Current Density ($mA/cm^2$) | Galv. Iso. | |
| [113] | N/A | Lower Limb Rehab. | 110×34.5 ×16.5 | NS | CM | 2 [Lower Leg] + 2 [Thigh] | Monophasic (PP:250 µs)/Symmetric Biphasic (PP&NP:250 µs and IP:NS) | Cont., CC, 0–35 mA, 100 Hz, NS | 7.83* | NS | NS | N/A |
| [99] | TensCare, Mynd | Acute Pain Relief | 120×38 ×11 | 15 | HG | 1 [Forehead] | Monophasic (PP:200 µs) | Cont., CC, 0–20 mA, 55/110 Hz, NS | 2.96* | 0.13 | NS | CE |
| [100] | paingone, Qalm | Acute Pain Relief | 120×38 ×11 | 15 | HG | 1 [Forehead] | Symmetric Biphasic (PP:200 µs) | Cont., CC, 0–17 mA, 55/110 Hz, NS | 3.56* | NS | NS | CE |
| [96] | paingone, Easy | Acute Pain Relief | Φ51× 13.5 | NS | HG | 1 [Painful Sites] | Monophasic* (PP:20–400 µs) | Cont., CC, 0–50 mA, 1–120 Hz, NS | 10.98* | NS | NS | CE |
| [98] | Cefaly Technology, CEFALY® | Acute Pain Relief | 66×47 ×17 | 25 | HG | 1 [Forehead] | Symmetric Biphasic (PP&NP:250 µs and IP:5 µs) | Cont., CC, 0–16 mA, 60/100 Hz, 0.5–10 kΩ | 3.58* | 0.19* | NS | FDA |
| [97] | Beurer, EM 50 | Acute Pain Relief | 193×95 ×15 | 47 | HG | 2 [Abdomen: Hypogastric] | Symmetric Biphasic (PP&NP:75–250 µs and IP:0 µs*) | Cont.*, CC, 0–80 mA, 8–100 Hz, 0–1 kΩ | 17.89* | 0.64* | NS | CE |
| [93] | NeuroMatrix, Quell® | Chronic Pain Relief | 98×74 ×11 | 62 | HG | 2 [Lower Leg] | Symmetric Biphasic (PP&NP:100–200 µs and IP:30 µs) | Cont., CC, 0–100 mA, 60–100 Hz, 0.5–10 kΩ | 20* | 0.71 | NS | FDA |
| [101] | N/A | Chronic Pain Relief | 48×28 ×NS | NS | CcC | 2 [Wrist/Ankle] | Monophasic (PP:0–500 µs) | Cont., CV, 0–100 V, 0–100 Hz, NS | NS | NS | NS | N/A |

(Continued)

| Ref. | General | | | | Electrode | | Electrical | | | | | Reg. Apvl. |
|---|---|---|---|---|---|---|---|---|---|---|---|---|
| | Make, Model | Intended Use | Dim. ($mm^3$) | Weight (g) | Type | Qt. Needed [Pos.] | Classification of Waveform (Patterns) | Other Stim. Parameters | Max. RMS Current (mA) | Max. Current Density ($mA/cm^2$) | Galv. Iso. | |
| [95] | DJO Inc., Compex Mini | Chronic and Arthritis Pain Relief, and Muscle Relaxation | 66×56 ×18 | NS | HG | 1/2 [Painful Sites] | Symmetric Biphasic (PP&NP:0–345 μs and IP:0 μs) | Burst/Cont., CC, 0–144 mA, 1–184 Hz, NS | 51.33* | 2.05* | NS | CE |
| [94] | DJO Inc., chattanooga® Wireless Professional | Acute, Chronic and Arthritis Pain Relief, and Muscle Imbalance Rehab. | Φ55× 16 | 62 | HG | 2–8 [Painful Sites] | Symmetric Biphasic (PP&NP:30–400 μs and IP:0 μs) | Burst/Cont., CC, 0–120 mA, 1–150 Hz, 0.5–1 kΩ | 41.56* | 1.66* | NS | CE |
| [116] | Beurer, EM 70 Wireless | Acute and Chronic Pain Relief, and Muscle Relaxation | 72×50 ×14 | 78 | HG | 1/3 [Painful Sites] | Symmetric Biphasic (PP&NP:30–300 μs and IP:0 μs*) | Cont., CC, 0–45 mA, 2–290 Hz, 0–1 kΩ | 18.77* | 0.75* | NS | CE |
| [117] | Beurer, EM 39 | Muscle Relaxation | 91×88 ×22 | ∼350 | SG* | 2 [Abdomen: Umbilical] + 2 [Lower Back] | Symmetric Biphasic (PP&NP:200 μs and IP:NS) | Burst/Cont., CC, 0–140 mA, 30–80 Hz, NS | 25.04* | 0.19* | NS | CE |
| [102] | Firstkind, geko™ T3 | Blood Circulation Improvement | 186×31 ×9.35 | 10 | HG | 1 [Knee] | Symmetric Biphasic (PP&NP:35–560 μs and IP:0 μs) | Cont., CC, 0–54 mA, 1 Hz, 0.2–3 kΩ | 1.81* | 13.3 | YES | FDA, CE |
| [103] | General Stim, Butterfly-shaped TTNS Device | OAB Management | 58.3×55.6 ×12.8 | 70 | HG | 1 [Behind Medial Malleolus] + 1 [Lower Leg] | Monophasic (PP:100–1,000 μs) | Cont., CC, 0–30 mA, 1–200 Hz, NS | 13.42* | NS | NS | NS |

(Continued)

| Ref. | General | | | | Electrode | | Electrical | | | | | Reg. Apvl. |
|---|---|---|---|---|---|---|---|---|---|---|---|---|
| | Make, Model | Intended Use | Dim. ($mm^3$) | Weight (g) | Type | Qt. Needed [Pos.] | Classification of Waveform (Patterns) | Other Stim. Parameters | Max. RMS Current (mA) | Max. Current Density ($mA/cm^2$) | Galv. Iso. | |
| [70] | Stimuli Technology, TENSI+ | OAB and Urge UI Management | 110×40 ×16 | 65 | SG | 1 [Behind Medial Malleolus] + 1 [Lower Leg] | Monophasic (PP:200 µs) | Cont., CC, 0–50 mA, 10 Hz, 0–1 kΩ | 2.24* | 0.2* | NS | CE |
| [71] | ZIDA, Zida® Control Sock | OAB and Urge UI Management | 65×40 ×17 | 26 | CF | 1 [Lower Leg] + 1 [Foot Bottom] | Monophasic (PP:200 µs) | Cont., CC, 0–156 mA, 20 Hz, NS | 9.87 | 1.23* | NS | FDA |
| [72] | Avation Medical, Vivally® | OAB and Urge UI Management | NS | NS | HG | 1 [Behind Medial Malleolus] + 1 [Foot Bottom] | Symmetric Biphasic (PP:40–600 µs) | Cont., CC, 20 mA, 20 Hz, NS | 4.38* | NS | NS | FDA |

Notes: Apvl.: approval; CC: constant current; CcC: composite-coated copper; CF: conductive fabric; CM: customised; Cont.: continuous; CV: constant voltage; Dim.: dimension; IP: interphase interval; Galv.: galvanic; HG: hydro gel; Iso.: isolation; Max.: maximum; N/A: not applicable; NP: negative phase; NS: not specified; Pos.: position; PP: positive phase; Qt.: quantity; Reg.: regulatory; Rehab.: rehabilitation; RMS: root-mean-square; SG: silicone graphite; Stim.: stimulation; SS: stainless steel; *: estimated.

Table 2.3. Selected specifications of commercially available TENS devices intended for TTNS.

| Parameters | NeuroTrac® Continence [63] | TPN 200 Premier Plus [64] | Geko™ T-1 [65] | TENSI+ [70] | Zida® Control Sock [71] | Vivally® [72] |
|---|---|---|---|---|---|---|
| Year | 2016 | 2018 | 2018 | 2021 | 2023 | 2024 |
| Manufacturer (Country) | Verity Medical Ltd. (Ireland) | Performance Health International Ltd. (UK) | Firstkind Ltd. (UK) | Stimuli Technology Ltd. (France) | Zida LLC (Israel) | Avation Medical Inc. (US) |
| Waveform Classification | Asymmetrical Biphasic | Asymmetrical Biphasic | Asymmetrical Biphasic | Asymmetrical Biphasic* | Monophasic | Symmetric Biphasic |
| Pulse Amplitude (@500Ω) | 0–90 mA | 0–80 mA | 0–54 mA | 0–50 mA | 0–156 mA | 20 mA (Fixed) |
| Stimulation Mode | Continuous | Continuous/Burst | Continuous | Continuous | Continuous | Continuous |
| Pulse Frequency (Continuous Mode) | 2–100 Hz | 2–150 Hz | 1 Hz (Fixed) | 10–20 Hz | 20 Hz (Fixed) | 20 Hz (Fixed) |
| Burst Frequency (Burst Mode Only) | N/A | 100 Hz (Fixed), 2 bps | N/A | N/A | N/A | N/A |
| Pulse Width | 50–450 µs | 30–260 µs | 35–560 µs | 200 µs | 200 µs (Fixed) | 40–600 µs |
| Output Channel | 2 | 2 | 1 | 1 | 1 | 1 |
| Electrode Type | Hydro Gel | Hydro Gel | Hydro Gel | Silicone Graphite | Conductive Textile | Hydro Gel |
| Electrode Size | 50×50 $mm^2$ | 50×50 $mm^2$ | NS | 40×28 $mm^2$ | 40×20 $mm^2$ | 50×22 $mm^2$ |
| Maximum Current Density | 0.76 $mA/cm^2$* | 0.63 $mA/cm^2$* | 1.33 $mA/cm^2$ | 0.20 $mA/cm^2$* | 1.23 $mA/cm^2$ | NS |
| Galvanic Isolation | Transformer | Transformer* | NS | NS | NS | NS |
| Comformity Assessment | CE & UKCA | CE & UKCA | CE & UKCA & FDA | CE | FDA | FDA |

Notes: bps: bursts per second; N/A: not applicable; NS: not specified; *: estimated.

## 2.3 Categorisation of Parameters

Following the review of various wearable electrical stimulation devices, it is essential to examine the parameters that govern the operation of these systems. The parameters of the pulses generated by a stimulator directly influence the safety and efficacy of an electrical intervention. An understanding of these parameters is important for the development of a TENS device tailored for OAB management, ensuring that the designed stimulator meet the design requirements while maintaining user safety.

### 2.3.1 Type of Stimulator

TENS devices on the market are commonly classified as either constant voltage (CV) or constant current (CC) devices. A CV device generates a stable voltage over time; however, the current delivered through the conductive path varies with the load impedance according to Ohm's Law [118]. In contrast, a CC device maintains a consistent current regardless of load variations.

Numerous studies across neuromodulation applications have demonstrated that CC stimulation outperforms CV stimulation in terms of therapeutic consistency, patient satisfaction, and efficacy. In spinal cord stimulation, a randomised controlled trial showed that 70% of chronic pain patients preferred CC over CV stimulation, reporting significantly greater pain relief and comfort [119]. Animal research for spinal cord stimulation in rat model also demonstrated that CC stimulation was more effective in reducing visceral pain responses than CV mode [120].

These findings collectively support the conclusion that CC provides more reliable dosing and superior adaptation to impedance variation, resulting in improved clinical outcomes. Given these established advantages, it is reasonable to adopt the CC stimulation to TTNS modality approach for managing OAB, where the stable and consistent stimulation is also important.

### 2.3.2 Classification of Waveform

In neuromodulation, stimulation pulses are typically classified based on waveform shape, polarity, and medical applications, with the key parameters summarised in Table 2.4.

Table 2.4. Summary of parameters for stimulation pulses.

| Parameters | Sub-category | | Presentation |
|---|---|---|---|
| Pulse Shape | Direct Current | | 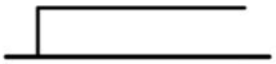 |
| | Alternating Current | |  |
| | Pulsed Current | *Monophasic* |  |
| | | *Symmetric Biphasic* | 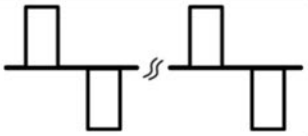 |
| | | *Asymmetric Biphasic (Balanced)* | 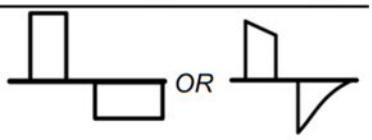 |
| | | *Asymmetric Biphasic (Unbalanced)* | 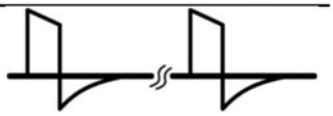 |
| Stimulation Mode | Continuous (Cont.) | |  |
| | Burst | | 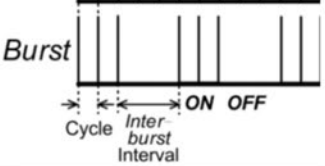 |
| Amplitude (or Intensity) | Low/High | | 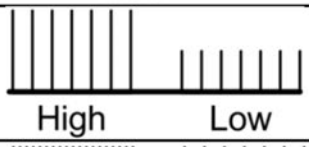 |
| Frequency | Low/High | |  |
| Pulse Width | Short/Long | | 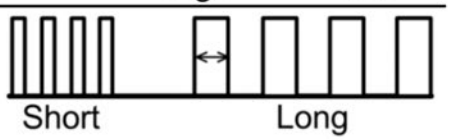 |

### Direct Current Pattern

A low-level direct current (Table 2.4), usually between 1 and 2 mA, is typically employed in transcranial direct current stimulation (tDCS) [121]. Delivered through two electrodes positioned on the scalp non-invasively, tDCS can safely modulates brain excitability without directly triggering action potentials, thereby minimising discomfort and reducing the risk of tissue damage [122].

### Pulsed Current Patterns

- **Monophasic Waveform** (Table 2.4): It is a single-phase, unidirectional pulse, characterised by either a positive (PP) or a negative phase (NP)—commonly referred to as anodic or cathodic, respectively [123]. Despite the difference in polarity, both forms represent a single phase of current flow and are functionally equivalent in practical applications. Due to its structural simplicity and ability to elicit localised physiological responses, the monophasic waveform is commonly employed in applications such as defibrillation and neural stimulation [124].

- **Symmetric Biphasic Waveform** (Table 2.4): This pulse shape consists of two phases (i.e., PP and NP), separated by an IP interval during which no net charge accumulates. The charges delivered in both phases are equal in magnitude but opposite in polarity, resulting in a net charge of zero. This characteristic makes the waveform suitable for preventing potential nerve or muscle damage from the long-term charge accumulation [125].

- **Asymmetric Biphasic Waveform** (Table 2.4): Similar to the symmetric biphasic waveform, this pulse consists of a PP and a NP; however, the shapes of the two phases differ. These pulses can be further classified into balanced (with equal accumulated charges, yielding a net zero charge) or unbalanced (where one phase exceeds the other in charge). Unbalanced pulses are more common in the literature. In balanced pulses, a short IP interval is often observed between the polarised phases.

#### Alternating Current Pattern

The sinusoidal waveform (Table 2.4) is the most common alternating current waveform used for electrical stimulation. Similar to the symmetric biphasic waveform, the sinusoidal waveform is biphasic and does not include an IP interval. This waveform is widely employed in transcranial alternating current stimulation for neurological research [126].

### 2.3.3 Amplitude

The amplitude (or intensity; Table 2.4) of a stimulation pulse is defined as the deviation from the baseline (0 V or 0 mA) to its peak value and is measured in V or mA, depending on whether the TENS device is of the CV or CC type.

### 2.3.4 Stimulation Mode

Stimulation could be delivered in continuous mode or burst mode, as illustrated in Table 2.4. In continuous mode, electrical pulses with defined frequency, amplitude, and pulse width are delivered continuously until the stimulation is terminated. In burst mode, a series of fixed-frequency pulses is followed by an interval with no stimulation, with this cycle repeating at a constant rate [123]. The burst mode is commonly described using the terms “ON time” and “OFF time” [105]. In some cases, this burst stimulation is designed to mimic the natural action potential patterns observed in neurons [123].

### 2.3.5 Frequency

In the context of electrical stimulation, the frequency (Table 2.4) typically refers to the repetition rate of the stimulation pulses, expressed in hertz (Hz). This is often termed the pulse repetition frequency and is defined as the number of complete pulse cycles delivered per second [127].

However, when stimulation is delivered in the form of square waves or other periodic waveforms, the signal contains not only a fundamental (principal) frequency corresponding to the pulse repetition rate, but also higher-order harmonics due to the sharp transitions inherent in the waveform. This is a

consequence of Fourier analysis, where a periodic square wave is represented as a sum of sinusoidal components (harmonics) at odd multiples of the fundamental frequency [128].

### 2.3.6 Pulse Width

Pulse width (Table 2.4) refers to the duration for which the pulse maintains its maximum amplitude. Alternatively, it can be measured as the time interval between the midpoints of the rising and falling edges of the pulse.

### 2.3.7 Output Channel

The output channel is the pathway through which electrical pulses are delivered from the device to the targeted tissues. Each channel can be independently controlled to deliver specific stimulation parameters. NMES/FES devices may be equipped with multiple channels to stimulate different muscles simultaneously, whereas typical TENS devices usually have fewer channels.

### 2.3.8 Electrode Type

In medical devices, electrodes often referred to as the "applied part" under the EN 60601-1 Standard [129], could be classified into three main categories based on their structural and functional characteristics: (1) wet electrodes, (2) dry electrodes, and (3) hybrid electrodes. Wet electrodes consist of a conductive base material, commonly silver/silver chloride (Ag/AgCl), in combination with an electrolyte medium such as conductive gel. The gel facilitates ionic charge transfer at the electrode-tissue interface and plays a key role in reducing contact impedance [130].

In contrast, dry electrodes rely on direct contact between the skin and a solid conductive material, including native metal (e.g., platinum or silver), stainless steel (e.g., SS316), or conductive silicone filled with graphite. These electrodes primarily operate through resistive or capacitive coupling and are widely used in reusable and wearable applications due to their durability and reduced risk of skin irritation [131]. Although dry electrodes eliminate the need for electrolyte in some monitoring applications (e.g., electrocardiogram (ECG), electromyography (EMG)), they typically require the

presence of an electrolyte (e.g., conductive gel, water or sweat) for neuro-stimulation purposes [73], [132]. This ensures reduced electrode-tissue impedance, thereby improving the users' comfort during the delivery of stimulation current [130], [133].

Hybrid electrodes represent a third category that integrates characteristics of both wet and dry electrodes. These electrodes are typically constructed using a flexible substrate—such as textile, silicone, or polymeric film—which is subsequently coated with a conductive layer. Common coating materials include silver-based inks, carbon composites, or metallic nanoparticles [134]. Depending on the design and intended applications, hybrid electrodes may operate as dry interfaces or incorporate a minimal electrolyte layer, including a thin hydrogel, water film, or moisture from the skin, to reduce their contact impedance [135].

### 2.3.9 Current Density

Although the size of these electrodes could be customised, their dimensions are often restricted by the maximum allowable current density, as determined by the EN 60601-2-10 Standard [136]. It is known that the current density ($J$) is defined by

$$J = \frac{I_{RMS}}{A_{ES}} \tag{2.1}$$

where $I_{RMS}$ denotes the root-mean-square (RMS) value of the current (generated by a stimulator), and $A_{ES}$ is the contact area between the electrode and the skin. For safety usage of a neuromodulatory device, the supplied maximum current density is regulated to remain below $2.0\,\mathrm{mA\,cm^{-2}}$ [136].

### 2.3.10 Conformity Assessment

Two common approval schemes for medical electronic devices are the Conformité Européene (CE) marking for the European Union (EU) market and the US FDA approval for the US market. Following Brexit, the United Kingdom (UK) now employs the UK Conformity Assessed (UKCA) marking, which generally aligns with CE requirements. Consequently, device manufacturers would have the flexibility to use either the UKCA or CE marking to commercialise their electronic products in the UK [137].

### 2.3.11 Summary

Evidence from the literature suggests that the stimulation frequency may be a key factor in the effectiveness of tibial neuromodulation for lower urinary tract symptoms [138]. For example, interventions for OAB and UI, which aim to inhibit bladder activity, typically operate at frequencies between 5 and 30 Hz [61], [103]. In contrast, both low-frequency (below 3 Hz) [61], [139], [140] and high-frequency (around 50 Hz) stimulation [141] have been shown to induce an excitatory effect on bladder storage function.

Stimulation amplitude (or intensity) has also been shown to have an impact on treatment efficacy, with a correlation between stimulation strength and neuromodulatory effects [142]. Pulse width has received less research attention, likely because many studies use a standard 200-µs waveform [34]. However, evidence regarding the influence of waveform shape on stimulation effectiveness for managing urinary symptoms remains inconclusive. Some studies suggest monophasic stimulation can activate nerves effectively at lower thresholds, potentially improving stimulation efficiency [143], [144]. Nevertheless, monophasic pulses could carry more risks of tissue damage or discomfort during long-term use [145]. Biphasic waveforms have also been widely utilised in clinical settings due to their reduced-net-charge profile, demonstrating the comparable efficacy and improved long-term tolerability [146]. Thus, waveform shape appears to have limited practical impact on clinical outcomes if other stimulation parameters (e.g., amplitude, frequency and pulse width) are properly optimised.

## 2.4 Classification of Drive Circuits

### 2.4.1 Wilson Current Mirror Topology

Wilson current mirror (WCM), named after George Wilson, is an improved current mirror configuration designed to provide a more accurate input-to-output current gain [147]. A typical WCM comprises three bipolar junction transistors (BJTs), enabling bidirectional current flow through the load. Two WCMs are implemented in the drive circuit, with one configured as a current source and the other as a current sink, both powered by high voltage ($\pm HV_{CC}$), as shown in Fig. 2.4. In medical device circuits, "high voltage" ($\pm HV_{CC}$) typically refers to any voltage significantly above or below standard low-voltage

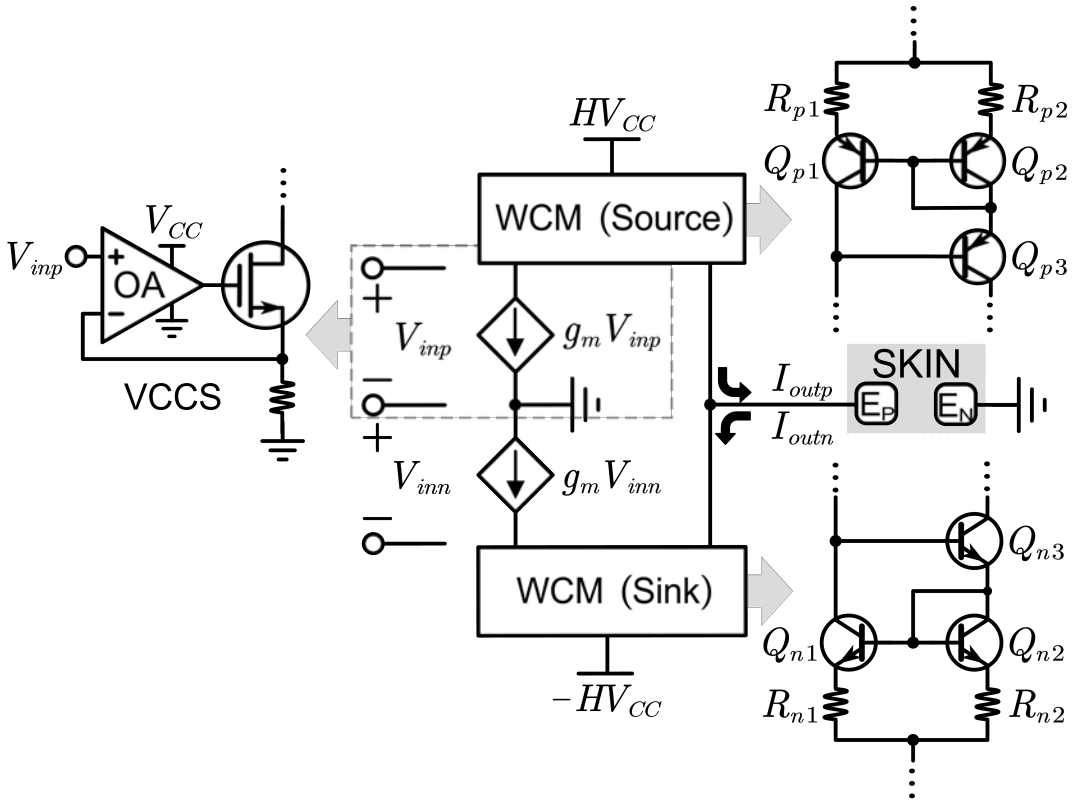


Fig. 2.4. WCM topology of drive circuit.

supply rails (e.g., $>$ 50 V or $<$ –50 V) [148]. Such voltage levels are generally sufficient to overcome the electrode-tissue impedance (ETI) safely and reliably during stimulation [148]. Additionally, the generated current can be regulated using a voltage-controlled current source (VCCS). This drive circuit topology has been utilised in previous studies [149], [150] to generate symmetric biphasic pulses with precise amplitude and pulse width.

### 2.4.2 H-bridge Topology

The H-bridge architecture is a fundamental circuit configuration that enables bidirectional current flow through a load (e.g., ETI) and has been extensively used in drive circuits for electrical stimulators in the literature [101], [151], [152], [153]. The primary advantage of this topology is its efficient control over both the polarity and amplitude of individual pulses. As shown in Fig. 2.5, it consists of four functional switches arranged in an "H" configuration, with each diagonal switch pair controlled

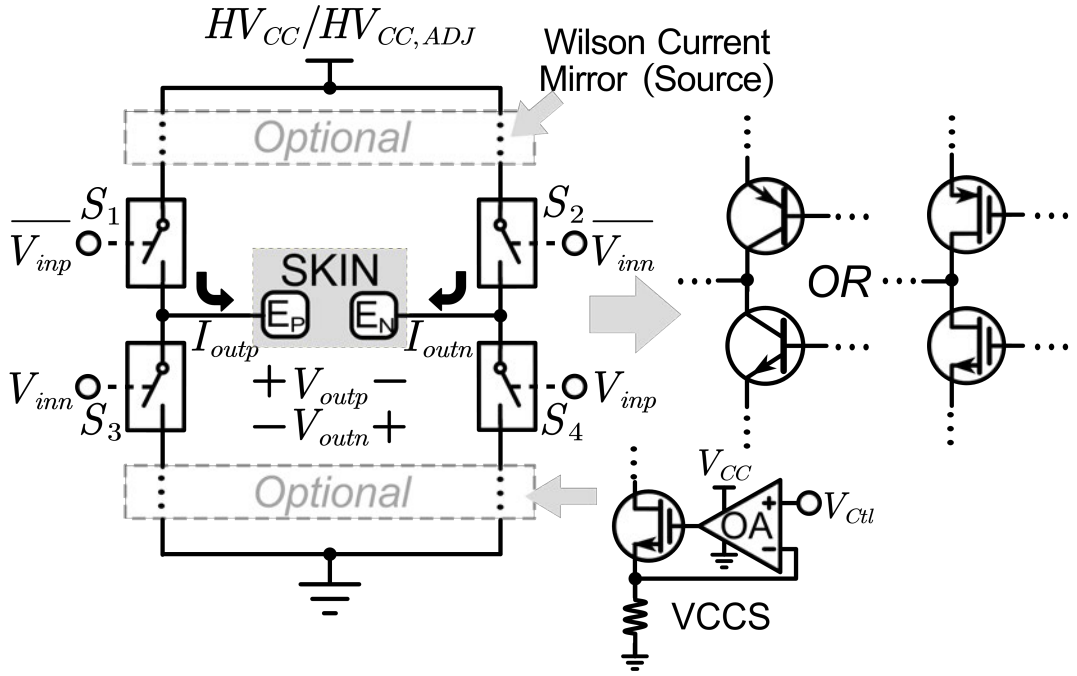


Fig. 2.5. H-bridge topology of drive circuit.

simultaneously to regulate output direction. These switches can be implemented using either BJTs or metal-oxide-semiconductor field-effect transistors (MOSFETs).

Applying a control voltage to the gate enables the corresponding MOSFET switch. This activation allows the high-side supply voltage ($HV_{CC}$ or the adjustable $HV_{CC,\,ADJ}$) to be directly applied across the load, thereby forming a CV configuration. The amplitude of the stimulation voltage pulses can be modulated through the $HV_{CC,\,ADJ}$.

When BJT-based switches are activated, they operate in saturation mode, resulting in a collector-emitter voltage drop ranging from 0.2 to 0.4 V. This drop could increase power dissipation and lead to a modest reduction in the effective stimulation voltage. Consequently, MOSFETs are generally preferred for CV operation. Although BJTs are less efficient in CV mode, they could be repurposed for CC drive configuration. This is achieved by integrating a pair of WCMs between the $+HV_{CC}$ and the high-side switches (i.e., $S_1$ and $S_2$). Furthermore, placing a pair of VCCSs between the lower-side switches (i.e., $S_3$ and $S_4$) and power ground also enables the transition from CV to CC operation, allowing for controlled current stimulation irrespective of load variation.

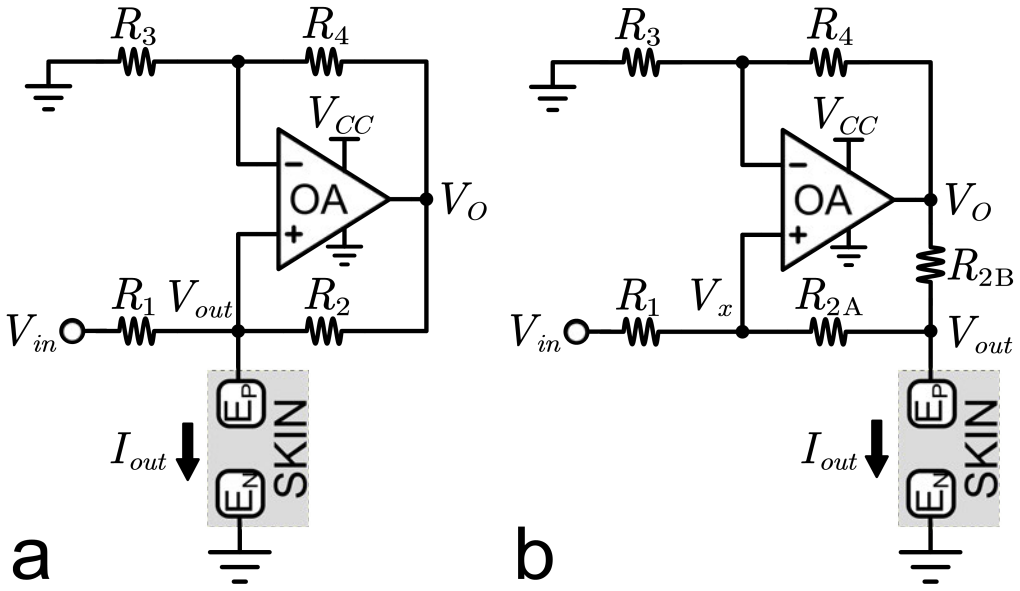


Fig. 2.6. HCS topology of drive circuits: (a) Basic configuration; (b) Improved configuration.

### 2.4.3 Howland Current Source Topology

#### Basic and Improved Configurations

The basic configuration of the Howland current source (HCS) was proposed by Howland at the Massachusetts Institute of Technology in the early 1960s [154]. The basic HCS provides a precise and stable current output that is independent of load resistance and is composed of an operational amplifier (OA) and four resistors arranged in a balanced bridge, as shown in Fig. 2.6(a). This circuit can both source and sink current in direct proportion to an input voltage, with the current-to-voltage relationship defined as:

$$I_{out} = \frac{1}{R_1} V_{in} + \frac{1}{R_3} \left( \frac{R_4}{R_2} - \frac{R_3}{R_1} \right) V_{out} \tag{2.2}$$

where the ratio of $R_4$ to $R_2$ is suggested to be equal to the ratio of $R_3$ to $R_1$ to eliminate influence of $V_{out}$. However, achieving perfectly matched resistor values in practical applications is challenging, which can result in performance degradation due to imbalances affecting output current stability and accuracy.

An improved HCS design, shown in Fig. 2.6(b), incorporates a fifth resistor to enhance overall performance. The mathematical relationship between input and output for this configuration is given as follows:

$$I_{out} = -\left(\frac{1}{R_{2A}} + \frac{1}{R_{2B}}\right)V_{in} + \left[\frac{R_1R_4 - R_3(R_{2A}+R_{2B})}{R_1R_{2B}R_3}\right]V_x \tag{2.3}$$

where $R_1R_4$ should match $R_3(R_{2A}+R_{2B})$, allowing the transconductance gain ($I_{out}/V_x$) to be $-(\frac{1}{R_{2A}} + \frac{1}{R_{2B}})$. This modification reduces sensitivity to resistor mismatches by enhancing bridge balance and compensating for tolerance variations, thereby improving the stability of the output current. The improved HCS is widely cited in the literature as a more effective drive circuit [155] and is particularly suited for applications requiring high precision in current control.

### Modified Configurations

While the improved HCS effectively delivers accurate current output, precise resistor matching remains crucial for optimal performance. Researchers have further modified drive circuits based on both basic and improved HCS configurations to meet specific application requirements [115], [156].

In Fig. 2.7(a), a unity-gain inverter, composed of an OA and two resistors, enables bidirectional constant current flow through the bio-impedance. While this topology supports biphasic output current, the sensing resistor $r_s$ is load-dependent and must satisfy the conditions specified in [157]:

$$r_s = \frac{(4R+2r+Z_{Load})r}{4R+2r} \tag{2.4}$$

where $Z_{Load}$ denotes the impedance of the load. Frequent adjustments to $r_s$ are required, as the impedance of the skin and underlying tissue is frequency-dependent and varies between individuals.

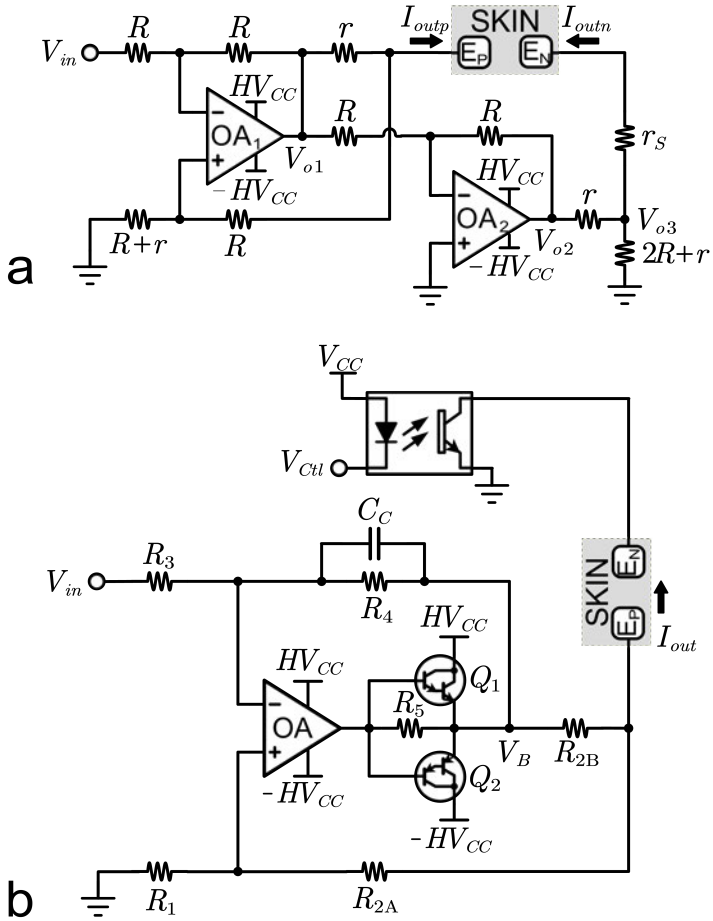


Fig. 2.7. Modified HCS topologies: (a) Biphasic output modification [156]; (b) Bootstrapped modification with an optocoupler to control the opening of the ground loop and the resulting current flow [115].

One of modified HCSs proposed by Barelli *et al.* [157] incorporates a bootstrapping technique, as illustrated in Fig. 2.7(b). This design utilises two Darlington pairs ($Q_1$ and $Q_2$) to significantly enhance the performance of the drive circuit. Firstly, the use of Darlington pairs increases the output voltage swing. This improvement allows the circuit to operate at higher voltage levels without distortion, thereby expanding the operational range. Secondly, the design enhances the current-driving capability of the OA, as these transistors are responsible for supplying current to the load, which effectively reduces the burden on the amplifier. Thirdly, the circuit maintains a linear relationship between the output current and the input voltage, a feature that is essential for precision applications. Additionally, a compensation capacitor ($C_c$) is added across a resistor ($R_4$), with the value suggested in the range of 3 to 10 pF [158]. This capacitor could help improve the response time and achieve a critically damped system behaviour [157].

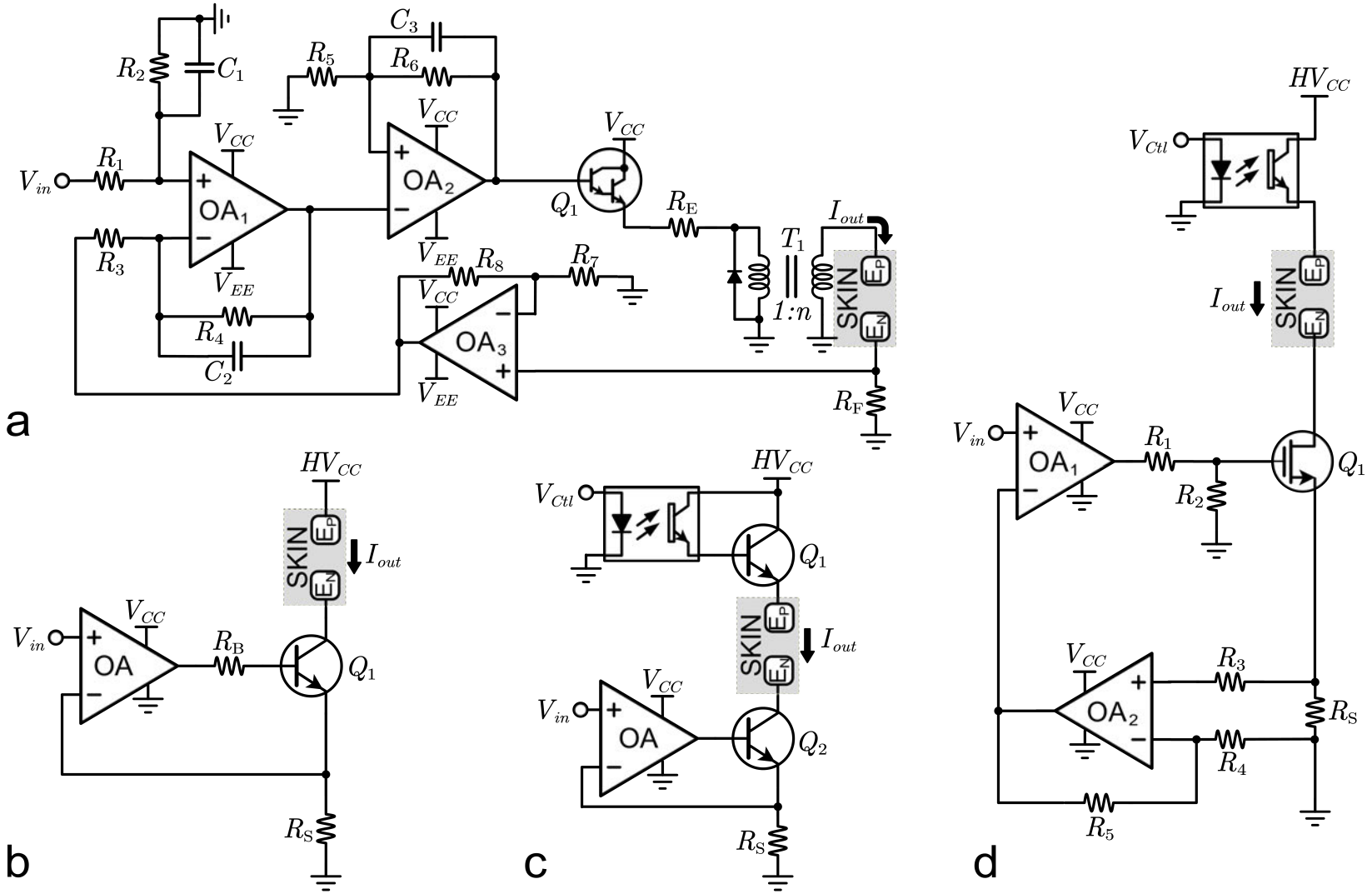


Fig. 2.8. Other hybrid topology of drive circuits: (a) Transformer-isolated VCCS with feedback [159]; (b) A typical VCCS [160]; (c) An optocoupler-isolated VCCS [161]; (d) An improved VCCS with feedback [162].

### Hybrid Topology

Velloso and Souza [159] proposed a drive circuit that utilises an OA in combination with one Darlington pair to construct a standard VCCS, which could enhance the overall current gain and improve output capability, as shown in Fig. 2.8(a). The inclusion of a feedback mechanism in this circuit is to optimise its output stability [159].

In contrast, the circuit shown in Fig. 2.8(b) represents a basic form of a VCCS [160]. In this design, the input voltage ($V_{in}$) is equivalently applied to a resistor connected to the base of a BJT. By using this configuration, the current flowing through the emitter is controlled, which is approximately equal to the ratio of $V_{in}$ to $R_F$. As the collector current of the BJT nearly matches the emitter current, the output current delivered through the load is directly proportional to the input voltage. A similar drive circuit topology (Fig. 2.8(c)) was proposed by Willand *et al.* [161]. The primary difference in this version is the inclusion of an optocoupler, which serves as a protective isolation, as it can create an optical barrier that isolates users from the high-voltage supply ($+HV_{CC}$).

Zhou *et al.* [162] proposed another optocoupler-isolated drive circuit, as shown in Fig. 2.8(d). This circuit includes an additional feedback network whose main function is to regulate the output current. It achieves this by continuously adjusting the gate voltage of a MOSFET based on the voltage sensed across a sensing resistor ($R_S$), thereby ensuring that the output current remains directly proportional to the input voltage.

### Summary

In the hybrid drive circuits, the optocouplers provide essential galvanic isolation between the low-voltage electronics and the high-voltage stimulation circuitry, thereby protecting the sensitive control electronics from damaging voltage transients. However, it should be explicitly noted that these implemented optocouplers (Fig. 2.8(c) and (d)) do not isolate the user side from the high-voltage supply; rather, users' isolation from high voltage shall be implemented separately using dedicated methods such as transformer isolation, adhering strictly to relevant medical safety standards [163]. Table 2.5 summarises additional parameters of the drive circuits collated from the recent literature, serving as both a reference and a resource for further studies.

Table 2.5. Summary of selected technical specifications of drive circuits.

| Ref. | Topology | Stim. Type | Amplitude or Intensity | Stim. Mode (Frequency) | Pulse Shape | Pulse Width | Galvanic Isolation |
|---|---|---|---|---|---|---|---|
| [149] | Wilson Current Mirror | CC | 0–100 mA | Cont. (NS) | Symmetric Biphasic | 100–600 µs (PP&NP) and 0 µs (IP) | NO |
| [150] | Wilson Current Mirror | CC | 0–60 mA | Burst (50 Hz) | Balanced, Asymmetric Biphasic | 2000 µs (PP), 500 µs (NP) and 0 µs (IP) | NO |
| [101] | H Bridge | CV | 0–100 V | Cont. (0–100 Hz) | Monophasic | 0–500 µs | NO |
| [152] | H Bridge | CV | 0–120 V | Cont. (5–50 Hz) | Symmetric Biphasic | 50–2000 µs (PP&NP) and 3.5 µs* (IP) | YES (Capacitor) |
| [153] | H Bridge | CV | 0–50 V | Cont. (100 Hz) | Symmetric Biphasic | 300 µs (PP&NP) and 100 µs* (IP) | NO |
| [151] | H Bridge (VCCS combined) | CC | 0–100 mA | Cont. (100 Hz) | Symmetric Biphasic | 10–1000 µs (PP&NP) and 100 µs* (IP) | NO |
| [164] | H Bridge (Wilson Current Mirror Combined) | CC | 0–150 mA | Cont. (50 Hz)/ Burst (2 kHz) | Symmetric Biphasic | NS | NO |
| [155] | Howland Current Source (Improved) | CC | 0.1–25.6 mA | Cont. (NS) | Sinosoidal | NS | NO |
| [156] | Howland Current Source (Modified) | CC | 0–25 mA | Cont. (100 Hz) | Symmetric Biphasic | 180 µs (PP&NP) and 40 µs (IP) | NO |
| [115] | Howland Current Source (Modified) | CC | 0–40 mA | Cont. (20 Hz) | Symmetric Biphasic | 300 µs (PP&NP) and 0 µs (IP) | NO |
| [165] | Other Hybrids | CC | 0–100 mA | Cont. (NS) | Monophasic | NS | YES (Transformer) |
| [159] | Other Hybrids | CC | 0–74 mA | Cont. (20–200 Hz) | Monophasic | 50–500 µs | YES (Transformer) |
| [160] | Other Hybrids | CC | 20 mA | Cont. (50 Hz) | Monophasic | 1–10 µs | NO |

(Continued)

| Ref. | Topology | Stim. Type | Amplitude or Intensity | Stim. Mode (Frequency) | Pulse Shape | Pulse Width | Galvanic Isolation |
|---|---|---|---|---|---|---|---|
| [161] | Other Hybrids | CC | 22 mA* | Cont. (NS) | Monophasic with Low-amplitude Prepulses (up to 10 ms) | 100–200 μs | NO |
| [162] | Other Hybrids | CC | 0–60 mA | Cont. (50 Hz) | Symmetric Biphasic/Balanced, Asymmetric Biphasic | 400 μs (PP&NP) and 100 μs* (IP)/400 μs (PP), 1200 μs (NP) and 100 μs* (IP) | NO |

Notes: CC: constant current; CV: constant voltage; IP: interphase; N/A: not applicable; NP: negative phase; NS: not specified; PP: positive phase; *: estimated.

## 2.5 Discussion

Monophasic pulse waveforms, when delivered using a bipolar electrode configuration (where the anode and cathode are positioned in close proximity at the same site), have been shown to yield lower neural activation thresholds and improved spatial selectivity compared to biphasic stimulation. Studies involving auditory and peripheral nerve models have demonstrated that monophasic stimulation can elicit equivalent or enhanced neural responses at reduced current amplitudes, while confining activation to more localised regions [166], [167]. These characteristics are of interest in TTNS applications, as they support reduced energy consumption, smaller power sources, and shorter stimulation durations, thereby improving system portability.

Despite these functional advantages, monophasic stimulation introduces safety considerations related to charge imbalance. Specifically, the use of monophasic pulses may lead to net charge accumulation at the electrode-tissue interface, potentially resulting in tissue irritation or damage [168]. In contrast, symmetrical biphasic waveforms maintain a net zero charge between the PP and NP, thereby minimising electrochemical reactions at the electrode-tissue interface [169]. This inherent charge balancing reduces the risk of ion accumulation and the associated tissue discomfort. Conversely, unbalanced, asymmetrical biphasic waveforms, in which the charge delivered during one phase does not equal that of the opposite phase, can lead to net charge buildup at the electrode site. This imbalance may result in increased local ionic accumulation, contributing to user discomfort and potential tissue irritation [169].

However, in low-frequency applications such as TTNS for OAB management (typically $\leq$ 30 Hz) and when limited to short pulse durations (e.g., $\leq$ 250 µs), these risks associated with monophasic pulses could be mitigated [138]. Appropriate design strategies, including the use of narrow pulse widths and long inter-pulse intervals, could maintain safe charge levels while retaining the efficacy and selectivity benefits of monophasic stimulation.

To implement monophasic patterns, a typical VCCS-based drive circuit (Fig. 2.8(b)) is determined to serve as a reference design for generating CC pulses. Galvanic isolation is considered a safety measure to reduce the risk of electrical faults and enhance user protection. The electrical characteristics and safety features of the proposed design (described in Chapter 4) are aligned with those found in existing clinically approved neuro-stimulators intended for TTNS, such as the NeuroTrac® Continence and Zida®

Control Sock. A comparative analysis (Table 2.3) of these stimulation devices' technical specifications is also utilised to inform and validate the proposed stimulator. Detailed explanations on circuit design and implementation, safety concerns, and performance verification are presented in subsequent chapters of the thesis.

# Chapter 3

# Textile Electrodes Feasibility Study

The seminal experiment conducted by Luigi Galvani, demonstrating that electrical stimulation could induce muscle contractions in frog's limbs, represented a pivotal milestone in medical science and established the foundation of modern electrophysiology [170]. This discovery initiated extensive investigations into the bio-electronic interface, with particular emphasis on the electrode-tissue interaction, subsequently driving the development of electrodes tailored for medical applications [171]. Early advancements in this field primarily relied on invasive electrode designs, such as needle electrodes, which required direct insertion into tissues to achieve effective stimulation or recording. While effective, these invasive approaches often pose challenges such as tissue damage, infection risks, and patient discomfort.

The demand for safer and more user-friendly solutions has driven the development of non-invasive surface electrodes. These electrodes have become indispensable tools in medical applications, particularly for diagnostic purposes. For instance, in electromyography (EMG), surface electrodes are employed to record the electrical activity of skeletal muscles, facilitating the diagnosis of neuromuscular disorders [172], [173], [174]. Similarly, in electroencephalography (EEG), surface electrodes positioned on the scalp record brain wave patterns, facilitating the diagnosis of neurological conditions such as epilepsy and sleep disorders [175], [176].

In past decades, non-invasive surface electrodes have extended their use to therapeutic applications, including neuromuscular or functional electrical stimulation (NMES/FES), and transcutaneous electrical nerve stimulation (TENS), further indicating their extensive adoption in medical industry. With advancements in medical electronics and emerging technologies, there is an increasing demand to

enhance the physical performance while expanding their variety of form factors and dimensions [171]. These developments have not only improved the efficacy of neuromodulation therapies but also broadened the potential applications of surface electrodes within neural science and biomedical engineering.

The electrode-tissue impedance (ETI) is an important parameter of medical electronic systems. While high ETI ranging from several hundreds of kΩ to a few tens of MΩ could introduce increased noise during bio-signal recording, thereby affecting quality of signals [177], [178]; however, these distorted signals could be analysed using post-processing techniques [179]. However, during electrical stimulation, a high ETI is most likely unacceptable, as it can exceed the compliance limit of the stimulator, preventing the device from delivering sufficient current to effectively activate targeted nerves or muscles [180].

Regarding the materials used for surface electrodes, gold, platinum, silver chloride (AgCl), and silver/silver chloride (Ag/AgCl) are commonly utilised. Gold and platinum electrodes are known for their durability and ease of maintenance [181]; however, the expensive manufacturing makes them unsuitable for use in disposable electrodes, particularly in sanitised clinical environments where single-use options are typically required. In contrast, Ag/AgCl electrodes with reasonable costs also provide good signals. However, when these metal electrodes are used in "dry" conditions, they become more susceptible to motion artifacts, which can compromise their performance and reliability [181].

To address this issue, a clinical approach is to penetrate these electrodes beneath the skin. Although this invasive (or percutaneous) method can provide high-quality signals, it comes with drawbacks. Invasive electrodes particularly implanted electrodes, could disrupt the surrounding microenvironment, causing immediate damage such as tissue punctures and microvascular disruptions [182]. These injuries often elicit a foreign body response, activating immune cells and promoting scar tissue formation [183]. Over time, this process results in dense fibrous encapsulation around the electrodes, elevating contact impedance and deteriorate their performance [184].

To this end, the pre-gelled Ag/AgCl electrode is introduced, featuring a soft and flexible contact interface [185]. Although effective, this non-invasive (or transcutaneous) gel electrode (GE) poses challenges for long-term use, particularly for patients with sensitive skin, as it may cause skin irritation or allergic reactions [66], [67]. In older patients, the removal of adhesive electrodes may damage their fragile skin [68], [69]. Moreover, the gel layer typically tends to dry out over time [67], leading to an increase in ETI and reduced therapeutic (stimulatory) effectiveness. Furthermore, with advancements

in technology, medical electronic devices are being developed in wearable modalities, necessitating a re-evaluation of electrode design (typically wearable electrodes). Despite the proven efficacy of pre-gelled electrodes, their designs are less suitable for integration into wearable, fabric-based garments.

To address these, dry surface electrodes made from flexible materials, such as conductive silicone (graphite) electrodes and conductive textile electrodes (TE), have attracted attention due to their natural softness. Although the use of these dry electrodes for bio-signals recording is well established, their application in electrical stimulation remains under-investigated. Additionally, the durability of integrating TE into wearable, fabric-based garments has made them a primary focus.

In present study, several TE prototypes were fabricated to explore their feasibility for electrical stimulation. The investigation focused on evaluating the ETI during short-term use and analysing stimulation-induced EMG responses, with performance compared to standard clinical-grade GEs.

## 3.1 Design and Fabrication of Textile Electrodes

A TE was constructed using a soft inner filling material such as a polyurethane (PU) sponge, a polyester sponge or a natural cotton pad (Fig. 3.1(a)–(c)), with dimensions of $5 \times 5$ cm$^2$. The filler material was positioned between two pieces of conductive textile material, made of jersey knit conductive fabric (1364, Adafruit Industries; Fig. 3.1(f)) or silver fibre knit conductive fabric (ZZB-1, SYG Radiation Protection Technology; Fig. 3.1(g)) and stitched together. The inclusion of filling material within the TE created a bulge that enhanced skin contact, particularly around the posterior ankle joint (or medial malleolus), compensating for insufficient electrode thickness that otherwise limited contact efficacy.

The metal connector (snap button, PMSOEHT Professional Accessories Store; Fig. 3.1(e)) positioned at the central backside of the TE facilitated connection to the external cable. Due to the lower linear resistance ($< 1$ Ω/ft in any direction across the material [186]) of the silver fibre knitted conductive fabric, TEs made from this conductive material were selected for the following assembly process. The cross-sectional view of an individual TE is illustrated in Fig. 3.1(h).

During assembly, the stitched edges of two TEs with identical inner filling material were encapsulated using an adhesive bandage (Tensplast®, BSN Medical, UK; Fig. 3.1(d)). This assembly maintained

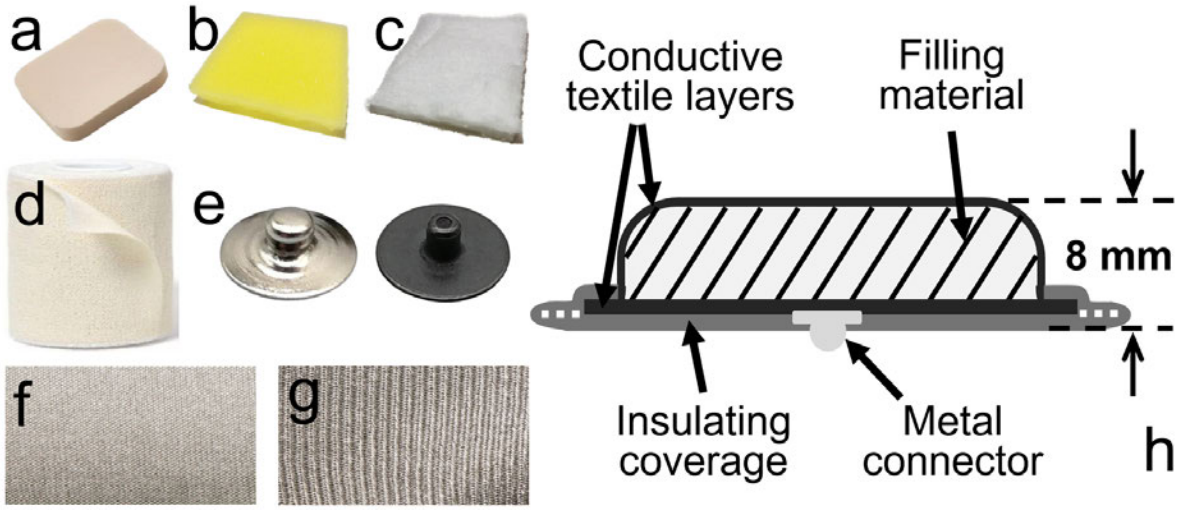


Fig. 3.1. A TE manufactured in-house and its relevant material [75]: (a) Polyurethane (PU) sponge; (b) Polyester sponge; (c) Natural cotton (chosen material); (d) Adhesive bandage for encapsulation; (e) A pair of metal connectors; (f) Knit jersey conductive fabric; (g) Silver fibre knitted conductive fabric (selected material); (h) The cross-sectional view of the TE.

a centre-to-centre separation distance of 10 cm between the TEs (Fig. 3.2), as per standard electrode placement protocol [187], [188] commonly employed for tibial neuromodulation in overactive bladder (OAB) management. Three TE prototypes were ultimately fabricated and subjected to subsequent comfort evaluations.

## 3.2 Study Protocol

### 3.2.1 Purpose

The objective of this study is to characterise the designed TE through measurement of ETI and evaluate whether the TE is capable of eliciting the basic physiological responses via transcutaneous electrical nerve stimulation (TTNS), as measured by EMG.

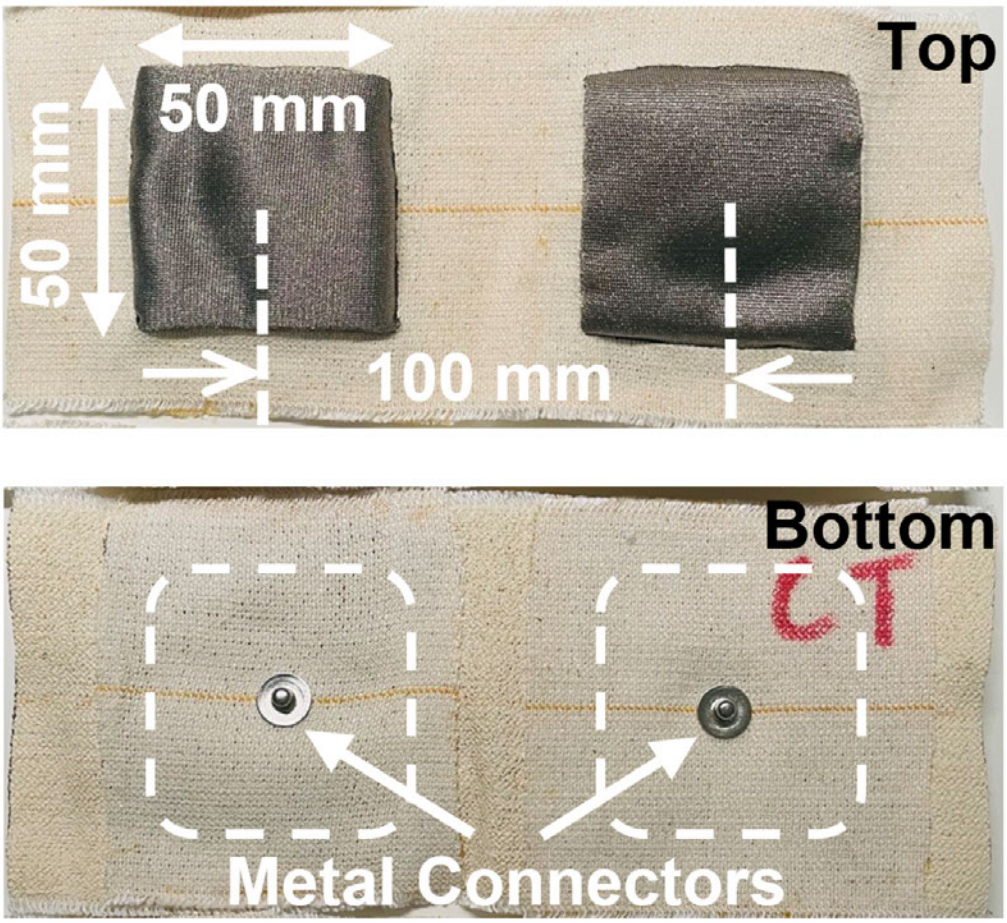


Fig. 3.2. Top and bottom views of a TE prototype.

### 3.2.2 Ethics and Recruitment

This study was reviewed and approved by the local ethics committee of The University of Edinburgh (Ref: RT2021/83413). Written informed consent (Appendix C) was obtained from all participants prior to the study.

Four healthy volunteers (one female and three males, age: $30 \pm 4$ years) were recruited for this study. They had no prior knowledge of the purpose of the trial beyond the context of the experiment, as described in the Participant Information Sheet (Appendix C).

### 3.2.3 Comfort Evaluation

Participants were instructed to assess the softness and comfort of various prototypes fabricated using two conductive materials and three inner filling materials, involving touching and squeezing. A 5-point Likert scale was utilised, where a score of 1 represented the lowest level of comfort and softness, and a score of 5 denoted the highest level.

Consequently, the cotton-filled TE prototype was rated the softest and most comfortable and was selected for all subsequent experiments. To ensure consistency and reliability of results, the same cohort of participants was employed in the entire feasibility study.

### 3.2.4 Skin Preparation

The following procedure was employed to prepare the skin surface before electrode application:

- Hair was removed from the targeted skin area using a disposable razor;
- The shaved skin was cleaned with cotton balls soaked in 70% isopropyl alcohol;
- A measured amount of electrolyte was uniformly applied to hydrate the skin surface prior to using TEs. However, this skin hydration step was not required when applying GEs.

### 3.2.5 Electrode-tissue Impedance (ETI) Measurement

ETI is an important performance metric for evaluating electrode quality [189]. Under typical dry TE conditions, the ETI generally ranges in the hundreds of kΩ; however, reducing this impedance is recommended for electrical intervention [190].

Following the skin preparation procedure, the cotton-filled TE prototype was attached to the skin surface of the right lower leg, with the ground (or cathodal) electrode positioned 1 cm behind the medial malleolus and the active (or anodal) electrode attached 10 cm proximally. The ETI was measured using a programmable LCR meter (HM8118, Rohde & Schwarz), as shown in Fig. 3.3.

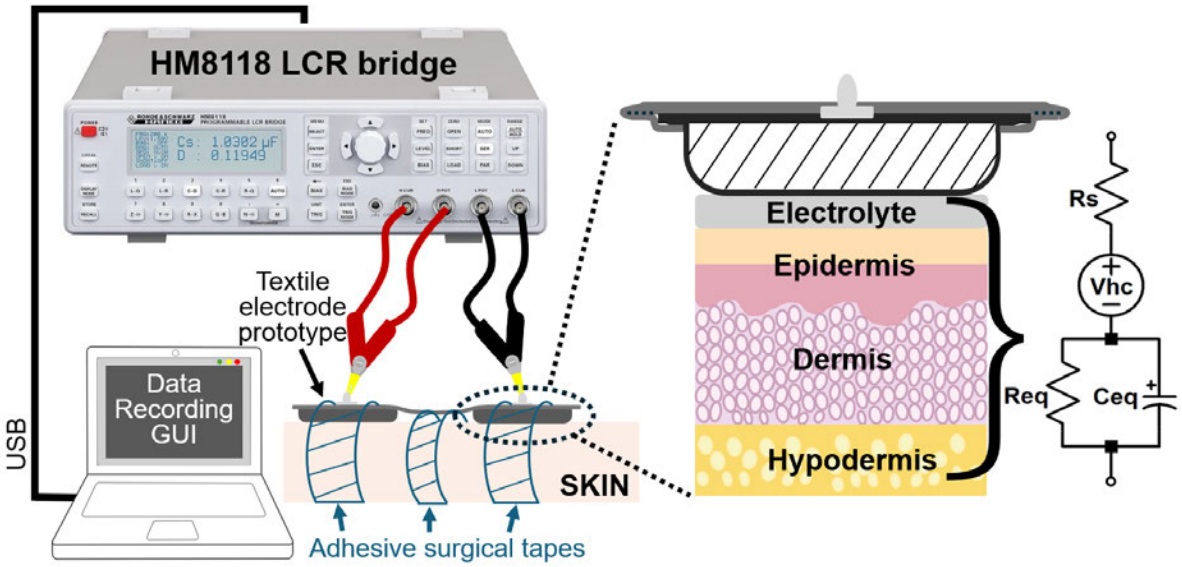


Fig. 3.3. Measurement of ETI with its equivalent electrical model.

The LCR meter applied a 1 V sinusoidal input across the skin through the TEs, with measurement frequencies swept from 20 Hz to 200 kHz in 42 increments. To ensure the precise positioning of the TEs on the skin surface, surgical tape was used to immobilise the prototype. For comparison, the TE prototype was subsequently replaced by two adhesive clinical-grade GEs (SA12, Med-Fit UK), which were placed at the same electrode locations without requiring surgical tape.

An electrolyte is necessary between the dry TE and cleaned skin; therefore, body moisturiser or deionised water was utilised during the skin preparation. Body moisturiser can be classified based on the nature of the dispersion medium and dispersed phase, as oil-in-water (O/W) or water-in-oil (W/O) types. In this experiment, the TE ETI was measured using multiple electrolyte types, including O/W (NIVEA™ Soft, Beiersdorf Global) and W/O (NIVEA™ Crème, Beiersdorf Global) body moisturisers as well as deionised water, and compared to that of the GEs. ETI was also measured at a constant frequency of 10 kHz over a one-hour period to evaluate the short-term feasibility of TE application.

### 3.2.6 Electromyography Recording

#### Setup

Stimulation-induced EMG signals were recorded using a NeuroRecorder (Blackrock Microsystems, Blackrock Neurotech). The EMG measurements verified the effective delivery of stimulation pulses to the neuromuscular system.

Given the small size of the foot muscles, a unipolar EMG recording arrangement was employed. Three small GEs ($15 \times 20$ mm$^2$, Spes Medica) were placed on the prepared right foot of the stimulated leg: (1) an active electrode positioned on the flexor hallucis brevis muscle, 3–5 cm proximal to the big toe; (2) a ground electrode placed on the fifth metatarsophalangeal joint on the lateral side of the foot to minimise noise; and (3) a reference electrode attached to the lateral malleolus. This arrangement provided a unipolar measurement. Surgical tape was also used to secure these EMG electrodes, ensuring consistent measurement of the evoked responses. The experimental setup is shown in Fig. 3.4(a)–(c).

Either type of stimulation electrodes (TEs or GEs) was connected to an FDA-approved clinical stimulator (DS7A, Digitimer), which is commonly utilised in experimental and clinical research applications [191], [192]. The order of electrode usage was randomised for each participant. Initially, TTNS was administered to each participant for 30 seconds, delivering 2 Hz stimulation pulses with a pulse width of 200 µs and an intensity level of 1 mA. Evoked EMG signals were continuously recorded during the TTNS. The stimulation intensity was then gradually increased, ranging from 1 to 50 mA or up to the maximum amplitude tolerable (i.e., maximum threshold) by each individual. The 30-second recording was repeated for each intensity level until reaching the maximum threshold, which was defined as a single TTNS procedure. Additionally, the procedure was repeated after a 15-minute rest period to prevent muscle fatigue, using different pulse width settings (50 and 100 µs) with the same participant during the session.

Before digitisation, the EMG signals were bandpass filtered at 10 to 500 Hz. A 50 Hz notch filter was also applied to attenuate the powerline noise. The EMG signals were subsequently sampled at a rate of 10 kHz and stored in the NS4 (i.e., Neuro Stream Four) format.

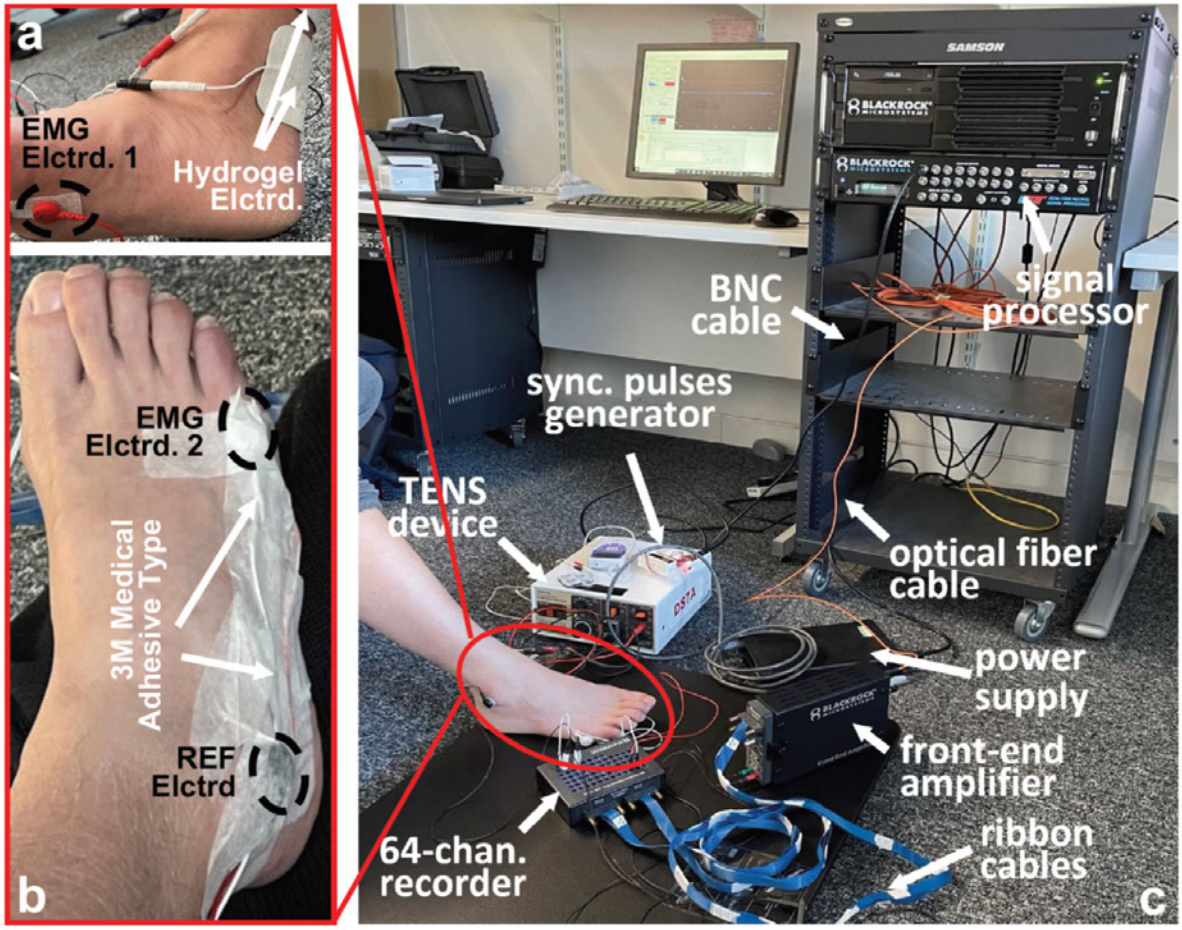


Fig. 3.4. Experimental setup of EMG recording [73]: (a) Illustration of the placement of an active EMG electrode and two stimulation electrodes, which can be either TEs or GEs. Only the cathodal GE is shown in this figure; (b) Positioning of the ground and reference EMG electrodes; (c) Overview of the cable connections between devices. Abbreviations: chan. – channel; Elctrd. – electrode; REF – reference; sync. – synchronisation.

### Recording-Stimulation Synchronisation

Synchronisation pulses were essential for enabling the signal processor (NeuroProcessor, Blackrock Neurotech) to effectively trigger the NeuroRecorder for recording evoked responses in Trigger Mode. The DS7A stimulator, primarily designed for single-pulse stimulation and manual activation via a press button, required additional components for continuous controlled operation. To address this, a custom pulse generator (Fig. 3.5) was developed to deliver 5 V transistor-transistor logic (TTL) pulses at 2 Hz, enabling the activation of the DS7A stimulator. Upon activation, the built-in module of the DS7A generated synchronisation triggers at 5 V TTL, 2 Hz, with a 1 ms pulse width.

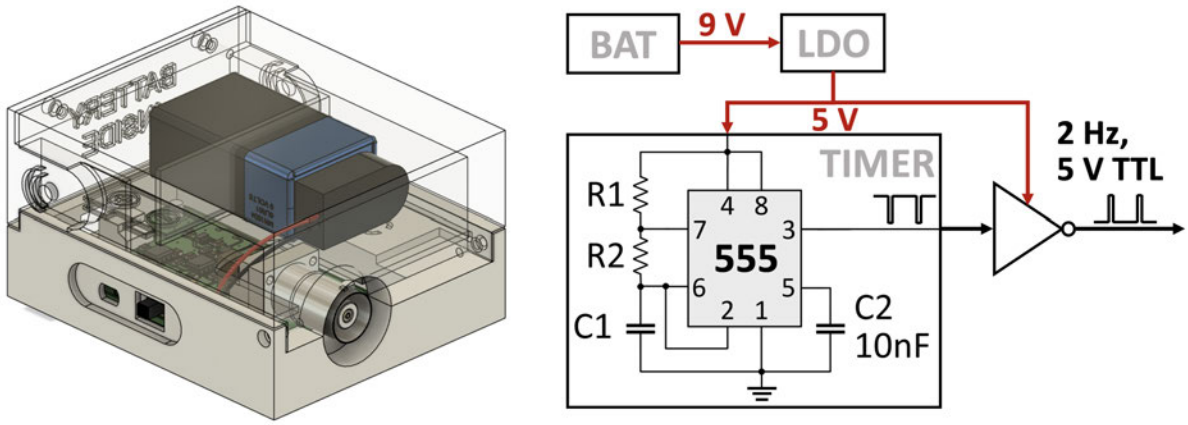


Fig. 3.5. Overview of a custom pulse generator for supplying the synchronisation pulses. Abbreviations: BAT – battery; LDO – Low-dropout (regulator); TTL – transistor-transistor logic.

### Data Processing and Analysis

The recorded EMG signals were segmented into 60 independent slices, each containing a single evoked EMG trace. This segmentation facilitated ensemble averaging to enhance signal quality. The mean, tenth and 90th percentile values of the processed data were subsequently calculated across all participants.

To extract the motor evoked potentials (MEPs) from raw datasets, synchronisation pulses were used to accurately determine the onset of each stimulation event. As the tibial nerve was stimulated at a frequency of 2 Hz, evoked EMG responses were expected to occur within a 500 ms period following each stimulus. A fixed-length time window of 100 ms was applied, starting 8 ms after the rising edge of the synchronisation pulse), in order to exclude stimulation artifacts. Within this 100 ms window, the peak-to-peak amplitude of the M-wave (or MEP) was identified and used for further analysis. This extraction method is illustrated in Fig. 3.6.

In addition, a normalised cross-correlation (NCC) analysis was performed to assess the similarity between two time-series EMG datasets ($X_i$ and $Y_i$, where $0 \leq i \leq N-1$). This method normalises amplitude differences between datasets to address scaling variations and computes the correlation coefficient $\Re$, as described in [193], and is formulated by:

$$\Re = \frac{\sum_{i=0}^{N-1}(X_i Y_i)}{\sqrt{\sum_{i=0}^{N-1} X_i^2}\sqrt{\sum_{i=0}^{N-1} Y_i^2}} \tag{3.1}$$

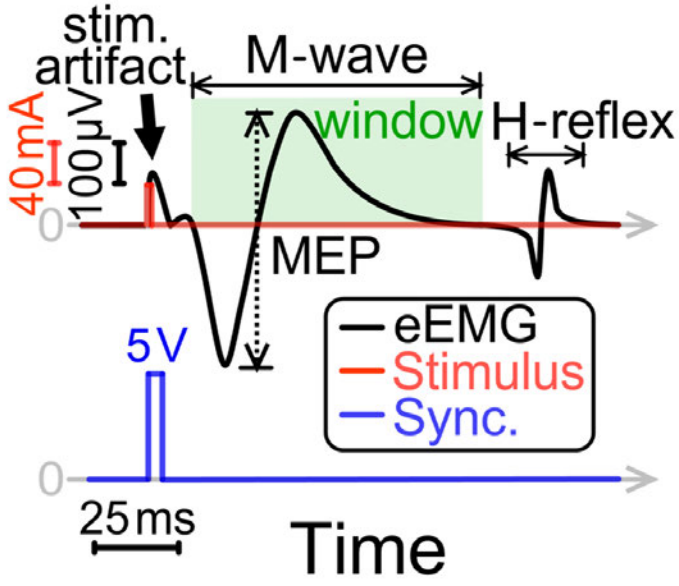


Fig. 3.6. Graphical representation of MEP calculation [75]. The M-wave represents the direct muscle response from TTNS, while the H-reflex reflects the spinal monosynaptic reflex pathway via sensory afferent activation. Abbreviations: eEMG – evoked electromyography; estim. – stimulation; Sync. – synchronisation.

The procedure involves shifting one dataset forward or backward relative to the other (known as the "time lag") to evaluate all possible alignments [194].

## 3.3 Results and Discussion

### 3.3.1 Result of ETI Measurement

In Fig. 3.7, the variation in ETI is shown based on the type of electrolyte applied to TEs, compared to GEs. TEs combined with a W/O moisturiser exhibit higher impedance compared to other electrolytes, likely due to the oil phase hindering ionic conductivity. When deionised water was used as an electrolyte, a small volume ($< 0.25$ mL) result in elevated ETI. While increasing the volume to 0.5 mL reduces ETI, yielding impedance values lower than those of standard GEs, particularly in the 5–10 kHz range. In contrast, TEs with an O/W moisturiser exhibit consistently lower impedance across all frequencies, suggesting improved conductivity due to its higher water content.

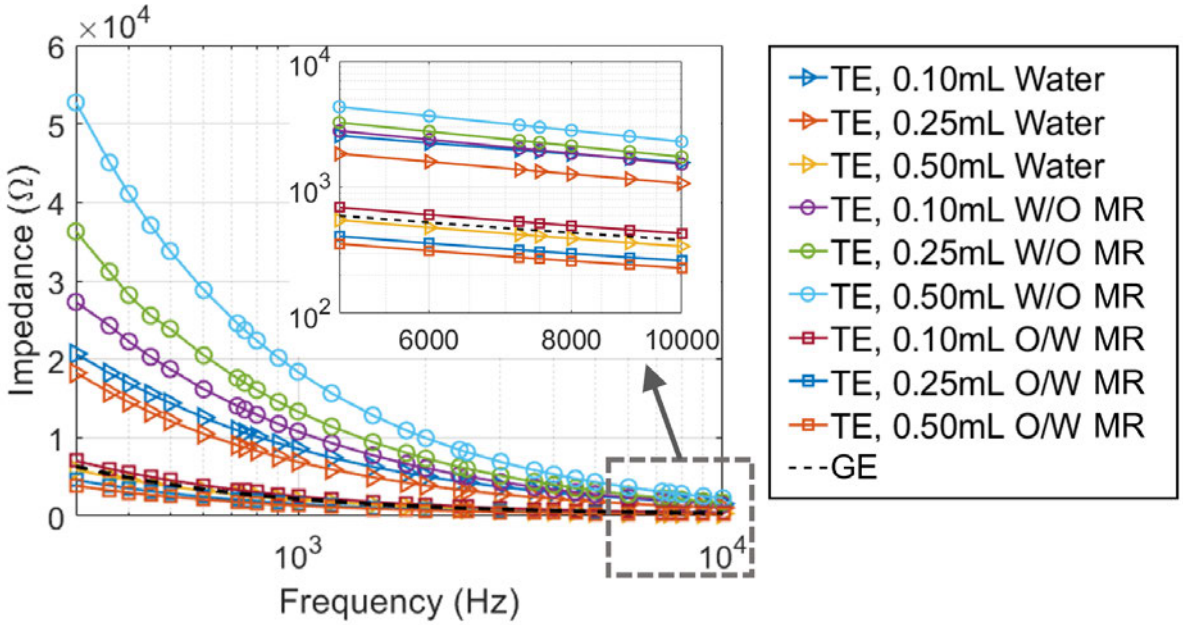


Fig. 3.7. Variance of ETI associated with different electrode and electrolyte types (with the volume of 0.1–0.5 mL) [73]. The main plot is presented on a semi-logarithmic (Log) scale (Log x-axis), while the inset plot is shown on a Log–Log scale. Abbreviations: GE – gel electrode; MR – moisturiser; O/W – oil-in-water; TE – textile electrode; W/O – water-in-oil.

In all electrolyte conditions, the ETI of the hydrated TEs and standard GEs progressively increases over time, as shown in Fig. 3.8(a). The highest rate of impedance change was identified by its slope (median = 34.03 $\Omega$/min) in the deionised water condition. In contrast, the lowest rate of ETI variation (median = 0.10 $\Omega$/min) occurred with the GE, as depicted in Fig. 3.8(b). Additionally, the condition with the least amount of W/O moisturiser showed the second-slowest rate (median = 1.98 $\Omega$/min). This steady trend may be attributed to the relatively slow absorption or evaporation rate of water molecules in the oil-based moisturiser. The baseline impedance is the highest in the W/O moisturiser condition, likely due to its higher oil content reducing conductivity at the electrode-tissue interface. Although the lowest baseline impedance was observed for 0.5 mL O/W moisturiser, its depletion rate (reflected by the slope of ETI trace, median = 6.94 $\Omega$/min; Fig. 3.8(b)) is close to that of 0.5 mL deionised water (median = 7.16 $\Omega$/min), raising concerns regarding its long-term usability.

A trade-off exists between the type of moisturiser and its applied volume. In real-life scenarios, particularly for older patients, body moisturisers may be applied before wearing the TEs-integrated garment prior to the scheduled therapeutic session. An amount of 0.5 mL or less of W/O moisturiser

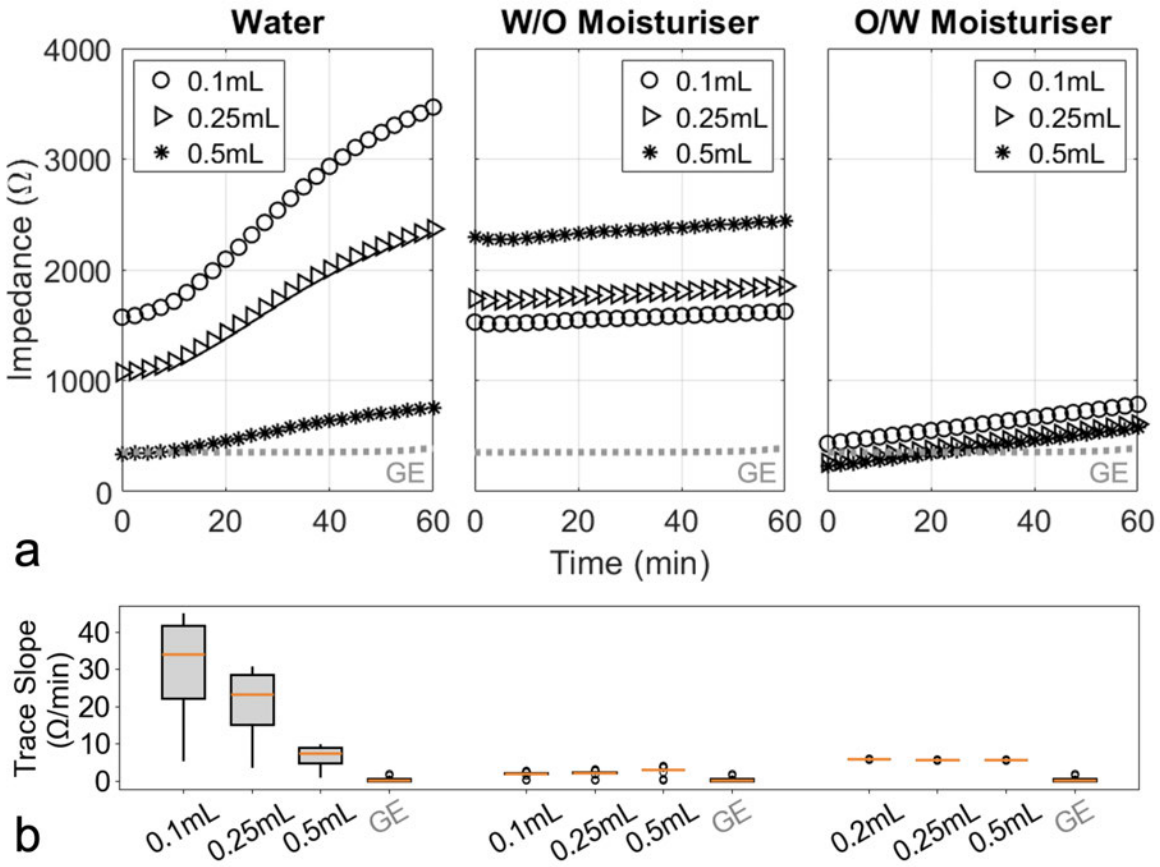


Fig. 3.8. (a) Change in TE ETI under different electrolyte conditions over time, with GE ETI shown as a reference (grey dotted lines) [73]; (b) Slope of ETI traces.

appears suitable in such cases, as it results in a reasonable baseline impedance and maintains a relatively low growth rate of ETI over time. In subsequent sections, the term "body moisturiser" or simply "moisturiser" refers specifically to the W/O moisturiser.

### 3.3.2 Result of EMG Recording

The evoked EMG responses recorded from each participant are presented in Fig. 3.9(a)–(d). These responses were elicited by electrical stimulation with intensities ranging from 10 to 34 mA, incremented in steps of 8 mA. For Participant 1, stimulation was terminated at 24 mA as the reported maximum threshold limited the maximum stimulation intensity during the session.

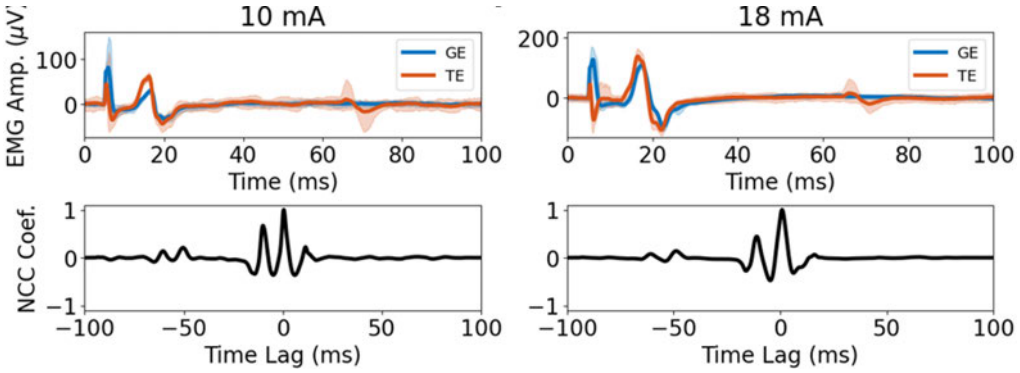


(a) Participant 1.

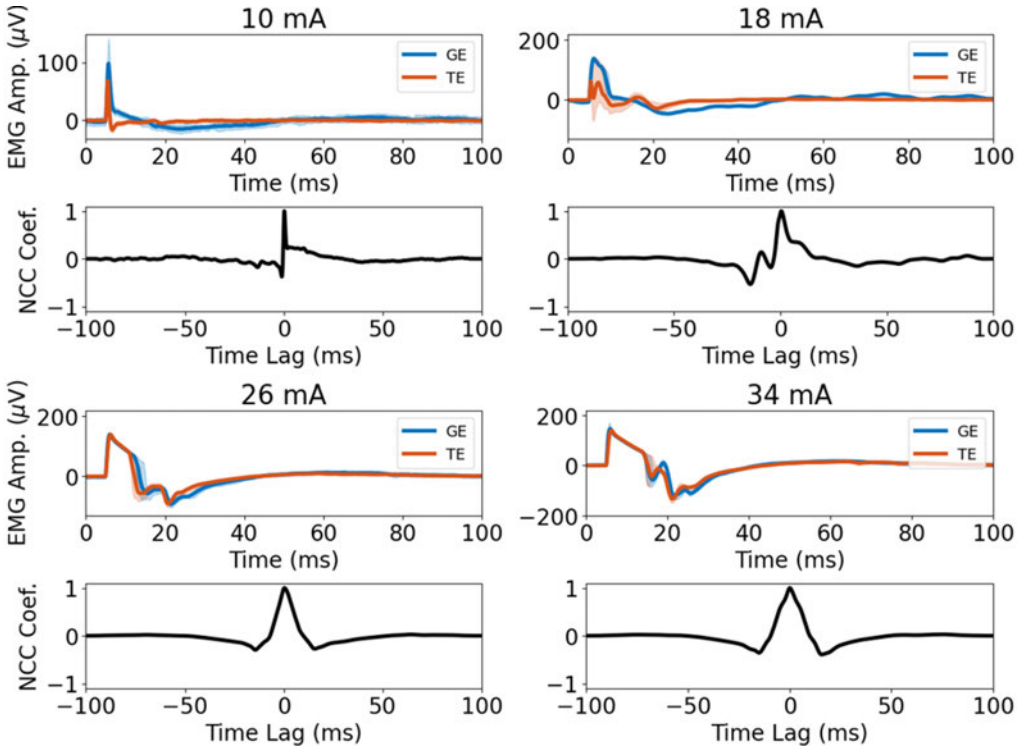


(b) Participant 2.

Fig. 3.9. EMG responses and its corresponding NCC values of all four participants. Abbreviations: Amp. – Amplitude; Coef. – Coefficient; GE – gel electrode; TE – textile electrode.

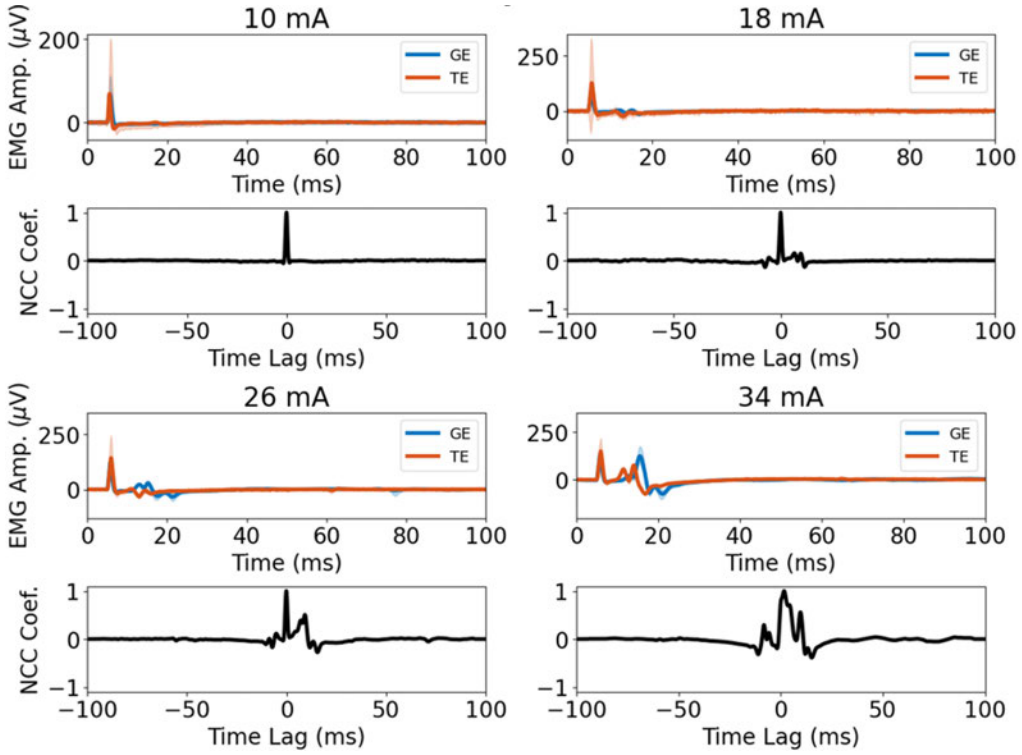


(c) Participant 3.

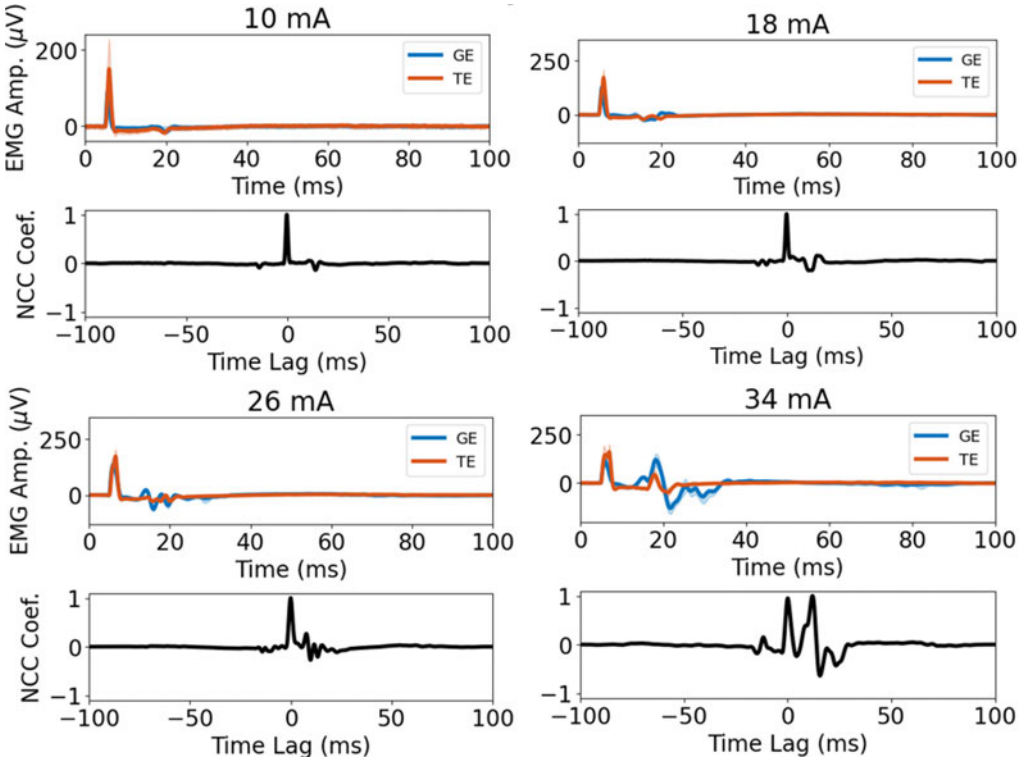


(d) Participant 4.

Fig. 3.9. Continued.

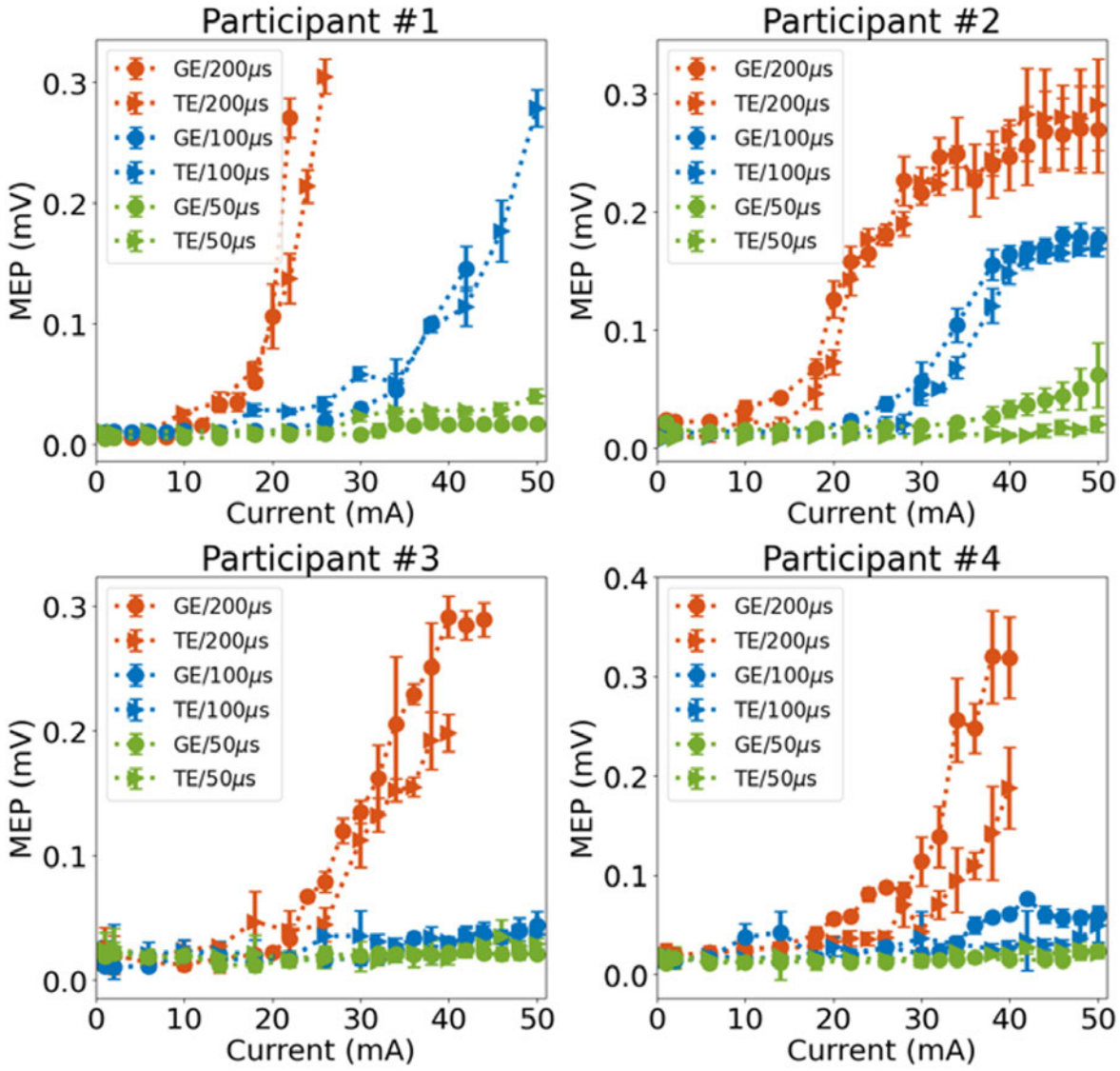


Fig. 3.10. Calculated MEP curves of all four participants.

All plots exhibit an initial peak, typically identified as a stimulation artifact, which appears immediately after the onset of electrical stimulation. Following a latency of a few milliseconds, evoked responses (referred to as M-waves) were observed across all four participants, particularly at stimulation intensities above 18 mA. The presence of M-waves confirms effective tibial nerve recruitment achieved through both TEs and GEs. The solid lines in the plots represent the mean value of multiple data slices, while the shaded regions indicate the tenth to 90th percentile range. A broader spread of data was observed in responses elicited using TEs, likely due to slight electrode movement during the stimulation.

The NCC subplots (displayed beneath the EMG traces) demonstrate that the correlation coefficient approaches unity, indicating a high degree of similarity between the evoked EMG traces at zero time lag. This finding demonstrates that TEs with body moisturiser as an electrolyte would effectively stimulate the tibial nerve, comparable to GEs.

The MEP (or recruitment) curves are shown in Fig. 3.10. For different pulse width conditions, the curves exhibit visually similar trends across all four participants. Despite variations in maximum threshold among participants, likely due to their physiological differences, typical sigmoidal curves were observed from the Participant 2. This observation further confirms that the feasibility of TEs during TTNS.

## 3.4 Limitations

The primary limitation of this study is the small sample size of participants. Furthermore, the inclusion criteria for participant recruitment should be adjusted to exclude individuals with sensitive skin, as their lower maximum threshold may result in data outliers. Another concern is the potential mismatch in TE positioning, as this could vary the ETI during stimulation and further affect the EMG recording. To address this, applying an external pressure to the TEs may be necessary in future studies.

## 3.5 Conclusion

This study demonstrates that the cotton-filled TE prototype, when combined with a body moisturiser, can exhibit electrical performance comparable to standard GEs and may offer certain advantages under specific conditions. The comparable evoked EMG responses and MEP curves indicate that TEs are a

feasible option for TENS applications including TTNS used for OAB management. Moreover, the soft and comfortable nature of TEs makes them suitable for integration into wearable garments, such as socks. Miniaturising the relatively large electrical stimulator to accommodate a TE-embedded wearable could provide a user-friendly solution for managing OAB, offering potential benefits for older patients.

# Chapter 4

# Wearable TENS Device

Overactive bladder (OAB) syndrome is a prevalent condition that significantly impacts patients' lives. Transcutaneous tibial nerve stimulation (TTNS) has emerged as a modern treatment modality that is non-invasive, safe, and effective, enabling home-based management of these urinary symptoms. TTNS offers a cost-effective alternative to conventional therapeutic methods, including medication and invasive neuromodulation.

A Bluetooth-enabled transcutaneous electrical nerve stimulation (TENS) device was developed specifically for TTNS to support home-based OAB management. The system comprises a designed miniaturised stimulator (named TENS*mini*) integrated into a wearable garment such as a sock featuring silver-fibre-knitted conductive textile electrodes (TEs). Compared to other clinical stimulators (Chapter 2, Section 2.2.1), this wearable design offers better compactness, improved safety and usability.

## 4.1 Wearable Textile Electrodes

To ensure precise electrode positioning during stimulation, the design integrates two TEs into a specially engineered sock (Yoga Flow Nana, Knitido). Unlike typical socks that may shift during the use due to variable fit and orientation, this sock employs anchor points around the toes and heel parts to secure it on the foot. A schematic representation of this design is provided in Fig. 4.1.

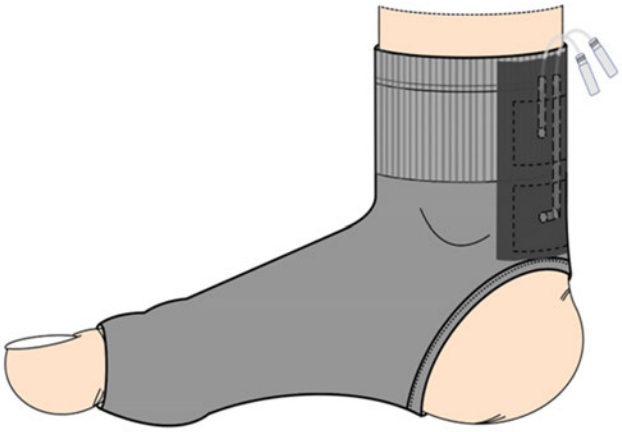

Fig. 4.1. Overview of a TEs-integrated wearable garment (based on a yoga sock).

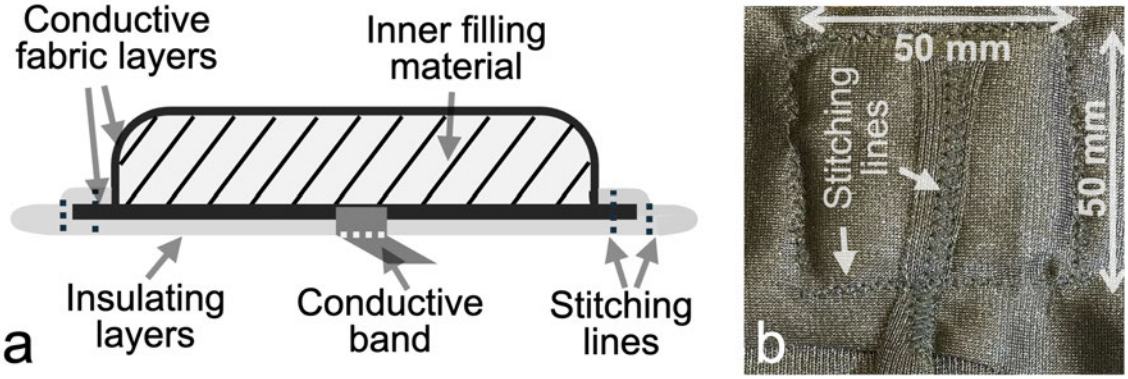


Fig. 4.2. (a) A cross-sectional view of the embedded TE; (b) A exterior view of the fabricated TE showing the surface stitching pattern and dimensions ($50 \times 50\,\mathrm{mm}^2$). The stitching lines secure the interior and exterior textile layers and establish the interconnection between the exterior-side textile and the conductive band.

Each TE was fabricated by layering two pieces of conductive fabric stitched together with an intermediate soft material (i.e., a piece of natural cotton) layer, as illustrated in Fig. 4.2(a). A *zigzag* stitching pattern (Fig. 4.2(b)) was employed to improve the connection between the soft conductive band and the TE bottom conductive fabric layer. The assembly process utilised a stitching machine (B380, Bernina).

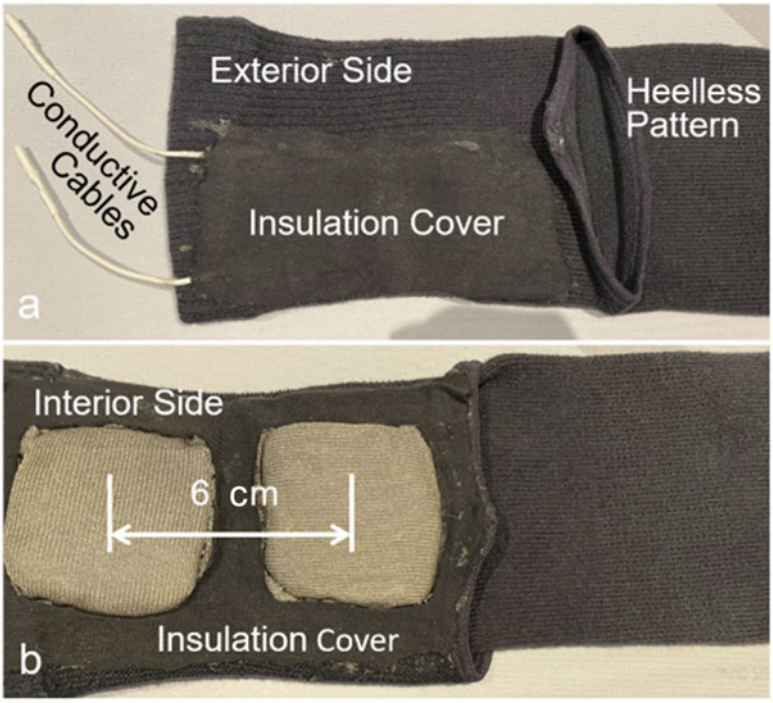


Fig. 4.3. (a) The exterior and (b) interior view of the implemented yoga-sock-based TEs.

Compared with the previous TE prototype (Chapter 3, Section 3.1), both central metal connectors have been replaced with flexible conductive bands composed of conductive textile. This modification was implemented because the metal connectors were challenging to encapsulate and could cause user discomfort during wear. For laboratory testing, the opposite end of these conductive bands was initially connected with conductive cables.

The dimension of each TE was adjusted to 40 $\times$ 40 mm$^2$ and the centre-to-centre separation distance between the two TEs was amended to 6 cm to accommodate the size constraints of the sock leg portion. Both electrode separations (i.e., 6 and 10 cm) are reported in clinical protocols for TTNS [187], [195], [196]. Although no comparative research has directly examined the impact of electrode separation distance on the therapeutic effectiveness of TTNS for OAB management, it is hypothesised that a between-electrode distance of 6 cm remains sufficient during TTNS with no significant difference in tibial nerve activation.

Two TEs were affixed to the interior side of the sock using fabric glue (5060774887240, D.A.Y. Republic). Conductive bands (fabricated from the same textile material and cut into band shapes) were positioned on the exterior side and encapsulated with a general-purpose elastic fabric that serves as an insulation cover. The appearance of this yoga-sock-based wearable is depicted in Fig. 4.3.

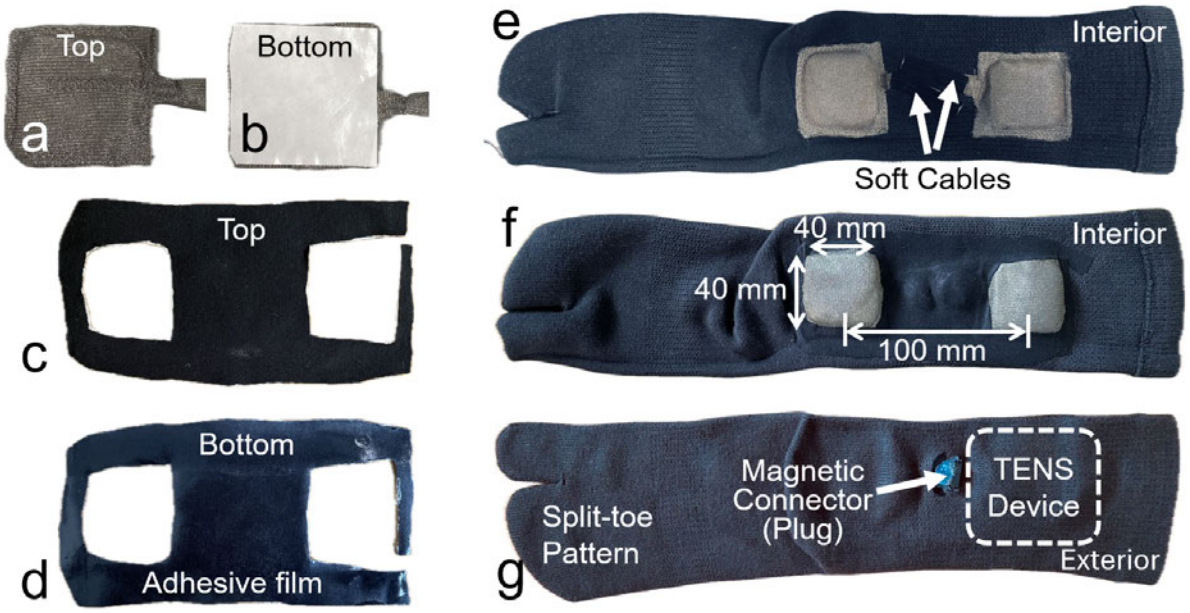


Fig. 4.4. (a) Top view of the textile electrode; (b) Bottom view of the textile electrode with the adhesive film applied, prior to removing the protective cover; (c) Top view of the elastic insulating layer; (d) Bottom view of the adhesive insulation layer after the protective cover has been peeled off; (e) Interior view of the split-toe sock before encapsulation, showing the placement of the soft cables; (f) Interior view of the encapsulated split-toe sock, with exposed electrodes measuring $40 \times 40$ mm$^2$ and separated by a distance of 100 mm (or 10 cm); (g) Exterior view of the split-toe sock, featuring a plug-type magnetic connector mounted to interface with an external electronic device.

Despite demonstrating the potential feasibility of the TEs-embedded yoga sock, several limitations were identified. The toeless and heelless design, originally intended to mitigate potential sock movement and improve electrode placement, was reported as difficult to wear by participants during pilot testing. This difficulty may be attributed to the inherent design of the yoga sock, which became increasingly challenging to align with the toe openings at the front of the yoga sock following the integration of the TEs.

The limited length of the sock's leg portion also restricted the recommended electrode separation distance (e.g., 10 cm [187], [188]). The reduced separation distance may cause a potential risk of short-circuiting between TEs. To address these issues, the original yoga sock was replaced with another sock (Tabi Midcalf Sock, Knitido). This sock was manufactured similarly to a conventional sock but featured a separation between the big toe and the other toes, facilitating correct self-identification of foot placement and improving electrode positioning compared to standard socks.

To attach the TEs to the sock, a polyurethane adhesive film (3206, Bemis) was applied to the back of each TE, and a hot press was used to secure them to the interior side of the sock. This adhesive film was chosen for its stretchable property compared to the rigidity of dried textile glue, enabling the sock to maintain its natural elasticity during use. The detailed breakdown of this TEs-embedded split-toe sock is illustrated in Fig. 4.4(a)–(g).

Furthermore, a pair of magnetic pogo-pin connector (MG03254x, Shenzhen Yiwei Technology) was incorporated to replace conductive cables, thereby interfacing the conductive TEs (embedded within the split-toe sock) with the proposed electronic device. The plug part of the magnetic connector was secured to the exterior of the sock using hot-melt adhesive, while the receptacle part was soldered on the hardware board of the electronic device. This wearable electrode design permits the sock to be worn unobtrusively and hand-washed like other garments when the electronic device is disconnected. The magnetic connector also ensures a fast and reliable connection between electrodes and the device, potentially improving the overall usability.

## 4.2 Hardware Design

### 4.2.1 Overview

There are three different functional modules in the proposed system: (1) A stimulation (STIM) module consisting of a 32-bit microcontroller unit (MCU) (STM32L433, STMicroelectronics) for central control, an isolated drive circuit (or output stage) and an electrodes detection circuit; (2) A power management module including a battery charger integrated circuit (IC) (BQ21040, Texas Instruments), a low-dropout (LDO) regulator IC (ADP7142, Analog Devices) and a boost converter IC (TPS61088, Texas Instruments); and (3) a Bluetooth® module (BT-11, Shenzhen DX Bluetooth). A graphical overview of the entire hardware system is illustrated in Fig. 4.5, detailing the connection between the hardware board and the TEs-embedded wearable garment (i.e., a split-toe sock) through a pair of magnetic connectors. The full schematic of the hardware and relevant bill of material can be found in Appendix B and B.5, respectively.

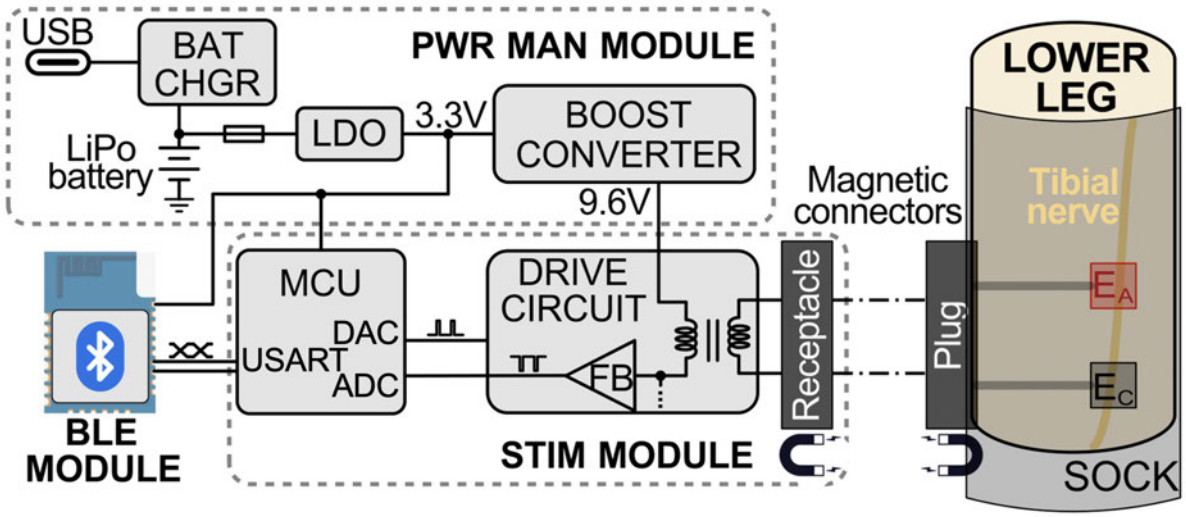


Fig. 4.5. A block diagram of the entire wearable system [75]. Abbreviations: ADC – analogue-to-digital converter; BAT CHGR – battery charger; BLE – Bluetooth® low energy; DAC – digital-to-analogue converter; LDO – low-dropout (regulator); LiPo – lithium polymer; FB – feedback; PWR MAN – power management; STIM – stimulation; USART – universal synchronous/asynchronous receiver/transmitter.

### 4.2.2 Stimulation Module

The stimulation module is an essential component of the proposed TENS device, as depicted in Fig. 4.5. To prevent leakage current, a continuous isolation between the patient and the electronic circuit, including battery-powered systems, is compulsory [129], [136]. Implementing galvanic isolation in medical equipment requires high-integrity isolation components and robust insulating barriers, such as clearance spaces on printed circuit boards (PCBs) or air gaps between the metal pins of ICs.

#### Determination of Methods for Galvanic Isolation

Commonly used isolation components include capacitors (which leverage electric fields), transformers (which utilise magnetic flux), and optocouplers (which rely on light transmission). However, uncertainty remains regarding the optimal option for this design. Accordingly, all three isolation options were evaluated during the design process, and the selection criteria for the final isolation component are detailed below.

**Isolation by Capacitor:** Capacitive isolation is widely used to prevent direct current (DC) flow between circuits while permitting the passage of alternating current (AC) signals. This approach is particularly advantageous in applications such as signal conditioning and data transmission, where it mitigates ground loops and unwanted current paths that could lead to equipment malfunction or damage. However, the performance of capacitive isolation diminishes at lower frequencies due to significant attenuation of low-frequency AC signals, thereby limiting its suitability for applications such as 20 Hz TTNS.

Another inherent limitation of capacitive isolation is its dependency on the capacitor's voltage rating, which defines the maximum isolation voltage. Exceeding this voltage rating may compromise capacitor integrity and introduce safety risks in high-voltage scenarios [197], as encountered in TENS applications. For example, generating a 50 mA pulsed current across a 2 kΩ load requires approximately 100 V across the load. High-voltage capacitors, such as aluminium electrolytic capacitors, can typically withstand several hundred volts, thereby addressing some of these high-voltage challenges [198]. To evaluate the feasibility of capacitive isolation in the proposed design, a simulation-based approach was implemented.

**Isolation through Optocouplers:** In the proposed design, the use of optocouplers would require an additional high-voltage power supply on the secondary (user) side to satisfy isolation requirements. This necessity would introduce a secondary battery and its associated power management circuitry, thereby increasing the complexity, cost, and physical dimensions of the device. Consequently, as optocoupler-based isolation is generally reserved for applications with less stringent size constraints (e.g., multi-channel neuromuscular or functional electrical stimulators (NMES/FES)) [115], [160]), it was not implemented in this design.

**Isolation via Transformers:** In TENS devices, transformers can serve as the isolation mechanism within the drive circuit by employing a step-up transformer. This transformer employed in the drive circuit could elevate the secondary voltage to the required compliance level, thereby enabling the delivery of a constant pulsed current through the electrode-tissue impedance (ETI). Based on the limitations of capacitive isolation (Chapter 5, Section 5.1) and unsuitability of optocoupler implementation, the transformer isolation is deemed the only viable option.

Despite the electrical advantages offered by transformers, their relatively large form factor poses significant challenges to the size and portability of electronic devices. Given the wide variety of PCB-mounted transformers available in the market, it is necessary to investigate the underlying physical parameters that influence these characteristics. Accordingly, the following analysis is conducted prior to finalising the transformer selection.

In transformers, the magnetic field generated by the primary and secondary coils plays a crucial role. The inductance arising from the flux coupling between these coils is known as mutual inductance ($M$), which for coupled coils is determined by

$$M = K\sqrt{L_P L_S} \tag{4.1}$$

where $K$ denotes the coupling coefficient varying between 0 and 1, and $L_P$ and $L_S$ represent the self-inductance of the primary and secondary windings, respectively.

Calculating the precise winding (or self-) inductance of a coil with complex geometry can be challenging. To simplify the calculation, a basic configuration of coil windings was considered, where both coils of the transformer are wound on opposite sides of a toroidal core [199]. To this end, the winding inductance of each coil is given by

$$L = \frac{N^2 A_c \mu_c}{l_F} \tag{4.2}$$

where $N$ indicates the number of turns on winding, $A_c$ denotes the cross-sectional area of the core through which the magnetic flux flows, $\mu_c$ presents the core's permeability, and $l_F$ depicts the length of the flux path within the core. Since the values of $A_c$, $\mu_c$ and $l_F$ are determined by the core's geometry and its physical properties, the self-inductance of the primary and secondary coils primarily depends on the number of turns. However, these parameters are typically not disclosed in the datasheets of most commercially available transformers. Consequently, a simulation-based approach was employed to investigate how variations in winding inductance affect the shape of the stimulation pulse, as illustrated in Chapter 5, Section 5.2.

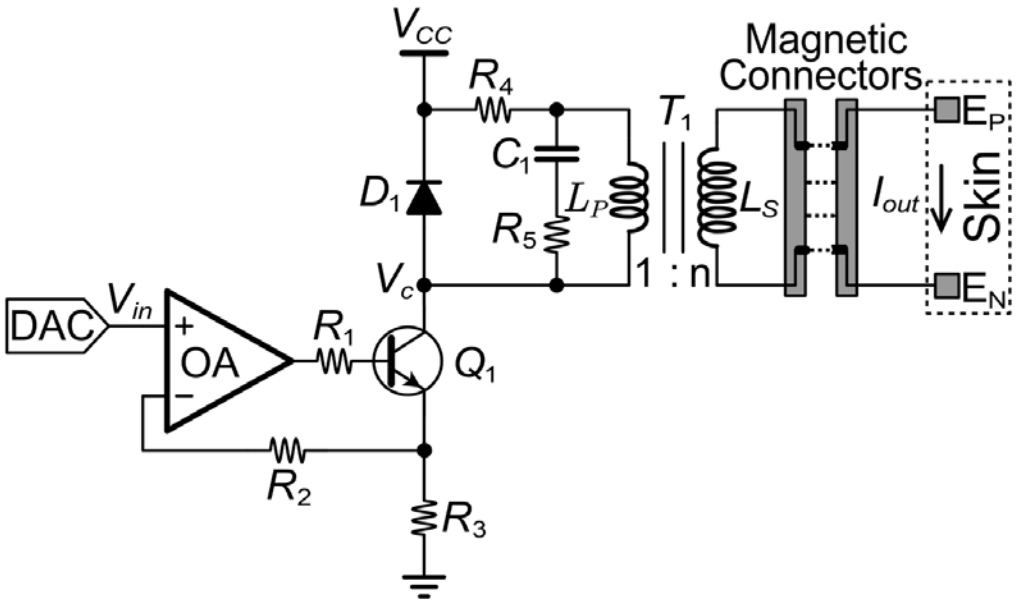


Fig. 4.6. A transformer-isolated drive circuit. Abbreviations: DAC – Digital-to-analogue converter; OA – operational amplifier.

### Transformer-isolated Drive Circuit

In conventional TENS devices, the drive circuit represents the final stage that directly interfaces with the skin and tissue via leads and electrodes [200]. A step-up transformer was incorporated into the design. This type of transformer facilitates the generation of the high secondary voltage required across the connected load (e.g., ETI) while ensuring a constant current flow. The transformer-isolated drive circuit implemented in the proposed hardware is based on a voltage-to-current conversion principle [201], as illustrated in Fig. 4.6.

In this circuit, the current on the primary side is regulated by the non-inverting terminal of an operational amplifier, which controls a bipolar junction transistor. The controllable and frequent switching of this transistor facilitates the transfer of current to the secondary winding of a transformer. Consequently, the transconductance gain ($g_m$) of this drive circuit is defined as:

$$g_m = \frac{I_{out}}{V_{in}} = \frac{1}{nR_3}\left(\frac{h_{FE}}{h_{FE}+1}\right) \tag{4.3}$$

where $h_{FE}$ represents the forward current transfer ratio.

Moreover, an RC snubber, comprising $R_5$ and $C_1$, was specifically implemented on the primary side of the transformer. This configuration could suppress voltage overshoots transferred from the secondary side during electrostatic discharge events caused by inadvertent user contact with the magnetic connector pins while the device is not in use [202].

### Electrode Disconnection Detection Circuit

Loose contact between the electrodes and the skin surface can significantly increase the ETI or even cause an open secondary circuit [203]. In such cases, parasitic capacitance may induce voltage build-up on the floating secondary, potentially exceeding insulation limits and posing safety risks in users [163]. Consequently, automatic detection of electrode connectivity is essential for ensuring system reliability and users safety.

To support this functionality and enable further circuit analysis (Fig. 4.6), the isolated transformer is modelled, for simplicity, as an ideal transformer (turns ratio = $1:n$) with perfect magnetic coupling ($K = 1$). The interaction between the primary and secondary sides is described by the following set of equations.

$$\begin{cases} V_{CC} - V_C - I_P R_4 = \dfrac{I_{out} Z_{Load}}{n} & (4.4) \\ I_P = n I_{out} & (4.5) \\ V_C = V_{in} + V_{CE} & (4.6) \end{cases}$$

where $V_C$ denotes the voltage measured at the collector terminal of the BJT, which is used to detect electrode disconnection on the secondary (user) side; $n$ represents the inverse of the conventional transformer turns ratio, defined here as the number of turns on the secondary winding per turn on the primary winding; $I_P$ is the current flowing through the primary side of the transformer; $Z_{Load}$ refers to the load impedance connected to the secondary side; and $V_{CE}$ is the collector-emitter voltage of the BJT.

By combining the relationships expressed in Equations (4.3)–(4.6), a unified expression is derived to describe the dependence of $V_C$ on the output load ($Z_{Load}$), as given by,

$$V_C = V_{CE} + \frac{n(V_{CC} - V_{CE})}{g_m Z_{Load} + n^2 g_m R_4 + n} \tag{4.7}$$

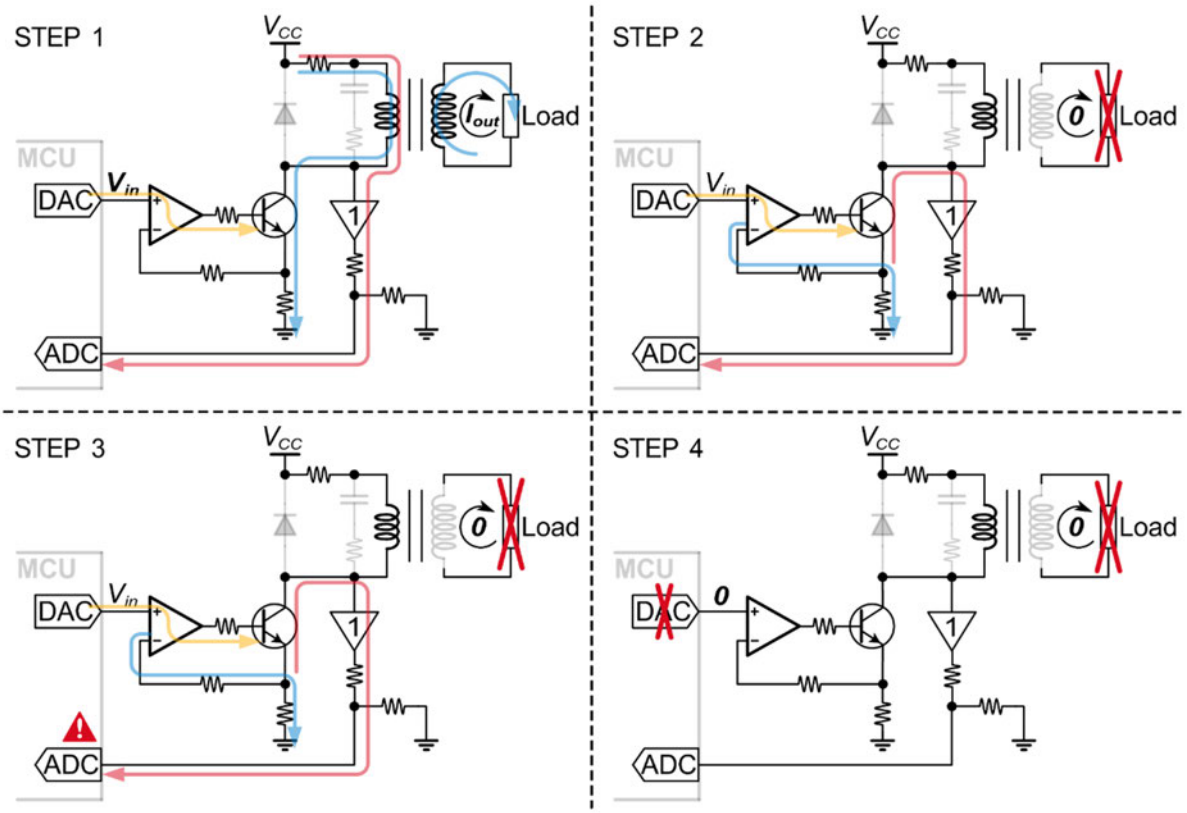


Fig. 4.7. Mechanism of electrodes connection detection. Abbreviations: ADC – analogue-to-digital converter; DAC – digital-to-analogue converter; MCU – microcontroller unit.

As the output load impedance ($Z_{Load}$) approaches infinity (open-circuit condition), the denominator in Equation (4.7) increases substantially, causing the collector voltage ($V_C$) to asymptotically approach the collector-emitter voltage ($V_{CE}$). This behaviour reflects an inverse relationship between $V_C$ and $Z_{Load}$.

To enable real-time monitoring of variations in $V_C$, a 12-bit built-in analogue-to-digital converter (ADC) was configured to continuously sample the collector voltage. A graphical illustration of this detection mechanism is provided Fig. 4.7, and the complete functional flow is outlined as follows.

- **Step 1:** During normal operation, the voltage $V_C$, measured at the collector of the BJT, is scaled down to a range of 0–3.3 V using a buffer and a voltage divider. This voltage is continuously monitored by a built-in ADC.
- **Step 2:** In the event of an electrode disconnection in the secondary circuit, the load current ceases, leaving only the low magnetising current in the primary winding. Although the BJT

remains active due to the applied base drive, the collector-emitter voltage ($V_{CE}$) decreases to a low value, indicating operation near saturation. Given that the emitter voltage ($V_E$) of BJT could be referenced to ground due to the near-zero current flowing through the primary side, the collector voltage ($V_C = V_{CE} + V_E$) also assumes a correspondingly low value.

- **Step 3:** At this moment, the small value of $V_C$ falls below the firmware-defined voltage threshold (0.9 V), leading to an interrupt event triggered by the ADC.
- **Step 4:** Upon detecting the interrupt events by the MCU, the built-in digital-to-analogue converter (DAC) peripheral is stopped, preventing generation of the input control pulses to the drive circuit in order to halt the stimulation.

### 4.2.3 Feasibility of Lithium Battery

In TENS applications that typically require a higher instantaneous supply current, 9 V alkaline batteries continue to be utilised in certain portable stimulators, such as the NeuroTrac® Continence [63] and TPN 200 Premier Plus [64]. However, most alkaline batteries are non-rechargeable and exhibit a bulky form factor [204], which poses a constraint on the compactness and lightweight requirements of wearable TENS devices. While nickel-metal hydride batteries serve as a rechargeable alternative, their energy density remains lower, and their physical dimensions are comparable to alkaline batteries, further limiting their suitability for wearable TENS devices [204].

To address these limitations, lithium-based battery technologies, such as lithium-ion (Li-ion) and lithium-polymer (LiPo) batteries, have emerged as the preferred choice due to their high energy-to-weight ratio, extended cycle life, and versatile form factors, making them well-suited for medical wearable [205]. While Li-ion batteries offer a higher energy density and longer lifespan, LiPo batteries provide greater mechanical flexibility and improved safety, offering them advantageous for small and thin device enclosures [206].

Despite these benefits, manufacturer datasheets often lack comprehensive information on the dynamic performance of LiPo batteries, particularly the details of maximum supply current. Therefore, an experimental analysis was performed to evaluate their feasibility as a front-end power source for a

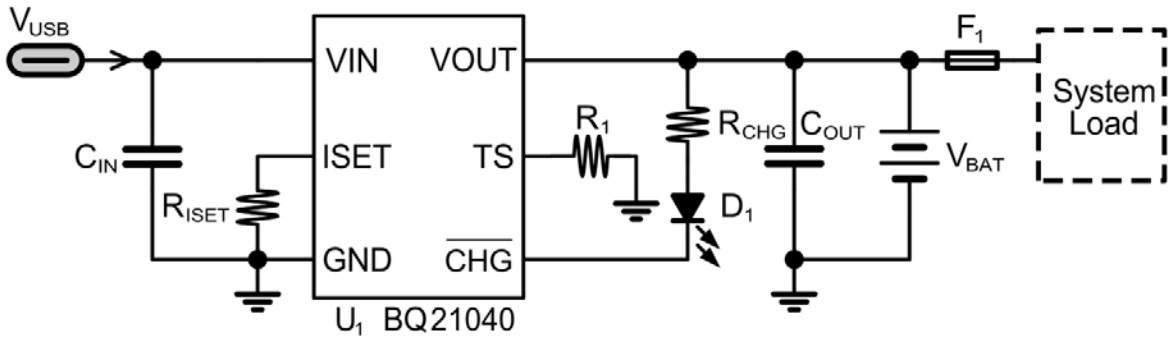


Fig. 4.8. A battery charger IC (BQ21040) and its peripheral passive components.

boost converter, potentially serving as a replacement for the conventional 9 V alkaline battery. The measurement methodology and experimental results are presented in Chapter 5, Section 5.4.

### 4.2.4 Power Management Module

#### Battery Charger

In accordance with the feasibility of using a 300 mAh LiPo battery (LP-402933-IS-3, BAK Technology), a battery management IC (BQ21040) was implemented to enable re-chargeability, providing a regulated charging function via a USB Type-C interface under a 5 V, 100 mA charging condition. The schematic of this charging module is illustrated in Fig. 4.8.

The charging current was configured using a resistor connected to the *ISET* pin, determined by [207],

$$R_{ISET} = \frac{K_{ISET}}{I_S} \tag{4.6}$$

where $K_{ISET}$ is fast-charging current factor (typically 540 A Ω for 0.06–1 A) [207]. In this design, a 5.1 kΩ $R_{ISET}$ was chosen to provide approximately 100 mA constant charging current.

Lithium battery manufacturers typically recommend 0–45 °C for charging and –20 to 60 °C for discharging [208]. The BQ21040 integrates a 50 µA internal current source, requiring a 10 kΩ negative temperature coefficient (NTC) thermistor ($R_1$) at the *TS* pin to enable temperature sensing. The thermistor's behaviour is characterised by its $\beta$ value, defined as [207]:

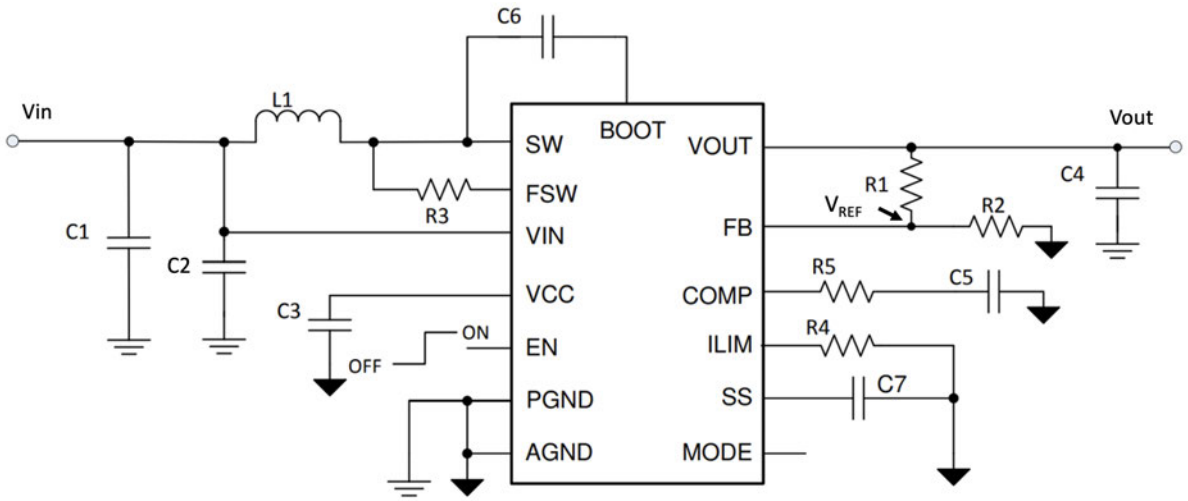


Fig. 4.9. A typical application circuit for boost converter IC (TPS61088) [209].

$$\beta = \frac{ln\left(\frac{R_{T1}}{R_{T2}}\right)}{\frac{1}{T_1} - \frac{1}{T_2}} \tag{4.7}$$

where $R_{T1}$ and $R_{T2}$ are resistances of the thermistor at temperatures $T_1$ and $T_2$ respectively. From the datasheet [207], the internal voltage thresholds at 45 °C and 0 °C are 260 mV and 1.28 V, respectively. Given the 50 µA current source, a thermistor ($R_1$) should be in the 5.2–25.6 kΩ range, yielding a $\beta$ of 3078.16 K. Accounting for a ±10% tolerance in resistance, a 10 kΩ thermistor with 3380 K (for $\beta$) was selected, and its derivations are detailed in Appendix A.

### Boost Converter

To maintain a stable supply voltage of 9 V, equivalent to that of an alkaline battery, a high-power-density synchronous boost converter (TPS61088) was employed to step up the 3.7 V output from a LiPo battery, providing a more compact and lightweight power solution. A typical application circuit recommended by the datasheet [209] is illustrated in Fig. 4.9.

Since inductor current ripple could introduce input-voltage fluctuations, particularly when parasitic inductance and resistance exist between *VIN* pin and inductor $L_1$, an adequate input capacitance is necessary to keep the voltage ripple below 100 mV. To this end, a 10 µF ceramic capacitor ($C_1$) is

typically adequate for most applications [209]. A 100 nF ceramic capacitor ($C_2$) was also placed near the *VIN* pin to minimise supply ripples and radio frequency interference.

The output voltage ($V_{out}$) was regulated by an external resistor divider consisting of $R_1$ and $R_2$, given by

$$V_{OUT} = \left(1 + \frac{R_1}{R_2} \cdot V_{REF}\right) \tag{4.8}$$

where $V_{REF}$ is the 1.2 V reference at the *FB* pin [209]. The switching frequency $f_{SW}$ can be programmed within 0.2–2.2 MHz by adding a resistor between *FSW* and *SW* pins [209]. In this design, a switching frequency of 600 kHz was selected, and the required $R_{FSW}$ was calculated by [209]:

$$R_{FSW} = \frac{4 \cdot \left(\frac{1}{f_{SW}} - t_{DELAY} \cdot \frac{V_{out}}{V_{in}}\right)}{C_F} \tag{4.9}$$

where $t_{DELAY}$ = 89 ns and $C_F$ = 23 pF are manufacturer-specified. Details on configurations of other pins are documented in [209].

#### LDO Regulator

The ADP7142 is characterised by its low quiescent current and operates as an LDO regulator across a 2.7–40 V input range, supplying up to 200 mA. In accordance with the datasheet guidelines [210], two 2.2 µF ceramic capacitors were placed at the *VIN* and *VOUT* pins (Fig. 4.10) to enhance transient response performance. To achieve a regulated constant 3.3 V supply for the MCU and Bluetooth module, the 3.3 V variant of the IC was selected.

## 4.3 Other Safety Considerations

### 4.3.1 Short-circuit Protection and Fault Prevention

To minimise the risk of short circuits, a 1 A fast-acting fuse is integrated between the power switch and the battery. Furthermore, a watchdog timer is implemented to continuously monitor system operation,

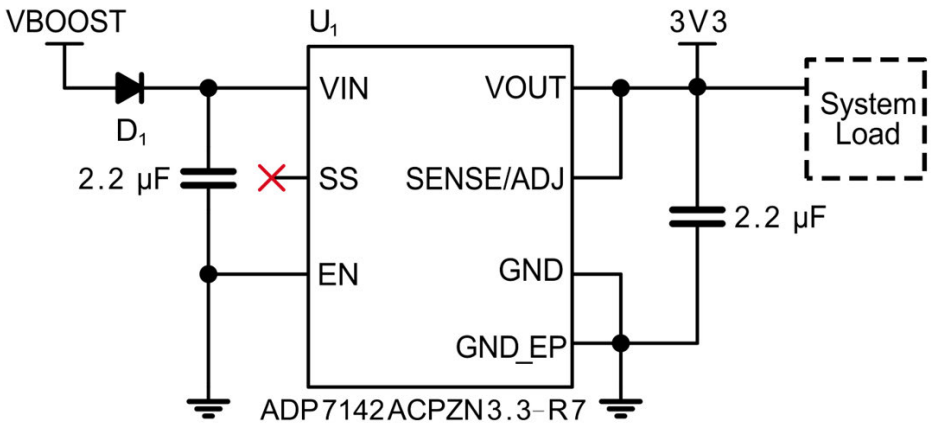


Fig. 4.10. A typical application circuit of LDO IC (ADP7142) [210].

enabling automatic reset in the event of a malfunction. These measures collectively enhance the stability and safety of the system.

### 4.3.2 Visual Indication

The visual indication in medical devices plays a key role in conveying essential information about the device's operational status and functionality. In this design, four light-emitting diodes (LEDs) are utilised as visual indicators, enabling the observation of the status of system through the device enclosure. The specific indications provided by these LEDs are detailed in Table 4.1.

## 4.4 Firmware Development

### 4.4.1 Overview

The firmware development process is critical to ensuring the reliable operation of electronic systems. The use of flowcharts prior to coding is beneficial as it provides a clear visualisation of the sequence of operations. Fig. 4.11 illustrates the sequential steps involved in the system's operational process for initiating stimulation.

Table 4.1. Description of LED indications.

| LEDs | Colour | Description of indication |
|---|---|---|
| LED 1 | Green | Device is powered on. |
| | Red/Off | Red: Battery charging in progress; Off: Battery fully charged. |
| LED 2 | Green | Electrical stimulation operating under normal conditions. |
| | Flash Red | Emergency stop activated. |
| LED 3 | Red | Overload detected ($> 10\,\text{k}\Omega$) or secondary circuit is open. |
| LED 4 | Green | BLE connected. |
| | Off | BLE disconnected. |

The process begins with system initialisation, followed by checks for Bluetooth connectivity and electrode connections. Upon successful verification of these conditions, stimulation parameters, including intensity, frequency, and pulse width are able to be controlled wirelessly using a mobile device. Conversely, if any condition check fails, the stimulation process will be halted and initialised.

### 4.4.2 Configuration of Standard MCU Peripherals

The utilised MCU peripherals are presented in Table 4.2. The detailed setups of these peripherals are described in the following context.

#### Direct Memory Access (DMA)

Multiple channels of the built-in direct memory access (DMA) were configured to streamline data transfer between memory and other peripherals. Two DMAs were employed in the system. The first DMA was assigned two channels: one for the universal synchronous/asynchronous receiver/transmitter (USART)

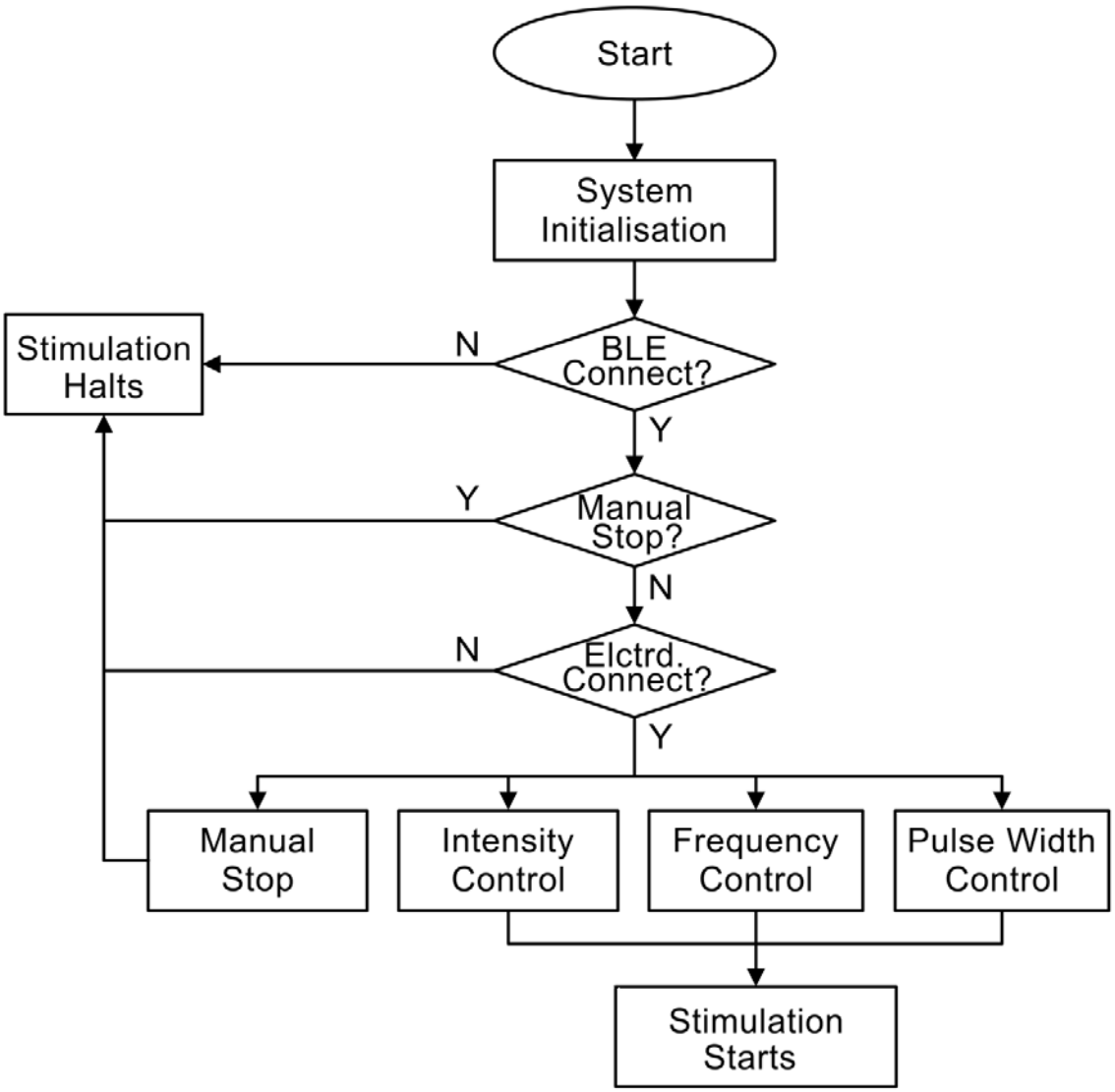


Fig. 4.11. A flowchart of the firmware development. Abbreviation: Elctrd. – electrode.

to support serial communication, and another for the DAC to enable continuous data conversion. The second DMA was allocated to the ADC to optimise real-time data acquisition.

### General-purpose Input/Output (GPIO)

The general-purpose input/output (GPIO) pins were primarily set up in "Output Push-Pull" mode to drive external LEDs, providing visual indication on system status. To reduce system energy consumption, unused GPIO pins were configured as "Analogue Input".

Table 4.2. Selected MCU peripherals.

| System Core | Analogue | Timer | Connectivity |
|---|---|---|---|
| DMA | ADC1 | TIM2 | USART1 |
| GPIO | DAC1 | TIM6 | USART2 |
| NVIC | | | |
| RCC | | | |
| SYS | | | |

### Nested Vectored Interrupt Controller (NVIC)

The nested vectored interrupt controller (NVIC) managed all system interrupts, ensuring prompt responses to events such as data conversion through the ADC or DAC, as well as data transmission and reception via USART. In this configuration, the "Global Interrupt" was enabled exclusively for the ADC.

### Reset and Clock Controller (RCC)

The reset and clock controller (RCC) was configured to distribute clock sources to various peripherals. The high-speed external (HSE) clock was set to 8 MHz, while the low-speed external (LSE) clock was configured to 32.768 kHz.

### System Debugging Interface

The system peripheral (SYS) in the MCU is a crucial component for system-level operations and debugging. Serial wire debug (SWD) interface was configured for system debugging. To this end, a debugging tool such as ST-Link V2 (STMicroelectronics, Switzerland) was used to interact with the MCU via this SWD interface to monitor and modify system state in real time.

#### ADC and DAC

The built-in ADC was set up in Single-ended mode for single-channel conversion. Its clock source was configured to operate in Asynchronous mode with a division factor of 10, and Timer (TIM) 2 was used to trigger each conversion, ensuring synchronised sampling. Similarly, the DAC output was configured to deliver analogue control signals to a GPIO with the Output Buffer disabled and was triggered by TIM 6.

#### Timers

As previously stated, timer (TIM) 2 was configured to trigger the ADC, with its pre-scaler and counter registers set to 99 and 7, respectively. Additionally, TIM 6 was employed to trigger the DAC, which provided input control signals to the drive circuit. The pre-scaler and counter register values for this configuration can be adjusted wirelessly through a mobile application, enabling amendment of the stimulation parameters.

#### USART

The USART was configured to facilitate communication between the MCU peripherals, such as the DAC, and the BLE module.

### 4.4.3 Summary

Based on the configuration of these peripherals, the firmware was developed using an open-source software STM32CubeIDE (STMicroelectronics, Switzerland). The pinout of the MCU and programming codes are provided in the Appendix B.

## 4.5 Wireless Control

The TENS*mini* device incorporates Bluetooth® connectivity, enabling wireless control via mobile devices. A typical Android application (BLE debugging assistant v2.4.2, Shenzhen Pixel LD Technology) was

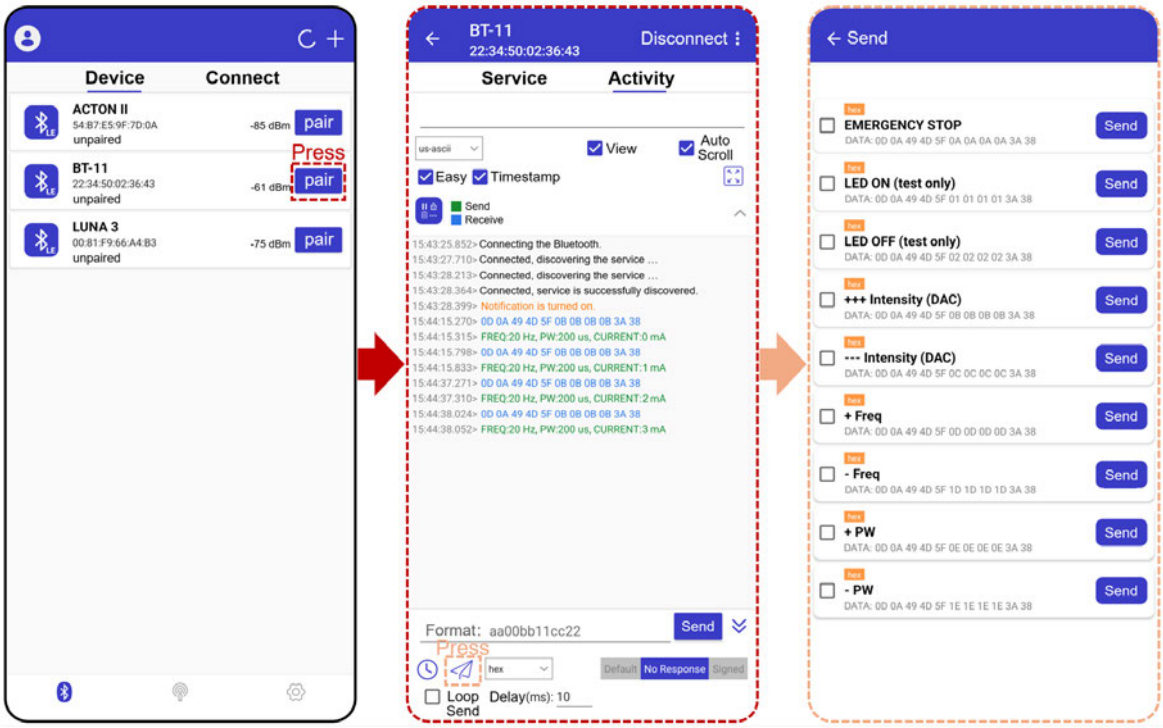


Fig. 4.12. An adapted mobile application for the wireless control of stimulation parameters via Bluetooth®.

chosen due to its compatibility and existing functionality. This application was adapted to meet the specific requirements of the TENS*mini*, with modifications to its control interface for parameter adjustments. The adapted interface, illustrated in Fig. 4.12, allows for control over stimulation parameters such as intensity, frequency and pulse width.

The adaptation primarily focused on aligning the user interface and communication protocol with the device operation. Preliminary testing demonstrated that the application successfully enabled wireless control of the device, with parameter adjustments reflected in the hardware responses. However, as this mobile application is based on a pre-existing framework, its customisation potential is inherently limited. While this approach offers a practical solution for wireless control, further development could improve integration and usability.

## 4.6 Implementation

### 4.6.1 Layer Stackup Configuration

The thickness of a PCB varies based on design requirements and manufacturer specifications, typically ranging from 1.0 to 2.0 mm. The 1.6 mm thickness, being the industry standard, was selected for this design. A multi-layer PCB architecture offers several advantages, including enhanced routing flexibility, improved signal integrity, and the capacity to accommodate higher component densities. The PCB for this design was developed using Altium Designer (Altium, Australia) with a standard six-layer stack-up configuration.

### 4.6.2 Board Size Optimisation

The board size was optimised by considering three factors: (1) the position and orientation of components, (2) the number of special components, and (3) the package of the components. Electronic components are typically assembled vertically on the top or bottom layer of the PCB. However, in specific cases, horizontal placement can further reduce the board size. For instance, commercially available TENS devices often feature vertically mounted transformers, leading to bulkier enclosures due to the transformers' height [74]. In contrast, this design incorporated a transformer positioned horizontally within a cut-out region of board. This approach reduced the overall enclosure thickness, thereby improving device wearability [74].

To further reduce the board size, small outline package was selected for most ICs and 0201 package was chosen for passive components during the PCB design. Additionally, overall dimension was also affected by size of special components, as these elements possess fixed dimensions that constrain the design. This design included three special components, including a transformer, a 470 μF aluminium electrolytic capacitor and a BLE module.

### 4.6.3 Board Manufacturing and Components Assembly

The fabricated six-layer PCB is shown in Fig. 4.13. The dimension of the PCB was measured 35 $\times$ 35 $mm^2$, and its complete layout can be found in Appendix B. Electronic components were distributed

across both sides of the PCB and assembled using solder paste and a reflow oven process. The board was powered by a 3.7 V, 300 mAh LiPo battery (LP-402933-IS-3, Shenzhen BAK Technology), sized 30 $\times$ 20 mm$^2$. The battery was positioned on the bottom side of the PCB when fitting into an enclosure.

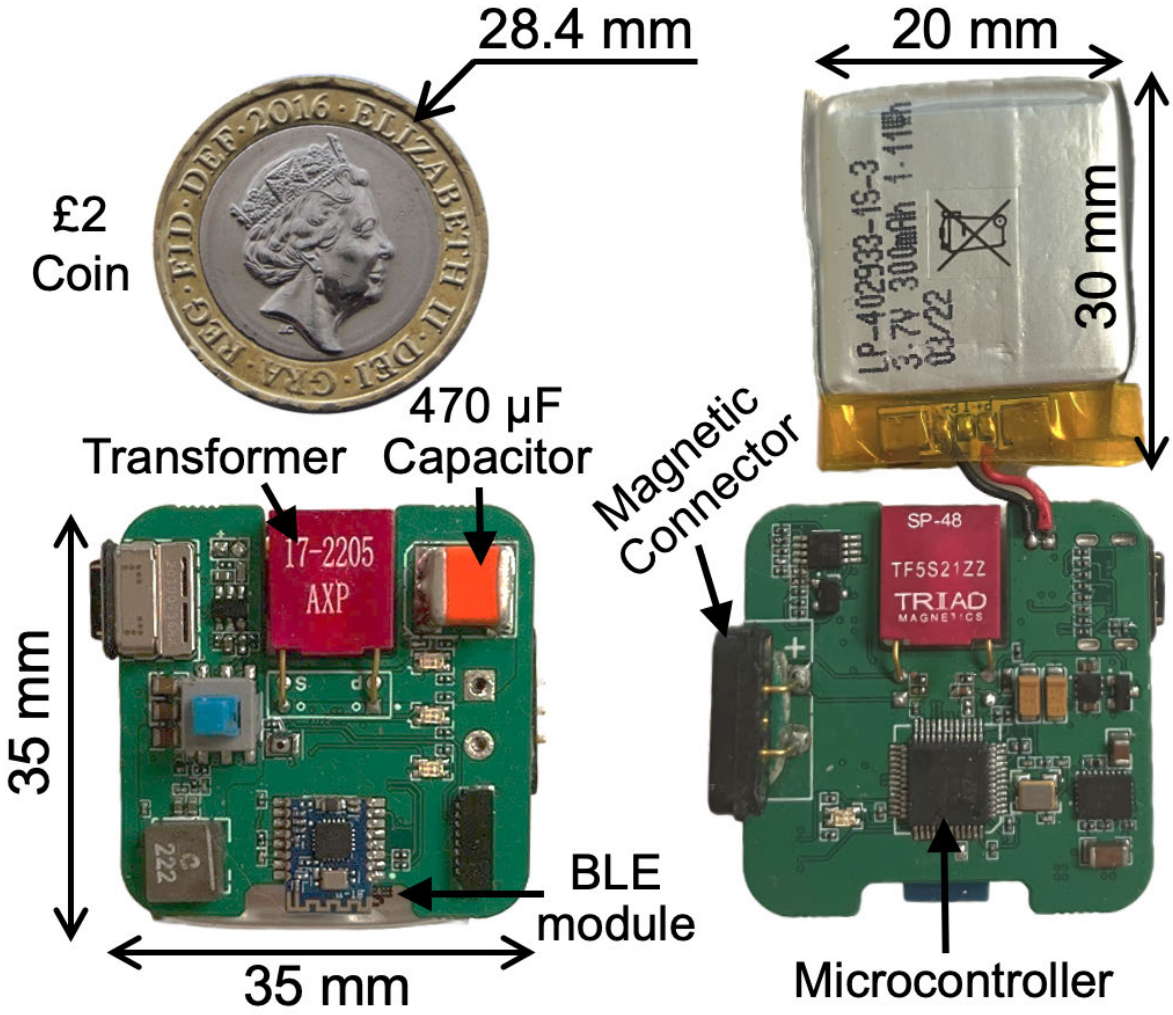


Fig. 4.13. An overview of a double-sided PCB powered by a 300 mA LiPo battery, shown alongside a £2 coin for size comparison

.

### 4.6.4 Enclosure Design and Fabrication

The device enclosure was designed using Fusion 360 (Autodesk, US) and fabricated with a 3D printer (Flashforge® Creator Pro 2, Zhejiang Flashforge 3D Technology) using polylactic acid (PLA) filament. The black-coloured switch button was 3D-printed using thermoplastic polyurethane (TPU), allowing the switch to be accessible from the top of the enclosure. Additionally, the protruding part of the enclosure in the front is designed to cover the magnetic connectors when connected with the sock, preventing accidental contact with the connector during the device use.

The final device dimensions were measured 38 $\times$ 38 $\times$ 21 mm$^3$, making it compact and feasible for mounting onto a sock, as shown in Fig. 4.14(a)–(c). The device remained securely attached via existing magnetic connectors, provided that the users remained relatively still during stimulation. However, for improved robustness, future iterations may incorporate either an additional pair of magnetic connectors, or a redesigned soft holding structure to better immobilise the device during movement.

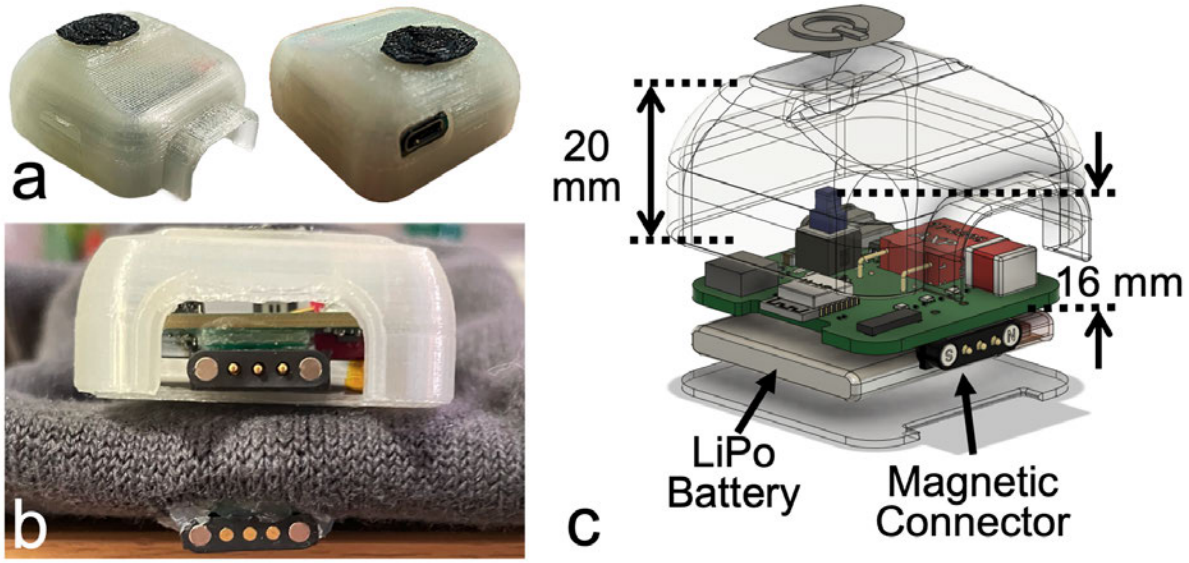


Fig. 4.14. (a) Isometric views of the custom 3D-printed enclosure, demonstrating different perspectives of the housing with flexible press button on the top and USB-C charging port on the back side; (b) Front view of the enclosure showing the alignment of a pair of magnetic connectors; (c) Overview of the enclosure with annotated dimensions, indicating the internal placement of the LiPo battery and magnetic connector.

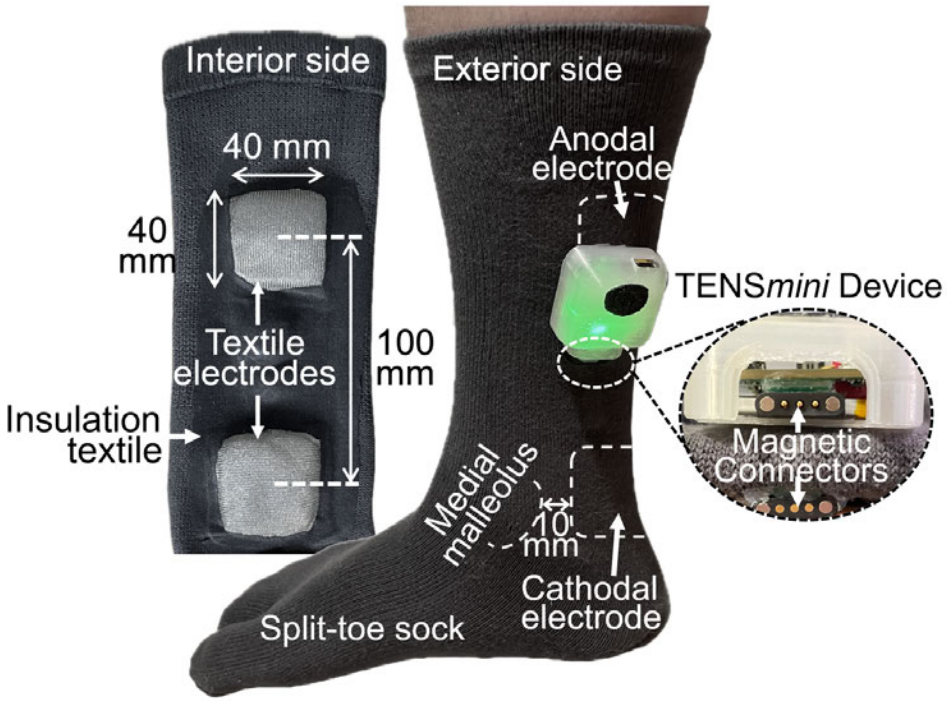


Fig. 4.15. A complete design (i.e., wearable TENS*mini*) intended for home-based OAB management [75].

### 4.6.5 Complete Wearable Design

A wearable, Bluetooth-enabled TENS device for TTNS was developed, as shown in Fig. 4.15. The entire design was composed of a miniaturised stimulator (i.e., TENS*mini*) fitted onto a split-toe sock that was integrated with two silver-fibre-knitted conductive TEs, making it convenient for users to manage their urinary conditions at home.

## 4.7 Other Conceptualised Implementation

The placement of the electronic device is important, as some users may find the initial positioning inappropriate due to its visibility during use. To address this, the device was repositioned to the upper lower leg near the knee. This adjustment required re-designing the PCB and enclosure with a curved shape to conform to the sock rim, allowing the device to remain concealed under trousers and improving user privacy.

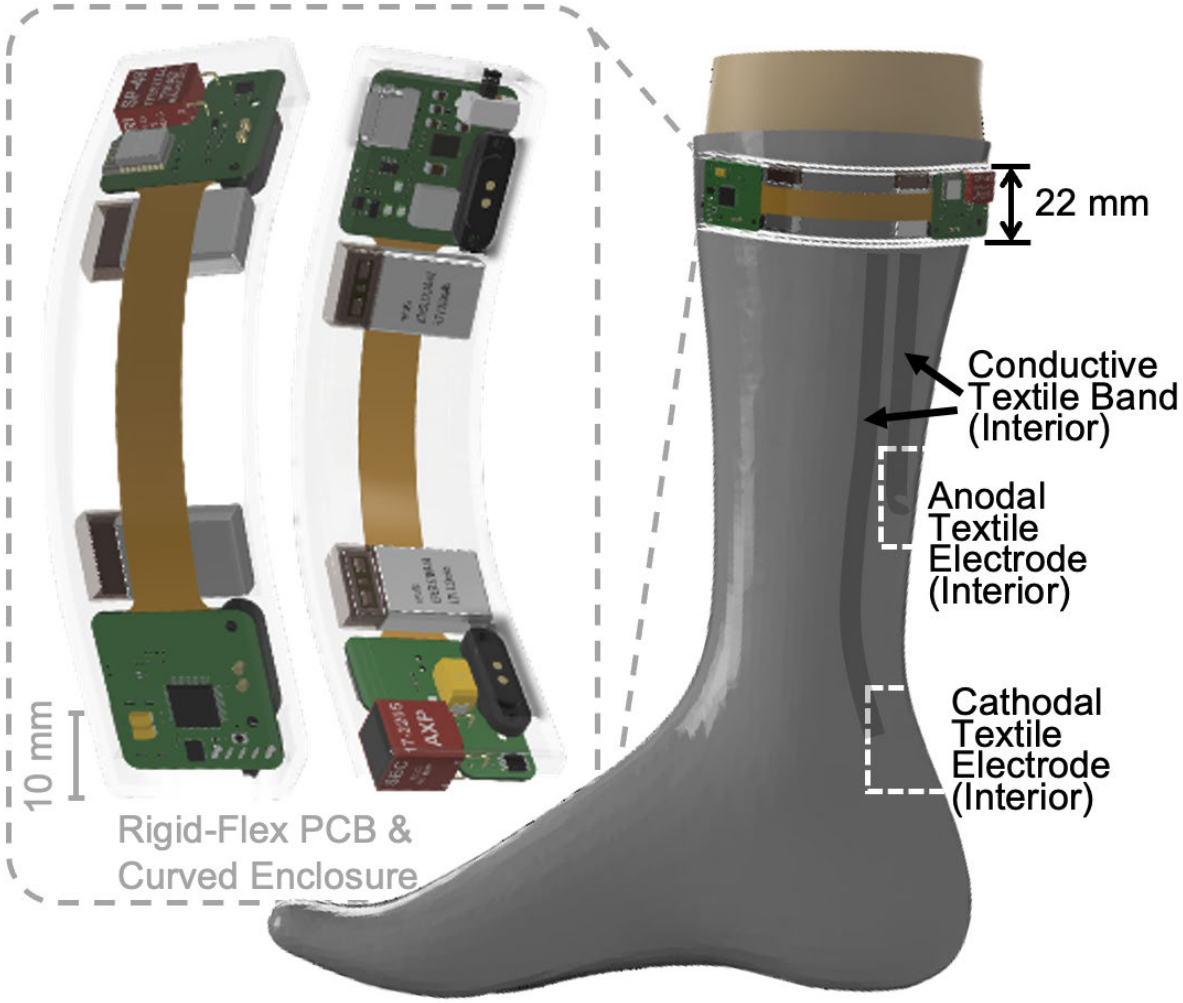


Fig. 4.16. The conceptualised implementation of the other wearable design using a rigid-flexible PCB and a curved enclosure.

To meet these design requirements, a mixed rigid-flexible PCB is proposed, as illustrated in Fig. 4.16. The flexible board between the two rigid sections facilitates the curved enclosure, while magnetic connectors on the rigid PCBs ensure secure attachment to the sock. Two 100 mAh LiPo batteries, chosen for their compact size and commercial availability, are positioned near each rigid section to evenly distribute the weight.

## 4.8 Conclusion

In summary, following the design of wearable TEs, circuit architecture, safety considerations, and hardware and firmware implementation, a smart wearable TENS*mini* device has been developed. This device is intended to serve as a potential alternative for home-based OAB management. The simulation and measurement results pertaining to its performance are presented in the subsequent chapter.

# Chapter 5

# Simulation and Measurement

This chapter details the methods and results of simulations and measurements conducted on the TENS*mini*'s hardware and its associated wearable textile electrodes (TEs). A comprehensive evaluation was performed, encompassing isolation technique selection (capacitor-based versus transformer-based approaches), verification of hardware functionality, and assessment of the short-term durability and washability of sock-based TEs. The aim was to rigorously validate the overall system performance, ensuring its suitability in managing overactive bladder (OAB) through transcutaneous electrical nerve stimulation (TTNS).

## 5.1 Limitations of Capacitive Isolation

The simulation was performed in LTspice software (Analog Devices, US), and its schematic is depicted in Fig. 5.1. The stimulation output was modelled using a voltage source in series with a 1 Ω resistor to mimic the constant current source.

In the initial simulation setup, the voltage source amplitude was configured to 100 V with a 200 µs pulse width, and the load was set to 1 kΩ. To block DC current in both directions, two isolation capacitors were placed in series, one at each terminal of the source, as recommended in [152]. Subsequently, the voltage source amplitude was reduced to 10 V, and the load was adjusted to 100 Ω, while preserving the 200 µs pulse width. The simulation outcomes for both configurations are presented as follows.

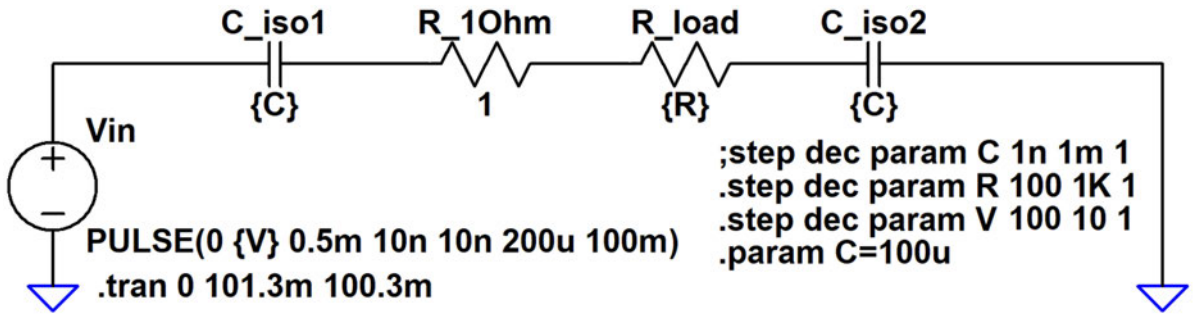


Fig. 5.1. The simulated schematic of capacitive isolation approach.

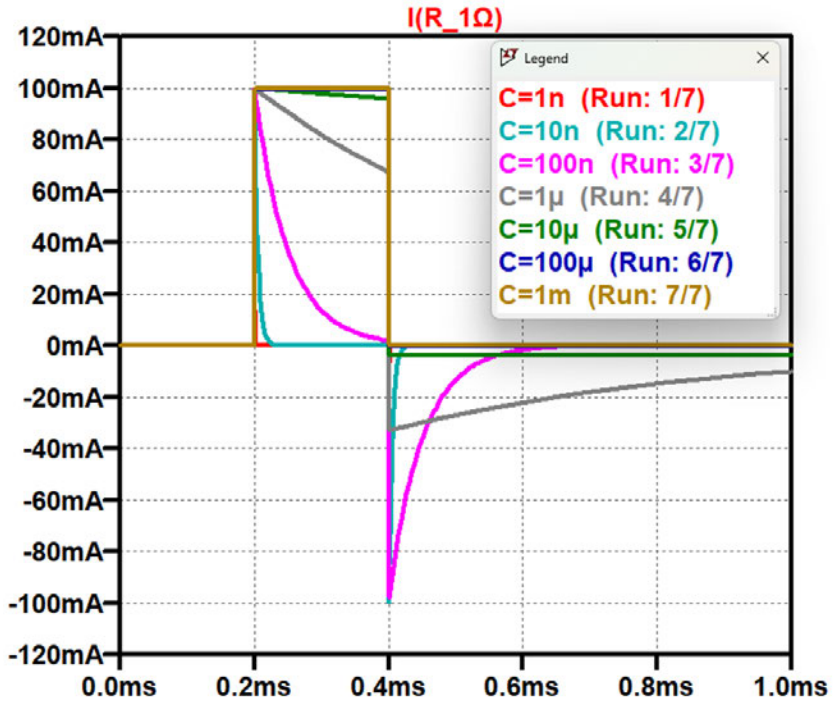


Fig. 5.2. Dependence of stimulation current pulses on isolation capacitance with a fixed output load (1 kΩ).

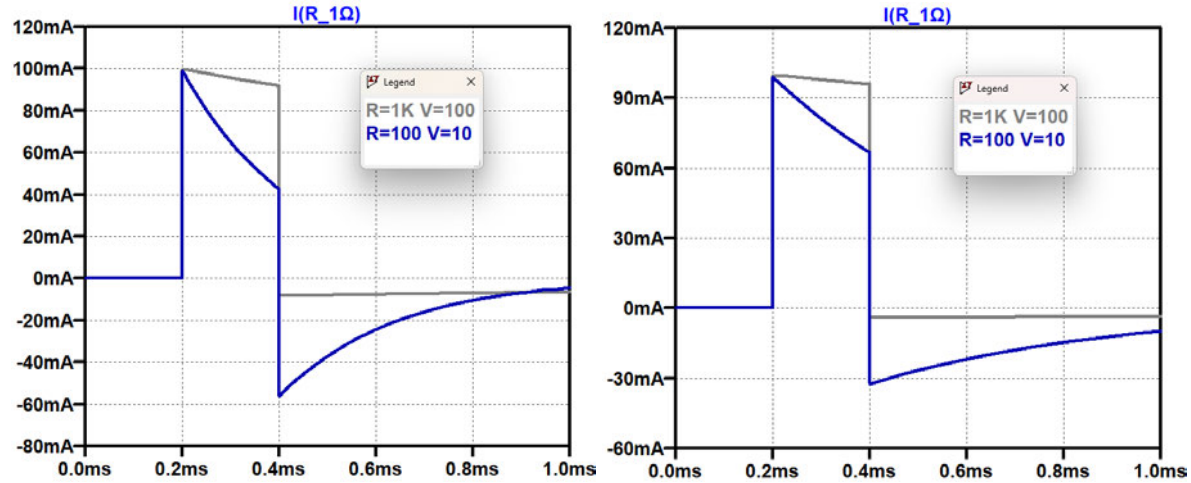


(a) Isolation capacitance of 4.7 µF.




(b) Isolation capacitance of 10 µF.

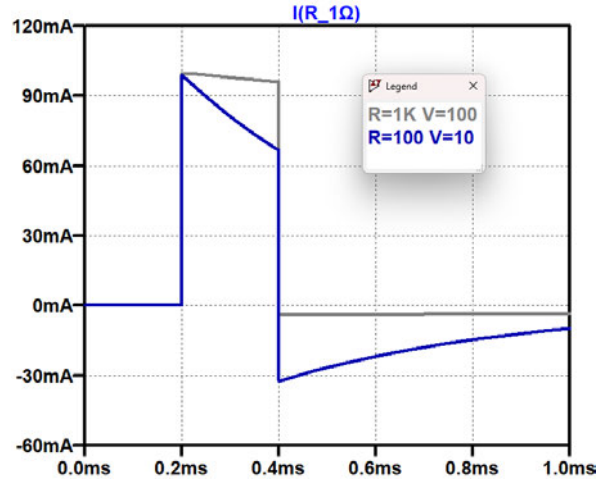


(c) Isolation capacitance of 47 µF.

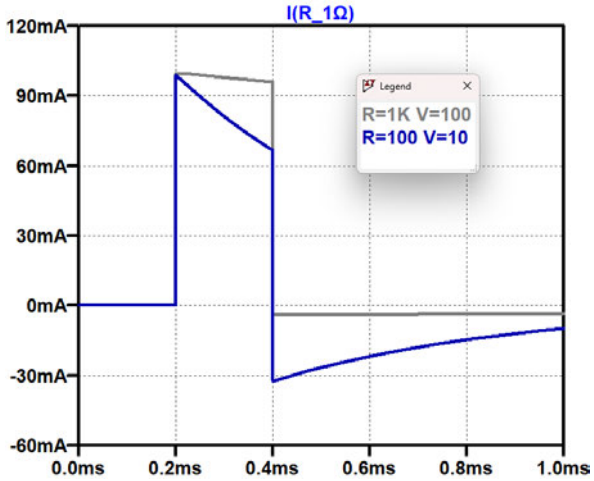


(d) Isolation capacitance of 100 µF.

Fig. 5.3. Variation in pulse shapes with increasing capacitance across four incremental steps.

While maintaining the output load consistently at 1 kΩ, increasing the isolation capacitance yields stimulation pulses that more closely resemble conventional monophasic waveforms, as illustrated in Fig. 5.2. In particular, for a 200 µs pulse width, capacitances exceeding 10 µF significantly enhance the pulse shape. However, when the load is reduced to 100 Ω, smaller capacitances produce notable pulse distortion relative to the 1 kΩ configuration, as shown in Fig. 5.3(a)–(d).

These findings suggest that isolation capacitance values of 100 µF or greater are preferable for more accurate pulse shaping. The underlying cause of waveform distortion is an insufficient time constant ($\tau = RC$) during the discharge phase, as detailed in Appendix A. A reduced $\tau$ leads to premature capacitor

Table 5.1. Estimated and practical isolation capacitance that maintain current drop within 10% during discharging.

| Load (Ω) | $\Delta I/I_0$ | Pulse Width (μs) | Calculated Capacitance (μF) | Capacitance in E6 Series (μF) |
|---|---|---|---|---|
| 100 | 1% | 200 | 199.0 | 220 |
| | 1% | 250 | 248.7 | |
| | 5% | 200 | 39.0 | 47 |
| | 5% | 250 | 48.7 | |
| | 10% | 200 | 19.0 | 22 |
| | 10% | 250 | 23.7 | |
| 1000 | 1% | 200 | 19.9 | |
| | 1% | 250 | 24.9 | |
| | 5% | 200 | 3.9 | 4.7 |
| | 5% | 250 | 4.9 | |
| | 10% | 200 | 2.4 | 2.2 |
| | 10% | 250 | 1.9 | |

discharge, thereby degrading the pulse profile. For wider pulse widths (e.g., 250 μs), increasing the isolation capacitance is essential to maintain the desired pulse shape and ensure waveform integrity.

According to Equation A.13 (Appendix A), larger capacitance values effectively reduce the proportion of discharge within a fixed time interval, in alignment with the pulse widths (200–250 μs) commonly employed in TTNS. To achieve a practical approximation of a monophasic pulse, up to 10% attenuation due to capacitor discharge was deemed acceptable. As summarised in Table 5.1, capacitances on the order of 220 μF or even 470 μF are confirmed to be optimal for sustaining a robust pulse shape under capacitive isolation conditions.

As previously noted, aluminium-electrolytic capacitors can provide high capacitance values and voltage ratings. Fundamentally, a capacitor can be modelled as a parallel-plate structure with two conductive plates separated by a dielectric layer, as illustrated in Fig. 5.4(a).

The capacitance of this parallel-plate structure is defined as:

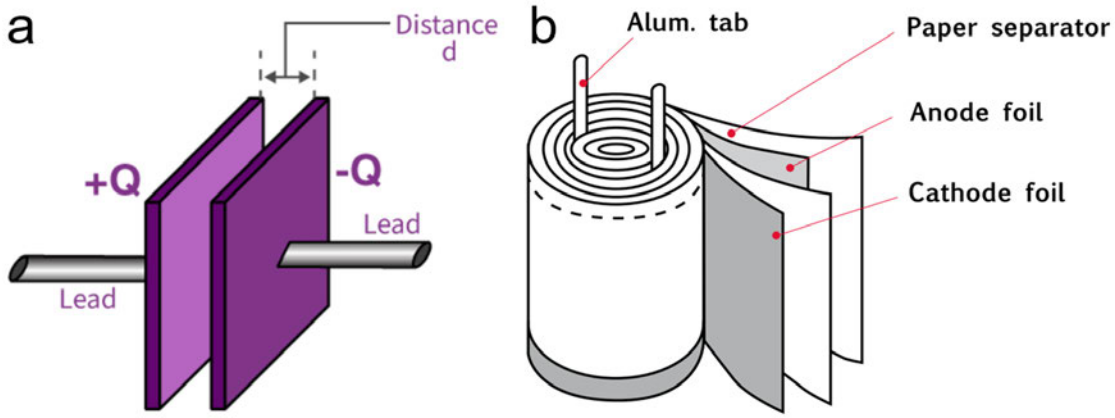


Fig. 5.4. (a) Schematic overview of a basic parallel plate capacitor [211]. (b) Structure of an aluminium-electrolytic capacitor [212].

$$C = \frac{\varepsilon \cdot A_p}{d_s} \tag{5.1}$$

where $\varepsilon = \varepsilon_0 \cdot \varepsilon_r$ (with $\varepsilon_0$ denoting the electric constant, approximately $8.854 \times 10^{-12}\ \mathrm{F m^{-1}}$, and $\varepsilon_r$ denoting the relative permittivity of the dielectric material), $A_p$ represents the overlapping area of the plates, and $d_s$ is the separation distance.

As the plate area ($A_p$) predominantly determines a capacitor's physical footprint, aluminium-electrolytic capacitors employing a rolled parallel-plate configuration (Fig. 5.4(b)) typically require a larger volume to achieve a substantial plate area. To investigate the relationship between capacitance and the cubic volume of these capacitors, data from the manufacturer's datasheet [213], including capacitance values, maximum voltage ratings, and volumetric dimensions were analysed.

From the manufacturer's data (Fig. 5.5), the linear trends indicate that higher capacitance values correspond to increased component dimensions. Moreover, at a constant capacitance, devices rated for higher voltages demand even larger volumes. For instance, a 200 µF surface-mounted aluminium-electrolytic capacitor rated at 100 V measures 18 mm in diameter and 16.5 mm in height, making it relatively large for miniaturised hardware.

Accordingly, employing two 220 µF, 100 V capacitors for capacitive isolation is deemed less suitable for wearable transcutaneous electrical nerve stimulation (TENS) devices, as the high-voltage and

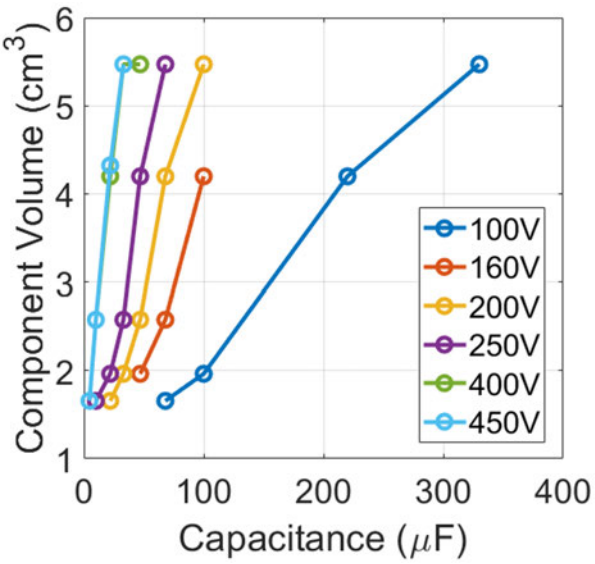


Fig. 5.5. Linear relationship between the volume of the capacitor and its capacitance.

high-capacitance requirements necessitate a relatively large enclosure, thereby diminishing overall device portability.

## 5.2 Determination of Winding Inductance

Transformer simulations are typically complex because of multiple parameters involved. To simplify the simulation in LTspice, the transformer's *k*-factor was fixed at one, ensuring a linear relationship between the primary and secondary windings [214]. The maximum voltage drop across the primary winding coil should not exceed 9 V that represents a typical maximum supply by a 9 V alkaline battery. Therefore, the voltage source connected (to the primary side) was set to an amplitude of 9 V, as shown in Fig. 5.6. On the secondary side, a 1 kΩ load was connected. The current through this load was assumed to be constant, with an expected value of approximately 100 mA, matching the maximum output of other clinical simulators (e.g., NeuroTrac® Continence device).

After several iterations of trial and error, a turns ratio of 1:20 was chosen, which achieved a maximum output of 120 mA under the configuration (Fig. 5.6). Additionally, the inductance of the secondary winding was varied from 10 mH to 100 H, and the current through a 1 Ω resistor connected with the load was recorded. Fig. 5.7 shows that when the secondary winding inductance is below 1 H, the output pulses exhibit distortion. This distortion is attributed to a low time constant ($L_S/R_L$) which leads to a rapid discharge of the secondary coil when connected to a 1 kΩ load. To achieve monophasic-like stimulation pulses with reduced distortion, the secondary inductance should exceed 5 H. Accordingly, a transformer (SP-48, Triad Magnetics) with a measured winding inductance of 12.1 H was selected. The datasheet-reported turns ratio of 1:25 [215] was considered suitable for the designed drive circuit based on the simulation results.

## 5.3 Drive Circuit Simulation

Since the transformer-isolated drive circuit constitutes one of core modules in the hardware design, several simulations were performed to determine other parameters related to the drive circuit. The schematic of the drive circuit was simulated using LTspice, as depicted in Fig. 5.8.

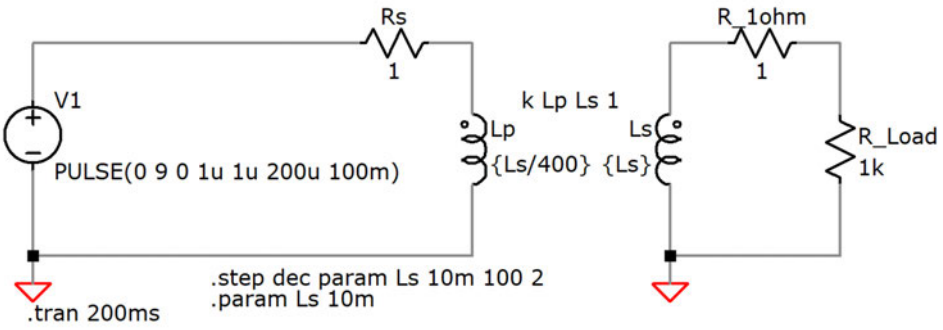


Fig. 5.6. Simulated circuit for transformer-isolated pulse generation with variable winding inductance.

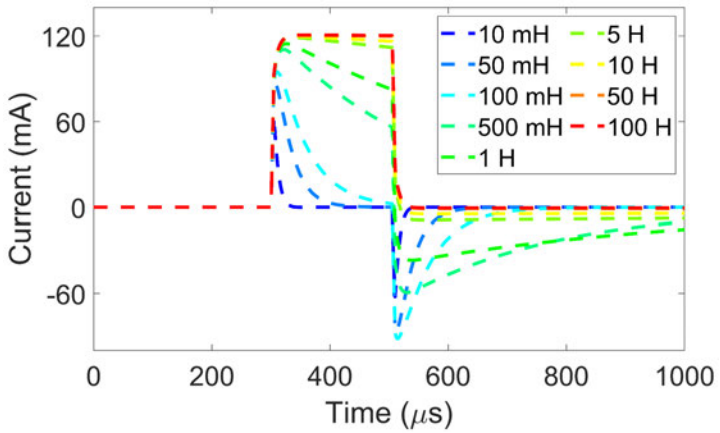


Fig. 5.7. Inductance-depended stimulation pulses (120 mA, 200 μs).

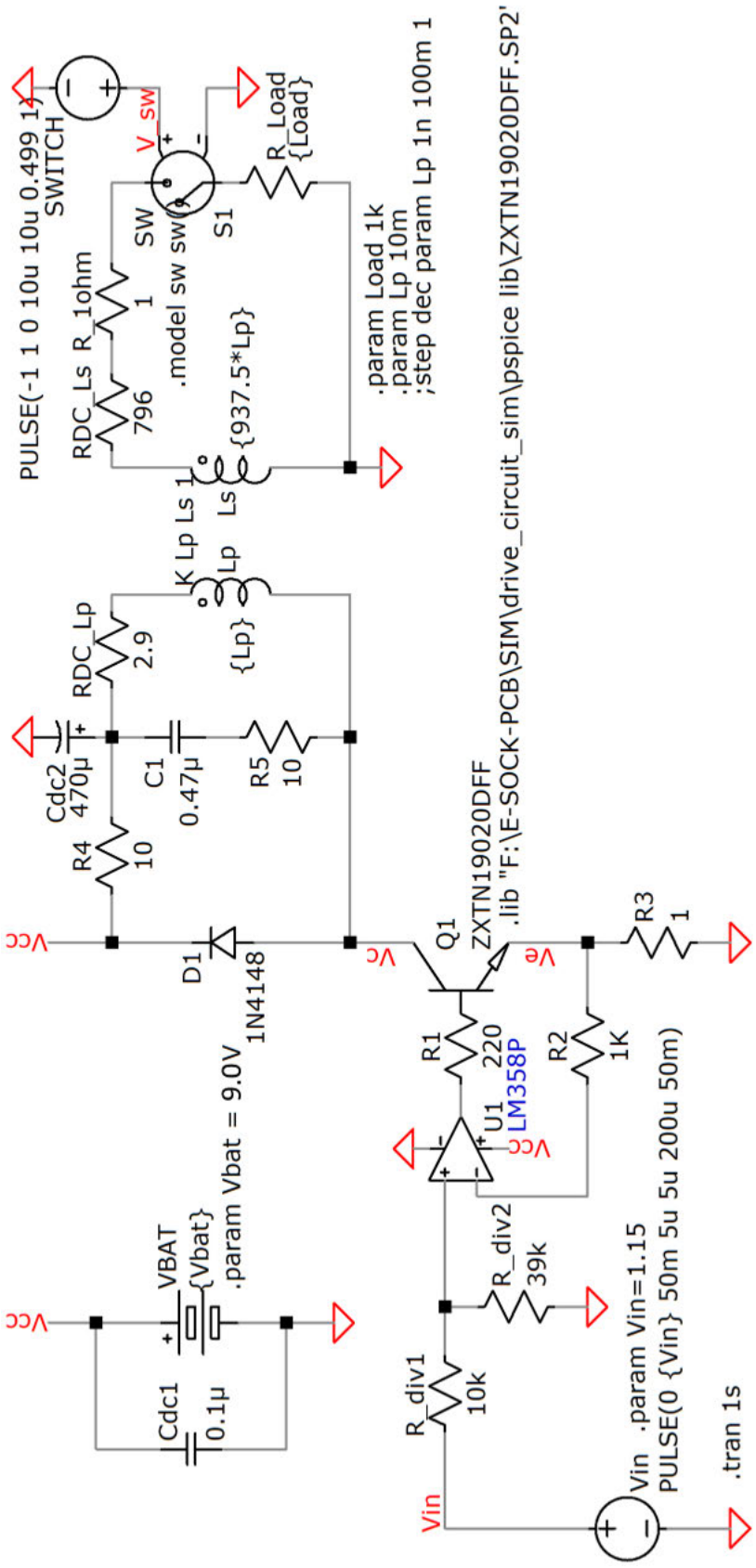


Fig. 5.8. Simulated schematic of the drive circuit.

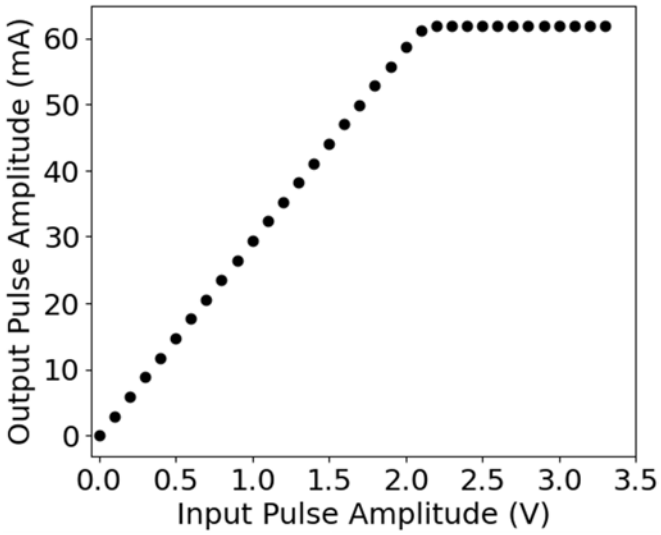


Fig. 5.9. The linearity between the input voltage control and stimulation current outputs.

### 5.3.1 Voltage-to-current Conversion

During simulation, the power supply remained constantly at 9 V. The input source ($V_{in}$) was configured in pulse mode, and the amplitude of pulsed input voltage was swept to up to 3.3 V, which is the maximum level provided by a typical microcontroller. The frequency and pulse width of the input pulses were fixed at 10 Hz and 200 µs, respectively. A one-ohm resistor was connected in the secondary loop to sense the output current. During the test, a voltage-controlled switch ($S_1$) remained closed, and the output load was fixed at 1 kΩ.

Fig. 5.9 illustrates the linear relationship between the input and output pulse amplitudes. It is observed that, under the aforementioned configurations, the maximum amplitude of the stimulation current pulses is approximately 60 mA.

### 5.3.2 Supply Voltage Optimisation

To evaluate the instantaneous current supply capability for the proposed TENS design, a lithium polymer (LiPo) battery in conjunction with a TPS61088 Boost Converter Evaluation Board or a 9 V alkaline battery was employed as the power source for the breadboard-implemented drive circuit. This circuit was identified as the primary power-consuming component of the TENS device.

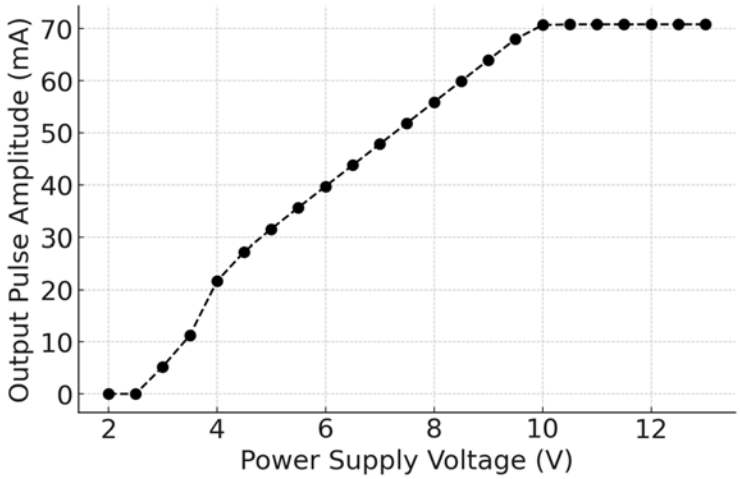


Fig. 5.10. Maximum pulse amplitude with respect to change in supply voltage.

Since the boost converter chip (i.e., TPS61088) can be configured to supply a maximum of 12.6 V, it was necessary to determine the voltage required by the drive circuit to deliver adequate stimulation pulses. Based on the simulation result (Fig. 5.9), an amplitude of 2.2 V for $V_{in}$ was expected to yield the sufficient amplitude (i.e., 60 mA) for output current pulses. Consequently, in this simulation, $V_{in}$ was fixed at 2.2 V and output load remained consistently 1 kΩ, while the power supply voltage ($V_{CC}$) was varied from 2 to 13 V.

The supply voltage influences the maximum amplitude of stimulation pulses; however, its effect diminishes when the supply voltage exceeds 10 V, as shown in Fig. 5.10. Therefore, it is reasonable to use a power supply voltage below 10 V while maintaining a sufficient stimulation amplitude such as 60 mA.

### 5.3.3 Electrode Detection Mechanism Simulation

The functionality of the electrode detection mechanism was evaluated by simulating the disconnection of the secondary circuit using a voltage-controlled switch ($S_1$; Fig. 5.8). Throughout the simulation, the collector voltage ($V_C$) was continuously recorded to monitor the circuit's behaviour.

When the switch is closed, stimulation pulses are continuously observed, as illustrated in Fig. 5.11. However, upon opening the switch, the secondary loop transitions into an open-circuit condition, leading to a voltage change in $V_C$.

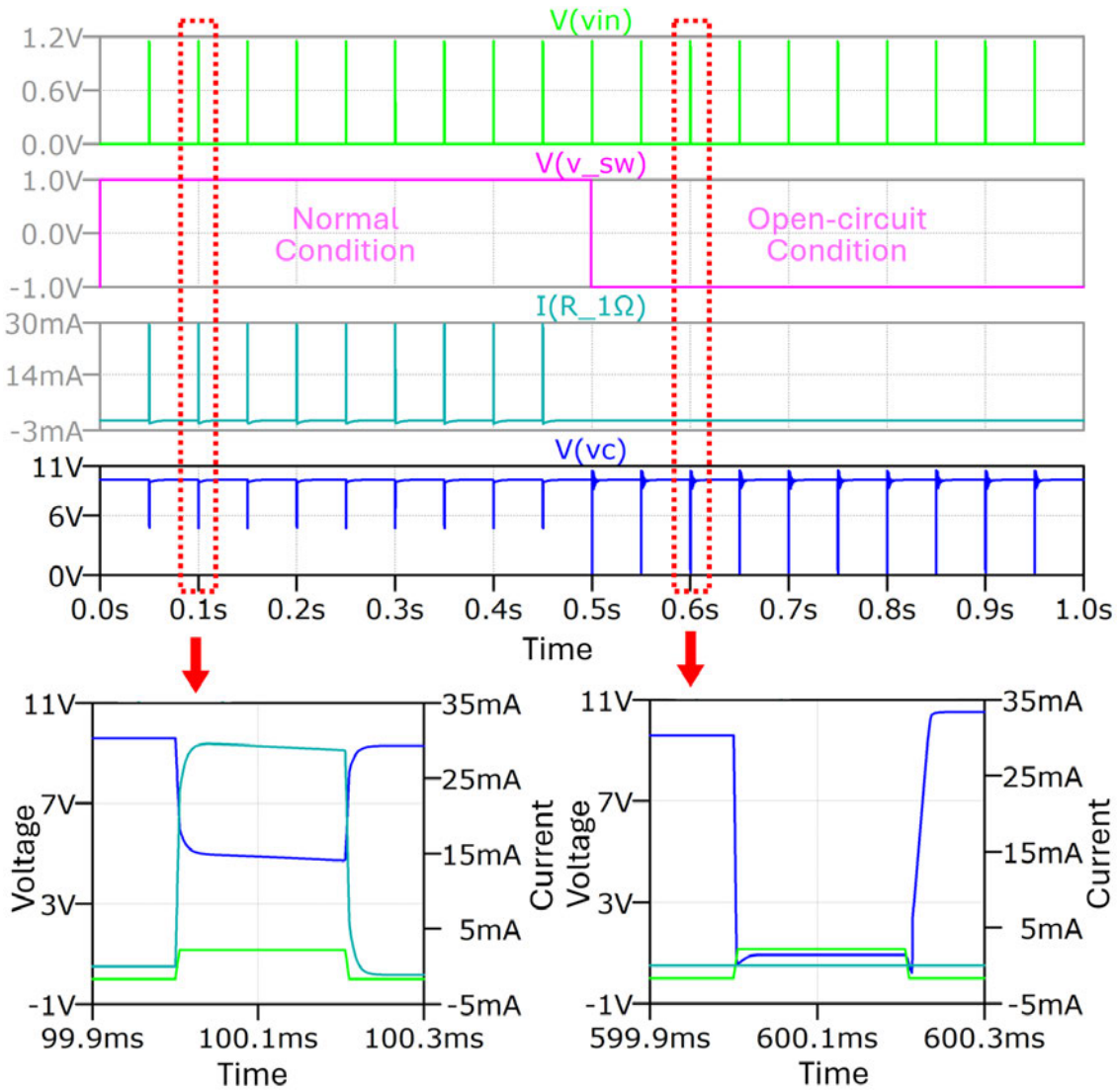


Fig. 5.11. Results of stimulation for normal and open-circuit conditions.

In practical scenarios, such an open-circuit condition may arise due to loose electrode contacts or device disconnection. Simulation results indicate that detecting electrode connectivity through the hardware circuit is feasible, aligning with expected outcomes.

## 5.4 Power Sources Characterisation

The experimental setup employed to evaluate power supply performance is illustrated in Fig. 5.12(a), with detailed interconnections between these modules (Fig. 5.12(b)). A 1 Ω, 5 W resistor was connected in series between the positive terminal of the power source (either a 9 V, 630 mA h alkaline battery (6LR61-9V, PKCELL) or a 3.3 V, 300 300 mA h LiPo battery and a boost converter) and the primary side of the drive circuit (i.e., $V_{CC}$ terminal; Fig. 4.6), functioning as a current-sensing element. On the secondary side of the drive circuit, a 1 kΩ resistor was utilised as the output load.

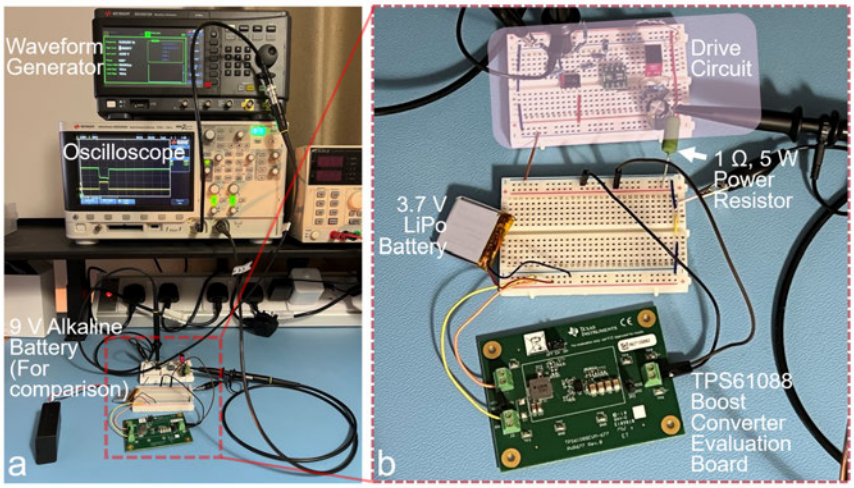


Fig. 5.12. (a) Experimental setup; (b) Connection between each module.

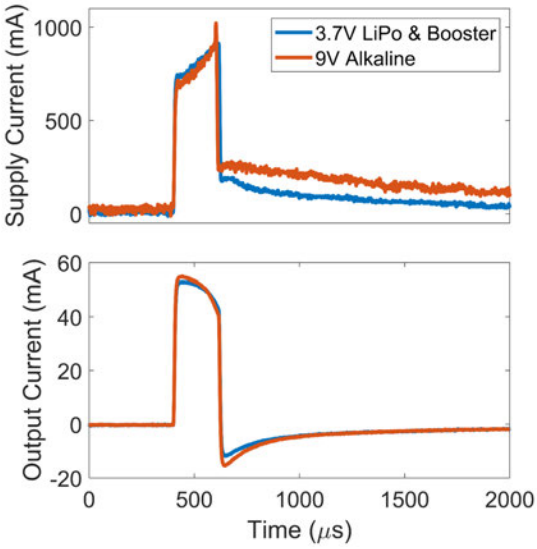


Fig. 5.13. Measured supply and output current using different power sources.

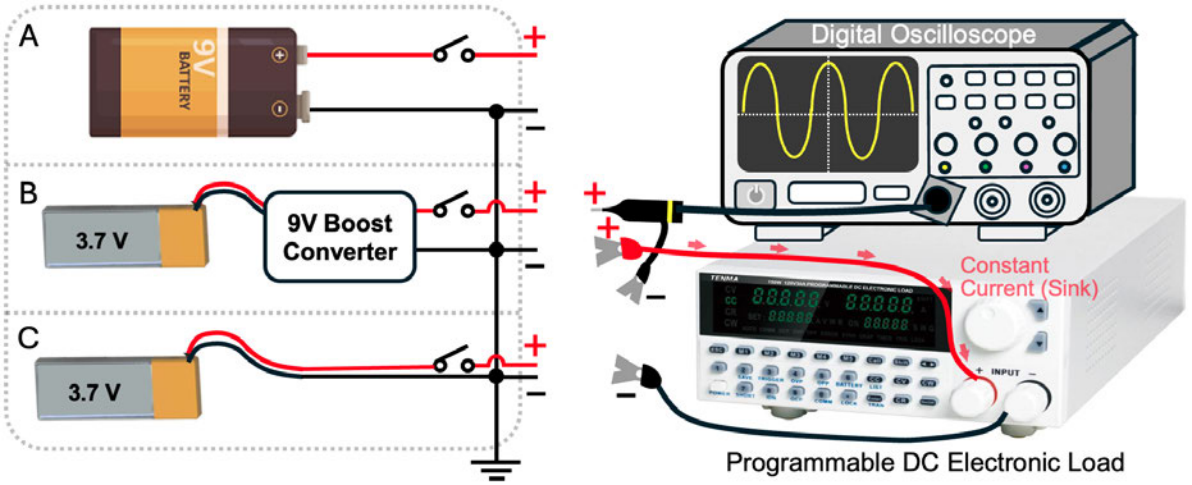


Fig. 5.14. Experimental setup for evaluating performance of different power sources: (a) A 9 V alkaline battery; (b) A 3.3 V LiPo battery associated with a boost converter module; (c) A 3.3 V LiPo battery.

A waveform generator (EDU33121A, Keysight Technologies; Fig. 5.12(a)) was configured to provide input control pulses at 20 Hz with a 200 µs pulse width, activating the drive circuit. Meanwhile, a digital oscilloscope (DSOX2014A, Keysight Technologies; Fig. 5.12(a)) was employed to measure the voltage across the 1 Ω resistor to determine the instantaneous current flowing through the primary-side circuit.

Measurement results (Fig. 5.13) demonstrate visually similar current profiles for both tested power supply options, each exhibiting peak currents below approximately 1 A. Considering the 20 Hz pulse frequency, the root-mean-square (RMS) value of the (pulsed) supply current was estimated to be 50 mA, derived from the area under the curve of each trace.

A separate experiment was performed to assess the sustainability and voltage stability of two distinct power sources (i.e., a 9 V alkaline battery, and a 3.3 V LiPo battery (300 mA h paired with a boost converter). These were compared against the performance of the same LiPo battery alone. compared with these of a LiPo battery alone. A programmable DC electronic load (Model 72-12310, TENMA) was employed to simulate a dynamic load (to sink constant current) for each power source. Additionally, a digital multimeter (Model 1908, Aim-TTi) was connected across the terminals of each power source to monitor the voltage during operation. The experimental setup is illustrated in Fig. 5.14.

Observations reveal all power sources can supply constant current of 1 A. However, none of the tested sources continuously sustained 1 A current for durations exceeding 15 minutes, as depicted in Fig. 5.15.

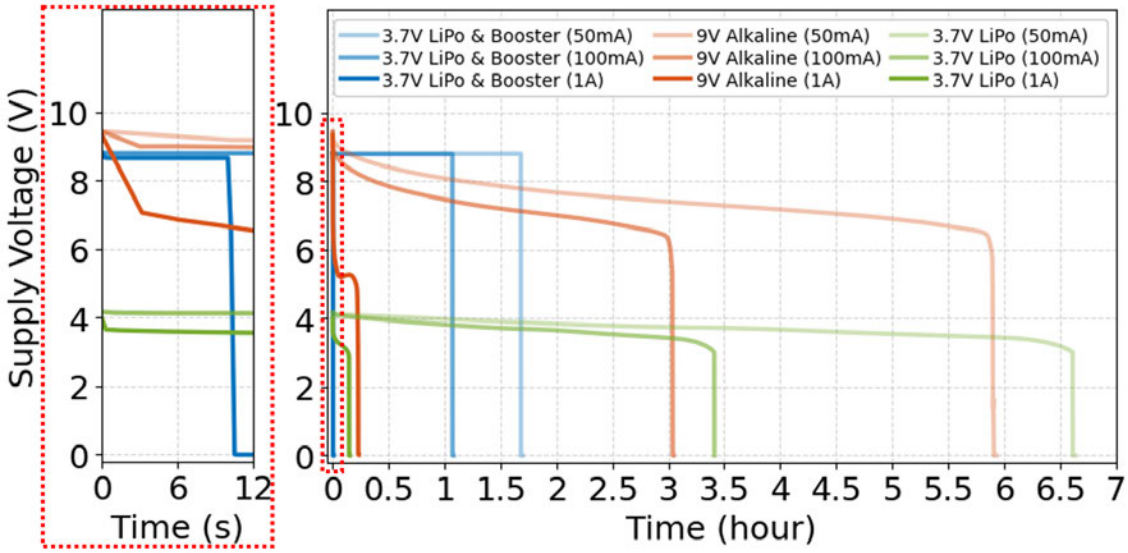


Fig. 5.15. Supply voltage varied with different consumed current.

Although a 9 V alkaline battery can directly power the drive circuit, its relatively large physical size imposes constraints on the overall device dimensions. In contrast, the LiPo battery with a boost converter shows the feasibility of sourcing 50 mA for one hour and 100 mA for approximately 1.7 hours.

To ensure compatibility with a typical 30-minute TTNS session, the minimum energy consumption (0.1103 W h) required for the proposed drive circuit was estimated. This estimation was based on the technical specifications of a clinically approved TENS device (i.e., NeuroTrac® Continence), which could operate with a 9 V alkaline battery to deliver 70 mA stimulation pulses at 100 Hz, 450 µs pulse width to a 1 kΩ load over a 30-minute duration [63]. Energy consumption for each supply source was calculated by integrating the area under the voltage trace and multiplying it by the corresponding constant current. The resulting values are summarised in Table 5.2 for comparison.

From Table 5.2, the total energy consumption of the 3.7 V LiPo battery combined with a boost converter is greater than the estimated requirement under both 50 and 100 mA conditions. This indicates that the chosen power source can sustain operation for more than 1.7 hours, enabling multiple 30-minute sessions using the proposed drive circuit.

Table 5.2. Summary of power and energy consumption for each power source.

| Power Sources | Consumed Current (A) | Maximum Power Rating (W) | Total Energy Consumption (Wh) |
|---|---|---|---|
| 3.7 V LiPo & Boost Converter | 0.05 | 0.0220 | 0.7405 |
| | 0.1 | 0.0882 | 0.9413 |
| | 1 | 8.8182 | 0.0248 |
| 9 V Alkaline | 0.05 | 0.0236 | 2.2128 |
| | 0.1 | 0.0944 | 2.2134 |
| | 1 | 9.3495 | 1.2030 |
| 3.7 V LiPo | 0.05 | 0.0104 | 1.2305 |
| | 0.1 | 0.0417 | 1.2580 |
| | 1 | 4.0016 | 0.4729 |

## 5.5 Boost Converter Simulation

To achieve an approximately 9 V supply voltage, calculations were performed to determine the appropriate values for the peripheral components of the selected boost converter chip (TPS61088). Table 5.3 lists the chosen values of all passive components, which theoretically enable the boost converter to deliver a constant 9.6 V output.

Table 5.3. Summary of component values utilised in the boost converter design.

| Component Designator | Selected Value |
|---|---|
| $C_1$ | 47 µF |
| $C_2$, $C_8$ | 100 nF |
| $C_3$, $C_4$ | 2× 1 µF |

Continued on next page

(Continued)

| Component Designator | Selected Value |
|---|---|
| $C_5$ | 39 pF |
| $C_6$ | 680 nF |
| $C_7$ | 8.2 nF |
| $C_9$, $C_{10}$, $C_{11}$, $C_{12}$ | 4× 22 µF |
| $R_3$ | 649 kΩ |
| $R_4$ | 90.9 kΩ |
| $R_{13}$ ($R_{FSW}$) | 249 kΩ |
| $R_4$ | 105 kΩ |
| $R_5$ | 45.2 kΩ |
| $L_1$ | 2.2 µH |

Utilising the values of electronic components (Table 5.3), the boost converter circuit was simulated using TINA-TI software (Texas Instruments, US), and its schematic is presented in Fig. 5.16.

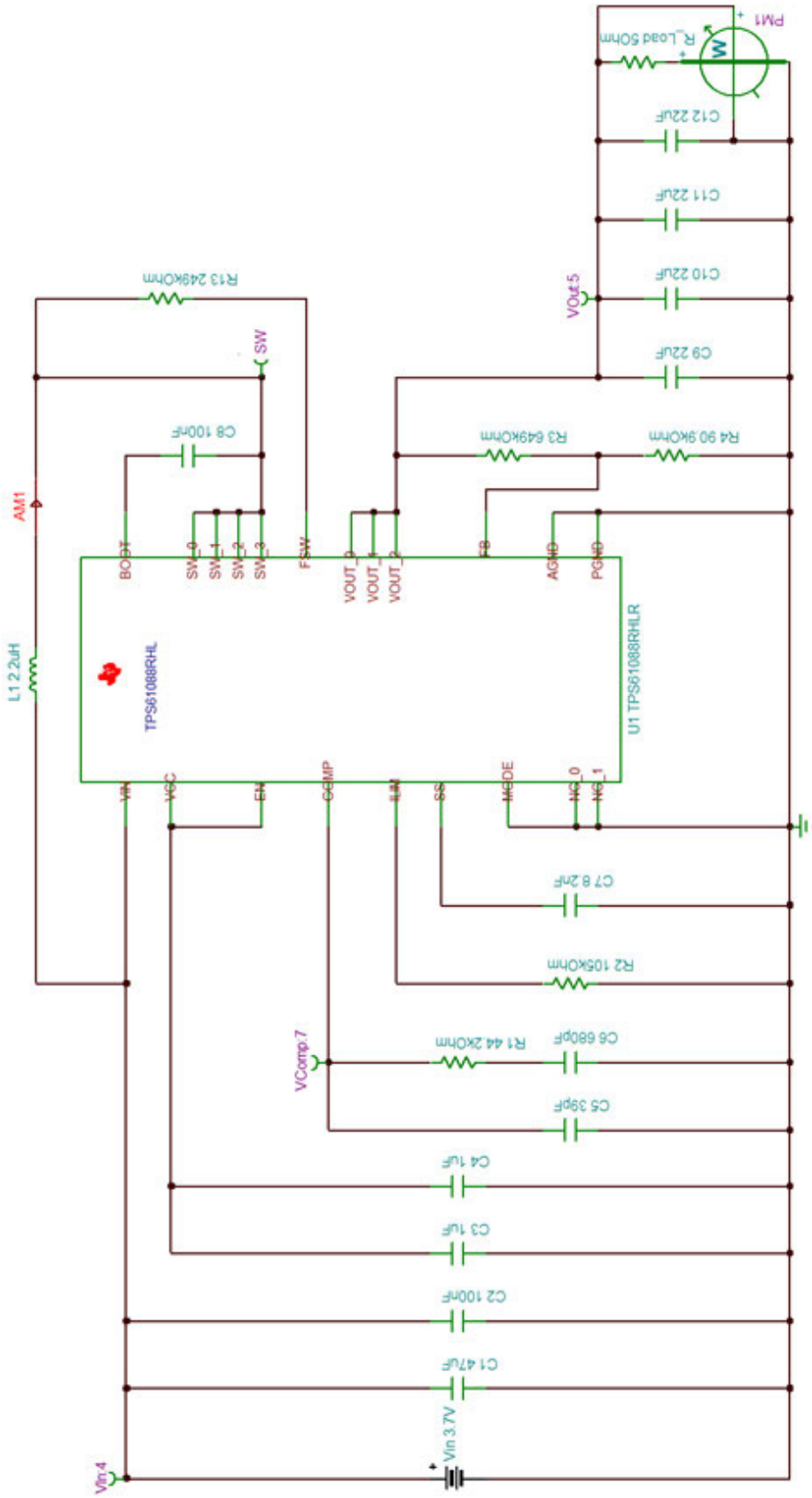


Fig. 5.16. Simulated schematic of the selected boost converter (TPS61088).

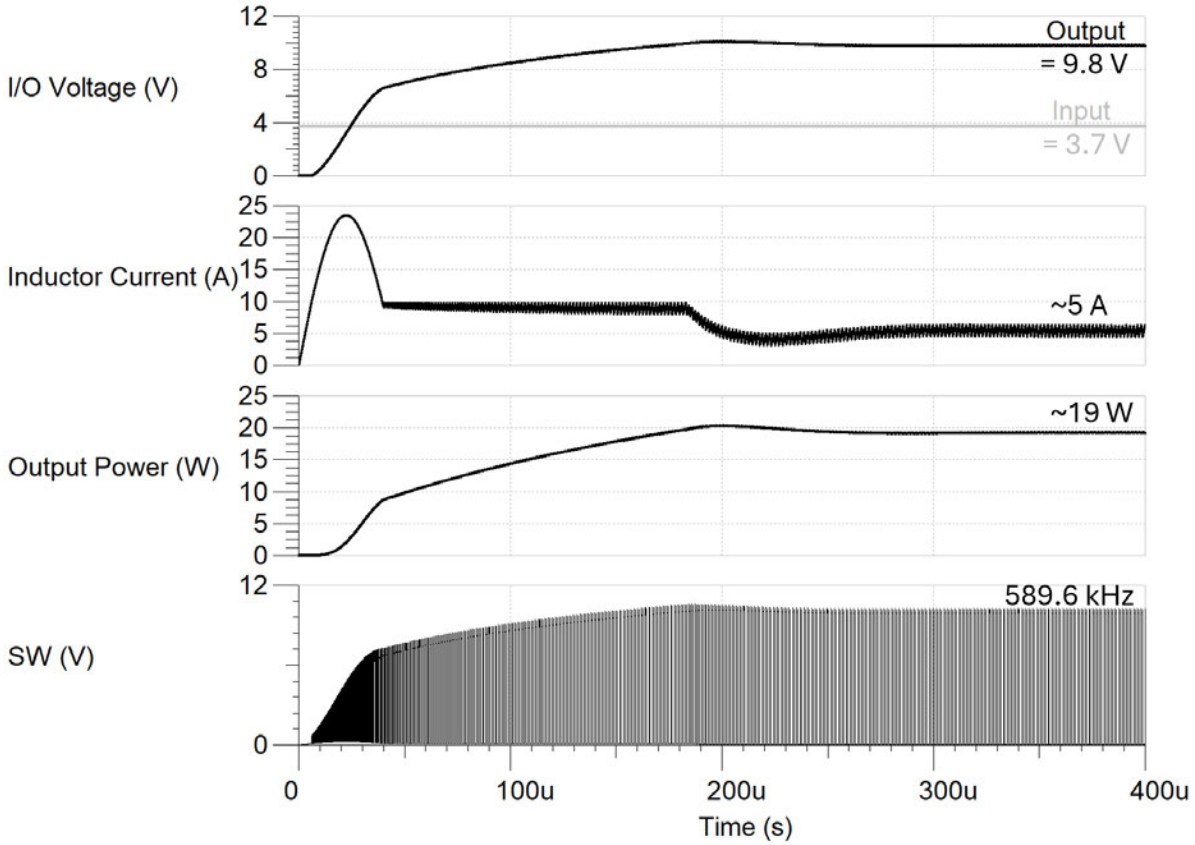


Fig. 5.17. Simulation results of the booster converter circuit.

The simulated results for the boost converter are presented in Fig. 5.17. A 3.7 V input voltage (which is the nominal voltage supplied by a single LiPo cell) was stepped up and maintained at 9.8 V. Under heavy load conditions (i.e., 5 Ω load), an inductor (output) current of 5 A is observed with noticeable ripples, resulting in an output power of approximately 19 W. A switching frequency of 589.6 kHz is measured, closely aligning with the targeted frequency of 600 kHz.

## 5.6 Test of Wearable TEs

### 5.6.1 Ethics and Recruitment

The following experiment protocols were reviewed and approved by the local ethics committee of The University of Edinburgh (Ref.: RT2021/83413). Written informed consent (Appendix C) was obtained from all participants prior to all experiments.

Five participants (two females and three males, age: 30 ± 2 years) were recruited for characterisation of the wearable textile electrodes (TEs). Participants were unaware of which electrodes (i.e., TEs or gel electrodes (GEs)) the author designed and what the author wanted to study. Furthermore, another person (a woman, 29 years old) was also recruited for the short-term durability and washability study of TEs.

### 5.6.2 Electrode Characterisation

To investigate the effect of pressure applied to the electrode-tissue interface, a force sensor (SXTSC, Sateco AG) was utilised to characterise this effect. A three-point measurement method, as described in [216], was employed to evaluate the performance of the designed TE (4 × 4 $cm^2$). For comparative analysis, a clinical-grade GE (SA12, Med-Fit UK) was also characterised using the same method.

The electrode placement configuration is illustrated in Fig. 5.18. Two GEs, each with dimensions of 4 × 4 cm, were positioned at locations (a) and (c) to serve as reference electrodes. The test electrode, either a TE or GE, was placed at position (b) in the centre. All electrodes were positioned on the posterior skin surface of the lower leg for each participant during the impedance measurement process.

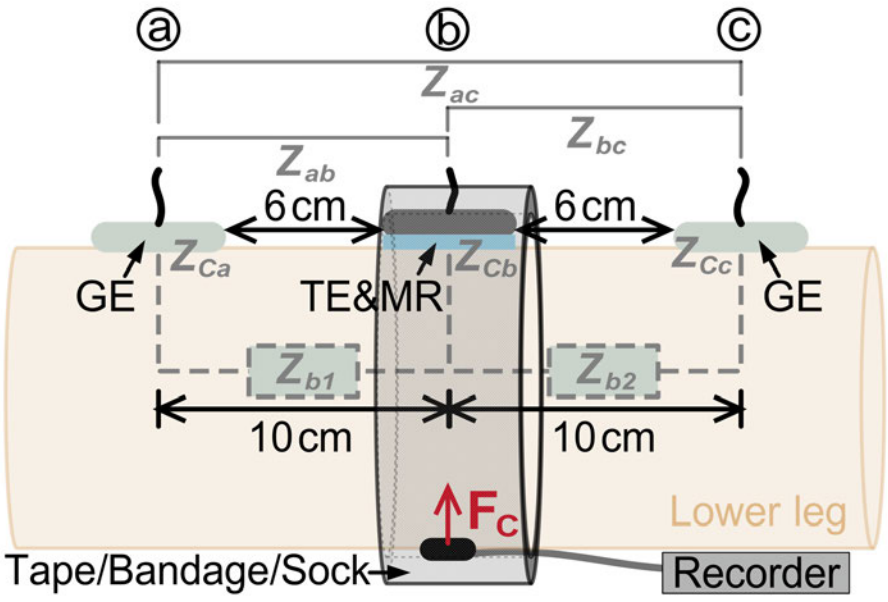


Fig. 5.18. Setup for three-point measurement of electrode characterisation, measuring the ETI under varying applied compression forces via an LCR meter [75]. Abbreviations: GE – gel electrode; MR – moisturiser; TE – textile electrode.

The centre-to-centre distance between adjacent electrodes was fixed at 10 cm, adhering to the standard protocol for tibial nerve stimulation [188]. Consequently, the impedance ($Z_{Cb}$) at the middle point (b), denoted as:

$$Z_{Cb} = \frac{Z_{ab} + Z_{bc} - Z_{ac}}{2} \tag{5.2}$$

where $Z_{ab}$, $Z_{bc}$ and $Z_{ac}$ denote the total impedance between the corresponding measurement points.

The central moisturised TE (Fig. 5.18) was secured to the skin using surgical tape, a compression band, or the leg portion of a sock, while the GEs were directly affixed to the skin. A force sensor was positioned on the anterior side of the lower leg, opposite the TE, to monitor an additional compression force uniformly applied around the leg's circumference. This compression force was varied between 0 N (achieved by gently securing the TEs to the skin surface using surgical tape without applying additional pressure) to up to 2 N (by using a compression band to apply controlled tightening over the TEs). The electrode-tissue impedance (ETI) was measured using an LCR meter over a frequency range of 20 Hz to 200 kHz [217].

The TEs were characterised under varying compression forces. For the stretchable leg portion of the sock, the corresponding compression force ranged from 0.8 to 1.1 N due to individual differences in the lower leg muscle size among participants. Such variation is unavoidable in real-world scenarios. In practice, sock sizes in the UK are broadly categorised (e.g., XS, S, M, L, XL), and even within these categories, compression levels can vary slightly depending on individual fit. For simplicity, the compression force applied by the leg portion of a typical medium-sized (UK 5–7) sock was hypothesised to 1 N, despite variations in leg size.

Fig. 5.19 illustrates that the GEs exhibited the lowest impedance levels, particularly at frequencies above 10 kHz. Within the frequency range of 10 to 20 kHz, the ETI of the TEs, when hydrated with 0.5 ml of body moisturiser, was comparable to that of the GEs. Moreover, increasing the compression force applied to the TEs further reduced their ETI, resulting in values lower than those observed for the GEs.

In general, greater compression improves electrode-skin contact by reducing resistance and minimising variations in contact impedance across different test subjects [218]. Applying external force to the TEs also enhances uniform and complete skin contact, thereby reducing ETI. However, forces exceeding 1 N

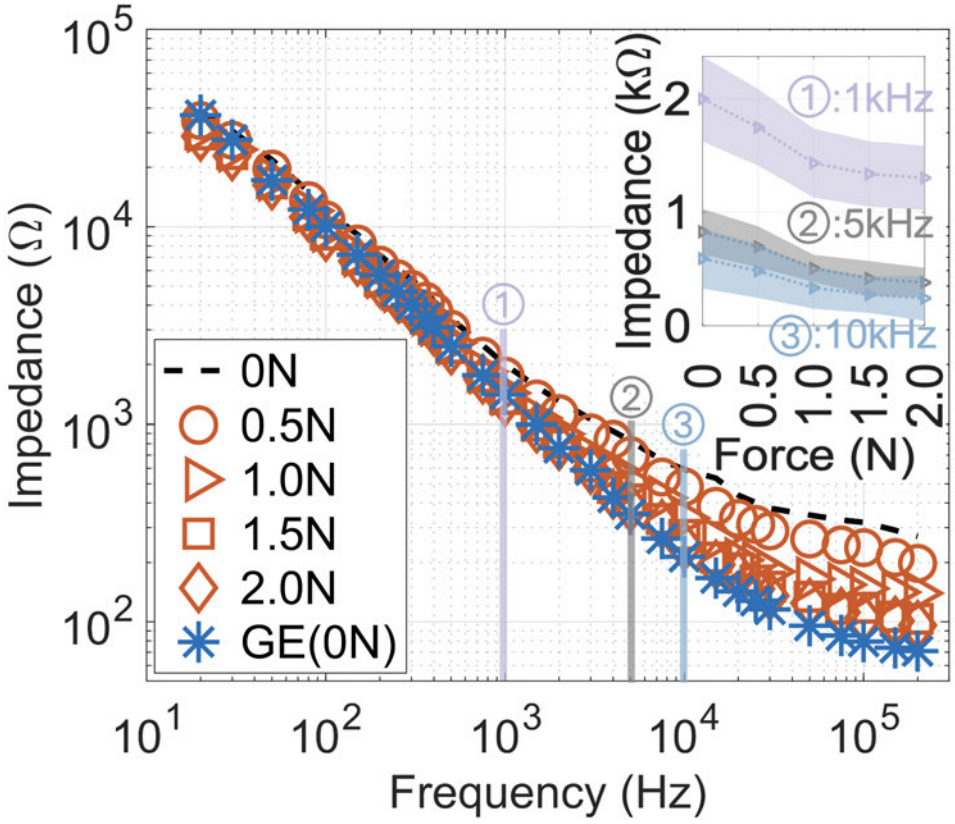


Fig. 5.19. The ETI of TEs under varying compression levels [75]. Abbreviation: GE – gel electrode.

were found to be impractical, as most participants reported discomfort or numbness when the applied force surpassed 1.5 N.

Although notable variations in the measured ETI were observed among participants, these variations decreased progressively as greater compression forces were applied. These results suggest that the combination of moisturiser-hydrated skin and additional compression improves electrode-skin contact, thereby enhancing the performance of the TEs.

### 5.6.3 Short-term Durability

To evaluate the stability of the TE-tissue interface over an extended period, additional tests were conducted with a new participant. The skin preparation procedure was consistent with previous methods, with a minor adjustment in the electrolyte type: either a body moisturiser or water was applied prior to

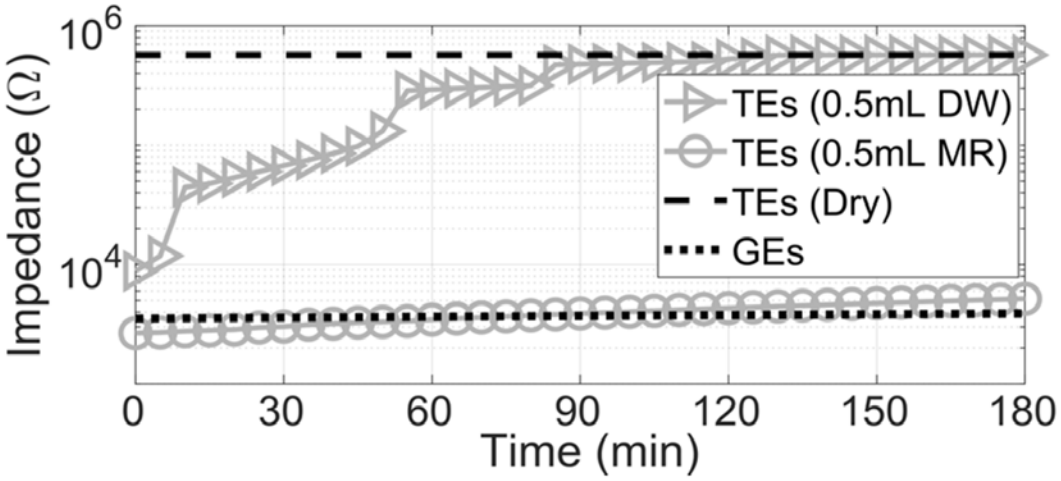


Fig. 5.20. Time-dependent ETI profiles of TEs hydrated with different electrolytes, compared to dry TEs and referenced GEs [75]. Abbreviations: DW – deionised water; MR – moisturiser.

monitoring impedance variations in the two TEs using an LCR meter. In real-life scenarios, tap water is often the most accessible electrolyte and is commonly used in literature [219], [132]. However, its composition can vary significantly based on geographic location and time, making it unsuitable for reproducible testing. Deionised water, on the other hand, provides stable and consistent properties, making it a more appropriate reference for controlled evaluations.

Given the practical relevance of electrolyte choice in real-world use, especially for home-based applications, this step also considered the scenario where the wearable device may be worn for several hours before stimulation begins. During this period, electrolyte drying may increase the ETI, potentially causing discomfort, such as sharp or stinging sensations, due to uneven current distribution at the electrolyte-tissue interface [220]. To address this concern, the study compared changes in ETI over time using a preferred body moisturiser, deionised water, and standard GEs.

The gel layer of the GE exhibited a slow drying process, as evidenced by a gradual increase in impedance over time. Conversely, the ETI of the TE hydrated with deionised water increased more rapidly over a 10-minute period compared to the TE hydrated with body moisturiser, as depicted in Fig. 5.20. This difference is likely attributable to the oil-based components of the body moisturiser, which act to reduce water evaporation.

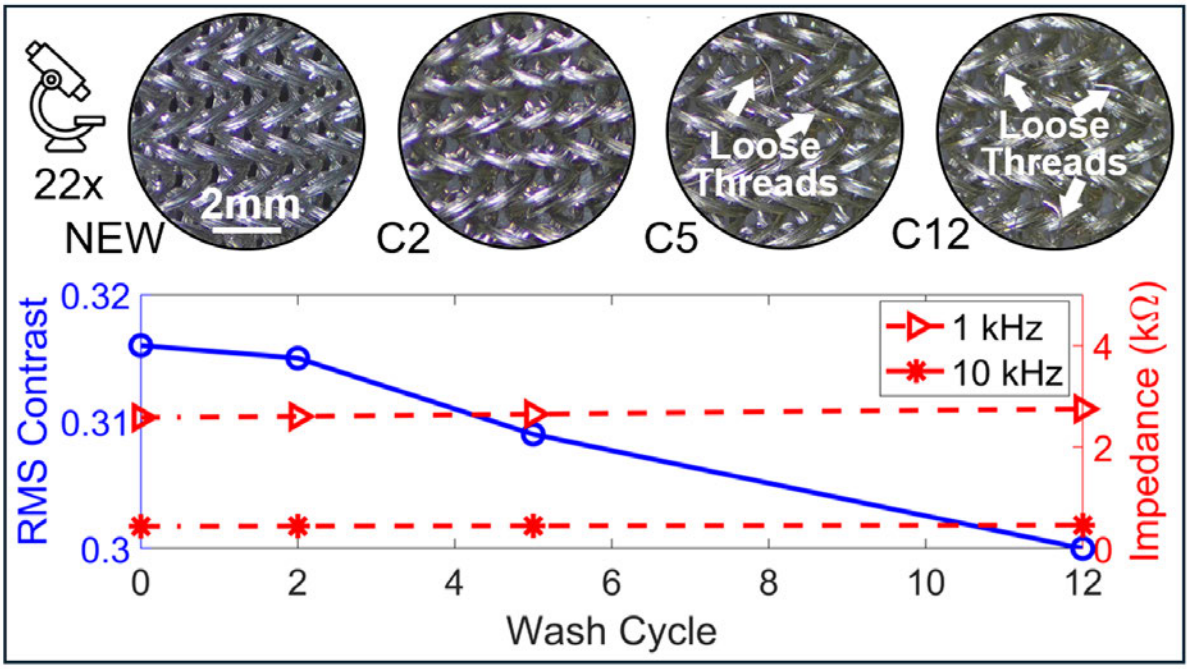


Fig. 5.21. Variance in surface appearance and electrical property of embedded TEs against multiple wash cycles [75]. Abbreviation: C – cycle (hand-washing).

Based on these observations, the application of 0.5 mL of body moisturiser per electrode site was found to be effective in maintaining stable impedance levels. This approach enables continuous stimulation for at least three hours without requiring re-hydration of the skin surface. Furthermore, no changes in elasticity or slippage were observed during the use of the socks.

### 5.6.4 Washability

A single participant was instructed to wear a newly constructed sock embedded with TEs on the first day of the experiment. The total impedance of the system was measured using an LCR meter. Afterward, the sock was hand-washed and air-dried. The TEs were then examined using a digital microscope (AO-V128S, AOSIV) at a magnification of 22×. This process was repeated daily over 12 consecutive days, resulting in a total of 13 days of data. The microscopic images were then analysed using the RMS contrast [221], which is defined as:

$$C_{RMS} = \sqrt{\frac{1}{n-1}\sum_{i=1}^{n}(x_i - \bar{x})^2} \tag{5.3}$$

where $x_i$ denotes a normalised gray-scale value, ranging from 0 to 1, and $\bar{x}$ represents the mean of $x_i$. Similarly, the impedances of the TEs were measured after each cycle.

The newly constructed TE exhibited the highest RMS contrast under microscopic observation, appearing as the most reflective surface. This reflectivity is attributed to the pristine silver-coated electrode surface, which effectively reflects ambient light. As illustrated in Fig. 5.21, the RMS contrast progressively decreased over 12 successive washing cycles conducted across 13 days, revealing an increasing presence of dark areas in the microscopic images. This reduction in contrast is likely due to partial degradation of the coated conductive surface. However, despite this surface degradation and the presence of loose threads, these factors did not impact the ETI of the TEs when hydrated with body moisturiser.

## 5.7 Electrical Assessment of TENS*mini* Device

The designed TENS*mini* device was configured to deliver constant current pulses across various output loads. Specifically, it generated 10 Hz pulses with an amplitude of 20 mA and a pulse width of 200 µs, which were applied to resistors with values ranging from 100 Ω to 10 kΩ. To monitor the pulsed current, a digital oscilloscope was used to measure the voltage drop across a 1 Ω resistor connected in series with the load.

The functionality of feedback mechanism was assessed by simulating an electrode disconnection, achieved by abruptly removing a 1 kΩ resistor from the secondary conduction path while the device operated under normal conditions at a pulse amplitude of 20 mA. The voltage of $V_C$ was continuously monitored using the oscilloscope, and the maximum current amplitude was recorded as the load resistance was varied.

### 5.7.1 Constant Current Stimulation Pulses

The waveform of the stimulation pulses generated by the proposed TENS*mini* device was measured and determined to be monophasic, as illustrated in Fig. 5.22(a). Both the simulated and measured pulses, along with their respective spectra, are presented in Fig. 5.22(b). A close resemblance was observed between the shapes and spectral compositions of the two waveforms.

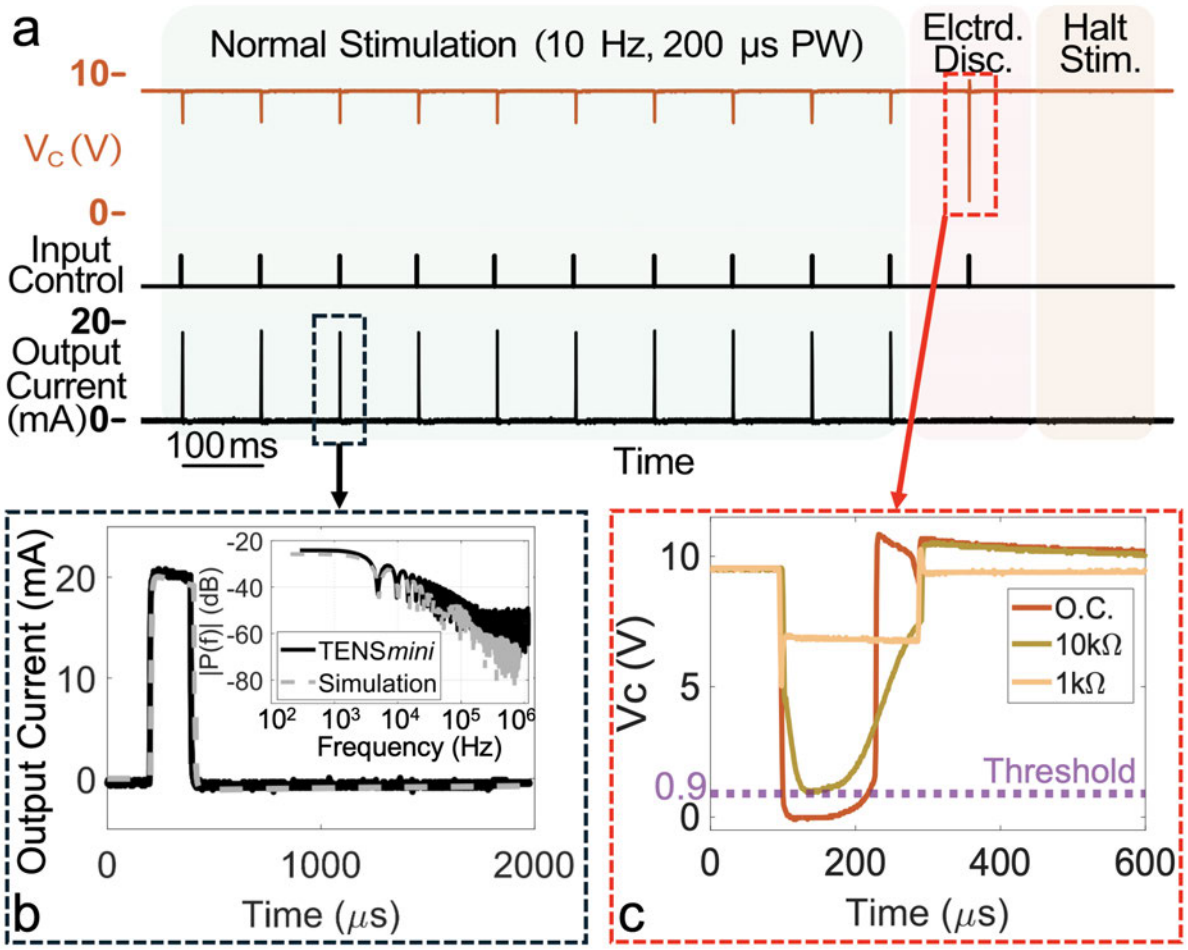


Fig. 5.22. Test results of the TENS*mini* device [75]: (a) Stimulation pulses and sensed voltage ($V_C$) under three scenarios: normal operation, electrode disconnection, and halted stimulation; (b) Comparison of simulated and measured monophasic stimulation pulses in the time and frequency domains; (c) Load-dependent $V_C$ waveforms with a predefined threshold (0.9 V) for detecting impedance exceedance during electrode disconnection events. Abbreviations: Elctrd. Disc. – electrode disconnection; O.C. – open circuit; PW – pulse width; Stim. – stimulation.

### 5.7.2 Electrode Disconnection Detection

The circuit was designed to ensure that, in the event of an electrode disconnection or a secondary open circuit, $V_C$ would abruptly drop below the defined threshold of 0.9 V, irrespective of the pulse amplitude, as shown in Fig. 5.22(c). This behaviour demonstrates the effectiveness of the proposed feedback mechanism in automatically halting stimulation when the connected load exceeds 10 kΩ. In practical

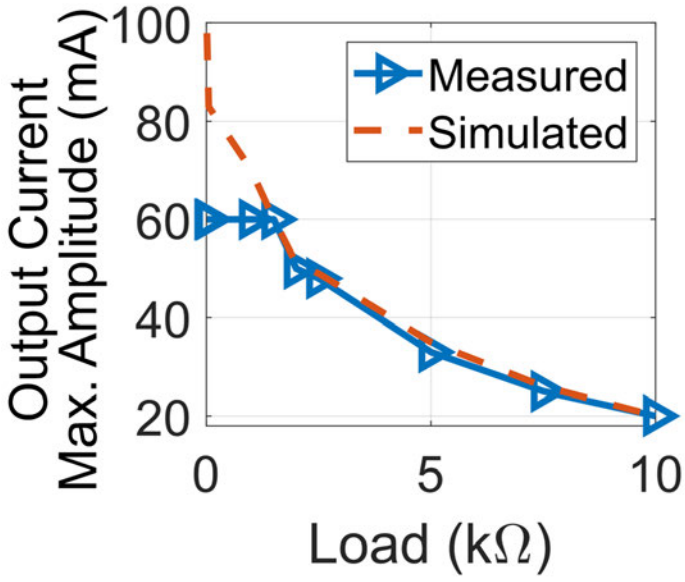


Fig. 5.23. Load-dependent output current maximum amplitude [75].

scenarios, such conditions may arise from a gradual increase in impedance, which is likely attributable to electrolyte depletion (e.g., from body moisturisers) or unintended detachment of the sock from the leg.

### 5.7.3 Maximum Amplitude of Stimulation Pulses

The drive circuit was evaluated using a resistive load of 1 kΩ. The maximum amplitude of the stimulation pulses was established based on prior findings in [222], which indicated that 50 mA is sufficient for transcutaneous tibial nerve stimulation (TTNS) to elicit sensory and motor responses in older patients. When the output load was increased to 10 kΩ, the maximum amplitude decreased gradually to 20 mA, as shown in Fig. 5.23.

This reduction in amplitude is attributed to the compliance voltage of the drive circuit, which is determined by the maximum secondary voltage of the transformer, assuming minimal voltage losses from other components.

Table 5.4. Selected technical specifications of TENS*mini* device comparable to other OAB management devices [75].

| Parameters | NeuroTrac® Continence [63] | TENSI+ [70] | Zida® Control Sock [71] | **TENS*mini*** |
|---|---|---|---|---|
| Dimension (inc. Bat.) (L × W × H) [Volume] | 119.2 × 69 × 28.7 $mm^3$ [236.1 $cm^3$] | 110 × 40 × 16 $mm^3$ [70.4 $cm^3$] | 65 × 40 × 17 $mm^3$ [44.2 $cm^3$] | **38 × 38 × 21 $mm^3$ [30.3 $cm^3$]** |
| Weight (inc. Bat.) | 100 g | 65 g | 38 g* | **31 g** |
| Bat. Type [Capacity] | 9V Alkaline [1200 mAh*] | 3.7V LiPo [NS] | 1.5 V AAA [1200 mAh*] | **3.3 V LiPo [300 mAh]** |
| Galvanic Isolation | Transformer | NS | NS | **Transformer** |
| Intensity Range (with Load) | 0–86 mA (1 kΩ) | 0–50 mA (1 kΩ) | 0–156 mA (500 Ω) | **0–60 mA (1 kΩ)** |
| Stimulation Frequency | 2–100 Hz | 10–20 Hz | 20 Hz (Fixed) | **1–100 Hz** |
| Pulse Width | 50–450 µs | 150–200 µs | 200 µs (Fixed) | **50–250 µs** |
| Device Control | Buttons on Device | Buttons on Device | Buttons on Device | **Mobile App via Bluetooth®** |
| Electrode type | Adhesive Gel | Silicone Graphite | Conductive Textile | **Conductive Textile** |
| Electrode Washability | N/A | N/A | NS | **12 Washes** |
| Accurate Electrode Positioning | N/A | N/A | No | **Yes** |

Notes: Batt.: Battery; LiPo: lithium polymer; N/A: not applicable; NS: not specified; *: estimated.

## 5.8 Comparison of Technical Specifications

The technical parameters of wearable TENS devices designed for TTNS are compared in Table 5.4. The designed TENS*mini* device is distinguished by its compact and lightweight design in comparison to alternative solutions. Enhanced safety features are incorporated, including an automatic electrode detection mechanism, and electrode misplacement is mitigated through the implementation of a split-toe sock design. Usability is further improved by the inclusion of a rechargeable LiPo battery, with a selected capacity of 300 mAh, which has been verified to support multiple 30-minute treatment sessions on a single charge. Additionally, the integration of a Bluetooth® module enables wireless control, further enhancing system functionality.

In numerous clinical studies addressing overactive bladder (OAB) treatment, stimulation parameters commonly employed include a frequency of 10 Hz and a pulse width of 200 µs [34]. However, consensus on the optimal parameter configuration remains lacking [223], [224], [56]. To accommodate this variability, the TENS*mini*, akin to NeuroTrac® Continence and TENSI+, provides a range of configurable options. Furthermore, lower frequency settings (e.g., 1 Hz) are required for the treatment of certain lower urinary tract conditions, such as urinary retention [225]. The capability to support 1 Hz stimulation has been incorporated into the proposed design, thereby expanding its potential therapeutic applications.

## 5.9 Conclusion

Laboratory testing of the TENS*mini* stimulator confirmed expected pulse generation and the effectiveness of its automatic shut-off function upon electrode disconnection, demonstrating its reliability and safety. Although the involvement of a single participant is acknowledged as a limitation, the findings offer valuable insights into the ETI consistency of the custom sock-based TEs. They provide preliminary evidence supporting the short-term durability and washability of the wearable electrodes. Additionally, these results underscore the potential of this wearable solution for home-based OAB management. However, further human pilot studies are required to assess its efficacy in TTNS and validate its practical applicability in real-world settings.

# Chapter 6

# Human Pilot Studies

Tibial nerve neuromodulation has been increasingly recognised as an effective treatment modality for managing overactive bladder (OAB). In recent years, various clinical trials have employed handheld or benchtop transcutaneous electrical nerve stimulation (TENS) devices to deliver tibial nerve stimulation. However, these devices have several limitations, particularly in patient adherence, which could be attributed to factors such as adhesive gel incompatibility and challenges in electrode positioning. To address these issues, a home-based OAB management device (wearable TENS*mini*) was developed with the objective of improved usability. While the performance of this device was evaluated in laboratory environments (Chapter 5, Section 5.7), its physiological effectiveness in real-world settings has not yet been assessed.

To explore the physiological responses induced by the TENS*mini* device, two pilot studies have been designed to evaluate (1) its efficacy of neuromuscular recruitment, and (2) its behavioural effectiveness on bladder functionality via transcutaneous tibial nerve system (TTNS). Neuromuscular recruitment via TTNS is not a novel concept, several prior studies have explored frequency-dependent effects (i.e., excitatory and inhibitory) in animal models [61], [140], [226]. However, these findings remain theoretical, as limited studies to date have fully investigated these effects in humans due to lack of non-invasive approaches.

Table 6.1. Measured and maximum allowed values of technical parameters of TENS*mini* device.

| Parameters | Measured Value | Maximum Allowed Value | Remarks |
|---|---|---|---|
| Dimension | $38 \times 38 \times 21$ mm$^3$ | – | – |
| Weight | 31 g | – | – |
| Battery [Capacity] | Lithium polymer [300 mAh] | – | – |
| Amplitude (PP value) | 1–50 mA | – | – |
| Amplitude (RMS value) | 4.05 mA | 50 mA (when $f \leq 400$ Hz) | Maximum frequency is 25 Hz. |
| Frequency ($f$) | 1–25 Hz | – | – |
| Pulse Width (PW) | 50–250 μs | – | – |
| Single-pulse Energy | 0.338 mJ | 300 mJ (when PW < 0.1 s) | PW is 250 μs. |
| Output Voltage (under OC condition) | 146 V | 500 V | – |

Notes: OC: open circuit; PP: peak-to-peak; PW: pulse width; RMS: root-mean-square; –: not applicable.

Both studies aim to evaluate whether the TENS*mini* device can elicit stimulatory responses and induce physiological responses related to bladder function in healthy participants, comparable to those produced by a clinically approved, research-grade stimulator. Demonstrating comparable efficacy would establish the potential of the device as an alternative to existing TTNS therapy and provide a basis for further clinical investigation in patients with OAB and related lower urinary tract disorders.

## 6.1 Pre-study Electrical Safety Test

In line with UK regulations, and ethical research practices [227], pre-study testing was conducted to ensure the device's safety during use. The test was carried out by Eurofins Scientific Ltd., a UKAS-accredited testing body. Compliance with the EN 60601-2-10:2012+A1:2016 Standard (Clause 201.12.4.104), which governs the limitation of output parameters, was verified [136]. A summary of these test results is presented in Table 6.1.

## 6.2 Pilot Study I: Tibial Nerve Recruitment

### 6.2.1 Ethics and Recruitment

The study protocol was reviewed and approved by the local ethics committee of The University of Edinburgh (Ref.: RT2021/83413). The study was advertised through The University of Edinburgh via internal mailing lists. Recruitment efforts were further expanded using personal social media channels and in-person advertisements, such as flyers and posters. The following exclusion criteria were applied:

- Individuals under the age of 18;
- Individuals with any pre-existing urinary tract disorders;
- Individuals with pre-existing cardiovascular conditions;
- Individuals with implanted medical devices, such as pacemakers or defibrillators;
- Individuals with uncontrolled epilepsy;
- Individuals with broken, fragile, thin, or infected skin at the treatment site (i.e., right foot ankle);
- Pregnant individuals;
- Individuals with nerve damage;
- Individuals lacking the capacity to provide informed consent.

Ten healthy participants (four women and six men, age range: 22–55 years) were recruited. Participants had no prior knowledge of the purpose of the trial beyond the context of the study, as described in the Participant Information Sheet (Appendix C). Written informed consent (Appendix C) was obtained from all participants prior to the study.

### 6.2.2 Study Protocol

#### Overview and Group Allocation

The previous study protocol including experimental setups for TTNS and electromyographic (EMG) recording was followed and adapted into this protocol. Participants used either a designed wearable OAB management device (TENS*mini*) or a clinical-grade device (DS7A). Each session lasted approximately 40 minutes.

Ten participants were assigned to two groups in pseudorandom order, with each group consisting of five participants. The procedure was counterbalanced to mitigate potential order effects, with participants in Group A using TENS*mini* followed by DS7A, and participants in Group B using DS7A followed by TENS*mini*. Each participant used both devices in two independent sessions, separated by a 15-minute rest period to minimise fatigue and carryover effects.

#### TTNS and EMG Recording Configuration

Before initiating TTNS, the stimulation sites on the posterior side of the lower right leg were prepared following the skin preparation procedure outlined in Chapter 3, Section 3.2.4. For the DS7A device, clinical-grade gel electrodes (GEs) were used, with their placement detailed in the same chapter. For the TENS*mini* device, participants wore a sock equipped with two built-in textile electrodes (TEs).

Both stimulators were set to deliver continuous constant-current stimulation pulses with a fixed frequency of 2 Hz and a pulse width of 200 μs. The current amplitude was increased in 2 mA increments, up to a maximum of 40 mA or until the participant experienced discomfort. At each amplitude level, 30 stimulation pulses were delivered.

Stimulation-evoked EMG signals were recorded using a NeuroRecorder (Blackrock Microsystems, Blackrock Neurotech). These recordings served to confirm the effective delivery of stimulation to the neuromuscular system. Details regarding the electrode placement for EMG recording can be found in Chapter 3, Section 3.2. Before digitisation, the EMG signals were bandpass filtered between 10 and 500 Hz. A 50 Hz notch filter was also applied to attenuate the powerline noise. The EMG signals were subsequently sampled at a rate of 10 kHz and saved in the NS4 format.

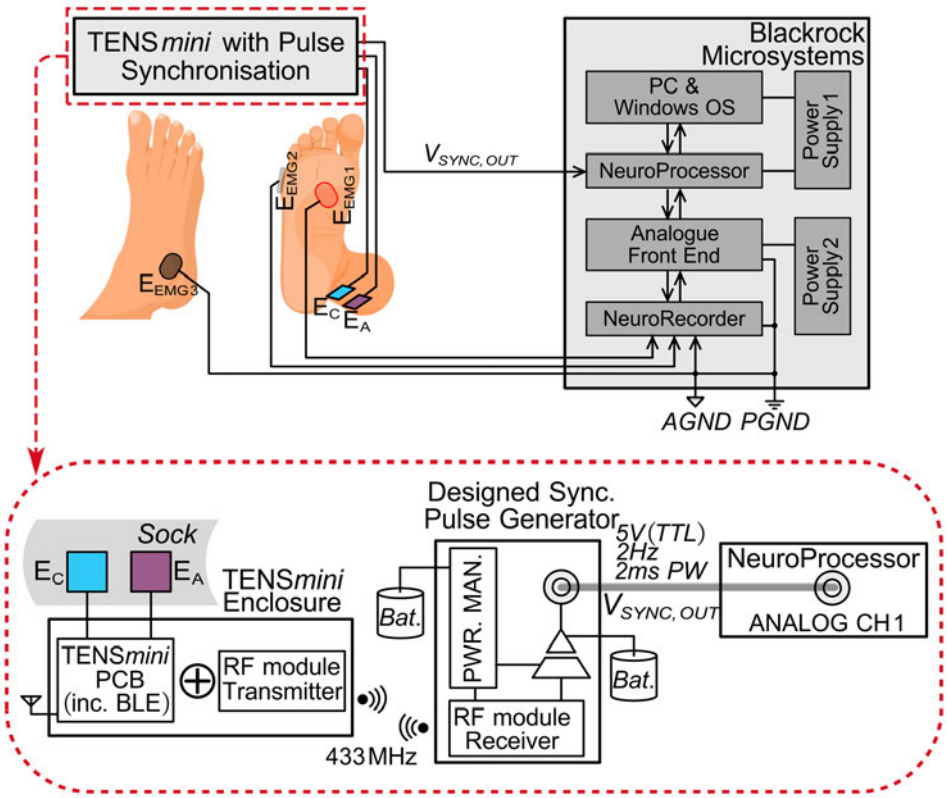


Fig. 6.1. Experimental setup showing the placement of three EMG electrodes with detailed configurations for synchronisation of stimulation through TENS*mini* device and EMG recording.

Synchronisation pulses are critical for enabling the NeuroProcessor to effectively trigger the NeuroRecorder for EMG signal acquisition in Trigger Mode. For the DS7A device, the same synchronisation method was re-employed in this study. A detailed description of the setup is also provided in Chapter 3, Section 3.2. For the proposed TENS*mini* stimulator, a 433 MHz receiver/transmitter pair (MDU-1015, HandsOn Technology) was utilised. The transmitter module was integrated into the TENS*mini* hardware board and housed within its enclosure, while the receiver module was incorporated into a custom-designed pulse generator. This generator was responsible for delivering synchronisation pulses to the NeuroProcessor. The detailed configuration is shown in Fig. 6.1.

### EMG Data Processing and Analysis

The recorded EMG signals were segmented into 30 independent slices, each containing a single evoked EMG trace, facilitating ensemble averaging. The mean, tenth, and 90th percentiles of the data sets

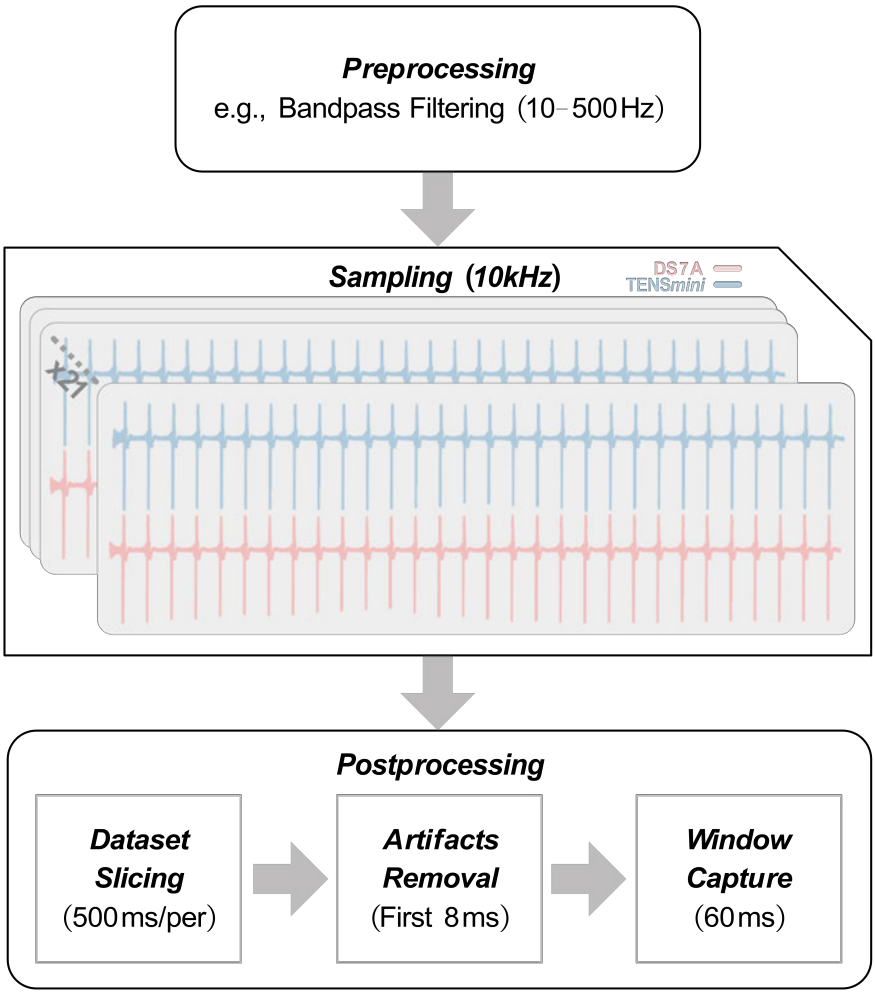


Fig. 6.2. EMG data processing pipeline."×21" denotes twenty-one recorded datasets, each corresponding to a different stimulation intensity step (in 2 mA increments), ranging from 0 mA up to a maximum of 40 mA.

were subsequently calculated across all participants. The peak-to-peak amplitude of the M-wave, or motor evoked potential (MEP), was analysed. MEPs are commonly used to assess nerve activation properties [228]. The start time of each EMG recording was determined by referencing the rising edge of the corresponding synchronisation pulse. To mitigate the influence of stimulation artifacts, the first 8 ms following stimulation onset were automatically excluded from the EMG signals. This exclusion window was approximated based on observations across all participant recorded datasets. After identifying the onset of the M-wave, a 60 ms time window was applied for MEP calculation. The data processing pipeline is illustrated in Fig. 6.2, and the graphical representation of the MEP calculation method can be found in Fig. 3.6 (Chapter 3).

The relationship between the MEP amplitude and stimulation amplitude (also known as the neuromuscular recruitment curve) is typically modelled using a Boltzmann sigmoidal curve [229], [230], [231]. However, due to the limited information available from neuromuscular recruitment curves induced by both TENS*mini* and DS7A stimulators (where MEPs increased up to the maximum tested amplitude of 40 mA, which could remain below the saturation point for most participants due to ethical constraints), it is not feasible to fully characterise or compare either stimulator using its modelled curve fit alone. Results and their limited interpretation are presented in Section 6.4.1. To compare the effectiveness of tibial nerve activation between two stimulators, further statistical analysis of MEP data at matched stimulation levels was conducted.

### Statistical Analysis of MEP Data

To evaluate the agreement and statistical equivalence between the TENS*mini* and the DS7A stimulators, a two one-sided t-test (TTOST) was employed. This method evaluates whether the observed mean difference between two conditions falls within a predefined equivalence margin ($\Delta$). In this study, the equivalence margin was set to $\pm 0.018$ mV (i.e., 20% of the overall mean MEP amplitude). The test computes two t-statistics: (1) one for the lower bound, testing $H_0: \mu_d \leq -\Delta$, and (2) the other for upper bound, testing $H_0: \mu_d \geq +\Delta$ (where $\mu_d$ is the mean of paired differences, that is the bias). Equivalence is concluded if both null hypotheses are rejected at the predetermined alpha level (i.e., 0.05), indicating the observed mean difference lies within the interval $(-\Delta, +\Delta)$ with sufficient statistical confidence.

In addition to equivalence testing (via TTOST), agreement between both stimulators was assessed using a Bland–Altman analysis. This method presents the paired difference of measurements against the mean of each pair, and includes limits of agreement (defined as $\mu_d \pm 1.96\sigma_d$, where $\sigma_d$ denotes the standard deviation of paired differences). Furthermore, intra-class correlation (ICC) was computed using a two-way mixed-effects model for absolute agreement ($ICC_{(3,1)}$), which is appropriate for evaluating device-level consistency. Confidence intervals (CI; 95%) and $F$-statistics were also reported to support the reliability analysis.

#### Comfort Evaluation of Electrodes

Upon completion of each TTNS session, the participants were instructed completed a survey questionnaire (Appendix C) to assess which class of electrodes (GE or TE) was more comfortable. A Likert scale (where 1 indicates total dissatisfaction and 5 represents the highest level of satisfaction) was utilised to quantify the user comfort (for both devices) and ease of wearing (specific to TENS*mini*).

## 6.3 Pilot Study II: Frequency-dependent Effects on Bladder Function

### 6.3.1 Ethics and Recruitment

The protocol of this study was reviewed and approved by the local ethics committee of The University of Edinburgh (Ref: RT977504). The recruitment was conducted using the approaches of the Pilot Study I, with the same exclusion criteria applied.

A total of 47 healthy volunteers (20 females and 27 males, age range: 21–52 years) were recruited for the second study. They had no prior knowledge of the purpose of the trial beyond the context of the study, as outlined in the Participant Information Sheet (Appendix C). Written informed consent (Appendix C) was obtained from all participants prior to the study.

### 6.3.2 Study Protocol

#### Purpose

The urge to urinate was specifically assessed in healthy participants, as it constitutes a reliable and non-invasive proxy for clinically relevant bladder function. By measuring the elapsed time until the initial sensation of urge and evaluating its intensity, afferent bladder somatosensation could be accurately quantified.

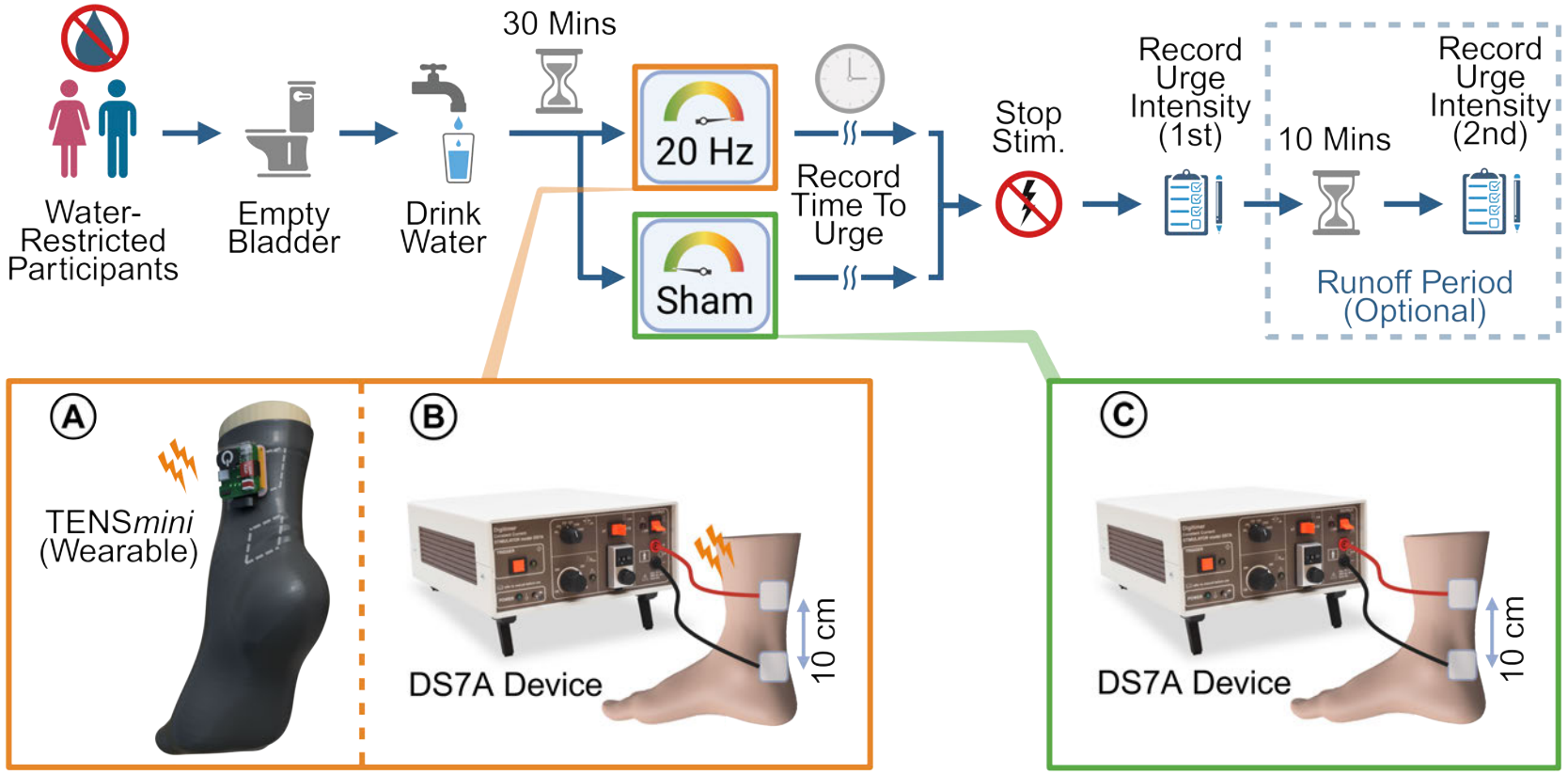


Fig. 6.3. Graphical overview of the study protocol, depicting Groups A and B receiving the TTNS from comparable stimulators (TENS*mini* versus DS7A), and Group C receiving a placebo stimulation [76]. Abbreviation: Stim. – Stimulation.

### Group Allocation

Participants were pseudo-randomly assigned to one of three groups, namely TENS*mini* (Group A), DS7A (Group B) or Sham (Group C), as depicted in Fig. 6.3. The allocation procedure was counter-balanced to mitigate potential order effects. A single-blinded, between-subjects design was employed. Participants were not informed about their group allocation. This protocol was inspired by an earlier work [225].

### Pre-TTNS Preparation

Participants were instructed to abstain from caffeine, nicotine, and other bladder modulating substances for a minimum of 12 hours before their scheduled sessions. They were also advised to refrain from fluid intake for at least two hours prior to arrival. Upon arrival, each participant received a briefing on the study and was instructed to completely empty their bladder in the nearby toilet. Subsequently, each participant was instructed to drink 750 mL of water.

A 30-minute waiting period was implemented to allow natural bladder filling before the initiation of TTNS. During this time, participants were instructed to remain seated and engage only in steady activities, such as casual conversation or desk work. This period was included to facilitate the natural and adequate accumulation of urine in the bladder prior to the onset of TTNS.

Near the end of the 30-minute period, the stimulation sites located on the posterior side of the lower right leg were prepared using an aforementioned procedure (Chapter 3, Section 3.2). The cathodal electrode was then placed 1 cm posterior to the medial malleolus and the anodal electrode 10 cm proximally. Clinical grade GEs were used for the DS7A stimulator. For TENS*mini*, conductive TEs integrated within the sock were used. For this group, we applied two (fingertip) dips (approximately 5 mL) of general purpose body moisturiser, e.g., NIVEA$^{TM}$ Crème [73]. For the controlled Sham group, all participants underwent identical skin preparation procedures and received placebo stimulation using GEs connected to the DS7A device. During the placebo session, DS7A device was turned on without delivering any pulses, and participants were informed that experiencing no sensation was normal. To minimise bias, identical instructions were also provided to participants in the other two experimental groups.

### TTNS and Urge Measurement

The stimulator (TENS*mini* or DS7A) was activated immediately after a 30 minute waiting period, delivering continuous TTNS at an initial frequency of 1 Hz with a pulse width of 200 μs. The intensity of stimulation was gradually increased through a Bluetooth-controlled mobile application until the motor threshold was reached, as indicated by the observable movement of the participant's big toe. Once the threshold was identified, the stimulation was stopped and the frequency was reconfigured to 20 Hz. Subsequently, the reset intensity was adjusted to the motor threshold level or a self-identified comfortable level for each participant. This intensity level was maintained throughout the TTNS session.

Identification of big toe movement was unnecessary for participants in the Sham group. The stimulation parameters of the placebo session were configured to a frequency of 20 Hz and a pulse width of 200 μs, with the intensity maintained at 0 mA. Participants were informed that the stimulator was functioning correctly as long as they reported no perceptible stimulation in the lower leg.

Participants were instructed to notify the researcher when they experienced their first urge to urinate, at which point the stimulation would be immediately stopped. When this urge was reported, the time since water ingestion was recorded. The participants were then asked to complete a validated urge intensity survey form (Table 6.2), rating their urgency on a scale from Level 0 (no urge) to Level 4 (desperate urge).

### Post-TTNS Testing

After completion of the initial portion of the study, participants were invited to undergo an optional final test, during which they passively waited for an additional ten minutes without TTNS. The post-TTNS testing was initially designed as an optional session due to ethical considerations regarding participant's tolerance of induced urge urinary sensation. At the end of this runoff period, participants once again completed the urge intensity survey form (Table 6.2).

Table 6.2. Urge intensity survey form [225].

| Description | Rated by Participant |
|---|---|
| Level 0: Convenience (No urge) | □ |
| Level 1: Mild Urge (Can hold for greater than one hour) | □ |
| Level 2: Moderate Urge (Can hold for 10–60 minutes) | □ |
| Level 3: Severe Urge (Can hold for less than 10 minutes) | □ |
| Level 4: Desperate Urge (Must go immediately) | □ |

#### Statistical Analysis

All data collected were recorded electronically and securely stored in compliance with The University of Edinburgh's data protection guidelines. Data analysis was performed using a Kruskal–Wallis test, followed by post hoc Mann–Whitney U tests adjusted for multiple comparisons. Non-parametric statistical methods were used due to the slight variation in sample sizes among the three test groups. Where non-parametric analysis was not possible (when analysing the effects of multiple factors on urge intensity), a mixed-factorial analysis of variance (ANOVA) was performed to examine the effects of two factors: (1) the 10-minute runoff period (Before vs. After) as the within-subject factor, and (2) three stimulation conditions including 20 Hz by TENS*mini*, 20 Hz via DS7A, and Placebo (sham stimulation) through DS7A, as the between-subject factor, followed by post hoc tests adjusted for multiple comparisons.

## 6.4 Results

### 6.4.1 Results of Pilot Study I

#### Evoked EMG Responses

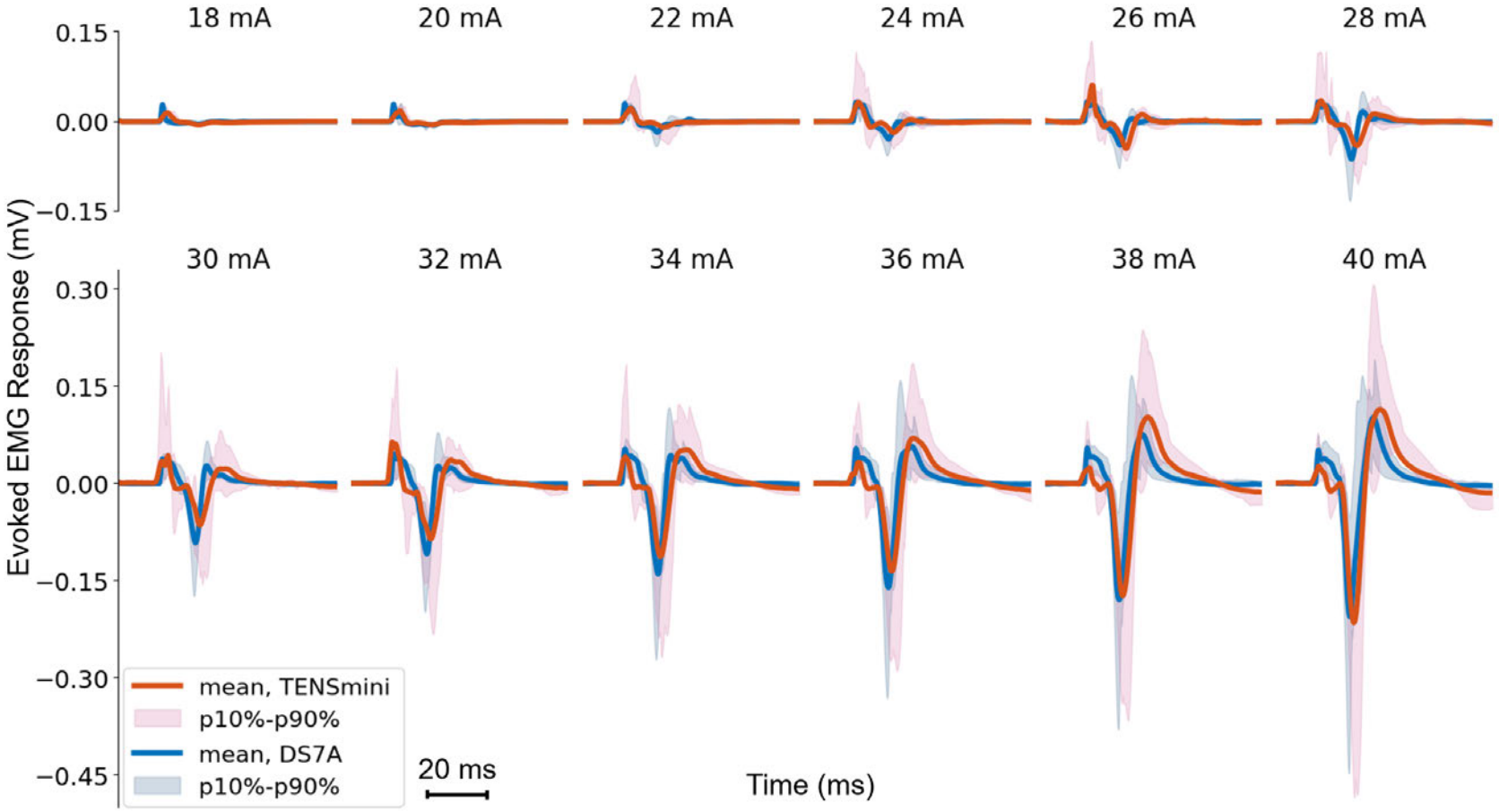


Fig. 6.4. Evoked EMG responses at varying stimulation amplitudes from 18 to 40 mA, in 2 mA increments [75].

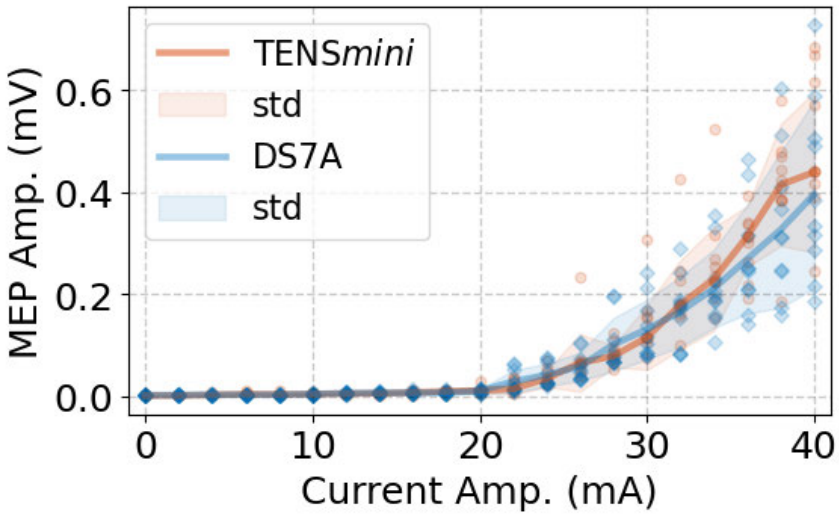


Fig. 6.5. Neuromuscular recruitment curves showing the relationship between MEP amplitude and stimulation amplitude for the TENS*mini* (pink) and DS7A (sky-blue) stimulators. Shaded areas represent ±1 standard deviation (std) across participants [75]. Abbreviation: Amp. – Amplitude.

Fig. 6.4 illustrates the mean EMG responses elicited by the designed wearable OAB management device (i.e., TENS*mini*; depicted in red) in comparison to those generated by the DS7A stimulator (depicted in blue). The shaded regions surrounding each mean response curve represent the tenth to 90th percentile range, reflecting inter-participant variability.

EMG responses evoked at stimulus intensities below 18 mA are not presented, as they provide limited information. A notable trend is observed where an increase in stimulus intensity corresponds to a proportional increase in the amplitude of the evoked EMG responses.

### Neuromuscular Recruitment Curves and Equivalence Testing

The mean MEP amplitude is plotted against stimulation current amplitude for the TENS*mini* and DS7A stimulators, as shown in Fig. 6.5. Both devices show overlapping recruitment patterns between 0 and 34 mA, with MEP amplitudes remaining near zero within the lower stimulation intensity range and a noticeable increase observed after 20 mA. Each trace represents the group-averaged response, with shaded regions indicating ±1 standard deviation across all participants.

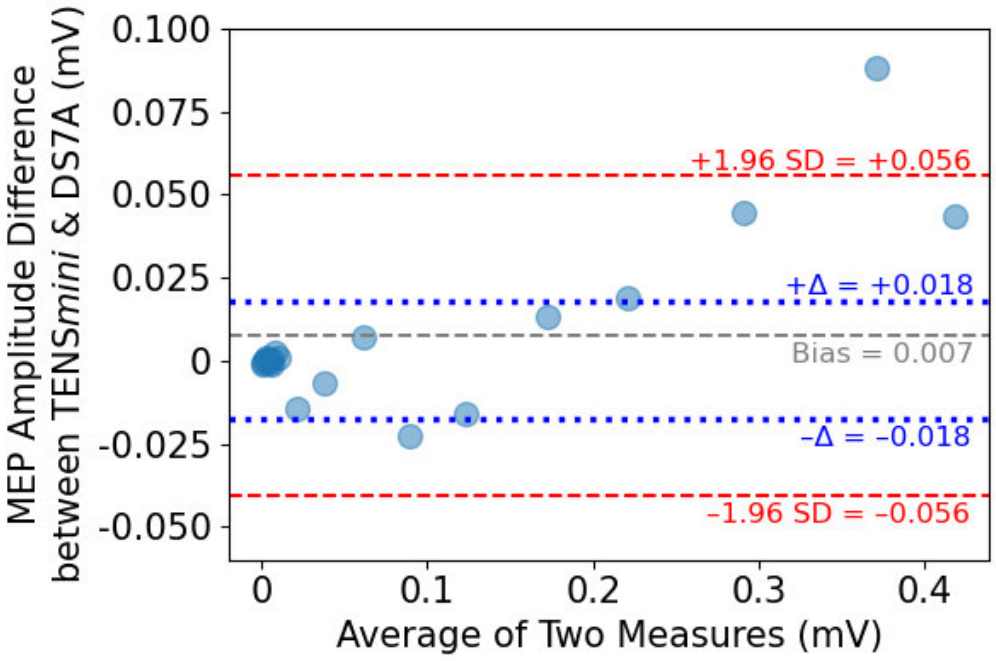


Fig. 6.6. Bland–Altman analysis for MEP amplitudes of TENS*mini* and DS7A.

The TTOST procedure indicated statistical equivalence between TENS*mini* and DS7A within a predefined equivalence margin (i.e., $\Delta = \pm\ 0.018$ mV), with $t_{lower} = 4.689$ ($p < 0.001$) and $t_{upper} = -1.905$ ($p = 0.036 < 0.05$). The mean difference in MEP between both devices was $0.007 \pm 0.0286$ mV. The Bland–Altman plot ( Fig. 6.6) showed most differences clustered near zero, with only one value exceeding the equivalence bounds and limits of agreement at higher stimulation intensity. The $ICC_{(3,1)}$ for absolute agreement was 0.982 (95% CI: [0.96, 0.99], $F = 112.85$, $p < 0.001$), indicating acceptable reliability between the two stimulators across the range of intensity (i.e., 0–40 mA).

### Comfort Evaluation Survey

For comfort, the wearable TENS*mini* achieved an average rating of 4, while the DS7A stimulator with GEs received a lower average rating of 1.5, as shown in Fig. 6.7. Regarding ease of wear, the process of putting on the sock was rated at approximately 3.5, whereas removing the sock received a higher average rating of 4.5.

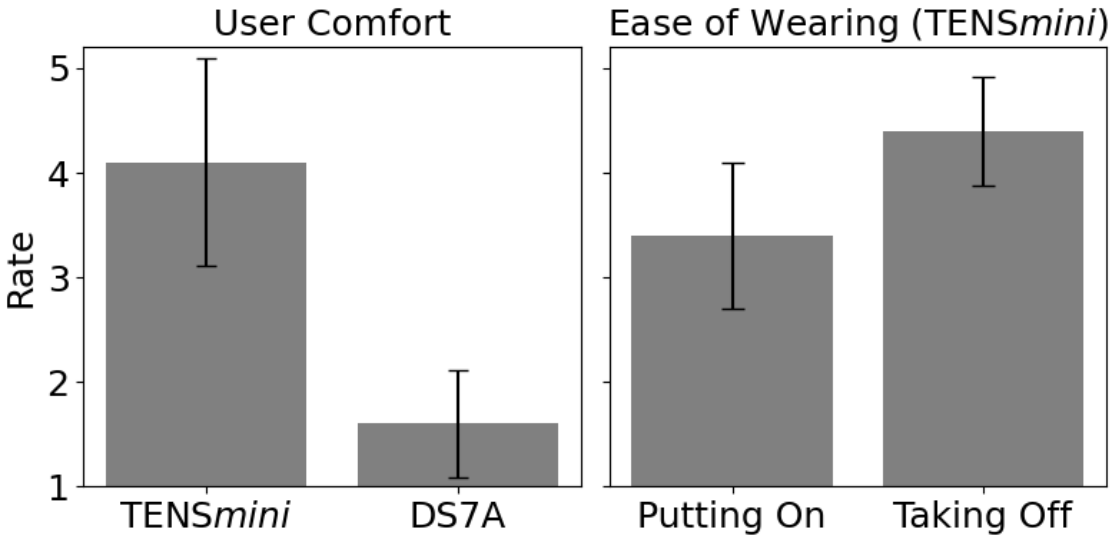


Fig. 6.7. Survey outcome related to user comfort (TENS*mini* versus DS7A) and ease of use (for TENS*mini* only) [75].

### 6.4.2 Results of Pilot II

#### Effects of TTNS on Micturition Reflex

A total of 16 participants were assigned to the TENS*mini* group and another 16 to the Sham group, while 15 participants were assigned to the DS7A group. Visual inspection indicated that the TENS*mini* and DS7A groups exhibited similar rank distributions[1], despite the presence of two outliers in the DS7A group, as depicted in Fig. 6.8. Statistical analysis demonstrated no significant difference between the time elapsed before the first urge (i.e., the duration of stimulation applied) across the TENS*mini* (11.9–52.4 min, mean: 36.72 min) and DS7A (8.1–56.25 min, mean: 37.4 min; $p = 1$) groups, revealing that their rank distributions[1] were likely identical. In contrast, both TENS*mini* and DS7A differed significantly from the Sham group (0–50.9 min, mean: 19.4 min; $p < 0.05$). This suggests that participants in the Sham group were likely to experience their initial urgency of micturition more quickly.

[1]Refers to the ordering of data points based on their relative magnitudes without assuming any specific underlying distribution (e.g., normal or exponential).

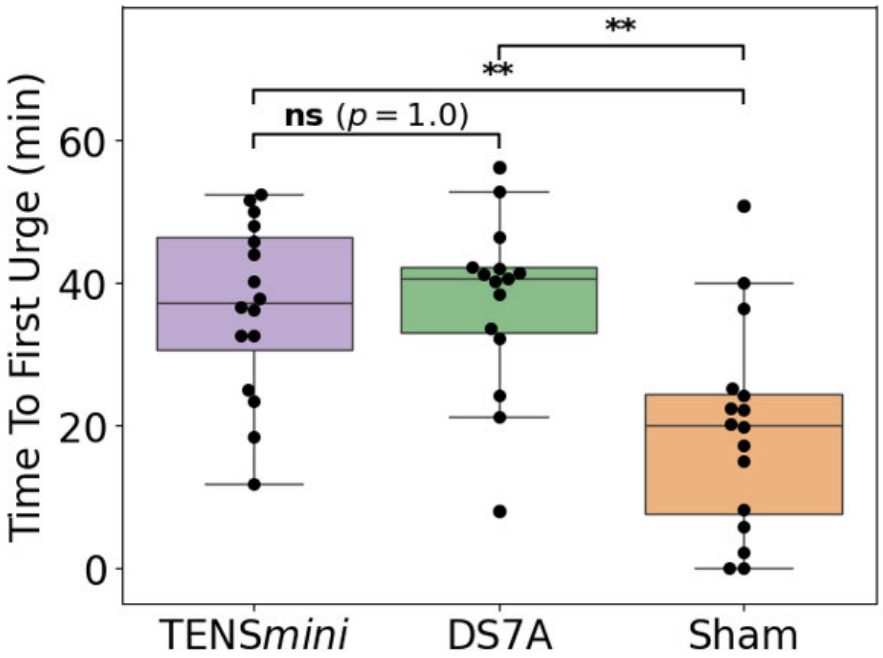


Fig. 6.8. Effect of 20-Hz TTNS on the time elapsed to the first sensation of urge [76]. Abbreviations: ns – non-significant; ∗∗ – significance at $0.01 < p < 0.05$.

### Effects of TTNS on Urge Intensity

The impact of the device on the intensity of the urge was evaluated at the onset of the first sensation of the urge and after a ten-minute runoff period. Although the post-TTNS evaluation session was optional, all participants (100%) attended it and completed the second survey.

A mixed-factorial ANOVA indicated that there was a significant main effect for the runoff period ($F_{(1,44)} = 65.19$, $p < 0.001$), indicating that participants reported significantly higher urge ratings after the runoff period compared to before, irrespective of three stimulation conditions. In contrast, no significant main effect was found for three stimulatory conditions ($F_{(2,44)} = 0.126$, $p = 0.9$), meaning the overall urge ratings did not differ significantly amongst three conditions.

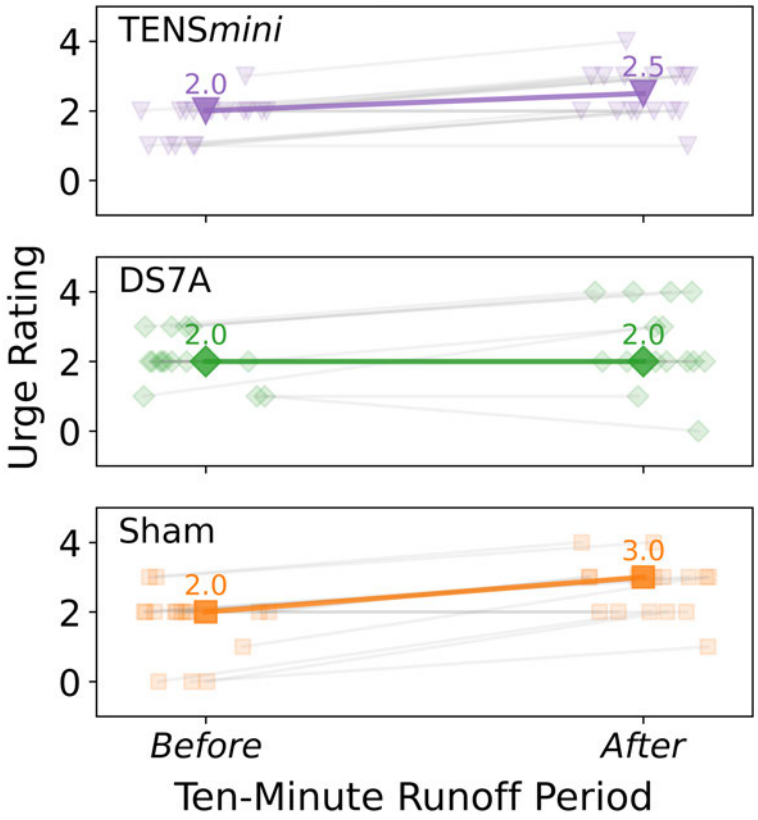


Fig. 6.9. Variance in self-reported urge intensity before and after the ten-minute runoff period [76]. Individual lighter data points were horizontally offset by applying a small random displacement ($\pm 0.15$) drawn from a uniform distribution. Darker points represent the median-value of these lighter points in each condition.

Post hoc pairwise testing (Fig. 6.9) using pooled data across all three stimulation conditions, confirming a significant overall increase in average urge intensity following the runoff period ($t_{(46)} = 7.644$, $p < 0.001$). The significant interaction effect between the two factors was also found ($F_{(2,44)} = 3.72$, $p = 0.03 < 0.05$), indicating that the increase in urge intensity from before to after the runoff period differed depending on the stimulator condition used. Specifically, this interaction highlighted that while all three conditions showed a general increase in urge intensity over time, the sham condition demonstrated a notably more rapid increase compared to the TENS*mini* and DS7A conditions (Fig. 6.9). However, post hoc analyses designed to isolate differences between specific conditions did not reveal significant pairwise differences, indicating that while the overall interaction is statistically significant, the precise differences among individual groups did not reach statistical significance in these comparisons.

Lastly, when comparing specifically the median scores at the end of the runoff period, participants using the TENS*mini* device reported a median urge intensity ($2.5 \pm 0.73$), closely matching the DS7A device group's median score ($2.0 \pm 1.19$).

## 6.5 Discussion

Ongoing debates in the academic literature regarding the relative efficacy of TTNS and PTNS in the management of OAB have consistently highlighted TTNS as safe and effective therapeutic option [34]. According to recent guidelines from the American Urological Association (AUA) [38], the importance of shared decision making between clinicians and patients has been emphasised. This collaborative approach allows therapy selection to be tailored to patient preferences, with TTNS frequently regarded as a preferable option due to its non-invasive nature.

In Pilot Study I, despite the larger inter-individual variation in EMG data caused by physiological differences among participants, the mean evoked EMG responses induced by both stimulators are visually comparable (Fig. 6.4). Equivalence testing via TTOST demonstrated that the mean difference in MEP amplitude between TENS*mini* and DS7A falls within the predefined equivalence margin. The $ICC_{(3,1)}$ value of 0.982 indicates excellent absolute agreement. Bland–Altman analysis revealed that paired differences remain near zero for stimulation intensity up to 28 mA, with a single outlier attributable to physiological variability amongst participants. Since most clinical protocols limit TTNS to motor threshold levels (typically below 30 mA for 10 Hz, 200 µs pulses), these results support that the wearable TENS*mini* device generates MEPs comparable to those produced by the DS7A.

Participant feedback from the survey (Fig. 6.7) indicates a preference for the TENS*mini* device, primarily due to the softer texture of its embedded TEs within the sock. Participants noted that removing the sock was easier than putting it on, likely because of the need to apply electrolytes to hydrate the skin before use. This feedback highlights the potential for improved user comfort with sock-based TENS*mini* design, which may positively impact patient adherence.

In the second study, the performance of a smart wearable device (TENS*mini*) was benchmarked against a clinically approved research-grade device (DS7A) in a cohort of 47 participants. The results demonstrated that the time to the first urge was significantly extended in both TTNS conditions compared to the control

condition. This observation is consistent with the hypothesised inhibitory effects of high-frequency (e.g., 20 Hz) tibial neuromodulation on bladder contractions, leading to an increased micturition threshold as the bladder volume expands [61], [140], [226]. These inhibitory effects appear to manifest immediately, in agreement with previous findings in animal models that have demonstrated transient modulation of bladder activity through TTNS [61], [140], [226].

The intensity of the urge findings indicate minimal lingering effects of TTNS. Although a significant interaction was observed, the changes in the intensity of the urge in the conditions of TENS*mini* and DS7A did not differ significantly from the control. This statistical significance may be attributed to the variability in the data from the small sample size. The absence of any lingering effects may appear unexpected given the known long-term impact of 20 Hz TTNS on bladder function [140], [226]. However, these effects are typically observed only after an extended stimulation protocol lasting approximately 12 weeks [232]. To this end, it is probable that the short-term nature of the present study accounts for the lack of significant differences in urge intensity observed between conditions. Nevertheless, the presence of a statistically significant result in this domain underscores the need for further investigation of the long-term therapeutic effectiveness of TENS*mini*, particularly in response to bladder dysfunction induced by brain damage (e.g. Stroke or Parkinson's disease) or peripheral neuropathy, as is common in the literature [233].

While TTNS is non-invasive and ostensibly appealing to patients, adherence gradually declines over time due to diminishing effectiveness and the burden of frequent self-administration. This results in most patients discontinuing treatment within eighteen months [234], [235]. In contrast, clinical evidence indicates that implantable tibial nerve stimulation devices such as the eCoin® (Valencia Technologies, US) and Revi™ (BlueWind Medical, US) demonstrate favourable long-term patient adherence and persistence due to their sustained effectiveness [236], [237]. Despite these apparent benefits however, these devices require semi-frequent surgical reimplantation. For instance, the eCoin® has a mean lifespan of 2.8 years due to its limited battery capacity [238], which could potentially offset some of the apparent long-term advantages.

Fortunately, recent advances in wearable TTNS technologies, notably Zida® Control Sock and Vivally®, may improve patient adherence and acceptance compared to another conventional benchtop or handheld TTNS devices. They achieve this end through enhanced convenience, and ease of use [104], [239].

Building on these advances, compared to Zida® the proposed TENS*mini* device offers a superior form factor, wireless control, and additional safety features (as detailed in [75]). Moreover, in contrast with Vivally® system, the TENS*mini* is designed to easily interface with a companion sock, thereby seamlessly integrating treatment into day-to-day life via a commonly utilised garment. This design aims to minimise disruption to daily routines and potentially improve patient adherence and treatment persistence.

## 6.6 Conclusion

In conclusion, the first study showed that the proposed TENS*mini* system achieved tibial nerve recruitment comparable to that of a clinical grade device. Results of the second study demonstrated that the TENS*mini* is able to induce identical short-term inhibitory effects on bladder function to a standard clinical benchmark. These findings indicate the feasibility of the proposed system as a portable solution for home-based OAB management. They further paves the way for further development of the TENS*mini*—a device that possesses both the benefits of a textile-based, wearable design and the potential for a personalised approach to lower urinary tract conditions. It is hypothesised that this device will improve treatment adherence and empower users.

# Chapter 7

# Conclusion and Future Work

## 7.1 Conclusion

The thesis has presented the design, development, and evaluation of a smart wearable neurostimulation system that integrates soft textile electrodes (TEs) with a custom-built, miniaturised stimulator (TENS*mini*) for the home-based management of overactive bladder (OAB) syndrome. The work brings together advances in materials engineering, embedded system design, and physiological validation (via human pilot trials) to propose a more user-friendly approach to neuromodulation therapy.

Importantly, the findings contribute to the growing body of literature on wearable bioelectronics and non-invasive neuromodulation, particularly transcutaneous tibial nerve stimulation (TTNS). While prior studies have focused on either improving electrode materials or designing stimulators, this work bridges both aspects in a unified system. The demonstration that cotton-based TEs, when hydrated with moisturiser, could achieve stimulation performance comparable to clinical-grade gel electrodes (GEs) supports the previous claims about the feasibility of textile-based interfaces, but adds more comprehensive assessments through physiological validation. Moreover, integrating these TEs into garments such as socks enhances durability and user acceptability, particularly among older adults or individuals with sensitive skin conditions, and those who place a high value on treatment privacy.

The TENS*mini* device itself introduces a platform that is not only functionally comparable to its clinical benchmark (DS7A) but also more practical for home-based use due to its enhanced portability. Its

consistent stimulation output and integrated safety features make it suitable for real-world deployment. Beyond OAB, this system has implications for broader applications of wearable neuromodulation. The tibial nerve is also implicated in other conditions such as chronic pelvic pain, interstitial cystitis, and even anxiety, indicating a broad therapeutic landscape for future exploration. Furthermore, the key features demonstrated in this system—including the comfortable textile-electrode design, integrated safety mechanisms, and device miniaturisation—could be adapted to target other peripheral nerves, such as the vagus or peroneal nerves, thereby expanding the scope of portable and non-invasive neuromodulation technologies.

In conclusion, this work advances the field of wearable neuromodulation by offering a validated, user-oriented system for managing OAB, while also laying the groundwork for future innovations in personalised therapy for a range of neurological and urological conditions. By situating technical innovation within a broader context of patient needs and healthcare delivery models, this thesis highlights how engineering solutions can meaningfully contribute to more inclusive and effective medical care.

## 7.2 Future Work

### Further Development of Wearable Electrodes

While this work has demonstrated the feasibility of embedding TEs into a sock-based form factor, further refinement of the wearable design remains an essential direction. For example, the current split-toe design may reduce electrode displacement, but this hypothesis has yet to be rigorously validated. A systematic investigation into electrode movement during daily activities (potentially using motion capture or imaging techniques) could generate more knowledge about biomechanical interaction between garment-based electrodes and skin. This understanding would not only benefit TTNS applications but could extend to any form of wearable electrotherapy such as functional electrical stimulation or biosignal monitoring including electromyography, electrocardiography.

Further work could also focus on transitioning from a semi-integrated to a fully integrated TE design. The current method of affixing electrodes with adhesive film is not fully optimised for repeated wear or ease of use. Future iterations could explore the use of textile knitting techniques to embed conductive pathways directly into the fabric structure, removing the need for adhesives entirely. Collaborations with

textile engineers or smart-fabric manufacturers could unlock novel fabrication strategies that optimise not just conductivity and durability but also aesthetic acceptability—an overlooked but important factor in user adherence. Moreover, improving connector design and ensuring compatibility with standard laundering processes would enhance the long-term practicality of such garments. This line of work could pave the way for more inclusive, age-friendly wearable health technologies, particularly for older adults.

### Adaptive and Intelligent Stimulation Systems

Although the present TENS*mini* platform delivers safe and consistent stimulation, the need for manual adjustment of intensity presents a barrier to fully autonomous home use. Physiological responses to stimulation vary across users and sessions, making fixed-intensity protocols suboptimal. An important area of future work involves developing adaptive stimulation algorithms that detect physiological thresholds (e.g., motor twitch response in the big toe during TTNS) and adjust stimulation parameters in real time.

One direction would involve embedding inertial sensors to detect subtle toe movement as an indicator of tibial nerve activation. This sensor data could feed into a closed-loop control system that auto-adjusts stimulation to remain below motor threshold, which may enhance both stimulation comfort and treatment effectiveness. This concept could be further developed by exploring the use of machine learning models trained on individual user response patterns to help estimate suitable stimulation intensity ranges over time. Such an approach may support more personalised therapy while potentially reducing the need for frequent intensity adjustments.

These innovations would also have applications outside of OAB. Similar adaptive control principles could be translated to neuromodulation for pain management, migraine therapy, or mental health treatments like vagus nerve stimulation, where patient variability and tolerance are key challenges.

### Miniaturisation and Seamless Integration

The current design of the TENS*mini* stimulator uses commercial off-the-shelf components, which constrains its miniaturisation in depth. An important next step is to migrate toward a custom application-

specific integrated circuit architecture. This would consolidate functionality into a smaller footprint, reducing the number of discrete components and enabling tighter integration into wearable textiles.

Such an advancement would allow the entire system, including electrodes, controller, and battery, to be housed discreetly within a single garment, indistinguishable from ordinary clothing. The implications are substantial: discreet therapeutic garments could reduce stigma and increase users adherence, particularly for those who require frequent and private treatment.

### Expanding Clinical and Societal Contexts

Beyond technical development, the long-term usability, acceptance, and effectiveness of the TENS*mini* system shall be evaluated in real-world settings. This includes qualitative assessments with diverse populations, particularly older adults with OAB or urge urinary incontinence. These studies should focus not only on device's functional performance but also on the lived experience of using the device.

In parallel, early-stage compliance with regulatory frameworks such as Conformité Européene (CE) or UK Conformity Assessed (UKCA) requirements should continue. Formal conformity assessments, safety validations of each subsystem (including integrated batteries and textile components), and reliable documentation will be prepared for future clinical trials. Following this, a randomised controlled trial should be conducted to evaluate its long-term therapeutic effectiveness and adherence in home environments. Beyond demonstrating efficacy for OAB, such a trial could explore cross-benefits, such as improvements in sleep quality, mood, or routine functioning, potentially linking TTNS to wider aspects of geriatric well-being.

### Cross-domain and Interdisciplinary Exploration

The insights and innovations from this research extend beyond the immediate application of OAB treatment. The methodology developed such as smart wearable stimulation, TEs integration, may be adapted for other therapeutic targets, including:

- Chronic pain management, especially for conditions like sciatica or diabetic neuropathy, where peripheral nerve stimulation is effective.

- Mental health, through portable vagus nerve stimulation as an adjunct for depression or anxiety.
- Post-stroke rehabilitation, using FES to assist motor recovery in a home setting.

This research also suggests opportunities for interdisciplinary work, particularly at the intersection of wearable electronics, data science, human-computer interaction, and personalised medicine. Future versions of the TENS*mini* system could incorporate connectivity features, such as integration with mobile applications or cloud-based platforms, enabling remote monitoring by clinicians.

# References


[1] M. J. Drake, "Fundamentals of terminology in lower urinary tract function," *Neurourol. Urodyn.*, vol. 37, S13–S19, S6 2018. DOI: 10.1002/nau.23768.

[2] M. P. Fitzgerald, U. Stablein, and L. Brubaker, "Urinary habits among asymptomatic women," *Am. J. Obstet. Gynecol.*, vol. 187, no. 5, pp. 1384–1388, 2002. DOI: 10.1067/mob.2002.126865.

[3] J. M. Latini, E. Mueller, M. M. Lux, M. P. Fitzgerald, and K. J. Kreder, "Voiding frequency in a sample of asymptomatic american men," *J. Urol.*, vol. 172, no. 3, pp. 980–984, 2004. DOI: 10.1097/01.ju.0000135890.08541.02.

[4] E. S. Lukacz, E. L. Whitcomb, J. M. Lawrence, C. W. Nager, and K. M. Luber, "Urinary frequency in community-dwelling women: What is normal?" *Am. J. Obstet. Gynecol.*, vol. 200, no. 5, 552.e1–552.e7, 2009. DOI: 10.1016/j.ajog.2008.11.006.

[5] J.-Y. Wang, L. Liao, M. Liu, B. Sumarsono, and M. Cong, "Epidemiology of lower urinary tract symptoms in a cross-sectional, population-based study: The status in china," *Medicine*, vol. 97, no. 34, 2018, Art. no. e11554. DOI: 10.1097/MD.0000000000011554.

[6] W. D. Steers, "Pathophysiology of overactive bladder and urge urinary incontinence," *Rev. Urol.*, vol. 4, S7–S18, Suppl 4 2002.

[7] M. Takeda, I. Araki, M. Kamiyama, Y. Takihana, M. Komuro, and Y. Furuya, "Diagnosis and treatment of voiding symptoms," *Urology*, vol. 62, no. 5, pp. 11–19, 2003. DOI: 10.1016/s0090-4295(03)00605-8.

[8] I. Milsom and D. E. Irwin, "A cross-sectional, population-based, multinational study of the prevalence of overactive bladder and lower urinary tract symptoms: Results from the EPIC study," *Eur. Urol. Suppl.*, vol. 6, no. 1, pp. 4–9, 2007. DOI: 10.1016/j.eursup.2006.10.003.

[9] B. T. Haylen *et al.*, "An international urogynecological association (IUGA)/international continence society (ICS) joint report on the terminology for female pelvic floor dysfunction," *Int. Urogynecol. J.*, vol. 21, no. 1, pp. 5–26, 2010. DOI: 10.1007/s00192-009-0976-9.

[10] Y. Cheng *et al.*, "Prevalence and trends in overactive bladder among men in the united states, 2005-2020," *Sci. Rep.*, vol. 14, no. 1, p. 16 284, 2024. DOI: 10.1038/s41598-024-66758-8.

[11] D. E. Irwin *et al.*, "Population-based survey of urinary incontinence, overactive bladder, and other lower urinary tract symptoms in five countries: Results of the EPIC study," *Eur. Urol.*, vol. 50, no. 6, pp. 1306–1315, 2006. DOI: 10.1016/j.eururo.2006.09.019.

[12] M. Abdel-Fattah *et al.*, "Invasive urodynamic investigations in the management of women with refractory overactive bladder symptoms (FUTURE) in the UK: A multicentre, superiority, parallel, open-label, randomised controlled trial," *The Lancet*, vol. 405, no. 10484, pp. 1057–1068, 2025. DOI: 10.1016/S0140-6736(24)01886-5.

[13] W. F. Stewart *et al.*, "Prevalence and burden of overactive bladder in the united states," *World J. Urol.*, vol. 20, no. 6, pp. 327–336, 2003. DOI: 10.1007/s00345-002-0301-4.

[14] W. S. Reynolds, J. Fowke, and R. Dmochowski, "The burden of overactive bladder on US public health," *Curr. Bladder Dysfunct. Rep.*, vol. 11, no. 1, pp. 8–13, 2016. DOI: 10.1007/s11884-016-0344-9.

[15] Cleveland Clinic, *Overactive Bladder*, (2022). Accessed: Dec. 1, 2024. [Online]. Available: https://my.clevelandclinic.org/health/diseases/14248-overactive-bladder.

[16] M. Przydacz, T. Golabek, P. Dudek, M. Lipinski, and P. Chlosta, "Prevalence and bother of lower urinary tract symptoms and overactive bladder in poland, an eastern european study," *Sci. Rep.*, vol. 10, no. 1, 2020, Art. no. 19819. DOI: 10.1038/s41598-020-76846-0.

[17] K. A. O. Tikkinen, T. L. J. Tammela, A. M. Rissanen, A. Valpas, H. Huhtala, and A. Auvinen, "Is the prevalence of overactive bladder overestimated? a population-based study in finland," *PLOS ONE*, vol. 2, no. 2, 2007, Art. no. e195. DOI: 10.1371/journal.pone.0000195.

[18] R. Reisch, "Interventions for overactive bladder: Review of pelvic floor muscle training and urgency control strategies," *Journal of women's health physical therapy*, vol. 44, no. 1, pp. 19–25, 2020. DOI: 10.1097/JWH.0000000000000148.

[19] S. Funada, T. Yoshioka, Y. Luo, A. Sato, S. Akamatsu, and N. Watanabe, "Bladder training for treating overactive bladder in adults," *Cochrane Database Syst. Rev.*, no. 10, 2023, Art. no. CD013571. DOI: 10.1002/14651858.CD013571.pub2.

[20] B. M. Brucker, R. K. Lee, and D. K. Newman, "Optimizing nonsurgical treatments of overactive bladder in the united states," *Urology*, vol. 145, pp. 52–59, Nov. 2020. DOI: 10.1016/j.urology.2020.06.017.

[21] P. I. Ellsworth, W. W. Cheung, and W. Huang. "Overactive bladder treatment & management." (2025). Accessed: Jun. 16, 2025. (2025), [Online]. Available: https://emedicine.medscape.com/article/459340-treatment?utm_source=chatgpt.com.

[22] K. Hesch, "Agents for treatment of overactive bladder: A therapeutic class review," *Bayl. Univ. Med. Cent. Proc.*, vol. 20, no. 3, pp. 307–314, 2007. DOI: 10.1080/08998280.2007.11928310.

[23] F. M. Chu and R. Dmochowski, "Pathophysiology of overactive bladder," *Am. J. Med.*, vol. 119, no. 3, pp. 3–8, 2006. DOI: 10.1016/j.amjmed.2005.12.010.

[24] N. Erdem and F. M. Chu, "Management of overactive bladder and urge urinary incontinence in the elderly patient," *Am. J. Med.*, vol. 119, no. 3, pp. 29–36, 2006. DOI: 10.1016/j.amjmed.2005.12.014.

[25] W. He, Y. Zhang, G. Huang, Y. Tian, Q. Sun, and X. Liu, "Efficacy and safety of vibegron compared with mirabegron for overactive bladder: A systematic review and network meta-analysis," *Low Urin. Tract Symptoms*, vol. 15, no. 3, pp. 80–88, 2023. DOI: 10.1111/luts.12475.

[26] K. E. Andersson, "On the site and mechanism of action of $\beta$3-adrenoceptor agonists in the bladder," *Int. Neurourol. J.*, vol. 21, no. 1, pp. 6–11, 2017. DOI: 10.5213/inj.1734850.425.

[27] C. R. Chapple *et al.*, "Safety and efficacy of mirabegron: Analysis of a large integrated clinical trial database of patients with overactive bladder receiving mirabegron, antimuscarinics, or placebo," *Eur. Urol.*, vol. 77, no. 1, pp. 119–128, 2020. DOI: 10.1016/j.eururo.2019.09.024.

[28] Cleveland Clinic, *Beta-agonist*, (2023). Accessed: Dec. 1, 2024. [Online]. Available: https://my.clevelandclinic.org/health/treatments/24851-beta-agonist.

[29] S. S. Hegde and R. M. Eglen, "Muscarinic receptor subtypes modulating smooth muscle contractility in the urinary bladder," *Life Sci.*, vol. 64, no. 6, pp. 419–428, 1999. DOI: 10.1016/S0024-3205(98)00581-5.

[30] L. Cox and A. P. Cameron, "OnabotulinumtoxinA for the treatment of overactive bladder," *Res. Rep. Urol.*, vol. 2014, no. 6, pp. 79–89, Jul. 2014. DOI: 10.2147/RRU.S43125.

[31] M. P. Feloney, K. Stauss, and S. W. Leslie, "Sacral neuromodulation," in *StatPearls*, Treasure Island (FL): StatPearls Publishing, 2025.

[32] B. Chughtai, D. Thomas, T. Sun, and A. Sedrakyan, "Failures of sacral neuromodulation for incontinence," *JAMA Surg.*, vol. 153, no. 5, pp. 493–494, 2018. DOI: 10.1001/jamasurg.2017.6093.

[33] S. Herroelen, C. Knowles, J. Kerrigan-Smith, T. Noone, T. Denison, and S. De Wachter, "Pudendal nerve stimulation for treatment of lower urinary tract symptoms: A systematic review of safety, technical feasibility and clinical efficacy," *Continence*, vol. 11, Sep. 2024, Art. no. 101685. DOI: 10.1016/j.cont.2024.101685.

[34] J. Booth, L. Connelly, S. Dickson, F. Duncan, and M. Lawrence, "The effectiveness of transcutaneous tibial nerve stimulation (TTNS) for adults with overactive bladder syndrome: A systematic review," *Neurourol. Urodyn.*, vol. 37, no. 2, pp. 528–541, 2018. DOI: 10.1002/nau.23351.

[35] J. Booth *et al.*, "A feasibility study of transcutaneous posterior tibial nerve stimulation for bladder and bowel dysfunction in elderly adults in residential care," *J. Am. Med. Dir. Assoc.*, vol. 14, no. 4, pp. 270–274, 2013. DOI: 10.1016/j.jamda.2012.10.021.

[36] B. Welk and M. McKibbon, "A randomized, controlled trial of transcutaneous tibial nerve stimulation to treat overactive bladder and neurogenic bladder patients," *Can. Urol. Assoc. J.*, vol. 14, no. 7, E297–E303, 2020. DOI: 10.5489/cuaj.6142.

[37] I. Ramírez-García, S. Kauffmann, L. Blanco-Ratto, A. Carralero-Martínez, and E. Sánchez, "Patient-reported outcomes in the setting of a randomized control trial on the efficacy of transcutaneous stimulation of the posterior tibial nerve compared to percutaneous stimulation in idiopathic overactive bladder syndrome," *Neurourol. Urodyn.*, vol. 40, no. 1, pp. 295–302, 2021. DOI: 10.1002/nau.24554.

[38] A. P. Cameron *et al.*, "The AUA/SUFU guideline on the diagnosis and treatment of idiopathic overactive bladder," *J. Urol.*, vol. 212, no. 1, pp. 11–20, 2024. DOI: 10.1097/JU.0000000000003985.

[39] N. Satyadev, M. Ameen, T. H. Do, and H. Wang, "Anticholinergic burden in patients treated for overactive bladder: Second-line therapy with tibial nerve stimulation as a solution," *Int. Urogynecol. J.*, vol. 35, no. 7, pp. 1375–1379, 2024. DOI: 10.1007/s00192-024-05791-7.

[40] P. Malladi and J. Panicker, "Audit results of transcutaneous tibial nerve stimulation (TTNS) therapy in adult patients with overactive bladder (OAB) symptoms," in *The 54th Annual Meeting of the International Continence Society*, Madrid, Spain, Oct. 2024.

[41] C. Goudelocke, J. Sobol, D. Poulos, E. Enemchukwu, S. Zaslau, and R. Dhir, "A multicenter study evaluating the FREquency of use and efficacy of a novel closed-loop wearable tibial neuromodulation system for overactive bladder and urgency urinary incontinence (FREEOAB)," *Urology*, vol. 183, pp. 63–69, 2024. DOI: 10.1016/j.urology.2023.10.007.

[42] Z. Zhang *et al.*, "Efficacy and safety of non-invasive low-frequency tibial nerve stimulator in overactive bladder," *Eur. J. Med. Res.*, vol. 30, 2025, Art. no. 40. DOI: 10.1186/s40001-024-02262-z.

[43] E. Leron, A. Y. Weintraub, S. A. Mastrolia, and P. Schwarzman, "Overactive bladder syndrome: Evaluation and management," *Curr. Urol.*, vol. 11, no. 3, pp. 117–125, 2018. DOI: 10.1159/000447205.

[44] C. Qin, Y. Wang, and Y. Gao, "Overactive bladder symptoms within nervous system: A focus on etiology," *Front. Physiol.*, vol. 12, 2021, Art. no. 747144. DOI: 10.3389/fphys.2021.747144.

[45] R. Chess-Williams and D. J. Sellers, "Pathophysiological mechanisms involved in overactive bladder/detrusor overactivity," *Curr. Bladder Dysfunct. Rep.*, vol. 18, no. 2, pp. 79–88, 2023. DOI: 10.1007/s11884-023-00690-x.

[46] M. Yao and A. Simoes, "Urodynamic testing and interpretation," in *StatPearls [Internet]*, (2025). Accessed: Jun. 16, 2025, Treasure Island (FL): StatPearls Publishing. [Online]. Available: http://www.ncbi.nlm.nih.gov/books/NBK562310/.

[47] M. E. Perkins and M. A. Vizzard, "Chapter five - transient receptor potential vanilloid type 4 (TRPV4) in urinary bladder structure and function," in *Current Topics in Membranes*, ser. Role of TRPV4 Channels in Different Organ Systems, S. K. Sonkusare, Ed., vol. 89, Academic Press, 2022, pp. 95–138. DOI: 10.1016/bs.ctm.2022.06.002.

[48] W. C. de Groat, D. Griffiths, and N. Yoshimura, "Neural control of the lower urinary tract," *Compr. Physiol.*, vol. 5, no. 1, pp. 327–396, 2015. DOI: 10.1002/cphy.c130056.

[49] Y. Igawa, "Peripheral neural control of the lower urinary tract," in *Neurourology: Theory and Practice*, L. Liao and H. Madersbacher, Eds., 2019, pp. 27–36.

[50] W. C. de Groat, "Integrative control of the lower urinary tract: Preclinical perspective," *Br. J. Pharmacol.*, vol. 147, S25–S40, S2 2006. DOI: 10.1038/sj.bjp.0706604.

[51] Physiopedia. "Male urinary incontinence." (2025). Accessed: Jun. 20, 2025. (), [Online]. Available: https://www.physio-pedia.com/Male_Urinary_Incontinence.

[52] C. J. Fowler, D. Griffiths, and W. C. de Groat, "The neural control of micturition," *Nat. Rev. Neurosci.*, vol. 9, pp. 453–466, Jun. 2008. DOI: 10.1038/nrn2401.

[53] G. Holstege and H. Collewijn, "Chapter 9 - central nervous system control of micturition," in *The Spinal Cord*, C. Watson, G. Paxinos, and G. Kayalioglu, Eds., San Diego, USA: Academic Press, 2009, pp. 130–147, ISBN: 978-0-12-374247-6.

[54] C. J. Granger and W. B. Cohen-Levy, "Anatomy, bony pelvis and lower limb: Posterior tibial nerve," in *StatPearls [Internet]*, Treasure Island (FL), 2023.

[55] A. Al-Danakh *et al.*, "Posterior tibial nerve stimulation for overactive bladder: Mechanism, classification, and management outlines," *Parkinsons Dis.*, vol. 2022, Mar. 2022, Art. no. 2700227. DOI: 10.1155/2022/2700227.

[56] L. Ghijselings, C. Renson, J. Van de Walle, K. Everaert, and A.-F. Spinoit, "Clinical efficacy of transcutaneous tibial nerve stimulation (TTNS) versus sham therapy (part i) and TTNS versus percutaneous tibial nerve stimulation (PTNS) (part II) on the short term in children with the idiopathic overactive bladder syndrome: Protocol for part i of the twofold double-blinded randomized controlled TaPaS trial," *Trials*, vol. 22, 2021, Art. no. 247. DOI: 10.1186/s13063-021-05117-8.

[57] R. Sonmez, N. Yildiz, and H. Alkan, "Efficacy of percutaneous and transcutaneous tibial nerve stimulation in women with idiopathic overactive bladder: A prospective randomised controlled trial," *Ann. Phys. Rehabil. Med.*, vol. 65, no. 1, 2022, Art. no. 101486. DOI: 10.1016/j.rehab.2021.101486.

[58] X. Li, X. Li, and L. Liao, "Mechanism of action of tibial nerve stimulation in the treatment of lower urinary tract dysfunction," *Neuromodulation*, vol. 27, no. 2, pp. 256–266, 2024. DOI: 10.1016/j.neurom.2023.03.017.

[59] Y.-S. Lim *et al.*, "Precise control of tibial nerve stimulation for bladder regulation via evoked compound action potential feedback mechanisms," *Nat. Commun.*, vol. 16, pp. 1–12, May 2025, Art. no. 4115. DOI: 10.1038/s41467-025-59436-4.

[60] D.-Y. Kim *et al.*, "Percutaneous tibial nerve stimulation for neurogenic bladder due to severe lumbosacral disc herniation," *J. Clin. Med.*, vol. 14, no. 7, 2025, Art. no. 2262. DOI: 10.3390/jcm14072262.

[61] K. Theisen *et al.*, "Frequency dependent tibial neuromodulation of bladder underactivity and overactivity in cats," *Neuromodulation*, vol. 21, no. 7, pp. 700–706, 2018. DOI: 10.1111/ner.12792.

[62] T. Yecies *et al.*, "Spinal interneuronal mechanisms underlying pudendal and tibial neuromodulation of bladder function in cats," *Exp. Neurol.*, vol. 308, pp. 100–110, Oct. 2018. DOI: 10.1016/j.expneurol.2018.06.015.

[63] Verity Medical Ltd., *NeuroTrac® Continence Operation Manual*, (2016). Accessed: Dec. 1, 2024. [Online]. Available: https://veritymedical.com/product/neurotrac-continence/.

[64] Performance Health International Ltd., *TPN 200 Premier Plus 09 153 1748*, (2018). Accessed: Dec. 1, 2024. [Online]. Available: https://www.performancehealth.co.uk/amfile/file/download/file/5013/product/120509/.

[65] J. H. Seth *et al.*, "Feasibility of using a novel non-invasive ambulatory tibial nerve stimulation device for the home-based treatment of overactive bladder symptoms," *Transl. Androl. Urol.*, vol. 7, no. 6, pp. 912–919, 2018. DOI: 10.21037/tau.2018.09.12.

[66] H. Zhou *et al.*, "Stimulating the comfort of textile electrodes in wearable neuromuscular electrical stimulation," *Sensors*, vol. 15, no. 7, pp. 17 241–17 257, 2015. DOI: 10.3390/s150717241.

[67] L. Euler, L. Guo, and N.-K. Persson, "A review of textile-based electrodes developed for electrostimulation," *Text. Res. J.*, vol. 92, no. 7, pp. 1300–1320, 2022. DOI: 10.1177/00405175211051949.

[68] M. F. de Faria, M. B. G. Ferreira, M. M. Dos Santos Felix, R. M. V. Bessa, and M. H. Barbosa, "Prevention of medical adhesive-related skin injury during patient care: A scoping review," *Int. J. Nurs. Stud. Adv.*, vol. 4, Apr. 2022, Art. no. 100078. DOI: 10.1016/j.ijnsa.2022.100078.

[69] L. Meng, Q. Fu, S. Hao, F. Xu, and J. Yang, "Self-adhesive, biodegradable silk-based dry electrodes for epidermal electrophysiological monitoring," *J. Chem. Eng.*, vol. 427, Jan. 2022, Art. no. 131999, ISSN: 1385-8947. DOI: 10.1016/j.cej.2021.131999. [Online]. Available: https://www.sciencedirect.com/science/article/pii/S1385894721035786.

[70] J.-N. Cornu, H. Hashim, C. D. Nunzio, V. G. Perez, R. Ferreira, and D. S. Elterman, "How i do it: Transcutaneous tibial nerve stimulation TENSI+ system," *Can. J. Urol.*, vol. 30, no. 6, pp. 11 756–11 761, 2023.

[71] ZIDA LLC, *Conquer Your Incontinence*, (2023). Accessed: Dec. 1, 2024. [Online]. Available: https://livezida.com/.

[72] Avation Medical, *Vivally® System*, (2025). Accessed: Mar. 6, 2025. [Online]. Available: https://avation.com/.

[73] W. Ju, A. McConnell-Trevillion, S. R. Khan, K. Nazarpour, and S. Mitra, "A feasibility study on textile electrodes for transcutaneous electrical nerve stimulation," in *21st IEEE Interregional NEWCAS Conf.*, Edinburgh, UK, Jun. 2023, pp. 1–5. DOI: 10.1109/NEWCAS57931.2023.10198106.

[74] W. Ju, S. R. Khan, K. Nazarpour, and S. Mitra, "TENSmini: A wearable electrical nerve stimulator for urinary incontinence management," in *22nd IEEE MELECON*, Porto, Portugal, Jun. 2024, pp. 1111–1115. DOI: 10.1109/MELECON56669.2024.10608726.

[75] W. Ju *et al.*, "Smart wearable TENS device for home-based overactive bladder management," *IEEE Trans. Biomed. Circuits Syst.*, pp. 1–12, Jan. 2025. DOI: 10.1109/TBCAS.2025.3527343.

[76] W. Ju, A. McConnell-Trevillion, D. A. Vaca-Benavides, S. D. Shenkin, S. Mitra, and K. Nazarpour, "Benchmarking tensmini for neuromodulation via tibial nerve stimulation," *IEEE Trans. Neural Syst. Rehabil. Eng.*, vol. 33, pp. 2135–2141, Jun. 2025. DOI: 10.1109/TNSRE.2025.3575009.

[77] R. Melzack and P. D. Wall, "Pain mechanisms: A new theory," *Science*, vol. 150, no. 3699, pp. 971–979, 1965. DOI: 10.1126/science.150.3699.971.

[78] C. N. Shealy, J. T. Mortimer, and J. B. Reswick, "Electrical inhibition of pain by stimulation of the dorsal columns: Preliminary clinical report," *Anesth. Analg.*, vol. 46, no. 4, pp. 489–491, 1967.

[79] C. Gilmore *et al.*, "Percutaneous peripheral nerve stimulation for the treatment of chronic neuropathic postamputation pain: A multicenter, randomized, placebo-controlled trial," *Reg. Anesth. Pain Med.*, vol. 44, no. 6, pp. 637–645, 2019. DOI: 10.1136/rapm-2018-100109.

[80] D. W. Dodick *et al.*, "Safety and efficacy of peripheral nerve stimulation of the occipital nerves for the management of chronic migraine: Long-term results from a randomized, multicenter, double-blinded, controlled study," *Cephalalgia*, vol. 35, no. 4, pp. 344–358, 2015. DOI: 10.1177/0333102414543331.

[81] R. D. Wilson, D. D. Gunzler, M. E. Bennett, and J. Chae, "Peripheral nerve stimulation compared with usual care for pain relief of hemiplegic shoulder pain: A randomized controlled trial," *Am. J. Phys. Med. Rehabil.*, vol. 93, no. 1, pp. 17–28, 2014. DOI: 10.1097/PHM.0000000000000011.

[82] H. Kloimstein *et al.*, "Peripheral nerve field stimulation (PNFS) in chronic low back pain: A prospective multicenter study," *Neuromodulation*, vol. 17, no. 2, pp. 180–187, 2014. DOI: 10.1111/ner.12139.

[83] D. R. Staskin, K. M. Peters, S. MacDiarmid, N. Shore, and W. C. de Groat, "Percutaneous tibial nerve stimulation: A clinically and cost effective addition to the overactive bladder algorithm of care," *Curr. Urol. Rep.*, vol. 13, no. 5, pp. 327–334, 2012. DOI: 10.1007/s11934-012-0274-9.

[84] P. Verrills, B. Mitchell, D. Vivian, and C. Sinclair, "Peripheral nerve stimulation: A treatment for chronic low back pain and failed back surgery syndrome?" *Neuromodulation*, vol. 12, no. 1, pp. 68–75, 2009. DOI: 10.1111/j.1525-1403.2009.00191.x.

[85] T. Marcelissen, R. Jacobs, P. van Kerrebroeck, and S. de Wachter, "Sacral neuromodulation as a treatment for chronic pelvic pain," *J. Urol.*, vol. 186, no. 2, pp. 387–393, 2011. DOI: 10.1016/j.juro.2011.02.2694.

[86] J. Hornberger, K. Kumar, E. Verhulst, M. A. Clark, and J. Hernandez, "Rechargeable spinal cord stimulation versus non-rechargeable system for patients with failed back surgery syndrome: A cost-consequences analysis," *Clin. J. Pain.*, vol. 24, no. 3, pp. 244–252, 2008. DOI: 10.1097/AJP.0b013e318160216a.

[87] D. E. Richardson and H. Akil, "Pain reduction by electrical brain stimulation in man. part 1: Acute administration in periaqueductal and periventricular sites," *J. Neurosurg.*, vol. 47, no. 2, pp. 178–183, 1977. DOI: 10.3171/jns.1977.47.2.0178.

[88] Y. Hosobuchi, J. E. Adams, and R. Linchitz, "Pain relief by electrical stimulation of the central gray matter in humans and its reversal by naloxone," *Science*, vol. 197, no. 4299, pp. 183–186, 1977. DOI: 10.1126/science.301658.

[89] S. A. Pilkington, "Rectal prolapse and sphincter operations," *Surgery*, vol. 29, no. 8, pp. 395–399, 2011. DOI: 10.1016/j.mpsur.2011.05.012.

[90] E. A. Tanagho and R. A. Schmidt, "Electrical stimulation in the clinical management of the neurogenic bladder," *J. Urol.*, vol. 140, no. 6, pp. 1331–1339, 1988. DOI: 10.1016/s0022-5347(17)42038-6.

[91] M. L. Stoller, "Afferent nerve stimulation for pelvic floor dysfunction," in *ICS-IUGA-ICCS 1999*, Art. no. 257, Denver, CO, 1999.

[92] J. H. Moe and H. W. Post, "Functional electrical stimulation for ambulation in hemiplegia," *Lancet*, vol. 82, pp. 285–288, Jul. 1962.

[93] NeuroMetrix Inc., Waltham, MA, USA, *Quell® User Manual*, (2017). Accessed: Dec. 1, 2024. [Online]. Available: https://www.quellrelief.com/wp-content/uploads/2018/04/Quell-User-Manual-Series-6-04.05.2018.pdf.

[94] DJO Global Inc., Lewisville, TX, USA, *chattanooga® Wireless Professional User Manual*, (2019). Accessed: Dec. 1, 2024. [Online]. Available: https://www.djoglobal.eu/media/storage.djoglobal.eu/en_UK/Documents/4626230_E_WIRELESS%20PROFESSIONAL%20USER%20MANUALPRACTICAL%20GUIDE_ENpdf_1fh83qo.pdf.

[95] DJO Global Inc., Lewisville, TX, USA, *COMPEX® MINI User Manual*, (2021). Accessed: Dec. 1, 2024. [Online]. Available: https://s3.amazonaws.com/assets.compex.com/en/manuals/INTL-CX192IF03+Rev+A+COMPEX+MIN+IFU+INTL+VERSION+DIGITAL.pdf.

[96] Paingone, *Paingone Easy User Manual*, (2021). Accessed: Dec. 1, 2024. [Online]. Available: https://uk.paingone.com/collections/paingone-easy.

[97] Beurer GmbH, *EM 50 Instructions for Use*, (2023). Accessed: Dec. 1, 2024. [Online]. Available: https://res.cloudinary.com/beurer/raw/upload/v1692803495/product-and-content-live-uk/90f9f55e82f891ab75ddf9043c720dbaaa86914291-22b6ef27f622741a23d60e.pdf.

[98] Cefaly Technology, *CEFALY Connected User Manual*, (2022). Accessed: Dec. 1, 2024. [Online]. Available: https://blog.cefaly.com/the-simple-guide-to-the-cefaly-device/.

[99] TensCare Ltd., *mynd User Manual*, (2021). Accessed: Dec. 1, 2024. [Online]. Available: https://tenscare.co.uk/cdn/shop/files/8.1.2_-_I-MYND-ML_UK_ES_DE_IT_Rev_2.5_12.24_-_eIFU.pdf?v=4763650683842608491.

[100] Paingone, *Paingone Qalm Instruction Manual*, (2020). Accessed: Dec. 1, 2024. [Online]. Available: https://uk.paingone.com/collections/paingone-qalm.

[101] P. Shi, J. Du, F. Fang, H. Yu, and J. Liu, "Design and implementation of an intelligent analgesic bracelet based on wrist-ankle acupuncture," *IEEE Trans. Biomed. Circuits Syst.*, vol. 14, no. 6, pp. 1431–1440, 2020. DOI: 10.1109/TBCAS.2020.3039063.

[102] Firstkind Ltd., *geko T-3 Instructions for Use*, (2021). Accessed: Dec. 1, 2024.

[103] X. Li, X. Li, Z. Zhou, H. Zhao, and L. Liao, "Feasibility of a transcutaneous tibial nerve stimulation device use in overactive bladder patients: A pilot study from a single tertiary care center," *Front. Neurol.*, vol. 13, Apr. 2022, Art. no. 872200. DOI: 10.3389/fneur.2022.872200.

[104] R. Cava and Y. Orlin, "Home-based transcutaneous tibial nerve stimulation for overactive bladder syndrome: A randomized, controlled study," *Int. Urol. Nephrol.*, vol. 54, pp. 1825–1835, May 2022. DOI: 10.1007/s11255-022-03235-z.

[105] E. L. Nussbaum, P. Houghton, J. Anthony, S. Rennie, B. L. Shay, and A. M. Hoens, "Neuromuscular electrical stimulation for treatment of muscle impairment: Critical review and recommendations for clinical practice," *Physiother. Can.*, vol. 69, no. 5, pp. 1–76, 2017. DOI: 10.3138/ptc.2015-88.

[106] L. L. Baker, *Neuromuscular electrical stimulation: a practical guide*, 4th ed. Downey, Calif.: Los Amigos Research & Education Institute, Rancho Los Amigos National Rehabilitation Center, 2000, ISBN: 978-0-9676335-0-3.

[107] National Coverage Determination (NCD), *Neuromuscular Electrical Stimulation (NMES)*, 160.12. (2006). Accessed: Dec. 1, 2024. [Online]. Available: https://www.cms.gov/medicare-coverage-database/view/ncd.aspx?ncdid=175&ncdver=2.

[108] Bioness Inc., *H200® Wireless User's Guide*, (2020). Accessed: Dec. 1, 2024.

[109] Bioness, Inc., *L300 Go® User's Guide*, (2023). Accessed: Dec. 1, 2024.

[110] Innovative Neurotronics Inc., *WalkAide® System User Manual*, (2010). Accessed: Dec. 1, 2024.

[111] Shenzhen XFT Medical Ltd., *XFT-2001E Nerve and Muscle Stimulator User Manual*, (2018). Accessed: Dec. 1, 2024.

[112] K. H. Ha, S. A. Murray, and M. Goldfarb, "An approach for the cooperative control of FES with a powered exoskeleton during level walking for persons with paraplegia," *IEEE Trans. Neural Syst. Rehabil. Eng.*, vol. 24, no. 4, pp. 455–466, 2016.

[113] J. Jung, D.-W. Lee, Y. Son, B. Kim, J. Gu, and H. C. Shin, "Volitional EMG controlled wearable FES system for lower limb rehabilitation," in *43rd Annu. Int. Conf. IEEE Eng. Med. Biol. Soc. (EMBC)*, Guadalajara, Mexico, 2021, pp. 7099–7102.

[114] C. Nam *et al.*, "An exoneuromusculoskeleton for self-help upper limb rehabilitation after stroke," *Soft Robot.*, vol. 9, no. 1, pp. 14–35, 2022.

[115] R. G. Barelli, V. F. Avelino, and M. C. F. Castro, "STIMGRASP: A home-based functional electrical stimulator for grasp restoration in daily activities," *Sensors*, vol. 23, no. 1, p. 10, 2022.

[116] Beurer GmbH, *EM 70 Instructions for Use*, (2020). Accessed: Dec. 1, 2024. [Online]. Available: https://pim.beurer.com/images/attribut/648.21_EM70_2020-06-16_02_IM1_BEU-min.pdf.

[117] Beurer GmbH, *EM 39 Instructions for Use*, (2019). Accessed: Dec. 1, 2024. [Online]. Available: https://res.cloudinary.com/beurer/raw/upload/v1692803488/product-and-content-live-uk/781fbededa3fd923f7ffe701e1272963176957c2f3-c24ab89c667e4c32a9b963.pdf.

[118] R. M. Kandadai, S. S. Meka, S. Kola, R. Alugolu, and R. Borgohain, "Constant current versus constant voltage DBS stimulators—changing trend," *Ann. Indian Acad. Neurol.*, vol. 26, no. 4, pp. 368–369, 2023. DOI: 10.4103/aian.aian_508_23.

[119] S. Washburn, R. Catlin, K. Bethel, and B. Canlas, "Patient-perceived differences between constant current and constant voltage spinal cord stimulation systems," *Neuromodulation*, vol. 17, no. 1, pp. 28–36, 2014. DOI: 10.1111/ner.12085.

[120] C. Qin *et al.*, "Is constant current or constant voltage spinal cord stimulation superior for the suppression of nociceptive visceral and somatic stimuli? a rat model," *Neuromodulation*, vol. 15, no. 2, pp. 132–143, 2012. DOI: 10.1111/j.1525-1403.2012.00431.x.

[121] A. J. Woods *et al.*, "A technical guide to tDCS, and related non-invasive brain stimulation tools," *Clin. Neurophysiol.*, vol. 127, no. 2, pp. 1031–1048, 2016. DOI: 10.1016/j.clinph.2015.11.012.

[122] M. A. Nitsche and W. Paulus, "Excitability changes induced in the human motor cortex by weak transcranial direct current stimulation," *J. Physiol.*, vol. 527, no. 3, pp. 633–639, 2000. DOI: 10.1111/j.1469-7793.2000.t01-1-00633.x.

[123] R. B. North *et al.*, "Glossary of neurostimulation terminology: A collaborative neuromodulation foundation, institute of neuromodulation, and international neuromodulation society project," *Neuromodulation*, vol. 25, no. 7, pp. 1050–1058, 2022. DOI: 10.1016/j.neurom.2021.10.010.

[124] Seizan Tanabe *et al.*, "Comparison of outcomes after use of biphasic or monophasic defibrillators among out-of-hospital cardiac arrest patients a nationwide population-based observational study | request PDF," *Circ.: Cardiovasc. Qual. Outcomes*, vol. 5, no. 5, 2012. DOI: 10.1161/CIRCOUTCOMES.112.965319.

[125] N. L. M. Cappaert, D. Ramekers, H. C. F. Martens, and W. J. Wadman, "Efficacy of a new charge-balanced biphasic electrical stimulus in the isolated sciatic nerve and the hippocampal slice," *Int. J. Neural. Syst.*, vol. 23, no. 1, 2013, Art. no. 1250031. DOI: 10.1142/S0129065712500311.

[126] A. Liu *et al.*, "Immediate neurophysiological effects of transcranial electrical stimulation," *Nat. Commun.*, vol. 9, Nov. 2018, Art. no. 5092. DOI: 10.1038/s41467-018-07233-7.

[127] M. Behringer, S. Grützner, J. Montag, M. McCourt, M. Ring, and J. Mester, "Effects of stimulation frequency, amplitude, and impulse width on muscle fatigue," *Muscle & Nerve*, vol. 53, no. 4, pp. 608–616, 2016. DOI: 10.1002/mus.24893.

[128] A. V. Oppenheim, A. S. Willsky, and S. Hamid, *Signals and Systems*. Prentice Hall, 1996.

[129] *Medical electrical equipment part 1: General requirements for basic safety and essential performance*, EN 60601-1:2006+A2:2021, Oct. 2021.

[130] M. S. Lee, A. Paul, Y. Xu, W. D. Hairston, and G. Cauwenberghs, "Characterization of ag/AgCl dry electrodes for wearable electrophysiological sensing," *Front. Electron.*, vol. 2, Jan. 2022. DOI: 10.3389/felec.2021.700363.

[131] H. Ullah *et al.*, "Recent advances in stretchable and wearable capacitive electrophysiological sensors for long-term health monitoring," *Biosensors*, vol. 12, no. 8, 2022, Art. no. 630. DOI: 10.3390/bios12080630.

[132] L. Euler, L. Guo, and N.-K. Persson, "Influence of the electrolyte concentration and amount on the performance of textile electrodes in electrostimulation: A systematic study," *Sensor Actuat. A-Phys.*, vol. 366, 2024, Art. no. 115010. DOI: 10.1016/j.sna.2024.115010.

[133] H. Wu *et al.*, "Materials, devices, and systems of on-skin electrodes for electrophysiological monitoring and human–machine interfaces," *Adv. Sci.*, vol. 8, no. 2, 2021, Art. no. 2001938. DOI: 10.1002/advs.202001938.

[134] N. Karim, S. Afroj, S. Tan, K. S. Novoselov, and S. G. Yeates, "All inkjet-printed graphene-silver composite ink on textiles for highly conductive wearable electronics applications," *Sci. Rep.*, vol. 9, May 2019, Art. no. 8035. DOI: 10.1038/s41598-019-44420-y.

[135] K. Yang, C. Freeman, R. Torah, S. Beeby, and J. Tudor, "Screen printed fabric electrode array for wearable functional electrical stimulation," *Sensor Actuat. A-Phys.*, vol. 213, pp. 108–115, Jul. 2014. DOI: 10.1016/j.sna.2014.03.025.

[136] *Medical electrical equipment part 2-10: Particular requirements for the basic safety and essential performance of nerve and muscle stimulators*, EN 60601-2-10:2015+A1:2016, Dec. 2016.

[137] GOV.UK, *Using the UKCA marking*, (2020). Accessed: Dec. 1, 2024. [Online]. Available: https://www.gov.uk/guidance/using-the-ukca-marking.

[138] D. A. Vaca-Benavides *et al.*, "The importance of electrical parameters on transcutaneous tibial nerve stimulation (TTNS) for overactive bladder syndrome: A systematic review and meta-analysis," *Age Ageing*, May 2025, (Accepted for publication).

[139] S. Li *et al.*, "Prolonged nonobstructive urinary retention induced by tibial nerve stimulation in cats," *Am. J. Physiol. Regul. Integr. Comp. Physiol.*, vol. 318, no. 2, R428–R434, 2020. DOI: 10.1152/ajpregu.00277.2019.

[140] Z. Moazzam, A. R. Duke, and P. B. Yoo, "Inhibition and excitation of bladder function by tibial nerve stimulation using a wirelessly powered implant: An acute study in anesthetized cats," *J. Urol.*, vol. 196, no. 3, pp. 926–933, 2016. DOI: 10.1016/j.juro.2016.04.077.

[141] M. Kovacevic and P. B. Yoo, "Reflex neuromodulation of bladder function elicited by posterior tibial nerve stimulation in anesthetized rats," *Am. J. Physiol. Renal. Physiol.*, vol. 308, no. 4, F320–F329, 2015. DOI: 10.1152/ajprenal.00212.2014.

[142] Y. Matsuta *et al.*, "Contribution of opioid and metabotropic glutamate receptor mechanisms to inhibition of bladder overactivity by tibial nerve stimulation," *Am. J. Physiol. Regul. Integr. Comp. Physiol.*, vol. 305, no. 2, R126–R133, 2013. DOI: 10.1152/ajpregu.00572.2012.

[143] L. Hofmann, M. Ebert, P. A. Tass, and C. Hauptmann, "Modified pulse shapes for effective neural stimulation," *Front. Neuroeng.*, vol. 4, Sep. 2011, Art. no. 9. DOI: 10.3389/fneng.2011.00009.

[144] J. E. Bucksot, C. R. Chandler, N. M. Intharuck, R. L. Rennaker, M. P. Kilgard, and S. A. Hays, "Validation of a parameterized, open-source model of nerve stimulation," *Journal of Neural Engineering*, vol. 18, Aug. 2021, Art. no. 042001. DOI: 10.1088/1741-2552/ac1983.

[145] J. A. Hokanson, C. L. Langdale, and W. M. Grill, "Pathways and parameters of sacral neuromodulation in rats," *Am. J. Physiol. Renal. Physiol.*, vol. 325, no. 6, F757–F769, 2023. DOI: 10.1152/ajprenal.00123.2023.

[146] Centers for Medicare & Medicaid Services. "Centers for medicare & medicaid services' (cms') healthcare common procedure coding system (hcpcs) level ii final coding, benefit category and payment determinations." (2024). Accessed: May 22, 2025. (), [Online]. Available: https://www.cms.gov/files/document/2024-hcpcs-application-summary-biannual-1-2024-non-drug-and-non-biological-items-and-services.pdf.

[147] Doug Mercer, *Chapter 11: The Current Mirror*, (2021). Accessed: Dec. 1, 2024. [Online]. Available: https://wiki.analog.com/university/courses/electronics/text/chapter-11.

[148] *Medical electrical equipment – part 1: General requirements for basic safety and essential performance*, EN 60601-1:2006+A2:2021, 2005.

[149] M. Yochum, S. Binczak, T. Bakir, S. Jacquir, and R. Lepers, "A mixed FES/EMG system for real time analysis of muscular fatigue," in *32nd Annu. Int. Conf. IEEE Eng. Med. Biol. Soc. (EMBC)*, vol. 2010, Buenos Aires, Argentina, 2010, pp. 4882–4885. DOI: 10.1109/IEMBS.2010.5627264.

[150] H.-P. Wang, Z.-G. Wang, X.-Y. Lü, Z.-H. Huang, and Y.-X. Zhou, "Design of a pulse-triggered four-channel functional electrical stimulator using complementary current source and time division multiplexing output method," in *37th Annu. Int. Conf. IEEE Eng. Med. Biol. Soc. (EMBC)*, vol. 2015, Milan, Italy, Aug. 2015, pp. 1671–1674. DOI: 10.1109/EMBC.2015.7318697.

[151] H. Qu *et al.*, "Development of a network FES system for stroke rehabilitation," in *33rd Annu. Int. Conf. IEEE Eng. Med. Biol. Soc. (EMBC)*, Boston, MA, USA, 2011, pp. 3119–3122. DOI: 10.1109/IEMBS.2011.6090851.

[152] S. Marzetti *et al.*, "Embedded learning for smart functional electrical stimulation," in *IEEE Int. Instrum. Meas. Technol. Conf. (I2MTC)*, Dubrovnik, Croatia: IEEE, May 2020, pp. 1–6. DOI: 10.1109/I2MTC43012.2020.9128681.

[153] R. Shirafkan, O. Shoaei, and M. K. Ahmadi, "A high efficient adiabatic transcutaneous electrical nerve stimulator (TENS) with current regulation," *AEU - Int. J. Electron.*, vol. 123, Aug. 2020, Art. no. 153275. DOI: 10.1016/j.aeue.2020.153275.

[154] A. Levido, *Howland Current Source*, (2021). Accessed: Dec. 1, 2024. [Online]. Available: https://circuitcellar.com/resources/quickbits/howland-current-source/.

[155] D. Rotermund, U. A. Ernst, and K. R. Pawelzik, *Open hardware for neuro-prosthesis research: A study about a closed-loop multi-channel system for electrical surface stimulations and measurements*, 2017. DOI: 10.1101/141184.

[156] D. R. P. Chamal, M. I. M. Fernando, W. P. M. W. Kulathunga, K. D. Pathirana, and N. W. Prins, "Design of a novel current controlling module for functional electrical stimulation (FES) system," in *6th Int. Conf. on Info. Tech. Res. (ICITR)*, Dec. 2021, pp. 1–5. DOI: 10.1109/ICITR54349.2021.9657272.

[157] D. Karpul, G. K. Cohen, G. D. Gargiulo, A. van Schaik, S. McIntyre, and P. P. Breen, "Low-power transcutaneous current stimulator for wearable applications," *Biomed. Eng. Online*, vol. 16, Oct. 2017, Art. no. 118. DOI: 10.1186/s12938-017-0409-9.

[158] "AN-1515 a comprehensive study of the howland current pump," Texas Instruments Corp., Dallas, TX, USA, SNOA474A, 2013. [Online]. Available: https://www.ti.com/lit/an/snoa474a/snoa474a.pdf?ts=1741303208303.

[159] J. B. Velloso and M. N. Souza, "A programmable system of functional electrical stimulation (FES)," in *29th Annu. Int. Conf. IEEE Eng. Med. Biol. Soc. (EMBC)*, Lyon, France, Aug. 2007, pp. 2234–2237. DOI: 10.1109/IEMBS.2007.4352769.

[160] T. Kitamura, Y. Hasegawa, T. Tsuji, and S. Sakaino, "Control using high-carrier frequency PWM in functional electrical stimulation," in *45th Annu. Int. Conf. IEEE Ind. Electron. Soc. (IECON)*, Lisbon, Portugal, Oct. 2019, pp. 5358–5363. DOI: 10.1109/IECON.2019.8926818.

[161] M. P. Willand and H. de Bruin, "Design and testing of an instrumentation system to reduce stimulus pulse amplitude requirements during FES," in *30th Annu. Int. Conf. IEEE Eng. Med. Biol. Soc. (EMBC)*, vol. 2008, Vancouver, BC, Canada, Aug. 2008, pp. 2764–2767. DOI: 10.1109/IEMBS.2008.4649775.

[162] Y. Zhou, Y. Fang, K. Gui, K. Li, D. Zhang, and H. Liu, "sEMG bias-driven functional electrical stimulation system for upper-limb stroke rehabilitation," *IEEE Sensors J.*, vol. 18, no. 16, pp. 6812–6821, 2018. DOI: 10.1109/JSEN.2018.2848726.

[163] J. G. Webster and A. J. Nimunkar, *Medical Instrumentation: Application and Design*, 5th. Wiley.

[164] S. Khosravani, N. Lahimgarzadeh, and A. Maleki, "Developing a stimulator and an interface for FES-cycling rehabilitation system," in *18th Iranian Conf. Biomed. Eng. (ICBME)*, Tehran, Iran, Dec. 2011, pp. 175–180. DOI: 10.1109/ICBME.2011.6168550.

[165] K. W. E. Cheng, Y. Lu, K.-Y. Tong, A. B. Rad, D. H. K. Chow, and D. Sutanto, "Development of a circuit for functional electrical stimulation," *IEEE Trans. Neural. Syst. Rehabil. Eng.*, vol. 12, no. 1, pp. 43–47, 2004. DOI: 10.1109/TNSRE.2003.819936.

[166] C. A. Miller, B. K. Robinson, J. T. Rubinstein, P. J. Abbas, and C. L. Runge-Samuelson, "Auditory nerve responses to monophasic and biphasic electric stimuli," *Hear. Res.*, vol. 151, no. 1, pp. 79–94, 2001. DOI: 10.1016/s0300-2977(00)00082-6.

[167] C. C. McIntyre and W. M. Grill, "Selective microstimulation of central nervous system neurons," *Ann. Biomed. Eng.*, vol. 28, no. 3, pp. 219–233, 2000. DOI: 10.1114/1.262.

[168] J. Rubinstein, C. Miller, H. Mino, and P. Abbas, "Analysis of monophasic and biphasic electrical stimulation of nerve," *IEEE Trans. Biomed. Eng.*, vol. 48, no. 10, pp. 1065–1070, 2001. DOI: 10.1109/10.951508.

[169] P. M. Hingne and K. A. Sluka, "Differences in waveform characteristics have no effect on the anti-hyperalgesia produced by transcutaneous electrical nerve stimulation (TENS) in rats with joint inflammation," *J. Pain*, vol. 8, no. 3, pp. 251–255, 2007. DOI: 10.1016/j.jpain.2006.08.008.

[170] IET, *Galvani's animal electricity experiments*, (2025). Accessed: Mar. 1, 2025. [Online]. Available: https://www.theiet.org/membership/library-and-archives/the-iet-archives/archives-highlights/galvanis-animal-electricity-experiments.

[171] H. Yuk, B. Lu, and X. Zhao, "Hydrogel bioelectronics," *Chem. Soc. Rev.*, vol. 48, no. 6, pp. 1642–1667, 2019. DOI: 10.1039/C8CS00595H.

[172] L. McManus, G. De Vito, and M. M. Lowery, "Analysis and biophysics of surface EMG for physiotherapists and kinesiologists: Toward a common language with rehabilitation engineers," *Front. Neurol.*, vol. 11, Oct. 2020, Art. no. 576729. DOI: 10.3389/fneur.2020.576729.

[173] M. Al-Ayyad, H. A. Owida, R. De Fazio, B. Al-Naami, and P. Visconti, "Electromyography monitoring systems in rehabilitation: A review of clinical applications, wearable devices and signal acquisition methodologies," *Electronics*, vol. 12, no. 7, p. 1520, 2023. DOI: 10.3390/electronics12071520.

[174] L. Cheng, J. Li, A. Guo, and J. Zhang, "Recent advances in flexible noninvasive electrodes for surface electromyography acquisition," *npj Flex. Electron.*, vol. 7, pp. 1–26, Aug. 2023, Art. no. 39. DOI: 10.1038/s41528-023-00273-0.

[175] G. A. Light *et al.*, "Electroencephalography (EEG) and event-related potentials (ERPs) with human participants," *Curr. Protoc. Neurosci.*, vol. 6, pp. 25.1–25.24, 2010. DOI: 10.1002/0471142301.ns0625s52.

[176] P. D. Emmady and A. C. Anilkumar, "EEG abnormal waveforms," in *StatPearls*, Treasure Island (FL): StatPearls Publishing, 2025.

[177] R. Dozio, A. Baba, C. Assambo, and M. J. Burke, "Time based measurement of the impedance of the skin-electrode interface for dry electrode ECG recording," in *29th Annu. Int. Conf. IEEE Eng. Med. Biol. Soc. (EMBC)*, vol. 2007, Lyon, France, Aug. 2007, pp. 5001–5004. DOI: 10.1109/IEMBS.2007.4353463.

[178] D. Henrich, K. Hoffmann, and T. Schmidt, "New dry electrodes with comparable performance as standard electrodes," *Biomed. Tech.*, vol. 58, Suppl 1 Sep. 2013. DOI: 10.1515/bmt-2013-4136.

[179] S. Chatterjee, R. S. Thakur, R. N. Yadav, L. Gupta, and D. K. Raghuvanshi, "Review of noise removal techniques in ECG signals," *IET Signal Process.*, vol. 14, no. 9, pp. 569–590, 2020. DOI: 10.1049/iet-spr.2020.0104.

[180] Digitimer Ltd., *The Importance of Skin-Electrode Impedance in Electrophysiological Recording and Stimulation*, (2024). Accessed: Dec. 1, 2024. [Online]. Available: https://www.digitimer.com/applications/the-importance-of-electrode-impedance-in-recording-and-stimulation/.

[181] J. Xu, S. Mitra, C. Van Hoof, R. F. Yazicioglu, and K. A. A. Makinwa, "Active electrodes for wearable EEG acquisition: Review and electronics design methodology," *IEEE Rev. Biomed. Eng.*, vol. 10, pp. 187–198, Jan. 2017. DOI: 10.1109/RBME.2017.2656388.

[182] C. Bennett *et al.*, "Neuroinflammation, oxidative stress, and blood-brain barrier (BBB) disruption in acute utah electrode array implants and the effect of deferoxamine as an iron chelator on acute foreign body response," *Biomaterials*, vol. 188, pp. 144–159, Jan. 2019. DOI: 10.1016/j.biomaterials.2018.09.040.

[183] A. Atala, D. J. Irvine, M. Moses, and S. Shaunak, "Wound healing versus regeneration: Role of the tissue environment in regenerative medicine," *MRS Bull.*, vol. 35, no. 8, 2010. DOI: 10.1557/mrs2010.528.

[184] T. Weigel *et al.*, "A three-dimensional hybrid pacemaker electrode seamlessly integrates into engineered, functional human cardiac tissue in vitro," *Sci. Rep.*, vol. 8, Sep. 2018, Art. no. 14545. DOI: 10.1038/s41598-018-32790-8.

[185] W. Pei *et al.*, "A pre-gelled EEG electrode and its application in SSVEP-based BCI," *IEEE Trans. Neural. Syst. Rehabil. Eng.*, vol. 30, pp. 843–850, Mar. 2022. DOI: 10.1109/TNSRE.2022.3161989.

[186] Adafruit Industries. "Knit conductive fabric - silver 20cm square." (2025). Accessed: Jun. 26, 2025. (), [Online]. Available: https://www.adafruit.com/product/1167.

[187] A. A. Bhide, V. Tailor, R. Fernando, V. Khullar, and G. A. Digesu, "Posterior tibial nerve stimulation for overactive bladder-techniques and efficacy," *Int. Urogynecol. J.*, vol. 31, no. 5, pp. 865–870, 2020. DOI: 10.1007/s00192-019-04186-3.

[188] M. L. Pierre, B. Friso, R. A. Casarotto, J. M. Haddad, E. C. Baracat, and E. A. G. Ferreira, "Comparison of transcutaneous electrical tibial nerve stimulation for the treatment of overactive bladder: A multi-arm randomized controlled trial with blinded assessment," *Clinics*, vol. 76, Aug. 2021, Art. no. e3039. DOI: 10.6061/clinics/2021/e3039.

[189] H. Ha *et al.*, "A bio-impedance readout IC with digital-assisted baseline cancellation for two-electrode measurement," *IEEE J. Solid-State Circuits*, vol. 54, no. 11, pp. 2969–2979, 2019. DOI: 10.1109/JSSC.2019.2939077.

[190] L. A. Geddes and L. E. Baker, *Principles of Applied Biomedical Instrumentation*, 3rd ed. Wiley, 1991, ISBN: 978-0-471-60899-8.

[191] O. FeldmanHall, D. Mobbs, D. Evans, L. Hiscox, L. Navrady, and T. Dalgleish, "What we say and what we do: The relationship between real and hypothetical moral choices," *Cognition*, vol. 123, no. 3, pp. 434–441, 2012. DOI: 10.1016/j.cognition.2012.02.001.

[192] D. V. Atanassova, I. A. Brazil, C. E. A. Tomassen, and J. M. Oosterman, "Pain sensitivity mediates the relationship between empathy for pain and psychopathic traits," *Sci. Rep.*, vol. 15, Jan. 2025, Art. no. 3729. DOI: 10.1038/s41598-025-87892-x.

[193] T. A. L. Wren, K. P. Do, S. A. Rethlefsen, and B. Healy, "Cross-correlation as a method for comparing dynamic electromyography signals during gait," *Journal of Biomechanics*, vol. 39, no. 14, pp. 2714–2718, 2006. DOI: 10.1016/j.jbiomech.2005.09.006.

[194] J. Luo and E. E. Konofagou, "A fast normalized cross-correlation calculation method for motion estimation," *IEEE transactions on ultrasonics, ferroelectrics, and frequency control*, vol. 57, no. 6, pp. 1347–1357, 2010. DOI: 10.1109/TUFFC.2010.1554.

[195] J. Booth *et al.*, "Tibial nerve stimulation compared with sham to reduce incontinence in care home residents: ELECTRIC RCT.," *Health Technol. Assess.*, vol. 25, no. 41, pp. 1–110, Jun. 2021. DOI: 10.3310/hta25410.

[196] S. A. Stalder *et al.*, "bTUNED: Transcutaneous tibial nerve stimulation for neurogenic lower urinary tract dysfunction," *BJU Int.*, vol. 132, no. 3, pp. 343–352, 2023. DOI: 10.1111/bju.16081.

[197] The Electricity Forum, *Understanding Capacitor Voltage Rating Limitations*, (2025). Accessed: Mar. 1, 2025. [Online]. Available: https://electricityforum.com/iep/power-quality/capacitor-voltage-rating?utm_source=chatgpt.com.

[198] TDK Corp., *Capacitors, Part 5 "Film Capacitors [2]"*, (2024). Accessed: Dec. 1, 2024. [Online]. Available: https://www.tdk.com/en/tech-mag/electronics_primer/8.

[199] Pulse Electronics, *Introduction to Transformer Magnetics*, (2020). Accessed: Dec. 1, 2024. [Online]. Available: https://www.pulseelectronics.com/wp-content/uploads/2020/12/Introduction-Transformer-Magnetics.pdf.

[200] D. C. d. Souza, M. d. C. Gaiotto, G. N. Nogueira, M. C. F. d. Castro, and P. Nohama, "Power amplifier circuits for functional electrical stimulation systems," *Res. Biomed. Eng.*, vol. 33, no. 2, pp. 144–155, 2017. DOI: 10.1590/2446-4740.07716.

[201] "Voltage-to-current (v-i) converter circuit with BJT," Texas Instruments Corp., Dallas, TX, USA, sboa325, 2021. [Online]. Available: https://www.ti.com/lit/pdf/sboa325.

[202] P. C. Todd, "Snubber circuits: Theory, design and application," Texas Instruments Corp., Dallas, TX, USA, 1993. [Online]. Available: https://e2e.ti.com/cfs-file/__key/communityserver-discussions-components-files/196/slup100.pdf.

[203] *IEEE standard requirements for instrument transformers*, IEEE Standard C57.13-2016, 2016.

[204] J. Thakur, P. Phogat, Shreya, R. Jha, and S. Singh, "Non-rechargeable batteries: A review of primary battery technology and future trends," *Phys. Chem. Chem. Phys.*, vol. 27, no. 8, pp. 4045–4077, 2025. DOI: 10.1039/D4CP04614E.

[205] Y. Zhang, Y. Zhao, J. Ren, W. Weng, and H. Peng, "Advances in wearable fiber-shaped lithium-ion batteries," *Adv. Mater.*, vol. 28, no. 22, pp. 4524–4531, 2016. DOI: 10.1002/adma.201503891.

[206] Blue Power, *Revolutionizing Power: The Future Of Energy With Custom-Shaped Ultra Thin Lipo Batteries*, (2024). Accessed: Mar. 1, 2025. [Online]. Available: https://www.cnbluepower.com/a-revolutionizing-power-the-future-of-energy-with-custom-shaped-ultra-thin-lipo-batteries.html.

[207] "Bq21040 0.8-a, single-input, single cell li-ion and li-pol battery charger," Texas Instruments Corp., Dallas, TX, USA, bq21040, 2019. [Online]. Available: https://www.ti.com/lit/ds/symlink/bq21040.pdf.

[208] Agwu Daberechi D., Opara F. K., Chukwuchekwa N., Dike. D. O., and Uzoechi L., "Review of comparative battery energy storage systems (bess) for energy storage applications in tropical enviroments," in *IEEE 3rd Int.Conf. Electro-Tech. Natl. Dev. (NIGERCON)*, Owerri, Nigeria, Nov. 2017.

[209] "TPS61088 10-a fully-integrated synchronous boost converter," Texas Instruments Corp., Dallas, TX, USA, TPS61088, 2021. [Online]. Available: https://www.ti.com/lit/ds/symlink/tps61088.pdf?ts=1741336300988&ref_url=https%253A%252F%252Fwww.google.com%252F.

[210] "40 v, 200 mA, low noise, CMOS LDO linear regulator," Analog Devices, Wilmington, MA, USA, ADP7142, 2024.

[211] BYJU'S, *Capacitor and Capacitance*, (2025). Accessed: Mar. 1, 2025. [Online]. Available: https://byjus.com/physics/capacitor-and-capacitance/.

[212] "Building an electrolytic capacitor," Kendeil Srl., Gallarate VA, Italy, 2025. [Online]. Available: https://www.kendeil.com/Portals/0/Tech-Academy/BUILDING_AN_ELECTROLYTIC_CAPACITOR.pdf.

[213] "Aluminium electrolytic capacitors," Nichicon Corp., Kyoto, Japan, CAT.8100L, 2025. [Online]. Available: https://www.nichicon.co.jp/english/series_items/catalog_pdf/e-lnk.pdf.

[214] "What is a transformer k-factor rating?" ABB Inc., NC, USA, 2025. [Online]. Available: https://search.abb.com/library/Download.aspx?DocumentID=1TQC194900E0001&LanguageCode=en&DocumentPartId&Action=Launch.

[215] "SP-48 audio transformer," Triad Magnetics, Perris, CA, USA, SP-48, 2024.

[216] R. R. Rajanna, N. Sriraam, P. R. Vittal, and U. Arun, "Performance evaluation of woven conductive dry textile electrodes for continuous ECG signals acquisition," *IEEE Sensors J.*, vol. 20, no. 3, pp. 1573–1581, 2020. DOI: 10.1109/JSEN.2019.2946058.

[217] S. R. Khan *et al.*, "Multi-modal portable respiratory rate monitoring device for childhood pneumonia detection," *Micromachines*, vol. 14, no. 4, 2023, Art. no. 708. DOI: 10.3390/mi14040708.

[218] V. Mihajlović and B. Grundlehner, "The effect of force and electrode material on electrode-to-skin impedance," in *2012 IEEE Biomed Circuits Syst Conf.*, Hsinchu, Taiwan, Nov. 2012, pp. 57–60. DOI: 10.1109/BioCAS.2012.6418511.

[219] S. M. M. Rahman, H. Mattila, M. Janka, and J. Virkki, "Impedance evaluation of textile electrodes for EEG measurements," *Text. Res. J.*, vol. 93, no. 7, pp. 1878–1888, 2023. DOI: 10.1177/00405175221135131.

[220] C. D. Solomons, M. Slovak, B. Heller, and A. T. Barker, "Reducing the sensation of electrical stimulation with dry electrodes by using an array of constant current sources," *Med. Eng. Phys.*, vol. 51, pp. 91–95, 2018. DOI: 10.1016/j.medengphy.2017.11.001.

[221] E. Peli, "Contrast in complex images," *J. Opt. Soc. Am. A*, vol. 7, no. 10, pp. 2032–2040, 1990. DOI: 10.1364/JOSAA.7.002032.

[222] D. McClurg *et al.*, "Stimulation of the tibial nerve—a randomised trial for urinary problems associated with parkinson's—the STARTUP trial," *Age Ageing*, vol. 51, no. 6, 2022, Art. no. afac114. DOI: 10.1093/ageing/afac114.

[223] G. Chen, L. Liao, and Y. Li, "The possible role of percutaneous tibial nerve stimulation using adhesive skin surface electrodes in patients with neurogenic detrusor overactivity secondary to spinal cord injury," *Int. Urol. Nephrol.*, vol. 47, no. 3, pp. 451–455, 2015. DOI: 10.1007/s11255-015-0911-6.

[224] V. Manríquez *et al.*, "Transcutaneous posterior tibial nerve stimulation versus extended release oxybutynin in overactive bladder patients. a prospective randomized trial," *Eur. J. Obstet. Gynecol. Reprod. Biol.*, vol. 196, pp. 6–10, 2016. DOI: 10.1016/j.ejogrb.2015.09.020.

[225] A. McConnell-Trevillion *et al.*, "Low-frequency tibial neuromodulation increases voiding activity—a human pilot study and computational model," *eLife*, Jun. 2025. DOI: 10.7554/eLife.106174.1.

[226] C. Tai, B. Shen, M. Chen, J. Wang, J. R. Roppolo, and W. C. de Groat, "Prolonged poststimulation inhibition of bladder activity induced by tibial nerve stimulation in cats," *Am. J. Physiol. Renal. Physiol.*, vol. 300, no. 2, F385–F392, 2011.

[227] *The medical devices regulations*, 618, 2002.

[228] K. Weise, O. Numssen, A. Thielscher, G. Hartwigsen, and T. R. Knösche, "A novel approach to localize cortical TMS effects," *NeuroImage*, vol. 209, Apr. 2020, Art. no. 116486, ISSN: 1053-8119. DOI: 10.1016/j.neuroimage.2019.116486.

[229] C. Kemlin *et al.*, "Redundancy among parameters describing the input-output relation of motor evoked potentials in healthy subjects and stroke patients," *Front. Neurol.*, vol. 10, 2019, Art. no. 535. DOI: 10.3389/fneur.2019.00535.

[230] S. M. M. Alavi, S. M. Goetz, and A. V. Peterchev, "Optimal estimation of neural recruitment curves using fisher information: Application to transcranial magnetic stimulation," *IEEE Trans. Neural. Syst. Rehabil. Eng.*, vol. 27, no. 6, pp. 1320–1330, 2019. DOI: 10.1109/TNSRE.2019.2914475.

[231] K. Nakagawa, K. L. Fok, and K. Masani, "Neuromuscular recruitment pattern in motor point stimulation," *Artif. Organs*, vol. 47, no. 3, pp. 537–546, 2023. DOI: 10.1111/aor.14445.

[232] H. J. Kendall, J. Schrijvers, and J. P. F. A. Heesakkers, "Tibial neuromodulation for lower urinary tract dysfunction (idiopathic overactive bladder and non obstructive urinary retention): A review of the literature," *Continence*, vol. 11, Sep. 2024, Art. no. 101326. DOI: 10.1016/j.cont.2024.101326.

[233] J. Mai *et al.*, "Prolonged inhibitory effects of repeated tibial nerve stimulation on the micturition reflex in decorticated rats," *Neuromodulation*, vol. 25, no. 8, pp. 1115–1121, 2022. DOI: 10.1016/j.neurom.2021.11.011.

[234] P.-A. Leroux, E. Brassart, S. Lebdai, A.-R. Azzouzi, P. Bigot, and J. Carrouget, "Transcutaneous tibial nerve stimulation: 2 years follow-up outcomes in the management of anticholinergic refractory overactive bladder," *World J. Urol.*, vol. 36, pp. 1455–1460, Apr. 2018. DOI: 10.1007/s00345-018-2296-5.

[235] M. te Dorsthorst, M. van Balken, D. Janssen, J. Heesakkers, and F. Martens, "Real-life patient experiences of TTNS in the treatment of overactive bladder syndrome," *Ther. Adv. Urol.*, vol. 13, Aug. 2021. DOI: 10.1177/17562872211041470.

[236] A. Rogers, S. Bragg, K. Ferrante, C. Thenuwara, and D. K. L. Peterson, "Pivotal study of leadless tibial nerve stimulation with eCoin® for urgency urinary incontinence: An open-label, single arm trial," *J. Urol.*, vol. 206, no. 2, pp. 399–408, 2021. DOI: 10.1097/JU.0000000000001733.

[237] J. P. F. A. Heesakkers *et al.*, "Two-year efficacy and safety outcomes of the pivotal OASIS study using the revi system for treatment of urgency urinary incontinence," *J. Urol.*, Mar. 2025. DOI: 10.1097/JU.0000000000004328.

[238] B. Kaaki *et al.*, "Six-month outcomes of reimplantation of a coin-sized tibial nerve stimulator for the treatment of overactive bladder syndrome with urgency urinary incontinence," *Female Pelvic Med. Reconstr. Surg.*, vol. 28, no. 5, pp. 287–292, 2022. DOI: 10.1097/SPV.0000000000001105.

[239] C. Goudelocke, R. Dhir, E. Shapiro, K. Cline, D. E. Poulos, and P. Hedges, "A multicenter prospective sham-controlled trial evaluating a physiologic closed-loop wearable tibial neuromodulation system for overactive bladder," *Urology*, vol. 195, pp. 16–22, Jan. 2025. DOI: 10.1016/j.urology.2024.09.018.

[240] Ametherm, *NTC Thermistors Steinhart and Hart Equation*, (2013). Accessed: Mar. 6, 2025. [Online]. Available: https://www.ametherm.com/thermistor/ntc-thermistors-steinhart-and-hart-equation/.

# Appendix A

# Expressions and Derivations

## A.1 Approximation Method of Beta Coefficient

The Steinhart and Hart Equation is recognised as the most accurate mathematical expression for describing the resistance-temperature relationship of negative temperature coefficient (NTC) thermistors [240]. The most common format is given by:

$$T = \frac{1}{A + B \cdot ln(R) + C \cdot [ln(R)]^3} \tag{A.1}$$

where $T$ denotes the temperature (in Kelvin). $A$, $B$ and $C$ represent coefficients are derived in the following.

Firstly, the thermistor's resistance is measured at three distinct temperatures, which should be evenly distributed and have a minimum difference of 10 degrees between each. Given that three temperature measurements have been obtained, Eq.(A.2)–(A.4) are given as follows:

$$\frac{1}{T_1} = \frac{1}{A + B \cdot ln(R_1) + C \cdot [ln(R_1)]^3} \tag{A.2}$$

$$\frac{1}{T_2} = \frac{1}{A + B \cdot ln(R_2) + C \cdot [ln(R_2)]^3} \tag{A.3}$$

$$\frac{1}{T_3} = \frac{1}{A + B \cdot ln(R_3) + C \cdot [ln(R_3)]^3} \tag{A.4}$$

Thereby, three coefficients (i.e., $A$, $B$ and $C$) can be determined as follows:

$$C = \left(\frac{\gamma_3 - \gamma_2}{L_3 - L_2}\right)(L_1 + L_2 + L_3)^{-1} \tag{A.5}$$

$$B = \gamma_2 - C \cdot ({L_1}^2 + L_1 L_2 + {L_2}^2) \tag{A.6}$$

$$A = Y_1 - L_1 \cdot (B + C \cdot {L_1}^2) \tag{A.7}$$

where $L_1 = ln(R_1), L_2 = ln(R_2), L_3 = ln(R_3), Y_1 = T_1^{-1}, Y_2 = T_2^{-1}, Y_3 = T_3^{-1}, \gamma_2 = \frac{Y_2 - Y_1}{L_2 - L_1}$, and $\gamma_3 = \frac{Y_3 - Y_1}{L_3 - L_1}$. If the resistance is known, Eq.(A.1) can be used to calculate the resistance. In contrast, if the temperature is known and the expected resistance is desired, use Eq.(A.8), as given below:

$$R = exp(\sqrt[3]{y - \frac{x}{2}} - \sqrt[3]{y + \frac{x}{2}}) \tag{A.8}$$

where

$$x = \frac{1}{C} \cdot \left(A - \frac{1}{T}\right) \tag{A.9}$$

and

$$y = \sqrt{\left(\frac{B}{3C}\right)^3 + \left(\frac{x}{2}\right)^2} \tag{A.10}$$

## A.2 Pulse Shape Analysis (Capacitive Isolation)

To maintain the monophasic shape of a stimulation pulse, a longer discharging time is essential. Achieving this requires careful consideration of the time constant ($\tau$), which is given by:

$$\tau = R_L \cdot C \tag{A.11}$$

where $R_L$ is the output load, and $C$ is the isolated capacitance.

The current during the discharging phase decreases over time following the equation:

$$I = I_0 \cdot e^{-\frac{t}{\tau}} \tag{A.12}$$

where $I_0$ represents the initial current, and t denotes the discharging time. The isolated capacitance can be derived based on the relationship between the discharging current and the time constant, given by

$$C = \frac{t}{R_L \cdot ln\left[\frac{I_0}{I(t)}\right]} \tag{A.13}$$

where $t$ denotes the pulse width of the stimulation pulse during discharging.

# Appendix B

# Design Material of TENS*mini*

## B.1 MCU Pinout Configuration

The pinout the microcontroller unit (MCU) is shown in Fig. B.1.

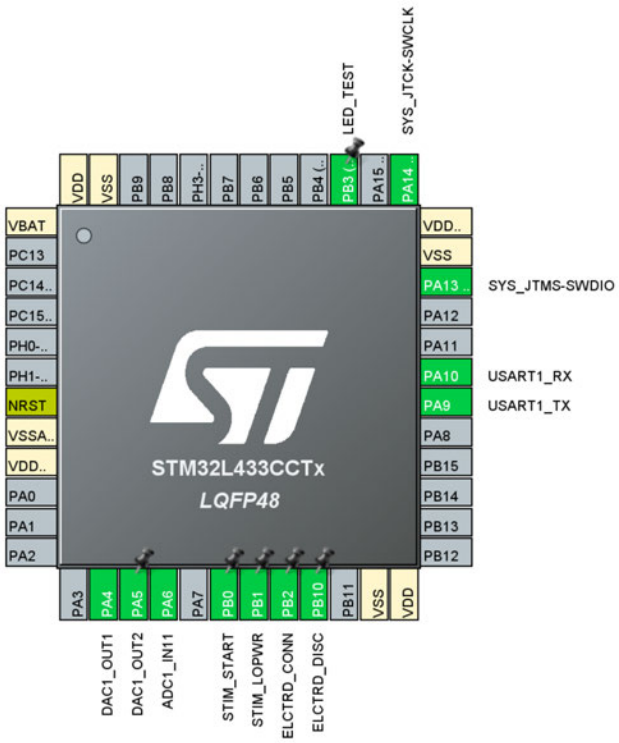


Fig. B.1. A pinout diagram of the MCU.

## B.2 Circuit Schematic

The complete circuit schematic of the *TENSmini* device is provided in Fig. B.2–Fig. B.5, detailing the hardware architecture.

## B.3 PCB Layout

The layout schematic of the six-layer printed circuit board (PCB) of the *TENSmini* is provided in Fig. B.6–Fig. B.8.

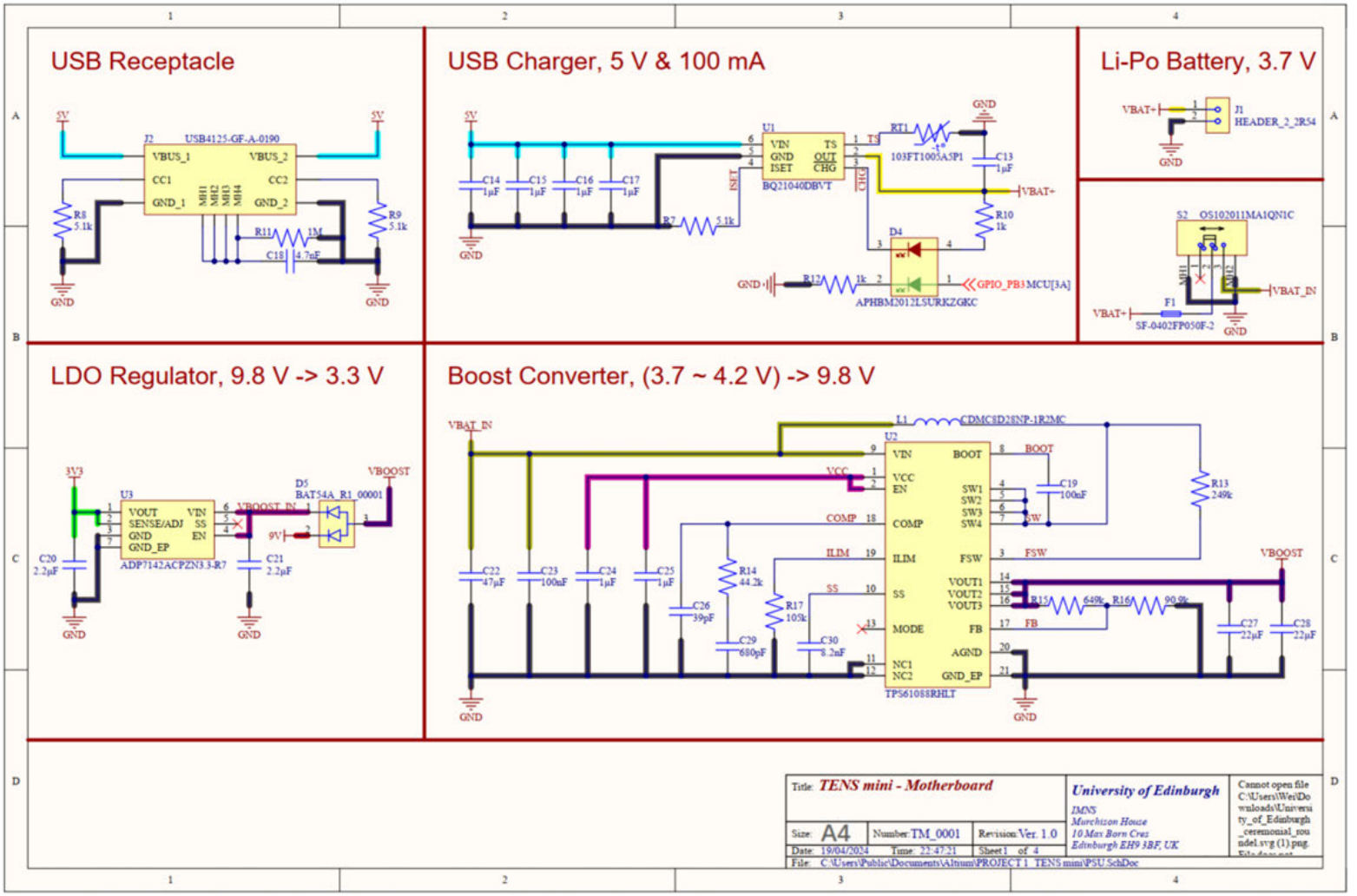


Fig. B.2. Schematic of power management module.

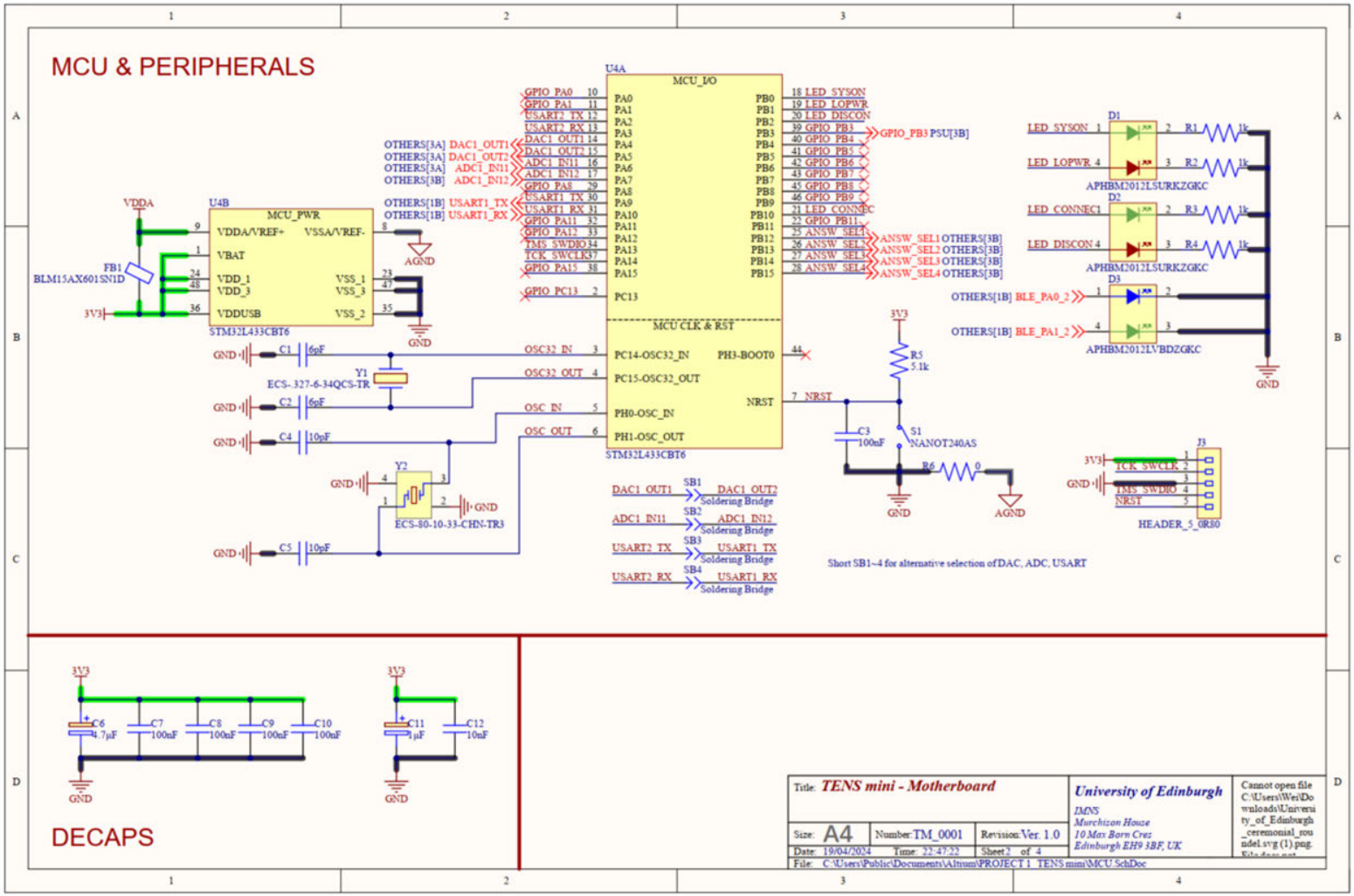


Fig. B.3. Schematic of microcontroller and its peripheral components.

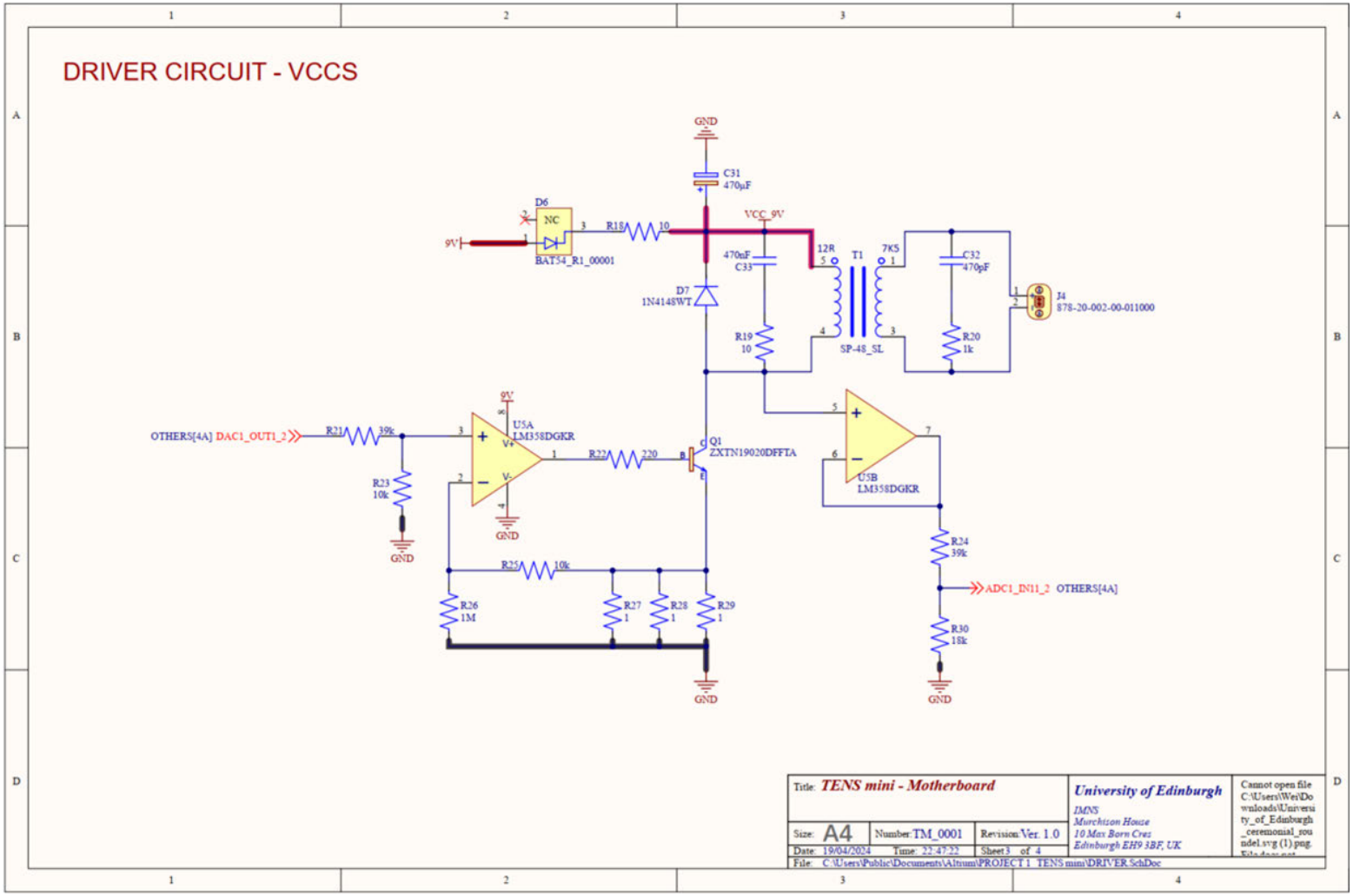


Fig. B.4. Schematic of stimulation module including a drive circuit.

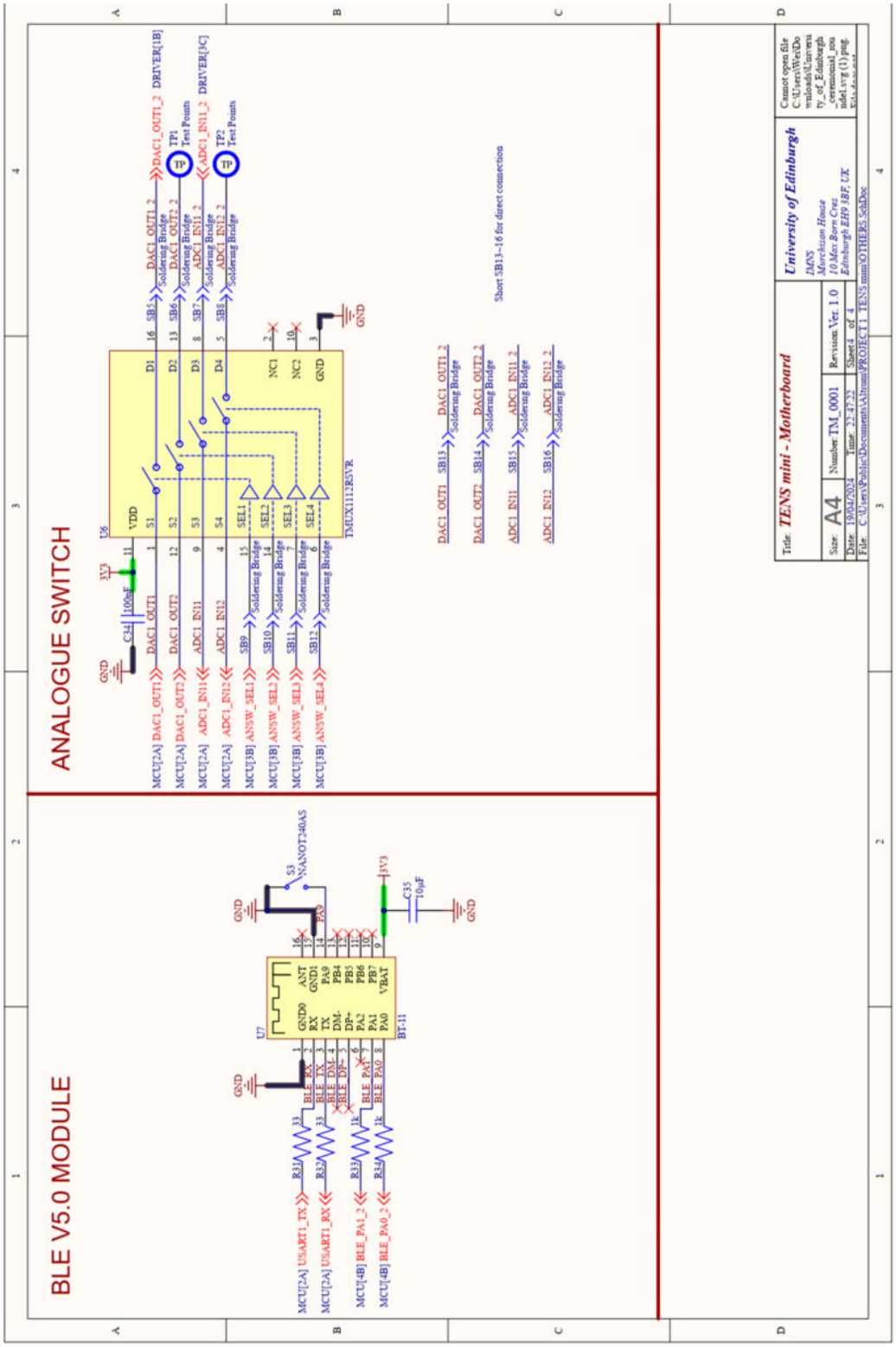


Fig. B.5. Schematic of other modules.

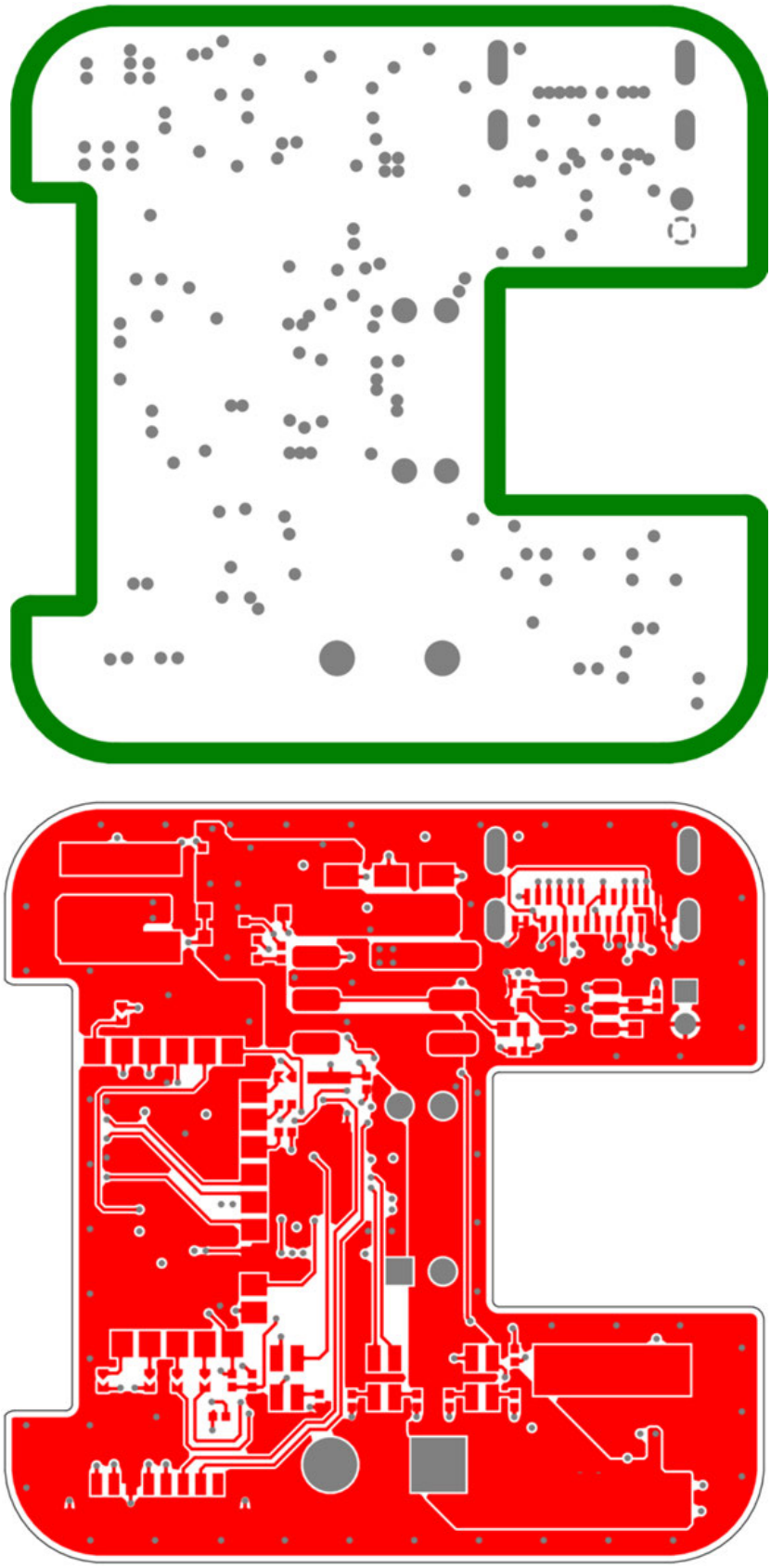

Fig. B.6. The top (left) and second layer (GND plane; right) of the PCB.

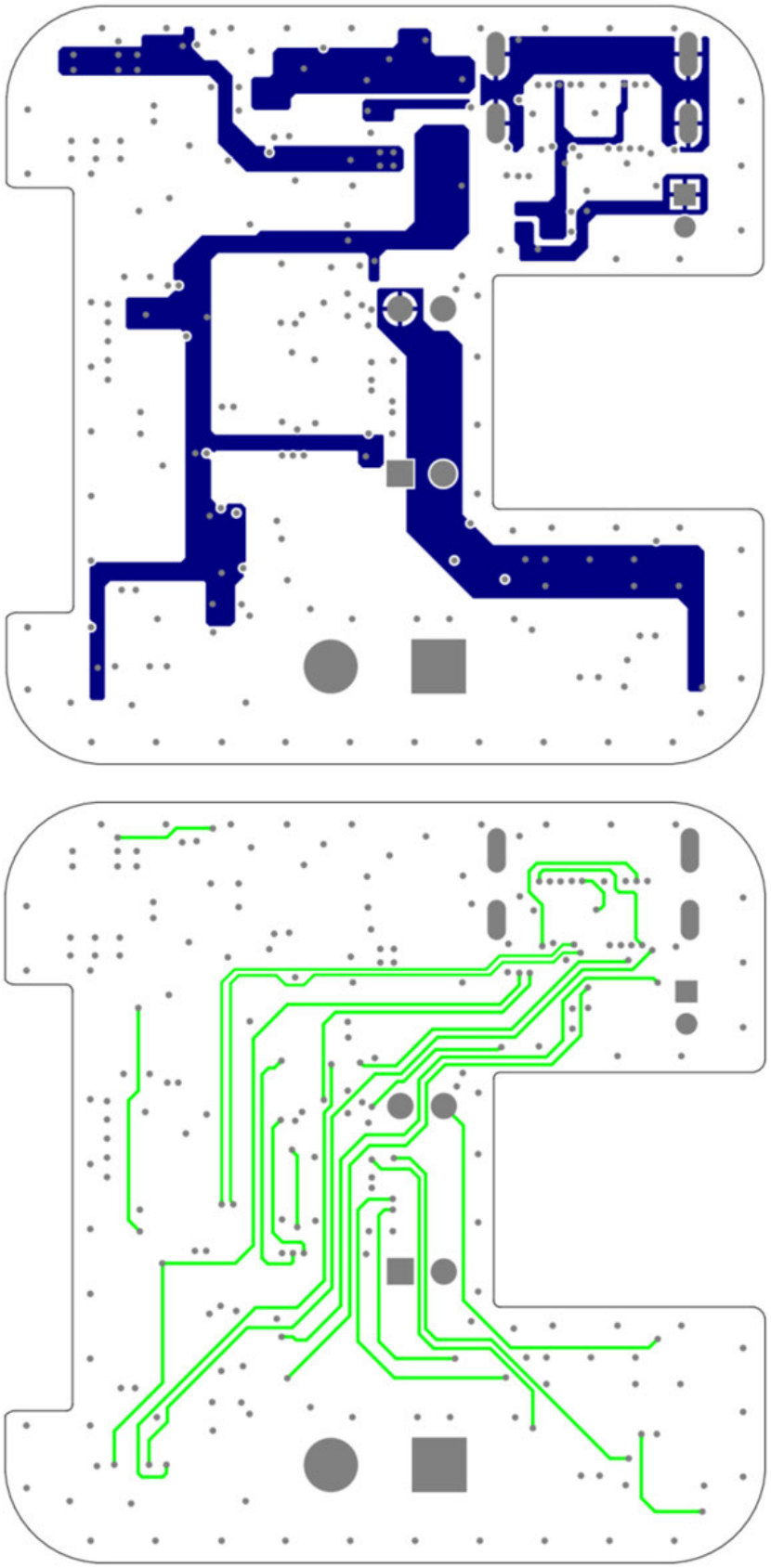

Fig. B.7. The third (signal; left) and fourth layer (power; right) of the PCB.

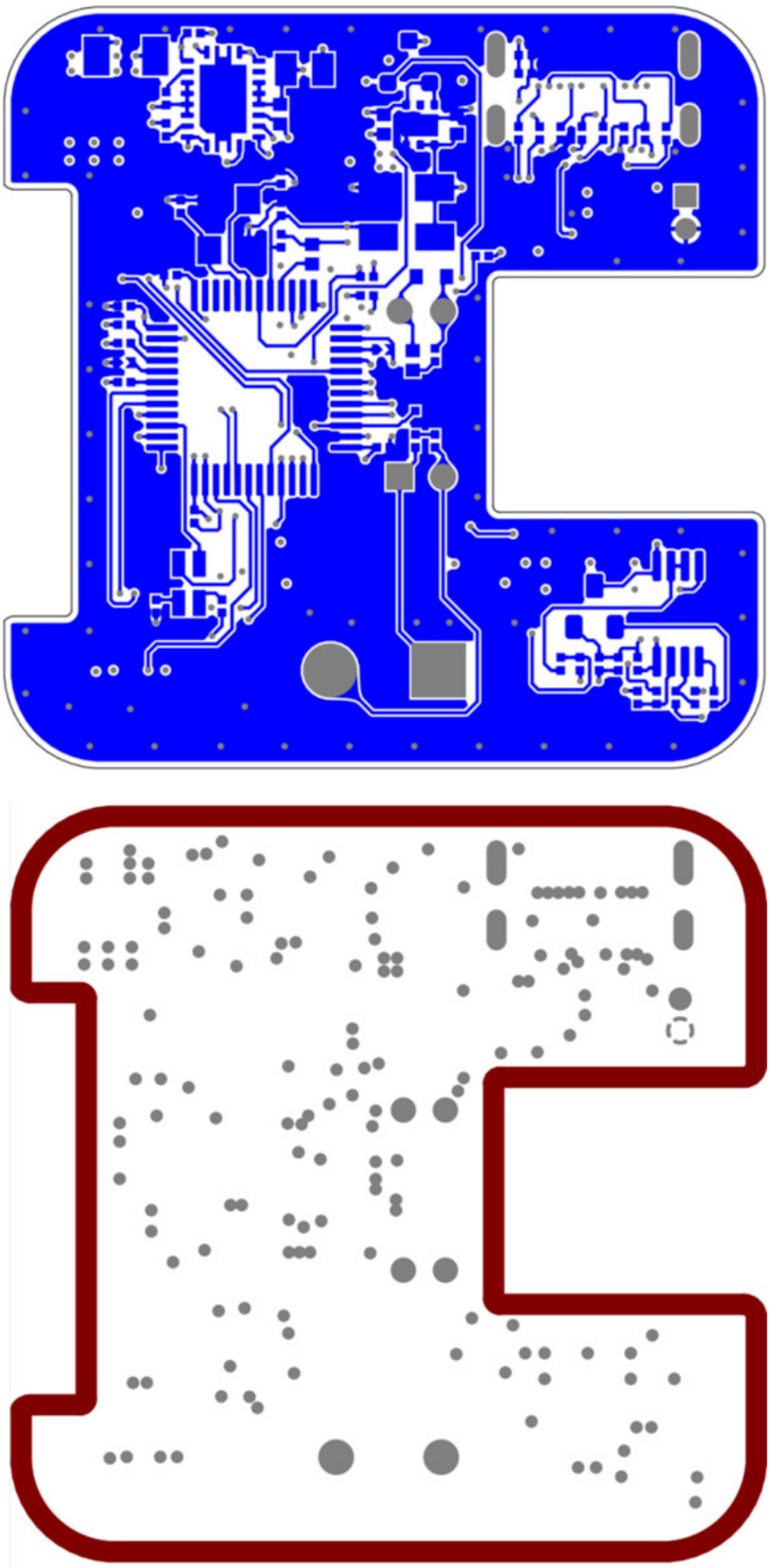

Fig. B.8. The fifth (GND plane; left) and bottom layer (right) of the PCB.

## B.4 Firmware

The firmware source code for the TENS*mini* device, including the *main.c* file, is publicly available in the GitHub repository.

## B.5 Bill of Material

A full bill of material related to the *TENSmini* is also provided in Table B.1.

Table B.1. Bill of material for the TENS*mini*'s PCB.

| Idx. | Description | Designator | Qt. | Manufacturer | Manufacturer P/N |
|---|---|---|---|---|---|
| 1 | Multilayer Ceramic Capacitors (MLCC) – 6 pF | C1, C2 | 2 | Murata | GRM0335C1H6R0BA01D |
| 2 | Multilayer Ceramic Capacitors (MLCC) – 0.1 $\mu$F | C3, C7, C8, C9, C10, C19, C23, C34 | 8 | Murata | GRM033R6YA104KE14D |
| 3 | Multilayer Ceramic Capacitors (MLCC) – 10 pF | C4, C5 | 2 | Murata | GRM0335C1H100JA01D |
| 4 | Tantalum Capacitors – 4.7 $\mu$F | C6 | 1 | KEMET | T491A475M025AT |
| 5 | Tantalum Capacitors – 1 $\mu$F | C11 | 1 | KEMET | T491A105K050AT |
| 6 | Multilayer Ceramic Capacitors (MLCC) – 0.01 $\mu$F | C12 | 1 | Murata | GRM033R71C103KE14D |
| 7 | Multilayer Ceramic Capacitors (MLCC) – 1 $\mu$F | C13, C14, C15, C16, C17, C24, C25 | 7 | Murata | GRM155R61H105KE05D |
| 8 | Multilayer Ceramic Capacitors (MLCC) – 4700 pF | C18 | 1 | Murata | GRM033R71E472KE14E |
| 9 | Multilayer Ceramic Capacitors (MLCC) – 2.2 $\mu$F | C20, C21 | 2 | Murata | GRM155R61E225ME11J |
| 10 | Multilayer Ceramic Capacitors (MLCC) – 47 $\mu$F | C22 | 1 | Murata | GRM31CR61C476ME44K |
| 11 | Multilayer Ceramic Capacitors (MLCC) – 39 pF | C26 | 1 | Murata | GRM0335C1H390JA01D |
| 12 | Multilayer Ceramic Capacitors (MLCC) – 22 $\mu$F | C27, C28 | 2 | Murata | GRM21BR61E226ME44L |

Continued on next page

(Continued)

| Idx. | Description | Designator | Qt. | Manufacturer | Manufacturer P/N |
|---|---|---|---|---|---|
| 13 | Multilayer Ceramic Capacitors (MLCC) – 680 pF | C29 | 1 | Murata | GRM0335C1H681JE01D |
| 14 | Multilayer Ceramic Capacitors (MLCC) – 8200 pF | C30 | 1 | Murata | GRM033R71E822KE14D |
| 15 | Tantalum Capacitors – 470 $\mu$F | C31 | 1 | Vishay Sprague | 597D477X9016H2T |
| 16 | Multilayer Ceramic Capacitors (MLCC) – 470 pF | C32 | 1 | Murata | GRM0335C1H471JE01D |
| 17 | Multilayer Ceramic Capacitors (MLCC) – 0.47 $\mu$F | C33 | 1 | Murata | GRM155R61H474KE11D |
| 18 | Multilayer Ceramic Capacitors (MLCC) – 10 $\mu$F | C35 | 1 | Murata | ZRB15XR61A106ME01D |
| 19 | Standard LEDs – Red/Green Low Current | D1, D2, D4 | 3 | Kingbright | APHBM2012LSURKZGKC |
| 20 | Standard LEDs – Blue/Green Low Current | D3 | 1 | Kingbright | APHBM2012LVBDZGKC |
| 21 | Schottky Diodes Rectifiers – Dual Cathode Common Anode | D5 | 1 | Pan Jit | BAT54A_R1_00001 |
| 22 | Schottky Diodes Rectifiers – Single | D6 | 1 | Pan Jit | BAT54_R1_00001 |
| 23 | General Purpose Diodes – Single | D7 | 1 | ON Semiconductor / Fairchild | 1N4148WT |
| 24 | Surface Mount Fuses – 0.5 A, Fast Acting | F1 | 1 | Bourns | SF-0402FP050F-2 |
| 25 | Ferrite Beads – 600 Ohms (@100 MHz) | FB1 | 1 | Murata | BLM15AX601SN1D |
| 26 | Headers Wire Housings – 2.54 mm, 2 Pins | J1 | 1 | - | - |

Continued on next page

(Continued)

| Idx. | Description | Designator | Qt. | Manufacturer | Manufacturer P/N |
|---|---|---|---|---|---|
| 27 | USB Connectors – Type C Receptacle (Female) | J2 | 1 | Global Connector Technology | USB4125-GF-A-0190 |
| 28 | Headers Wire Housings – 0.80 mm, 5 Pins | J3 | 1 | - | - |
| 29 | Headers Wire Housings – Magnetic Spring-Loaded Target Connector, 2 Pins | J4 | 1 | - | - |
| 30 | Power Inductors – 1.2 $\mu$H | L1 | 1 | Sumida | CDMC8D28NP-1R2MC |
| 31 | Bipolar Transistors (BJT) – NPN, 20VDC | Q1 | 1 | Diodes Zetex | ZXTN19020DFFTA |
| 32 | Thick Film Resistors – 1 kΩ | R1, R2, R3, R4, R10, R12, R20, R33, R34 | 9 | Yageo | RC0201JR-071KL |
| 33 | Thick Film Resistors – 5.1 kΩ | R5, R7, R8, R9 | 4 | Yageo | RC0201FR-075K1L |
| 34 | Thick Film Resistors – 0 Ω | R6 | 1 | | |
| 35 | Thick Film Resistors – 1 MΩ | R11, R26 | 2 | Yageo | RC0201JR-071ML |
| 36 | Thick Film Resistors – 249 kΩ | R13 | 1 | Yageo | RC0201FR-07249KL |
| 37 | Thick Film Resistors – 44.2 kΩ | R14 | 1 | Vishay | CRCW020144K2FNED |

Continued on next page

(Continued)

| Idx. | Description | Designator | Qt. | Manufacturer | Manufacturer P/N |
|---|---|---|---|---|---|
| 38 | Thick Film Resistors – 649 kΩ | R15 | 1 | Vishay Semiconductors | CRCW0402649KFKEDC |
| 39 | Thick Film Resistors – 90.9 kΩ | R16 | 1 | Vishay | CRCW040290K9FKED |
| 40 | Thick Film Resistors – 105 kΩ | R17 | 1 | Yageo | RC0201FR-07105KL |
| 41 | Thick Film Resistors – 10 Ω | R18, R19 | 2 | Yageo | RC0201JR-1310RL |
| 42 | Thick Film Resistors – 39 kΩ | R21, R24 | 2 | Yageo | RC0201JR-0739KL |
| 43 | Thick Film Resistors – 220 Ω | R22 | 1 | Yageo | RC0201JR-07220RL |
| 44 | Thick Film Resistors – 10 kΩ | R23, R25 | 2 | Yageo | RC0201JR-1310KL |
| 45 | Thick Film Resistors – 1 Ω | R27, R28, R29 | 3 | Yageo | RC0201JR-071RL |
| 46 | Thick Film Resistors – 18 kΩ | R30 | 1 | Yageo | RC0201JR-0718KL |
| 47 | Thick Film Resistors – 33 Ω | R31, R32 | 2 | Yageo | RC0201FR-0733RL |
| 48 | Negative Temperature Coefficient (NTC) Thermistors – 10 kΩ, 3370 K | RT1 | 1 | Semitec | 103FT1005A5P1 |
| 49 | Switches – Tactile | S1, S3 | 2 | ITT CK | NANOT240AS |
| 50 | Switches – Slide | S2 | 1 | ITT CK | OS102011MA1QN1C |

Continued on next page

(Continued)

| Idx. | Description | Designator | Qt. | Manufacturer | Manufacturer P/N |
|---|---|---|---|---|---|
| 51 | Soldering Bridges | SB1, SB2, SB3, SB4, SB5, SB6, SB7, SB8, SB9, SB10, SB11, SB12, SB13, SB14, SB15, SB16 | 16 | - | - |
| 52 | Audio/Signal Transformers - 55.3:1 | T1 | 1 | Triad Magnetics | SP-48 |
| 53 | Battery Management – 0.8 A, Single-cell Li-Ion/Li-Po | U1 | 1 | Texas Instruments | BQ21040DBVT |
| 54 | Switching Voltage Regulators – Boost | U2 | 1 | Texas Instruments | TPS61088RHLT |
| 55 | LDO Voltage Regulators – 3.3 VDC | U3 | 1 | Analog Devices | ADP7142ACPZN3.3-R7 |
| 56 | ARM Cortex-M4 Microcontrollers (MCU) – 80 MHz | U4 | 1 | STMicroelectronics | STM32L433CBT6 |
| 57 | Operational Amplifiers – General Purpose, 2 Ch., 700 kHz | U5 | 1 | Texas Instruments | LM358DGKR |
| 58 | Analogue Switch – 4× SPST, 5 V | U6 | 1 | Texas Instruments | TMUX1112RSVR |
| 59 | Bluetooth Low Energy (BLE) Modules – Ver. 5.0, 2.4 GHz, UART | U7 | 1 | DX Bluetooth | BT-11 |
| 60 | Crystals – 32.7680 kHz | Y1 | 1 | ECS International | ECS-.327-6-34QCS-TR |

Continued on next page

(Continued)

| Idx. | Description | Designator | Qt. | Manufacturer | Manufacturer P/N |
|---|---|---|---|---|---|
| 61 | Crystals – 8.0000 MHz | Y2 | 1 | ECS International | ECS-80-10-33-CHN-TR3 |

# Appendix C

# Sheets and Forms

All Participant Information Sheets and consent forms for the textile electrodes feasibility study (Chapter 3) and both human pilot studies (Chapter 6), are provided in full in this Appendix. Additionally, the survey questionnaire administered during Pilot Study I (Chapter 6) is also included.

## Participant Information Sheet 1

| | |
|---|---|
| Project title: | **A wearable incontinence management system** |
| Principal investigator (PI): | **Kia Nazarpour** |
| Researcher(s): | **Wei Ju, Srinjoy Mitra, Lynda Webb, Sadeque Reza Khan** |
| PI contact details: | |

This study was certified according to the Informatics Research Ethics Process, RT number **2021/83413**. Please take time to read the following information carefully. You should keep this page for your records.

**Who are the researchers?**
The team are members of Edinburgh Neuroprosthetics Laboratory. Kia Nazarpour is Principal Investigator. Srinjoy Mitra, Lynda Webb, and Sadeque Reza Khan are senior researchers within the team. They may be accompanied by PhD students, e.g. Wei Ju, while conducting this project.

**What is the purpose of the study?**
We work to develop a wearable system, e.g. a sock, to enhance the efficacy of clinical practice in the management incontinence. You are being asked to take part in a research study to help in understanding the wearability and efficacy of the proposed system.

**Do I have to take part?**
No – participation in this study is entirely up to you. You may decide to stop being a part of the research study at any time without explanation. You have the right to ask that any data you have supplied to that point be withdrawn or destroyed. You have the right to refuse to answer or respond to any question that is asked of you. You have the right to have your questions about the procedures answered (unless answering these questions would interfere with the study's outcome). If you have any questions as a result of reading this information sheet, you should ask the researcher before the study begins. You will have the option of taking part in the longer or shorter experiments.

**What will happen if I decide to take part?**
We will ask you to wear the proposed system, e.g. a sock, and give us feedback about various factors, e.g. comfort, weight, etc. Upon the initial feedback, we may use a technique called non-invasive electrical stimulation to send tiny pulses to your leg and we ask you to report your sensation. We may also measure the electrical activity of

your muscles, the so-called the electromyographic signals, from your leg/foot. In some experiments, we may also monitor the movement of your leg/foot with a video stream or with a sensor. These are well-known, safe and clinically certified techniques and are widely used in both academia and the NHS. As such the risks associated with our research is minimal. The experimental protocol will be as the following:

After skin preparation, e.g. wiping off any dirt from the skin with clinical level (NHS-approved) wipes, you wear a sock and embedded electronic sensors will be placed on your skin to stimulate currents or measure the activity of your muscles. Sensors will usually be placed by an experimental operator; however, you will also have the option to place them yourself. Once sensors are placed, a brief calibration routine will be performed. We may increase the stimulation current to induce a very small twitch in your foot. This level of stimulation is significantly below the pain threshold, i.e. you will not feel any pain.

In various stages of the trial, you may be asked for your opinions on the sock. Your views may be used to provide contextual information for our research. If we quote you in any research output, it will be anonymous so it cannot be traced back to you.

**Time Commitment**

Between different experimental sessions, there will be rest period of up to 30 minutes during which you can relax. The sensors may remain attached to you during the break. Therefore, we may ask that your body movement will have to be under the supervision of the research team. If the experiment takes more than 90 minutes, we will provide light refreshment, e.g. fruits, biscuits and tea/coffee. In the case of long recording sessions, buffet lunch will be provided. Please see the Participants' Rights section for more details.

Depending on the study question, you may be asked to return to the laboratory, up to five time, to repeat the same experiment. Before you sign up in study, you will know whether it is a one-day or a multi-day study.

**Are there any risks associated with taking part?**

There are no risks associated with participation. All equipment and systems have been tested for safety. The experimental protocol is safe.

If recommended by the UK and/or Scottish Government or The University of Edinburgh Health and Safety guidelines, if required, all experimental operators will be wearing personal protection equipment (PPE). You will also be given the option of wearing such equipment. If required, social distancing measures will be maintained when contact is not necessary. The laboratory space will be clean. Any surfaces you may come into contact with will have been cleaned prior to the experiment.

**What will happen to the results of this study?**
The results of this study may be summarised in published articles, reports and presentations. Quotes or key findings will be anonymised. With your consent, information can also be used for future research. Your experimental data will be anonymised and archived on a public data repository as per the requirement of the funding agency.

**Data protection and confidentiality.**
The data we collect do not contain any personal information about you except your initials for data management and your age for statistical analysis purposes. If you would like your data to be completely anonymised you must inform us as soon as possible, preferably before signing this document. No one will link the data you provided to the identifying information you supply.

Your data will be processed in accordance with Data Protection Law. All information collected about you will be kept strictly confidential. Your data will be referred to by a unique code, e.g. participant number. Your data will only be viewed by the research team.

All electronic data will be stored on a password-protected encrypted computer, on the School of Informatics' secure file servers and all paper records will be stored in a locked filing cabinet in the PI's office. Your consent information will be kept separately from your responses in order to minimise risk.

**What are my data protection rights?**
The University of Edinburgh is a Data Controller for the information you provide. You have the right to access information held about you. Your right of access can be

exercised in accordance Data Protection Law. You also have other rights including rights of correction, erasure and objection. For more details, including the right to lodge a complaint with the Information Commissioner's Office, please visit www.ico.org.uk. Questions, comments and requests about your personal data can also be sent to the University Data Protection Officer at dpo@ed.ac.uk.

**Who can I contact?**

Kia Nazarpour will be glad to answer your questions about this study at any time. You may contact him at . If you want to find out about the final results of this study, you can contact Dr Nazarpour directly. If you wish to make a complaint about the study, please contact inf-ethics@inf.ed.ac.uk. When you contact, please provide the study title and detail the nature of your complaint.

**Signature**

By signing below, you are agreeing that:

- you have read and understood the Participant Information Sheet 1,
- questions about your participation in this study have been answered satisfactorily,
- you are aware of the potential risks (if any), and
- you are taking part in this research study voluntarily (without coercion).

Participant's Name (Printed)*: _____

Participant's signature*: _____

Date: _____

**Participants wishing to preserve some degree of anonymity may use their initials.*

THE UNIVERSITY of EDINBURGH
informatics

# Participant Consent Form

| | |
|---|---|
| Project title: | **A wearable incontinence management system** |
| Principal investigator (PI): | **Kia Nazarpour** |
| Researcher(s): | **Wei Ju, Srinjoy Mitra, Lynda Webb, Sadeque Reza Khan** |
| PI contact details: | |

By participating in the study you agree that:

- I have read and understood below participant information sheets (PIS) and I have had the opportunity to ask questions, and that any questions I had were answered to my satisfaction.

| PIS1 | PIS2 | PIS3 |
|---|---|---|
| | | |

- My participation is voluntary, and that I can withdraw at any time without giving a reason. Withdrawing will not affect any of my rights. In addition, should I not wish to answer any particular question or questions, I am free to decline.
- I consent to my anonymised data being used in academic publications and presentations.
- I understand that my anonymised data will be stored for the duration outlined in the Participant Information Sheet.

**Please tick yes or no for each of these statements.**

| | | Yes | No |
|---|---|---|---|
| **1.** | I agree to being video recorded for approved research purposes. | | |
| **2.** | I allow my data to be used in future ethically approved research. | | |
| **3.** | I understand that my responses will be kept strictly confidential. I give permission for members of the research team to have access to my anonymised data and responses. I understand that my name will not be linked with the research materials, and I will not be identified or identifiable in the report or reports that result from the research. | | |
| **4.** | I agree to take part in this study. | | |

| | | |
|---|---|---|
| Name of Participant | Date | Signature |
| Name of person taking consent | Date | Signature |
| *To be signed and dated in presence of the participant* | | |
| Name of Principal Investigator | Date | Signature |

*Once this has been signed by all parties the participant can receive a copy of the signed and dated consent form, participant information sheets and any other written information provided to the participants. A copy of the signed and dated consent form will be kept with the project's main documents in a secure location.*

# Participant Information Sheet

| | |
|---|---|
| Project Title: | Non-invasive Electrical Stimulation on Posterior Tibial Nerve for Urinary Incontinence Rehabilitation: A Pilot Study Based on a Designed Wearable Stimulator: TENS*mini* |
| Principal investigator (PI): | Srinjoy Mitra |
| Researcher(s): | Srinjoy Mitra; Kianorsh Nazarpour; Wei Ju; David Vaca-Benavides |
| PI Contact Details: | |

This study is recorded by School of Engineering Ethics Team with submission of a self-assessment form on 26th Feb 2024. Please take time to read the following information carefully. You should keep this page for your records.

**Who are the researchers?**

The team members are from Institute for Integrated Nano and Micro Systems, and Edinburgh Neuroprosthetics Laboratory, The University of Edinburgh. Srinjoy Mitra is Principal Investigator. Srinjoy (academic), Kia (academic), Wei (PhD student) and David (PhD student) collaborate within the team. They may be accompanied by students/trainees in conducting this project.

**What is the purpose of the study?**

Researchers and clinicians at the University of Edinburgh are developing a device that stimulate the nerves with electric pulses to help with various medical conditions. Similar devices are available on the high street, e.g., Boots, and they are called TENS machines. Our device is smaller and lighter. It also allows us to control the electric current more effectively. We would like to invite you to a take part in this study so that we can test the function of this device in a pilot study.

**Do I have to take part?**

No – participation in this study is entirely up to you. You may decide to stop being a part of the research study at any time without explanation. You have the right to ask that any data you have supplied to that point be withdrawn or destroyed. You have the right to refuse to answer or respond to any question that is asked of you. You have the right to have your questions about the procedures answered (unless answering

these questions would interfere with the study's outcome). If you have any questions as a result of reading this information sheet, you should ask the researcher before the study begins.

**What will happen if I decide to take part?**

The experiment will take place at Edinburgh Neuroprosthetics Laboratory, School of Informatics at the University of Edinburgh.

We will attach the device on your body, near a nerve, e.g., your tibial nerve near your posterior ankle bone. Firstly, we turn the device on and step by step increase the stimulation current until you feel a tiny tingle on your leg or foot, and we will continue to increase the current intensity until we see your big toes start twitching and moving.

Secondly, we will record the EMG induced by different current intensity ranging from 0 mA up to 40 mA or your maximum tolerance of stimulation. We will repeat the process several times for comparison and statistical purposes. The bench-top stimulator DS-07A is an FDA-cleared device. The other wearable stimulator has not been certified as a clinical-approved device yet, but the many considerations has been taken regarding electrical safety, as seen in [the risk section]. All our EMG recording systems are certified medical device (CE and FDA approved).

**Time Commitment**

The experiment will not take more than 1.5 hours. We will provide light refreshment, e.g., fruits, biscuits and tea or coffee. Please see the Participants' Rights section for more details.

**Are there any risks associated with taking part?**

We have designed the stimulator to comply with all safety requirements. If you are interested, please see Appendix 1 which lists all safety measures that we have included.

We need the results of this experiment to ensure that the stimulator works, and we have enough data to support us in applying for medical certification.

All systems associated with EMG (recording from muscles) are safe as they have received international safety certificate.

The electrical stimulation protocol (which is 10 Hz frequency, 200 microsecond for pulse width, a stimulation period within 30 minutes) is safe and is used on a daily basis by NHS Lothian clinicians (neurophysiologist).

**What will happen to the results of this study?**

The results of this study may be summarised in published articles, reports and presentations. Quotes or key findings will be anonymised. With your consent, information can also be used for future research. Your experimental data will be anonymised and archived on a public data repository as per the requirement of the funding agency.

**Data protection and confidentiality.**

The data we collect do not contain any personal information about you except your initials for data management and your age for statistical analysis purposes. If you would like your data to be completely anonymised, please inform us as soon as possible, preferably before signing this document. No one will link the data you provided to the identifying information you supply.

Your data will be processed in accordance with Data Protection Law. All information collected about you will be kept strictly confidential. Your data will be referred to by a unique code, e.g. participant number. Your data will only be viewed by the researcher/research team.

All electronic data will be stored on a password-protected encrypted computer, on the School of Informatics' secure file servers and all paper records will be stored in a locked filing cabinet in the PI's office. Your consent information will be kept separately from your responses in order to minimise risk.

**What are my data protection rights?**

The University of Edinburgh is a Data Controller for the information you provide. You have the right to access information held about you. Your right of access can be exercised in accordance Data Protection Law. You also have other rights including rights of correction, erasure and objection. For more details, including the right to lodge a complaint with the Information Commissioner's Office, please visit www.ico.org.uk. Questions, comments and requests about your personal data can also be sent to the University Data Protection Officer at dpo@ed.ac.uk.

**Who can I contact?**

Srinjoy Mitra will be glad to answer your questions about this study at any time. You may contact him at . If you want to find out about the final results of this study, you can contact Dr Srinjoy Mitra directly. If you wish to make a complaint about the study, please contact School of Engineering Ethics Team (Ethics.Eng@ed.ac.uk). When you contact, please provide the study title and detail the nature of your complaint.

**Signature**

By signing below, you are agreeing that:

- You have read and understood the Participant Information Sheet,
- Questions about your participation in this study have been answered satisfactorily,
- You are aware of the potential risks (if any), and
- You are taking part in this research study voluntarily (without coercion).

Participant's Name (Printed)*: _____

Participant's signature*: _____

Date: _____

**Participants wishing to preserve some degree of anonymity may use their initials.*

**Appendix: Safety Considerations**

1. A Quick-Action Fuse (with 200 mA hold current) has been fitted to prevent overall current sourced by a lithium-polymer (Li-Po) battery to be greater than 200 mA. Under test, the overall current consumed by the electronic system (with maximum current stimulation output) were below 150 mA. This is the DC current used for powering a micro-controller (MCU) and other hardware peripherals, including a Bluetooth Low Energy (BLE) v5.0 module and a driving stage (voltage-to-current converter, for current stimulation purposes).
2. A transformer was used to remain the safe air gap (electrical isolation) between electronic circuitry and electrodes non-invasively contacted with human skin. The transformer only operates on ac supply.
3. Safety regulations IEC 60601-2-10:2012, 201.4.2 RISK MANAGEMENT PROCESS for ME EQUIPMENT or ME SYSTEMS: MANUFACTURERS shall include, within their RISK ANALYSIS, the risk associated with the potential use of their STIMULATORS and accessories to deliver current exceeding 10 mA or current densities for any electrode exceeding 2 $mA/cm^2$. For our designed STIM, maximum delivered current (RMS) is less than 8.94 mA, and current density should be less than 0.56 $mA/cm^2$ if the size of the electrode is 4 by 4 cm. Within the safe level of current density, the minimum size of electrode used for our designed system could be reduced to 2.12 by 2.12 cm.
4. Safety Mechanism: Automatically shut off the stimulation programme once the disconnection of electrodes or overload issues (due to electrolyte dries out) are detected by circuit.
5. Emergency Stop button from controller side to shut down the stimulation programme for emergency prevention, could also be designed into the circuit board itself.
6. A further module such as a Watchdog timer to be added in the future generation of PCB to avoid the run-away coding and would effectively improve the system robustness and stability.

THE UNIVERSITY of EDINBURGH
School of Engineering

# Participant Consent Form

| | |
|---|---|
| Project Title: | Non-invasive Electrical Stimulation on Posterior Tibial Nerve for Urinary Incontinence Rehabilitation: A Pilot Study Based on a Designed Wearable Stimulator: TENS*mini* |
| Principal investigator (PI): | Srinjoy Mitra |
| Researcher(s): | Srinjoy Mitra; Kianorsh Nazarpour; Wei Ju; David Vaca-Benavides |
| PI Contact Details: | |

By participating in the study, you agree that:

- I have read and understood the participant information sheets (PIS) and I have had the opportunity to ask questions, and that any questions I had were answered to my satisfaction.
- My participation is voluntary, and that I can withdraw at any time without giving a reason. Withdrawing will not affect any of my rights. In addition, should I not wish to answer any particular question or questions, I am free to decline.
- I consent to my anonymised data being used in academic publications and presentations.
- I understand that my anonymised data will be stored for the duration outlined in the Participant Information Sheet.

**Please tick yes or no for each of these statements.**

| | | Yes | No |
|---|---|---|---|
| **1.** | I agree to being video recorded. | | |
| **2.** | I allow my data to be used in future ethically approved research. | | |
| **3.** | I understand that my responses will be kept strictly confidential. I give permission for members of the research team to have access to my anonymised data and responses. I understand that my name will not be linked with the research materials, and I will not be identified or identifiable in the report or reports that result from the research. | | |
| **4.** | I agree to take part in this study. | | |

| | | |
|---|---|---|
| _____ | _____ | _____ |
| Name of Participant | Date | Signature |
| _____ | _____ | _____ |
| Name of person taking consent | Date | Signature |

*To be signed and dated in presence of the participant.*

| | | |
|---|---|---|
| _____ | _____ | _____ |
| Name of Principal Investigator | Date | Signature |

*Once this has been signed by all parties the participant can receive a copy of the signed and dated consent form, participant information sheets and any other written information provided to the participants. A copy of the signed and dated consent form will be kept with the project's main documents in a secure location.*

THE UNIVERSITY of EDINBURGH informatics

## Participant Information Sheet

| | |
|---|---|
| Project title: | **Exploring the Frequency-Dependent Effects of Neural Stimulation** |
| Principal investigator (PI): | **Kia Nazarpour** |
| Researcher(s): | **Aidan McConnell-Trevillion, Wei Ju, Srinjoy Mitra, Lynda Webb, Ingrid Hoeritzauer** |
| PI contact details: | |

This study was certified according to the Informatics Research Ethics Process, RT number **977504**. Please take time to read the following information carefully. You should keep this page for your records.

### Who are the researchers?

The research will be carried out by Aidan McConnell-Trevillion and Wei Ju, both research assistants at the School of Informatics. They will be supported by members of the Edinburgh Neuroprosthetics Laboratory and research partners including: Kia Nazarpour, the Principal Investigator; and Srinjoy Mitra, Lynda Webb, and Ingrid Hoeritzauer, senior researchers and academics within the team.

### What is the purpose of the study?

We are working to validate ongoing computational neuroscience research in healthy human participants. To do so, we use safe and approved stimulators to activate nerves of the leg, non-invasively from the surface of the skin. You are being asked to take part because the research team wants to examine how neural stimulation affect your bladder function, in our search for therapeutic benefits of neural stimulation.

### Why have I been asked to take part?

As a healthy adult, you have been asked to take part in this study to validate ongoing computational research in a safe and controlled environment.

**Do I have to take part?**

No - participation in this study is entirely up to you. You may decide to stop being a part of the research study at any time and without any explanation. You have the right to ask that any data you have supplied up until the point of your exit be withdrawn and/or destroyed. You have the right to refuse to answer or respond to any question that is asked of you. You have the right to have your questions about the procedures answered (unless answering these questions would interfere with the study's outcome). If you have any questions as a result of reading this information sheet, you should ask the researcher before the study begins.

**What will happen if I decide to take part?**

If you decide to take part, after providing informed, written consent, the research team will work with you to schedule a timeslot for the experiment that works for your schedule.

We will ask that you attend a session in the morning, and abstain from any caffeinated beverages, or cigarettes for 12 hours prior to attending the experiment **and any fluids at all for 2 hours before attending.**

When you arrive at the lab, the following will happen:

1. **Empty your bladder and drink water:** You'll be asked to use the restroom first, to empty your bladder as much as reasonably possible, and asked to drink a bottle of water (750ml).
2. **Wait 30 minutes:** Relax and read, do puzzles, or any other activity you can perform while stationary to pass the time
3. **Main Experiment:** We will use a safe nerve electrical stimulation device (approved as safe to for use in the UK, EU, and the USA) to gently stimulate a nerve near your ankle. Before we do so, the research team will cleanse the area near your

ankle with medically approved disinfectant wipes and, if needed, shave a small patch of hair with a sterile razor to allow us to place stick on electrodes to your skin. The stimulation will not be painful. You will barely feel it. You might feel a small twitching in a few of your toes.

4. **Wait until you need to pee**: We will tell you that you can let us know if you feel the urge to go to the toilet at any time.
5. **Tell us when you need to urinate:** Once you first feel the urge to go to the toilet, we'll stop the experiment and ask you to answer a short question about how strong your urge to pee is at that moment.
6. **Continue (Optional)**: If you feel able, we will ask if you are willing to remain for a further 10 minutes at which point we will ask you the same question about how strong your urge to pee is. This section of the experiment helps us see if the stimulation affects your urge to urinate, or if it is just because more time has passed.

**Is there any risk in taking part?**

There are no foreseen risks involved, the stimulation device has been approved as safe upon rigorous testing by independent organisations. The stimulation protocol is currently used as a standard research method globally. It is painless and safe.

If you feel at any point that you urgently need to urinate, or for any other reason, you may stop participating in the study without justification. If you report a strong urge to urinate during the questionnaire the research team will cease your participation in the study.

You may also cease participation in the study at any point during the optional 10-minute section of the experiment.

**How do I know if I can take part?**

To ensure we can address our research question, you cannot participate in the experiment if you meet any of the following criteria:

- You are younger than 18 years of age

- You have any form of pre-existing urinary tract disorder
- You have pre-existing cardiovascular conditions
- You have any form of implanted treatment devices (pacemakers, defibrilators, etc.)
- You have uncontrolled epilepsy
- You have broken/fragile/thin/infected skin around the treatment site (ankle)
- You are currently pregnant or believe there is a considerable risk of you being so at the moment.
- You have nerve damage
- You for any reason do not currently possess the capacity to provide informed consent.

**How long will the experiment take?**

The research team do not expect the experiment to take longer than two hours. Though we do ask that you restrict your intake of caffeinated beverages and cigarettes for **12 hours** before attending the session, and any fluid intake **2 hours before** attending the session.

**What will happen to the results of the study?**

The results of this study may be summarised as published articles, reports, and presentations. With your consent, information obtained during this study may be used for future research. Your experimental data will be anonymised and archived on a public repository as per the requirements of the project funding body. At this point, the data will be completely anonymised, and as such there will be no way to link any information available back to you.

**Can I be informed of the results of the study?**

Yes, you can reach out to study PI, Prof Nazarpour, on
and ask for study results.

**Data protection and confidentiality:**

The data we collect during the study will not contain any personal information about you, except for your initials for data management. If you would like your data to be completely anonymised you must inform us as soon as possible, preferably before signing this document. Otherwise, your data will be stored in a pseudo-anonymised form. Your data will only be linked to an ID number, the key for which will be stored separately from the rest of your data, on a secure/encrypted University of Edinburgh server. We store the data in this manner to allow the research team to destroy your data if you wish to withdraw from the experiment. Please note however, that this will not be possible if you choose to fully anonymise your data, as the research team will have no way of determining which set of stored data is yours.

Your data will be processed in accordance with UK Data Protection law. Your data will only be viewed by the research team. Any subsequent use of your data in reports, publications etc. will be in a form that makes it impossible to link the information back to you.

All electronic data will be stored on a password-protected encrypted computer, on the School of Informatics' secure file servers. All paper records will be stored in a locked filing cabinet in the PI's (Prof Kia Nazarpour) office. Your confirmation of consent will be kept separately from your research data to minimise risk.

**What are my data protection rights?**

The University of Edinburgh is a Data Controller for the information you provide. You have the right to access information held about you. Your right to access can be exercised at any point in accordance with UK Data Protection Law. You also have other rights including rights of correction, erasure and objection. For more details, including the right to lodge a complaint with the Information Commissioner's Office, please visit www.ico.org.uk. Questions, comments and requests about your personal data can also be sent to the University Data Protection Officer at dpo@ed.ac.uk.

**Who can I contact?**

Kia Nazarpour will be glad to answer your questions about this study at any time. You may contact him at .If you wish to make a complaint about the study, please contact inf-ethics@inf.ed.ac.uk. When you make contact, please provide the study title and detail the nature of your complaint.

**Signature**

By signing below, you are agreeing that:

- You have read and understood the information sheet
- You do not to your knowledge meet any of the listed exclusion criteria
- Any and all questions about your participation in this study have been answered satisfactorily
- You are aware of the potential risks (if any)
- You are taking part in this research study voluntarily (without coercion) and are of sound mind to provide consent

Participant's Name (Printed)*: _____

Participant's Signature*: _____

Date: _____

**OPTIONAL** Contact Email Address: _____

**Participants wishing to preserve some degree of anonymity may use their initials.*

THE UNIVERSITY of EDINBURGH
informatics

# Participant Consent Form

| | |
|---|---|
| Project title: | **Exploring the Frequency-Dependent Effects of Neural Stimulation** |
| Principal investigator (PI): | **Kia Nazarpour** |
| Researcher(s): | **Aidan McConnell-Trevillion, Wei Ju, Srinjoy Mitra, Lynda Webb, Ingrid Hoeritzauer** |
| PI contact details: | |

By participating in the study, you agree that:

- I have read and understood below participant information sheets (PIS) and I have had the opportunity to ask questions, and that any questions I had were answered to my satisfaction.
- My participation is voluntary, and that I can withdraw at any time without giving a reason. Withdrawing will not affect any of my rights. In addition, should I not wish to answer any particular question or questions, I am free to decline.
- I consent to my anonymised data being used in academic publications and presentations.
- I understand that my anonymised data will be stored for the duration outlined in the Participant Information Sheet.

**Please tick yes or no for each of these statements.**

| | | Yes | No |
|---|---|---|---|
| **1.** | I agree to being video recorded for approved research purposes. | | |
| **2.** | I allow my data to be used in future ethically approved research. | | |
| **3.** | I understand that my responses will be kept strictly confidential. I give permission for members of the research team to have access to my anonymised data and responses. I understand that my name will not be linked with the research materials, and I will not be identified or identifiable in the report or reports that result from the research. | | |
| **4.** | I agree to take part in this study. | | |

| | | |
|---|---|---|
| _____ | _____ | _____ |
| Name of Participant | Date | Signature |
| _____ | _____ | _____ |
| Name of person taking consent | Date | Signature |
| *To be signed and dated in presence of the participant* | | |
| _____ | _____ | _____ |
| Name of Principal Investigator | Date | Signature |

*Once this has been signed by all parties the participant can receive a copy of the signed and dated consent form, participant information sheets and any other written information provided to the participants. A copy of the signed and dated consent form will be kept with the project's main documents in a secure location.*

## Participant Information Sheet

| | |
|---|---|
| Project title: | **Exploring the Frequency-Dependent Effects of Neural Stimulation Part II: Wearable TENS*mini* Validation** |
| Principal investigator (PI): | **Srinjoy Mitra** |
| Researcher(s): | **Wei Ju, Srinjoy Mitra, Aidan McConnell-Trevillion, Lynda Webb, Ingrid Hoeritzauer, Kianoush Nazarpour** |
| PI contact details: | |

This study was certified according to the School of Engineering Research Ethics and Integrity Process. Please take time to read the following information carefully. You should keep this page for your records.

**Who are the researchers?**

The research will be carried out by Wei Ju, a PhD student at the School of Engineering. He will be supported by Srinjoy Mitra, Principal Investigator, and research collaborators including Aidan McConnell-Trevillion, Kia Nazarpour, Lynda Webb, and Ingrid Hoeritzauer from the School of Informatics.

**What is the purpose of the study?**

We are working to validate ongoing computational neuroscience research in healthy human participants. To do so, we use a design wearable stimulator (TENS*mini*) to activate the tibial nerve of the leg, non-invasively from the surface of the skin. You are being asked to take part because the research team wants to examine how neural stimulation affect your bladder function, in our search for therapeutic benefits of neural stimulation.

**Why have I been asked to take part?**

As a healthy adult, you have been asked to take part in this study to validate ongoing computational research in a safe and controlled environment.

**Do I have to take part?**

No - participation in this study is entirely up to you. You may decide to stop being a part of the research study at any time and without any explanation. You have the right to ask that any data you have supplied up until the point of your exit be withdrawn and/or destroyed. You have the right to refuse to answer or respond to any question that is asked of you. You have the right to have your questions about the procedures answered (unless answering these questions would interfere with the study's outcome). If you have any questions as a result of reading this information sheet, you should ask the researcher before the study begins.

**What will happen if I decide to take part?**

If you decide to take part, after providing informed, written consent, the research team will work with you to schedule a timeslot for the experiment that works for your schedule.

We will ask that you attend a session in the morning, and abstain from any caffeinated beverages, or cigarettes for 12 hours prior to attending the experiment **and any fluids at all for 2 hours before attending.**

When you arrive at the lab, the following will happen:

1. **Empty your bladder and drink water:** You'll be asked to use the restroom first, to empty your bladder as much as reasonably possible, and asked to drink a bottle of water (750 mL).
2. **Wait 30 minutes:** Relax and read, or any other activity you can perform while stationary to pass the time
3. **Main Experiment:** We will use a wearable stimulator to gently stimulate a nerve near your ankle. Before we do so, the research team will cleanse the area near your ankle with medically approved disinfectant wipes and, if needed, shave a small patch of hair with a sterile razor to allow us to fit textile electrodes (they are

embedded within a sock) to your skin. The skin surface will then be hydrated with the general-purpose body moisturizer (1.0 mL NIVEA Cream). The stimulation will not be painful. You will barely feel it. You might feel a small twitching in a few of your toes.

4. **Wait until you need to pee**: We will tell you that you can let us know if you feel the urge to go to the toilet at any time.
5. **Tell us when you need to urinate:** Once you first feel the urge to go to the toilet, we'll stop the experiment and ask you to answer a short question about how strong your urge to pee is at that moment.
6. **Continue (Optional)**: If you feel able, we will ask if you are willing to remain for a further 10 minutes at which point we will ask you the same question about how strong your urge to pee is. This section of the experiment helps us see if the stimulation affects your urge to urinate, or if it is just because more time has passed.

**Is there any risk in taking part?**

There are no foreseen risks involved, the stimulation protocol is currently used as a standard research method globally. It is painless and safe, although the stimulation device (TENS*mini*) is a designed device. The previously study based on TENS*mini* device was conducted very successfully without any complaints from attended participants and had a School of Engineering Research Ethics and Integrity Self-Assessment Form submitted and recorded on 28/02/2024.

If you feel at any point that you urgently need to urinate, or for any other reason, you may stop participating in the study without justification. If you report a strong urge to urinate during the questionnaire the research team will cease your participation in the study.

You may also cease participation in the study at any point during the optional 10-minute section of the experiment.

**How do I know if I can take part?**

To ensure we can address our research question, you cannot participate in the experiment if you meet any of the following criteria:

- You are younger than 18 years of age
- You have any form of pre-existing urinary tract disorder
- You have pre-existing cardiovascular conditions
- You have any form of implanted treatment devices (pacemakers, defibrilators, etc.)
- You have uncontrolled epilepsy
- You have broken/fragile/thin/infected skin around the treatment site (ankle)
- You are currently pregnant or believe there is a considerable risk of you being so at the moment.
- You have nerve damage
- You for any reason do not currently possess the capacity to provide informed consent.

**How long will the experiment take?**

The research team do not expect the experiment to take longer than two hours. Though we do ask that you restrict your intake of caffeinated beverages and cigarettes for **12 hours** before attending the session, and any fluid intake **2 hours before** attending the session.

**What will happen to the results of the study?**

The results of this study may be summarised as published articles, reports, and presentations. With your consent, information obtained during this study may be used for future research. Your experimental data will be anonymised and archived on a public repository as per the requirements of the project funding body. At this point, the data will be completely anonymised, and as such there will be no way to link any information available back to you.

**Can I be informed of the results of the study?**

Yes, you can reach out to study PI, Dr Srinjoy Mitra, on and ask for study results.

**Data protection and confidentiality:**

The data we collect during the study will not contain any personal information about you, except for your initials for data management. If you would like your data to be completely anonymised you must inform us as soon as possible, preferably before signing this document. Otherwise, your data will be stored in a pseudo-anonymised form. Your data will only be linked to an ID number, the key for which will be stored separately from the rest of your data, on a secure/encrypted University of Edinburgh server. We store the data in this manner to allow the research team to destroy your data if you wish to withdraw from the experiment. Please note however, that this will not be possible if you choose to fully anonymise your data, as the research team will have no way of determining which set of stored data is yours.

Your data will be processed in accordance with UK Data Protection Law. Your data will only be viewed by the research team. Any subsequent use of your data in reports, publications etc. will be in a form that makes it impossible to link the information back to you.

All electronic data will be stored on a password-protected encrypted computer, on the School of Informatics' secure file servers. All paper records will be stored in a locked filing cabinet in the PI's (Dr Srinjoy Mitra) office. Your confirmation of consent will be kept separately from your research data to minimise risk.

**What are my data protection rights?**

The University of Edinburgh is a Data Controller for the information you provide. You have the right to access information held about you. Your right to access can be exercised at any point in accordance with UK Data Protection Law. You also have other rights including rights of correction, erasure and objection. For more details, including the right to lodge a

complaint with the Information Commissioner's Office, please visit www.ico.org.uk. Questions, comments and requests about your personal data can also be sent to the University Data Protection Officer at dpo@ed.ac.uk.

**Who can I contact?**

Srinjoy Mitra will be glad to answer your questions about this study at any time. You may contact him at . If you wish to make a complaint about the study, please contact Ethics.Eng@ed.ac.uk. When you make contact, please provide the study title and detail the nature of your complaint.

**Signature**

By signing below, you are agreeing that:

- You have read and understood the information sheet
- You do not to your knowledge meet any of the listed exclusion criteria
- Any and all questions about your participation in this study have been answered satisfactorily
- You are aware of the potential risks (if any)
- You are taking part in this research study voluntarily (without coercion) and are of sound mind to provide consent

Participant's Name (Printed)*: _____

Participant's Signature*: _____

Date: _____

**OPTIONAL** Contact Email Address: _____

**Participants wishing to preserve some degree of anonymity may use their initials.*

THE UNIVERSITY of EDINBURGH
School of Engineering

# Participant Consent Form

| | |
|---|---|
| Project title: | **Exploring the Frequency-Dependent Effects of Neural Stimulation Part II: Wearable TENS*mini* Validation** |
| Principal investigator (PI): | **Srinjoy Mitra** |
| Researcher(s): | **Wei Ju, Srinjoy Mitra, Aidan McConnell-Trevillion, Lynda Webb, Ingrid Hoeritzauer, Kianoush Nazarpour** |
| PI contact details: | |

By participating in the study, you agree that:

- I have read and understood below participant information sheets (PIS) and I have had the opportunity to ask questions, and that any questions I had were answered to my satisfaction.
- My participation is voluntary, and that I can withdraw at any time without giving a reason. Withdrawing will not affect any of my rights. In addition, should I not wish to answer any particular question or questions, I am free to decline.
- I consent to my anonymised data being used in academic publications and presentations.
- I understand that my anonymised data will be stored for the duration outlined in the Participant Information Sheet.

**Please tick yes or no for each of these statements.**

| | | Yes | No |
|---|---|---|---|
| **1.** | I agree to being video recorded for approved research purposes. | | |
| **2.** | I allow my data to be used in future ethically approved research. | | |
| **3.** | I understand that my responses will be kept strictly confidential. I give permission for members of the research team to have access to my anonymised data and responses. I understand that my name will not be linked with the research materials, and I will not be identified or identifiable in the report or reports that result from the research. | | |
| **4.** | I agree to take part in this study. | | |

| _____ | _____ | _____ |
|---|---|---|
| Name of Participant | Date | Signature |
| _____ | _____ | _____ |
| Name of person taking consent | Date | Signature |
| *To be signed and dated in presence of the participant* | | |
| _____ | _____ | _____ |
| Name of Principal Investigator | Date | Signature |

*Once this has been signed by all parties the participant can receive a copy of the signed and dated consent form, participant information sheets and any other written information provided to the participants. A copy of the signed and dated consent form will be kept with the project's main documents in a secure location.*

A Survey for Participants

## BEFORE THE TEST

*Now that you are wearing the sock, please take a moment to rate the following items on a scale from 1 to 5 where 1 Indicates total dislike (disagree) and 5 represents high satisfaction (agree). Rate each item based on your experience, using the entire scale. Your honest feedback, reflecting your personal feelings and experiences, is valued.*

1. How was your experience of putting the sock on (easiest: 5, hardest: 1)?
   5 4 3 2 1

2. What is your opinion about its comfortability related to material of the sock?
   5 4 3 2 1

3. How does the device look to you (e.g., colour, shape)?
   5 4 3 2 1

4. What is your opinion of the device's discretion (or how do you feel the visibility of the device) (like: 5, dislike: 1)?
   5 4 3 2 1

5. What do you think of applying body moisturiser before wearing the sock (like: 5, dislike: 1)?
   5 4 3 2 1

## AFTER THE TEST

6. How comfortable would you describe the stimulation received by DS-07A?
   5 4 3 2 1

7. How comfortable would you describe the stimulation received by TENS*mini* Sock?
   5 4 3 2 1

8. Would you recommend TENS*mini* Sock to someone who needs it (such as for treatment of overactive bladder syndrome (OBS))?
   5 4 3 2 1

9. Would you like to use the TENS*mini* Sock while doing other daily activities (i.e., walking, cooking, etc.) at the same time?
   5 4 3 2 1

10. How was your experience of taking the sock off (easiest: 5, hardest: 1)?
    5 4 3 2 1